2013

Waves, currents and sediment transport modelling at the Wave Hub site

Gonzalez-Santamaria, Raul

http://hdl.handle.net/10026.1/1527

Waves, currents and sediment transport modelling at the Wave Hub site

by

Raúl González-Santamaría

A thesis submitted to Plymouth University

in partial fulfilment for the degree of

Doctor of Philosophy

School of Marine Science and Engineering

Faculty of Science and Technology

Plymouth University

October 2012

Abstract

Waves, currents and sediment transport modelling at the Wave Hub site

Author: Raúl González-Santamaría

This research project uses an integrated modelling system to investigate the effects of a wave farm on nearshore sediment transport at the Wave Hub site. The Wave Hub project is a large scale demonstration site for the development of the operation of arrays of wave energy generation devices located at the southwest coast of the UK where multiple field measurements took place. Particular attention of this study was paid to the interaction between waves and tides due the presence of the wave farm and its effects on radiation stress, bottom stress, and consequently on the sediment transport and the coast adjacent to the wave farm, using an integrated complex numerical modelling system. The modelling system consisted of the SWAN model for waves and the ROMS model for currents, and a sediment transport model for morphological computations. The two-way coupled SWAN and ROMS models with nested model grids were set up and run with and without the wave farm at the Wave Hub site. The results from this study show that tidal elevation and tidal currents have a significant effect on the wave height and direction predictions, and tidal forcing and wind waves have a significant effect on the bed shear-stress, mainly during spring tide. Also, the wave radiation stresses can considerably alter the long-shore and cross-shore velocity components. Interactions between waves and tides at the Wave Hub site are found to be important when modelling coastal morphological change due to the presence of wave energy devices. The wave action can impact on bottom boundary layer and mixing in the water column, which consequently impact on the nearshore sediment transport and the resulting morphological changes. Model results indicate that wave and long-shore currents are attenuated in the area sheltered by the wave farm. Bed-load rates show a decrease in magnitude when the wave farm is present, even during storm conditions. Wave impacts on averaged flood and averaged ebb tidal cycles show significant changes during flooding cases, when including the wave farm, it has major effects for the averaged flood cases on current speeds, bottom stresses, suspended sediments and bed-load transports. The results highlight the importance of the interactions between waves and tides when modelling coastal morphology with presence of wave energy devices. It was observed that the presence of the wave farm has significant impacts on the nearshore circulation, bed shear stresses and sediment transport. The morphological changes are also altered by the wave farm. This integrated modelling system provides a useful tool to help the study of physical impacts of a wave farm on coastal areas, which is the key element for the wave resource characterization, ocean circulation, sediment transport, morphodynamic changes and environmental impact assessment for the on-going Wave Hub projects.

Content

List of symbols

u_t	Total velocity of a water particle
U	Time-averaged velocity
u_w	Wave-induced velocity
u'	Velocity fluctuation due to turbulence
τ_0	Bed shear-stress
ρ	Density of water
u_*	Friction velocity
θ	Shields parameter
g	Acceleration due to gravity
ρ_s	Density of sediment grains
s	Specific density (ρ_s/ρ)
d	Characteristic diameter (usually the median grain diameter) of the sediment
u	Horizontal x-component of the wave velocity
v	Transversal y-component of the wave velocity
w	Vertical z-component of the wave velocity
k	Wave number
h	Water depth
z	Surface elevation
ω	angular frequency
a	Wave amplitude
η	Wave-averaged free surface elevation
E	Total energy density
R	Forcing Residual

$\propto, \beta$	Traditional tensor notation instead of *i, j.*
$N(\sigma, \theta; x, y, t)$	Action density function
σ	Intrinsic frequency
θ	Wave direction
t	Time
c_x and c_y	Wave celerity
S_{tot}	Effects of generation, dissipation, and nonlinear wave-wave interactions
D	Total water depth *D=h+η*
f	Coriolis parameter
H_z	Grid cell thickness
K_M, K_c	Vertical eddy viscosity and diffusivity
p	Pressure
ν and ν_θ	Molecular viscosity and diffusivity
S_{py}, S_{px}	Vertical radiation stress
A_r	Roller area
D_{50}	Median grain diameter
ρ_s	Mean sediment density
w_s	Vertical settling velocity
δ_{wbl}	Thickness of the BBL
τ_{sf}	Bottom skin-friction stress
τ_{ce}	Critical stress for erosion
$\vec{\Phi}$ and $\vec{\theta_{sf}}$	Vectors in the direction of the mean current and perpendicular to the current
τ_c	Bottom stress from currents
τ_w	Bottom stress from waves

q_{blx} and q_{bly}	Horizontal bed-load transport rates
D	Total water depth
D_{50}	Median grain diameter
E_s	Erosion source term
E_0	Erosion rate for each sediment class
F_{CC} F_{CS} F_{SS} F_{SC}	Hyperbolic functions
H_z	Grid cell thickness
K_H	Eddy diffusivity
K_M	Eddy viscosity
L	Wave length
N	Wave action density
N_{bed}	Number of bed layers
Q_b	Fraction of breaking waves
R_z	Wave roller shape function
S_w	Wave energy source/sink term
S_{xx} S_{xy} S_{yx} S_{yy}	Vertically varying horizontal radiation stresses
T	Near bottom average wave period
T^*	Ratio of τ_{wc}/τ_{ce}
u_*	Friction velocity due to currents
u_{*wc}	Friction velocity due to combined waves and currents
w_s	Sediment settling velocity
x	Horizontal direction
y	Horizontal direction
z	Vertical elevation
z_a	Active layer thickness

z_0	Total bottom roughness length
z_{oN}	Grain size bottom roughness
z_{oST}	Sediment transport bottom roughness
z_{oBF}	Bedform bottom roughness
z_{oMIN}	Minimum bottom roughness
z_r	Reference elevation for BBL
k	von Karman's constant (0.41)
lr	Ripple wave length
r	Density
r_0	Reference density
r_s	Sediment density
r_{water}	Water density
n	Kinematic viscosity
n_y	Tracer kinematic diffusivity
s	Wave frequency (relative to currents)
τ_c	Bottom stress due to currents alone
τ_{ce}	Bottom critical erosion stress
τ_m	Mean bottom stress due to combined waves+currents
τ_{sf}	Total skin friction bottom stress, (maximum combined wave+current)
τ_{sfm}	Skin friction component due to form drag
τ_w	Bottom stress due to waves alone
τ_{wc}	Combined bottom stress due to waves and currents

List of figures

13

To My Family

Acknowledgment

I would like to express my gratitude and acknowledgement to all those persons and institutions that have been important in this research study.

I am grateful to my supervisory team. My deepest gratitude to Dr. Qingping Zou and Dr. Shunqi Pan for their patience, support and guidance in this study. To Dr. Vanesa Magar for her encouragement in this work.

My thanks and acknowledgement to the National Council of Science and Technology – Mexico for the awarded scholarship and to Plymouth University for the opportunity to further this study.

I want to extend my thanks to the School of Marine Science and Engineering, in particular to the people in the Coastal and Ocean Engineering Research Group for their advice and support.

To all those who I have forgotten to mentioned here but have given me support during this study I would like to thank you.

Author's Declaration

At no time during the registration for the degree of Doctor of Philosophy has the author been registered for any other University award without prior agreement of the Graduate Committee.

Further material presented in this thesis has been published in two journal papers, one of them under review, and three conference proceedings. Relevant scientific conferences, five international and five national, were attended at which work was often presented.

Relevant publications

- Gonzalez R., Zou Q., Pan S., 2013, Impacts of a wave farm on waves, currents and coastal morphology in South West England, Journal of Estuaries and Coasts, SI: Renewable Ocean Energy. DOI: 10.1007/s12237-013-9634-z.
- Gonzalez R., Zou Q., Pan S., 2011, Numerical modelling of wave-tide interactions at a wave farm in the southwest of England, Journal of Coastal Research, SI 64, ISSN 0749-0208.
- Gonzalez R., Zou Q., Pan S., 2012: Modelling of the impact of a wave farm on nearshore sediment transport, Proceedings International Conference on Coastal Engineering.
- Gonzalez R., Zou Q., Pan S., 2011, The impact of a wave farm on large scale sediment transport, Proceedings European Wave and Tidal Energy Conference.
- Gonzalez R., Zou Q., Pan S., Padilla R., 2010: Modelling wave-tide interactions at a wave farm in the southwest of England, Proceedings International Conference on Coastal Engineering.

Conferences attended:

- Gonzalez R., Zou Q., Pan S., Waves, currents and sediment transport modelling at the Wave Hub site, CCOSE seminar series. (Oral presentation), January 2013, Plymouth, UK.

- Gonzalez R., Zou Q., Pan S., Modelling of the impact of a wave farm on nearshore sediment transport, International Conference on Coastal Engineering. (Oral presentation), July 2012, Santander, Spain.

- Gonzalez R., Zou Q., Pan S., The effect of a wave energy installation on large scale sediment transport, Blue Horizons Conference. (Poster), December 2011, Plymouth, UK.

- Gonzalez R., Zou Q., Pan S., The impact of a wave farm on large scale sediment transport, European Wave and Tidal Energy Conference. (Oral presentation), September 2011, Southampton, UK.

- Gonzalez R., Zou Q., Pan S., Numerical modelling of wave-tide interactions at a wave farm. International Coastal Symposium. (Poster), May 2011, Szczecin, Poland.

- Gonzalez R., Zou Q., Pan S., Modelling wave-tide interactions at the Wave Hub site, Peninsula Research Institute for Marine Renewable Energy. (Oral presentation), April 2011, Plymouth, UK.

- Gonzalez R., Zou Q., Pan S., Waves and tides at a wave farm in the southwest of England, Young Coastal Scientists and Engineers conference. (Oral presentation), March 2011, Liverpool, UK.

- Gonzalez R., Zou Q., Pan S., Modelling wave-tide interactions at a wave farm in the southwest of England, International Conference on Coastal Engineering. (Oral presentation), July 2010, Shanghai, China.

- Gonzalez R., Zou Q., Pan S., Wave and tide interactions at a wave farm in the southwest of England, Joint Numerical Sea Modelling Conference. (Oral presentation), May 2010, Rotterdam, Netherlands.

- Gonzalez R., Zou Q., Pan S., Wave and tidal currents at the Wave Hub site, Peninsula Research Institute for Marine Renewable Energy. (Oral presentation), March 2010, Penryn Cornwall, UK.

Word count of main body of thesis: 40,289

Signed: Raúl González-Santamaría

Date: 31 October 2012

1. Introduction

Marine energy is about connecting the energy from the sea - including waves, tidal streams and use of tidal range - to generate electricity. Some 25% of the world's wave and tidal technologies are being developed in the UK, which has the best wave and tidal resource in Europe (www.wavehub.co.uk).

The UK is widely regarded as a world leader in the development of marine renewable energy due to the high level of marine energy resource, its skilled expertise and the world-class complementary testing facilities at Wave Hub in Cornwall. In May 2011 an analysis released by the Carbon Trust found that total marine energy capacity could be 27.5GW in the UK by 2050, which would be capable of supplying to the grid the equivalent of over a fifth of current UK electricity demand. Also, the report shows that the UK could create over 68,000 jobs. These jobs would be developed thanks to growing export markets in countries like Chile, Korea and America as well as Atlantic-facing European states which benefit from powerful waves or tidal currents, including South West England in the UK (http://www.wavehub.co.uk). To help the development of renewable energy, a number of test and demonstration sites have been established in the UK, and the Wave Hub Project is one of them

1.1 The Wave Hub project

Located at the southwest coast of England, the Wave Hub project aimed to create one of the world's largest wave farms for demonstration and testing wave energy converter devices (Figure 1.1). Recent studies at the Wave Hub site suggest that wave induced currents are important in controlling sediment movement (SWRDA, 2006). Better

understanding of tidal effects on waves and sand transport is crucial to wave resource characterization and environmental impact assessment of the wave farm at the Wave Hub site.

1.2 Previous studies at the Wave Hub site

A numerical study carried out by SWRDA (2006) suggested that the wave energy converters (WECs) installed at the Wave Hub site would cause a reduction between 3% - 5% of wave height in the adjacent coast of the Wave Hub, as well as changes in tidal currents and bathymetry. However, in their study a hydrodynamic model, Flow3D, was forced by four tidal constituents during a storm to assess the impact of the deployed WECs on tidal currents and sediment transport. Key areas of study are the estimated wave height attenuation and tidal currents in the lee of the Wave Hub site and the associated impact on sedimentation, beach topography and beach state. Tidal currents recorded maximum current velocity of 1.2 m/s, in comparison of the admiralty pilot reported tidal currents between 0.5 and 1.0 m/s on the north coast of Cornwall during spring tides. To assess the WECs effect on the studied area, wave dragon devices were used. Model results suggest that sediment transport for this case study changes significantly at the Wave Hub site, but the impact of the wave farm on the adjacent nearshore zone remains an unresolved issue.

Millar et al (2007) carried out a study at the Wave Hub site using the wave model SWAN (Booij et al, 1999), to estimate the impact of WECs on the nearshore wave climate. They assumed a transmission rate through the wave farm of 90%, and analysed the distribution of the wave energy transmitted through the WECs to the adjacent nearshore region. By comparing the SWAN model results with field observations from wave buoys, they concluded that the average reduction in significant wave height was of

the order of 1cm, and that the stretch of the coast most likely to be affected was between St Ives Bay and St. Agnes (Figure 1.1).
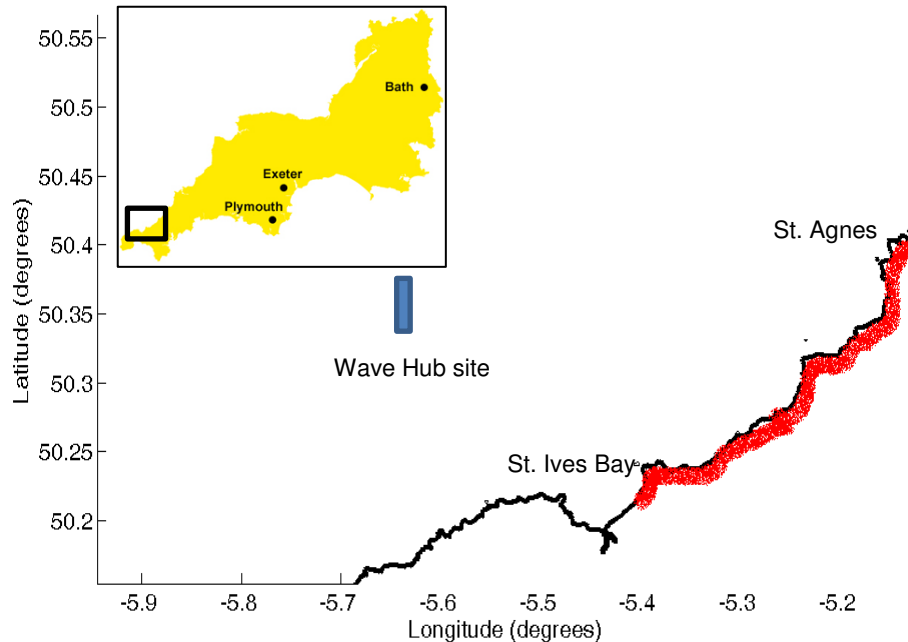
Figure 1.1 Location of the Wave Hub site and the affected area by the wave farm (red shaded line) suggested by Millar et al (2007).

Buscombe and Scott (2008) indicate that the sediment transport due to tides is believed to be weak and unquantified in this region, and the volume of transported sand is limited in comparison with other sectors of the English coasts. Also, they suggest that not only storm events may cause movement of sand on the inner shelf, but also their effects are greater in the near-shore zone where significant cross- and long-shore sediment transport takes place. Hence, wave-induced currents are more important in controlling sediment movement. Even, the prevailing winds are from the South and West, easterly winds can also produce significant movement of sediment. Therefore, there is currently a lack of studies in the near-shore areas in the lee of the wave farm.

Following the previous studies of wave-tide interactions at this area (Gonzalez-Santamaria et al, 2011), the main aim of the present study is to investigate the effect of a wave farm on the wave field, bed shear stresses, sediment transport and morphological changes, particularly along the shoreline behind the wave farm. We use the integrated and fully coupled wave-current numerical modelling system, incorporated with a morphological module, to gain insight into how the wave farm affects the currents and bottom friction at the Wave Hub site, as well as sediment transport and the resulting morphological changes.

1.3 Objectives of the study

The aim of the present study is to investigate the effects of a wave farm on the wave field, bed shear stresses, sediment transport and morphological changes, particularly along the shoreline behind the wave farm.

Particular aims:

- To investigate wave-tide interactions and their effects on sediment transport at the wave-farm coast, looking at the relationships of wave-currents and bottom stresses. Also, to assess on how waves, tidal currents and winds affect the wave-induced currents at the Wave Hub site and the near-shore zone, as well as their impact on the sediment transport.

- To setup a modelling system able to predict wave-current interactions and morphology changes, all affected by the wave farm.

The use of an integrated and fully coupled wave-current numerical modelling system, extended with the sediment transport modules to gain insight into how the wave farm

affects the current and bottom friction at the Wave Hub site, as well as sediment transport and the resulting morphological changes.

It is found that at an open coast the waves are modified by the flow through the water level and the current field. Changes in water level are reflected in changes of water depth. This, in turn, leads to changes in wave propagation, producing shoaling, refraction and wave breaking. Changes in the current field modify the wave patterns due to current refraction and, in cases of strong opposing currents, wave blocking. As accounted by Reniers (2012), when the flow is modified by the waves, the bottom friction is enhanced. Bottom friction then forces longshore currents, wave-induced set-up and horizontal and vertical circulations.

The current research study has been carried out by a complex modelling system and validated against measured observations. Model results show great accuracy when comparing with available wave buoy data and sea surface elevations, also a high correlation has been found between bottom friction, bottom stresses and bedload transports due to offshore wind fields and thus wind-waves, particularly in nearshore areas. However, due to the limited wave observations, velocity current measurements and sediment transport data, the model has not been validated in full.

1.4 Structure of the thesis

The thesis has been structured in the following chapters:

Chapter 2 consists on the review of renewable energies, particularly the energy extracted from wind-induced ocean waves through wave energy devices. The review of the Wave Hub project, which is the main focus on this research, is also addressed. Also, the review of the theory behind the modelling of wave-current interaction and sediment transport.

Chapter 3 reviews the theory of the applied numerical models to study wave modelling, ocean modelling, wave-current interactions and sediment transport. Then, the description of the coupled modelling system: the wave models and tide and ocean circulation models.

Chapter 4 provides the validation of the modelling system is carried out. First the validations of sea surface elevations and wave parameters during storm conditions. Then, the implementation of the coupled modelling system, analysing the effects of the wave farm on hydrodynamics and bottom stresses.

Chapter 5 presents the results of impacts of the wave farm that are modelled by the operational system testing and validating the results during storm conditions, even analysing the wave farm effects on the wave-current interactions.

Chapter 6 then presents the results of the effects of the wave farm on suspended sediment transport, bedload transport rate and morphology changes, and finally the analysis of bottom bed changes during and after the storminess period.

Chapter 7 gives the concluding remarks of the overall research outcomes and recommendations for future research.

2. Literature Review

2.1 Introduction

All societies require energy services to meet basic human needs (e.g. lighting, cooking, space comfort, mobility, communication) and to serve productive processes. Delivery of energy services needs to be secure and has low environmental impacts. Sustainable social and economic development requires assured and affordable access to the energy resources necessary to provide essential and sustainable energy services. Renewable energy (RE) sources play a role in providing energy services in a sustainable manner and, in particular, in mitigating climate change. In the Special Report on Renewable Energy Sources and Climate Change Mitigation by Moomaw et al, (2011) they estimate that RE accounted for 12.9% of the total 492 Exa-Joules (EJ) of primary energy supply in 2008 (IEA, 2010a). The largest RE contributor was biomass (10.2%), with the majority (roughly 60%), of the biomass fuel used in traditional cooking and heating applications in developing countries but with rapidly increasing use of modern biomass as well, 0.6 Hydropower represented 2.3%, whereas other RE sources accounted for 0.4%.

The RE resource in the ocean comes from different sources, each with different origins and requiring different technologies for conversion. Lewis et al. (2011) have identified six ocean energy sources, these are:

- Waves, derived from the transfer of the kinetic energy of the wind to the upper surface of the ocean.

- Tidal Range (tidal rise and fall), derived from the gravitational forces of the Earth-Moon-Sun system.

- Tidal Currents, derived from water flow resulting from the filling and emptying of coastal regions as a result of the tidal rise and fall.

- Ocean Currents, derived from wind-driven and thermohaline ocean circulation.

- Ocean Thermal Energy Conversion (OTEC), derived from temperature differences between solar energy stored as heat in upper ocean layers and colder seawater, generally below 1,000 m.

- Salinity Gradients (osmotic power), derived from salinity differences between fresh and ocean water at river mouths.

Ocean wave energy (as distinct from internal waves or tsunamis), is energy that has been transferred from the wind to the ocean. As the wind blows over the ocean, air-sea interaction transfers some of the wind energy to the water, forming waves, which store this energy as potential energy (in the mass of water displaced from the mean sea level) and kinetic energy (in the motion of water particles). The most energetic waves on earth are generated between 30º and 60º latitudes by extra-tropical storms. Wave energy availability characteristically varies seasonally and over shorter time periods, with seasonal variation typically being greater in the northern hemisphere. Annual variations in the wave climate are usually estimated by the use of long-term averages in modelling, using global databases with reasonably long histories (Lewis et al, 2011). Figure 2.1 shows a map of the global offshore average annual wave power distribution; the largest power levels occur off the west coasts of the continents in temperate latitudes, where the most energetic winds and greatest fetch areas occur.

The rate of energy input to waves is typically 0.01 to 0.1 W/m^2; this is a small fraction of the gross solar energy input, which averages 350 W/m^2, but waves can build up over oceanic distances to energy densities averaging over 100 kW/m (Cruz, 2008). Normally the highest average levels of wave power are found on the lee side of temperate zone oceans. On an annual basis, the highest levels in the Northern Hemisphere are off the west coast of the British Isles, also in Iceland and Greenland.
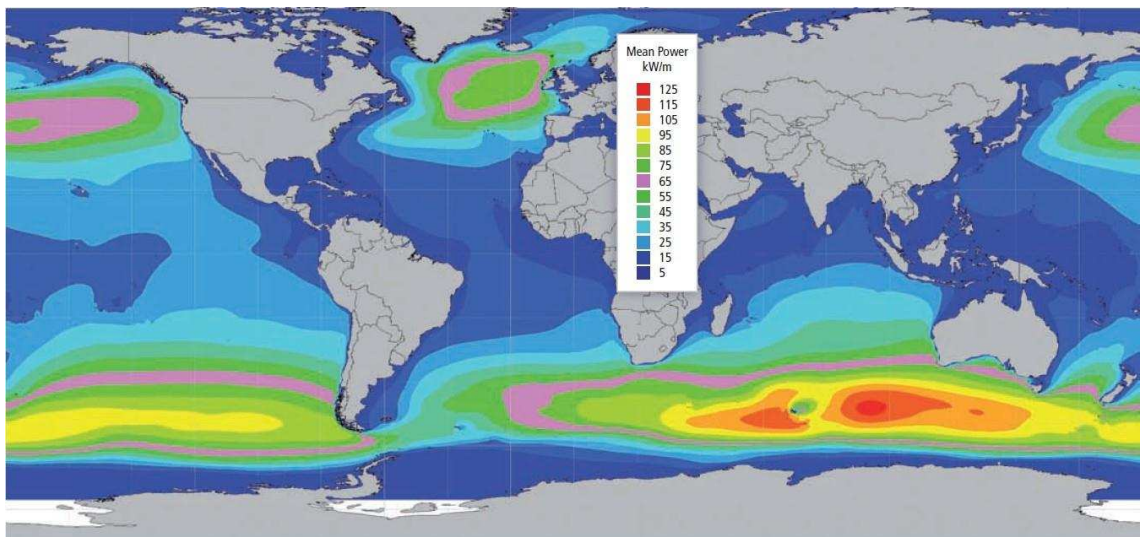
Figure 2.1 Global offshore annual wave power level distribution (after Cornett, 2008).

In terms of wave energy resource in Figure 2.1, there are some attractive areas in the globe when looking for a suitable site to locate a wave farm. On an average day, about 1 TW/h of wave energy enters to the coastal waters of the British Isles; this energy is about the same amount of energy which is used in electricity in the British Isles on an average day. The challenge is to choose a location which provides not only the adequate resource but also all the necessary conditions to ensure the continuous and reliable operation of the wave energy converters (Cruz, 2008). The UK has some of the largest wave and tidal energy resources in Europe. Allowing for technical, practical and environmental limitations, wave energy alone could generate up to one-sixth of the

UK's electricity consumption. The UK Government is committed to increasing the amount of electricity generated by renewable energy sources to 20% by 2020. This will help to address increasingly important energy and environmental issues including the security of energy supplies, climate change, resource depletion and environmental pollution.

2.2 The Wave Hub Project

In the Southwest of England a project called Wave Hub is being developed and funded by local authorities, industry and prestigious universities. The project started in 2003 from the initiative of the local government because the region has the potential to generate substantial amounts of electricity from its wave and tidal stream resources, and has the skills and facilities to support development of the industry. The Wave Hub is an electrical grid connection point approximately 10 nautical miles (16km) offshore into which wave energy devices will be connected.

Wave Hub is a ground-breaking renewable energy project that is being developed in response to the Government's initiative to increase the use of UK's renewable energy resources (SWRDA, 2006). It aims to create the UK's first offshore demonstration facility for proving the operation of arrays of wave energy generation devices. When fully operational, the Wave Hub site will be the world's largest test site for wave energy converters. The Wave Hub is located off the coast of Cornwall, in the Southwest of England (Figure 2.2). Recent studies at the Wave Hub site, suggest that wave-induced currents are important in controlling sediment movement (SWRDA, 2006). However, the tidal control on sand transport is uncertain on the Wave Hub coast (Buscombe and Scott, 2008).

A modelling study by SWRDA (2006) suggests that the Wave Hub would cause between 3% - 5% reduction to wave height between Hayle and Newquay, as well as minor changes to surface tidal currents and offshore bed elevations. Key areas are the estimated wave height attenuation and tidal currents in the lee of the Wave Hub site and the associated impact on sedimentation, beach topography and beach state.
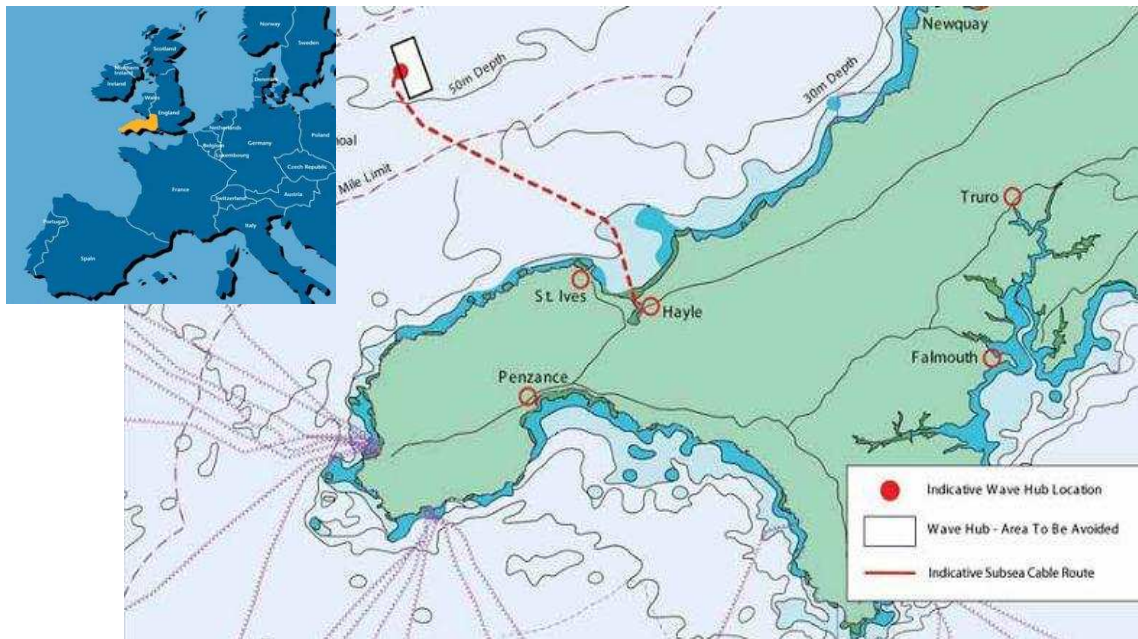
Figure 2.2 The Wave Hub site is located 16 kilometres off the north coast of Cornwall (north east of St Ives) in South West England (after www.wavehub.co.uk).

SWARDA & ASR Ltd (2007) performed a review of the Wave Hub project, reviewing Millar et al (2006) and SWRDA (2006) studies. They used the SWRDA data and their own model to conduct a scientific examination of the likely impacts of the Wave Hub. They concluded that the impact on wave height is expected to be low at less than five percent or less than five centimetres off a metre-high wave. In the same report by SWARDA & ASR (2007) they concluded that neither Millar et al (2006) nor SWRDA (2006) presented calibration of the wave models to the local environment, or even the

effect of the devices on the wave period. Hence a number of open questions still remain on the impacts of waves and wave-induced currents on the sea bed and on the coastal evolution in the area.

2.2.1 Hydrodynamics around the Wave Hub area

SWRDA (2006) deployed a buoy in 2005 to observe wave parameters and tidal currents, recording maximum velocities of 1.2 m/s, on the other hand, the admiralty pilot reports tidal streams on the north coast of Cornwall at a spring tide rate of 1 to 2 knots (0.5 to 1.0 m/s). In a study by Babtie (2002) the effects of waves and tidal currents on sediment transport were investigated, modelling the inter-tidal area in St Ives Bay; the analysis investigated the dynamics at seven locations within this area. In their study it seems that the transport of sediment is mainly cross-shore but there is no data that quantifies the transfer of material between the nearshore and offshore during storm (winter) and calm (summer) conditions; even the numerical study does not state where the ebb dominated flow is. However, SWRDA (2006) assumes that the dominated flow may be in the vicinity of the Hayle estuary (see Figure 2.2).

Generally, it is accepted that transport in the offshore zone is mainly related to currents, as the influence of waves is limited to shallow water depths. Unfortunately, there is no admiralty information about tidal currents for St Ives Bay; however there is information for the South West. For example, it has been reported that tidal current speeds range from 0.72 m/s off to Lundy up to 3.0 m/s in the Bristol Deep (Babtie, 2002). There is no data available for sediment transport during storm conditions. In the report by SWRDA (2006) it is suggested that there is very little published information to date regarding sediment transport in the transitional zone and the nearshore zone.

2.2.2 Morphodynamics around the Wave Hub area

The north Cornwall beaches are characterised by low erosion rates due to high inputs of sediment from offshore. They are characterised by large tidal ranges and significant wave heights, thus large redistributions of material during storms are a strong seasonal component to beach change. On nearly all of the beaches, dominant controls are also played by some combination of intertidal rock outcrops (rip channels at high tide) and streams which discharge directly into the beach. For any given beach, on/offshore exchanges of material are likely to be more significant than the exchanges along-shore; this depends on the beach and on the environmental conditions, as well as the timescales of observation. Moreover, the influence of the rivers on the coast that discharge directly into the beaches, is poorly studied, thus the sediment transport impact is not well understood. (Buscombe & Scott, 2008). Waves cause strong seasonal on/offshore movements of sediment at the shore. According to SWRDA (2002), wave-induced currents are considerably more important than tide-induced currents in nearshore sediment transport affecting beaches.

A study by Babtie (2002) suggests that this on/offshore sediment transfer might not be as significant as what it could be due to tidal currents, which move sediment in the opposite direction (from Hayle estuary to Black Cliff). Also, the net movement of material appears to be from the west to the east. Along this frontage the sediment moves westwards (clockwise direction), into the Hayle estuary where it has the opportunity to either settle or be transported further along-shore on an ebb tide.

In the report by Buscombe and Scott (2008) most of the beaches of the Southwest of England have been characterised. The report covers 53 beaches and coves, for each of them physiography and physical attributes (of the region) are given. The morphodynamic classification for 15 major beaches within the regions are discussed.

The coasts of Devon and Cornwall in the Southwest of England experience some of the most energetic wave conditions (with significant wave heights of 2–3m) and the largest mean spring tide ranges (4-9 m) in the UK. Atlantic swell waves with moderate energy (0.5-1.5 m) during spring and summer enable the development of rhythmic bar morphology on the intermediate beaches at the low water stand, generating morphologically controlled rip current systems. Large tidal ranges introduce hazards such as tidal cut off through high water levels, and horizontal speed of shoreline movement, and enhanced rip current velocities on the ebbing tide. In the same report by Buscombe and Scott (2008) the following beaches in the North of Cornwall were characterised:

- Saunton Sands: this is an ultra-dissipative beach, characterised by a low gradient and fine sand (D50=0.19 mm), has a mean spring tidal range of 7.9 m and shows very subdued intertidal morphology due to cross shore translation of high energy surf zone processes during the tidal cycle.

- Constantine Bay, Perranport, and Sandymouth: these are intermediate (reflective/dissipative) beaches, characterised by a low-tide terrace and rip, and by low-tide bar/rip morphologies. These beaches have the highest calculated rip current risk and fall into the low tide bar/rip beach type (Scott et al, 2007). They are characterised by a steep, often coarse, reflective high water beach face, a wide (400-600 m) subdued dissipative intertidal zone (swash bar sometimes present) and well developed intermediate low water bar and rip circulation systems.

2.3 Effect of currents on waves

The present study is focused on the analysis of wave induced currents and tide induced currents, thus the need to understand these processes is compulsory. The effect of currents on waves is evident in the tidal modulation of significant wave height and especially in wave period. The modulation of apparent (absolute) period must be attributable to the unsteady current (Wolf and Prandle, 1999).

According to Wolf and Prandle (1999), there are some important concepts to keep in mind when considering the impact of currents on waves:

• Wave generation by wind – the effective wind is that relative to the surface current, the wave age (c_p/U^*) and effective surface roughness may be important. Here c_p is the wave phase speed and U^* is the friction velocity of the wind. The effective fetch also changes in the presence of a current.

• Wave propagation – current refraction is dependent on the spatial variation of currents, which could decrease or increase towards the coast. Generally, shoaling depths will increase the tidal amplitude towards the coast until friction reverses this trend. The waves will tend to turn towards the direction of the current axis.

- Doppler shift – the effect of a steady current on intrinsic (relative) wave frequency.

- Steepening of waves on an opposing current due to shorter wavelength and increased wave height. This is a consequence of the principle of conservation of wave action.

- Modulation of absolute frequency of the waves by unsteady currents and modulation of intrinsic frequency by propagation over spatial gradients of current.

- Wave-current bottom stress – various empirical theories for wave-current interaction in the bottom boundary layer suggest that the friction coefficient experienced by waves in a current regime will be larger than if there were no currents.

- Effect of vertical current shear stresses on wave breaking – wind-driven surge currents would be relevant to this.

Waves can be affected by the presence of currents due to refraction, modification of bottom drag and blocking (Bolanos et al, 2008). An impact of currents on waves modifies the wave period: the waves will propagate faster when their direction of propagation is the same as the current direction. Also, the water depth will have an influence on the waves, so low tide affects the waves more than high tide, due to bottom influence on the waves (Pleskachevsky et al. 2009).

2.4 Effect of waves on currents

The effect of waves on currents can be seen in an apparent decrease in tidal current amplitude with increasing wave height. This is attributed here to an increased bottom friction coefficient for the current flow due to the presence of waves (Wolf and Prandle, 1999). This friction of the wave with the bottom leads to wave energy loss and to the appearance of radiation stresses, which in turn cause long-shore currents and wave set-up. Also, the effective surface drag coefficient for wind-driven surge currents may change with wave age. Prandle (1977) shows that bottom friction has little effect on depth-averaged tidal current in water depths greater than 50m (Wolf and Prandle, 1999).

Currents can be modified by waves due to an increase in turbulence, Stokes drift, Langmuir circulation, radiation stress and indirectly by a modification of the wind stress. The behaviour of the Stokes drift has been theoretically measured and modelled in several ways (Bolanos et al, 2008). The wave energy can be transferred to currents (radiation stress): this effect occurs when strong energy gradients appear, especially in shallow water. The waves lose their energy here due to stronger bottom friction, and as a consequence they slow down (Pleskachevsky et al. 2009).

2.5 Tidal currents

In addition to wave's effect, we need to understand tides and tidal currents, particularly in the UK where large tidal ranges exist. Tidal currents are tidal streams that vary from place to place, and are sensitive to changes of depth and to the influence of coastal embayments and headlands (Howarth, 1982). In the oceans, well away from the influence of the coast, both the direct tidal forcing and the Coriolis accelerations act to induce circulation of the semi-diurnal current ellipses in a clockwise sense in the northern hemisphere and in an anticlockwise sense in the southern hemisphere. On the continental shelf the sense of rotation is usually controlled by the bathymetry and by coastal wave reflections. Another important influence on the sense of ellipse rotation near a coastline is the presence of shelving beach or an embayment. In a pure standing wave system, currents are rectilinear with maximum amplitudes near the nodes or amphidromes such as in the southern North Sea, and southern entrance to the Irish Sea. The strongest currents are observed in the English Channel and Dover Straits, in the Irish Sea and North of Ireland (Pugh, 1987).

One of the most distinctive features of the Continental Shelf Sea is the relative strength of the tidal currents compared with those that occur in the deep sea. From the point of

view of fluid flow this feature is easy to explain. Just as flow through a large-diameter pipe accelerates as the pipe's diameter decreases, so a slow tidal flow in the deep sea accelerates to fast tide over the shallow continental shelf. In shelf regions, tidal currents are usually ten times stronger than currents from other sources (wind or convection due to fresh water from rivers) (Dyke, 2007). Tidal currents may be broken down into their harmonic constituent ellipses or rotary components, measured, analysed, and predicted in the same way as tidal levels (Pugh, 1987). Tidal currents can also be specified by the amplitude and Greenwich phase lag of the two components of the tidal current vector, each of which can be determined independently from harmonic (or response) analysis in the form of a tidal ellipse, instead of the individual components. Four parameters completely describe the tidal ellipse and hence the tidal current for a single constituent (Kantha and Clayson, 2000). The ellipse parameters for tidal currents are the semi-major and semi-minor axes, inclination and phase angles. The inclination angle is the angle which the semi-major axis makes with the x- (east) axis. The phase angle is the angle corresponding to the time of maximum velocity. The calculation of these parameters is beyond the scope of this research.

The current associated with a tidal constituent is a two dimensional periodic vector and as such can be approached in three different but complementary ways. Each describes the motion in terms of the four parameters - the amplitudes and phases of two orthogonal components; the amplitudes and phases of a clockwise and anticlockwise rotating vector, (an ellipse described by the motion), its maximum and minimum amplitude and the phase and direction of the maximum. The first orthogonal components, usually in the east and north directions, is the easiest for analysis and computation but is lacking because the choice of directions is arbitrary, having no dynamical significance. The second is not only a step between the other two but also

has dynamical significance because of Earth's rotation (in the northern hemisphere clockwise motion is favoured). The third; the ellipse parameters may be presented in four separate contour maps, are independent of a coordinate system and make most sense for presentation purposes (Howarth, 1990).

Tidal currents play an important role around tidal inlets, estuaries and open coasts, where the currents are strong enough to cause significant bottom changes. The propagation of tides along the ocean coasts and shallow waters normally are described by the shallow water equations, as tidal wave lengths are large compared to the water depth (Roelvink and Reniers, 2012).

2.6 Wave-current interaction

The main sources of energy in the coastal region are in the following order: tides, surges and wind waves. Tides and surges have a significant impact on shallow water waves. Interactions occur between these different 'waves' because the tides and surges change the mean water depth and current field experienced by the waves (Wolf and Prandle, 1999). The wave current interaction equations have been studied extensively (e.g. Longuet-Higgins and Stewart, 1962, 1963; Bowen, 1969; Grant and Madsen, 1979). Stokes drift is a well known second order wave process describing the net transport due to waves (Bolanos et al, 2008). Surge and tides are both long waves with periods of several hours, surface gravity (wind waves) have periods of several seconds (Figure 2.3), thus linear wave theory is sufficiently accurate, in the depths of water concerned greater than 12.5m mean depth, and significant wave heights less than 5m, for the purposes of dispersion (Wolf and Prandle, 1999).

The term wave-current interaction is commonly used to define the complex nearshore interaction of currents and the wave motion. To understand this process we require the

derivation of the depth-integrated, time averaged equations of momentum and continuity. Some assumptions help to simplify such equations since this particular nearshore zone is highly turbulent: from integrating differential equations over the depth from the bottom to the free surface, applying the appropriate boundary conditions which are affected significantly by contributions of bottom friction, bottom stress and surface stress (Svendsen, 2006).
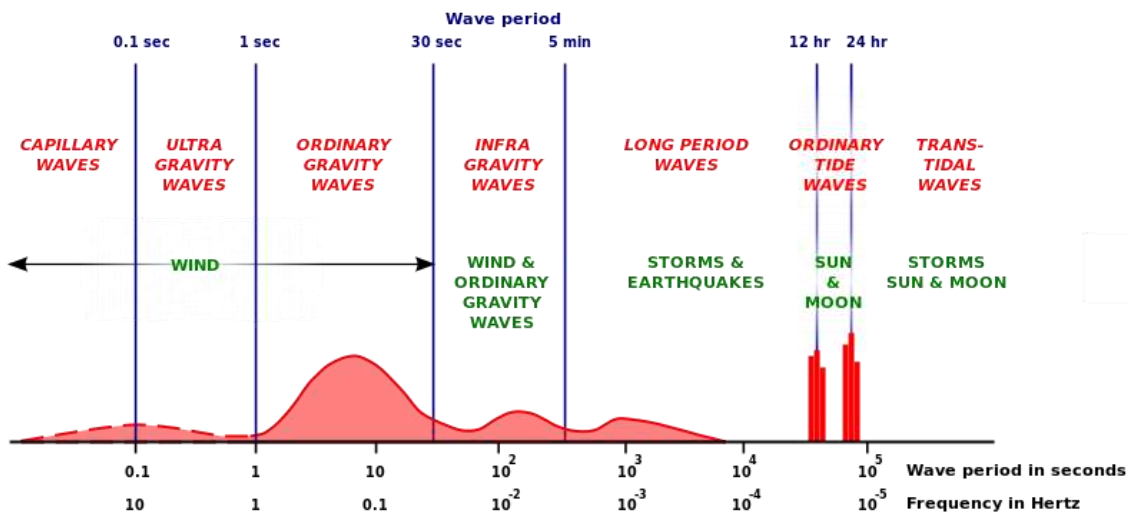
Figure 2.3 Classification of the spectrum of ocean waves according to the wave period (after Munk, 1950)

In order to study the wave-current interactions, we need to separate the waves from the currents, and their physical mechanisms. The total velocity of a water particle u_t is divided in three parts: the time-averaged current velocity; the oscillatory part representing the wave motion; and the turbulent fluctuation. Thus we have:

$$u_t = U + u_w + u'$$

(2.1)

where, u is the time-averaged velocity, u_w is wave-induced velocity and u' is the velocity fluctuation due to turbulence.

Waves and currents are coupled through the following physical mechanisms: i) surface shear stress, the effect of surface waves on the drag coefficient; ii) bottom shear stress, waves enhance the turbulent mixing, therefore, waves modify the bottom stress experience by currents (Grant & Madsen, 1979; Zou, 2004); and iii) radiation stress which represents the excessive momentum flux within the circulation due to the presence of waves (Longuet-Higgins and Stewart, 1964; Zou, 2006).

The forces acting on the free surface are a combination of wind shear stresses and surface pressure that together add up to the total stress. In case of strong winds blowing over waves, these create a pressure distribution and a shear stress distribution on the sloping surface. The shear stress is larger in the upstream side where the pressure is smaller. At the rear side of the wave the pressure is strongly negative and the shear stress is small (Svendsen, 2006).

A theoretical model presented by Pradeep et al (2011) describes the current velocity within and outside a wave–current boundary layer, to quantify the associated bed shear stresses for wave–current interaction at an arbitrary angle. The model indicates that the wave–current interaction angle is not significant for wave–current flow properties.

2.7 Bottom friction

Another term to assess the tides induced currents and waves induced currents is the bottom friction which is responsible for energy dissipation at the sea bed, it may reach a few watts per square meter, which is comparable to the energy input by the wind for moderate winds (Cavaleri et al, 2007). Within the bottom friction, the bottom stress is responsible for the sediment transport and the mixing column of water.

2.7.1 The bed shear-stress

Currents and waves effects on the sediment dynamics take place primarily through the friction they exert on the sea bed. This is expressed in terms of bed shear-stress, which is the frictional force exerted by the flow per unit area of bed (Soulsby, 1997). The bed shear-stress has units of force per unit area, which can also be written in units of velocity, as the friction velocity (or shear velocity), u_* which is defined through the relationship $\tau_0 = \rho u_*^2$, or $u_* = (\tau_0/\rho)^{\frac{1}{2}}$, and ρ is the density of the water.

Friction velocity can be related to the turbulent fluctuations in the real velocity components. A dimensionless form of the bed shear-stress and its relationship to the sediment is the Shields parameter defined by:

$$\theta = \frac{\tau_0}{g(\rho_s - \rho)d} = \frac{u_*^2}{g(s-1)d} \tag{2.2}$$

where g is the acceleration of gravity, ρ is the is the density of the water, ρ_s is the density of sediment grains, s is the specific density (ρ_s/ρ), and d is the characteristic diameter (usually the median grain diameter) of the sediment.

Soulsby (1997), states that the generated bed shear-stress depends not only on the speed of flow, but also on the roughness of the sea bed. This can be measured using either the Nikuradse roughness (related to grain size) or by the roughness length (derived from the velocity profile).

2.7.2 Bottom friction dissipation

The physics of the influence of a current on bottom friction dissipation is not fully understood. Bottom friction dissipation represented by the bottom friction, is regularly considered in shallow water modelling. With the exception of particular conditions as the southern and northern sea, bottom friction is rarely the dominant process for the proper evaluation of the wave conditions. There is a fair idea of the physics involved, but a lack of a solid quantification of the energy lost in the process (Cavaleri et al, 2007).

The same approach used for wave-bottom conservative interactions is usable also for currents. The level of interaction depends on the amplitude and the spatial scale of the current variations. The modifications of waves when interacting with currents are not interesting only on themselves, but also for remote sensing, both from space and from coastal measurements. A strong limitation to the operational implementation of the extensive theory available is the lack of sufficiently accurate description of the current field in the open sea. The difficulty of the problem increases considerably once we consider the currents as three-dimensional. Even, a better description of the current field is required to evaluate its effect on the wave field.

Another problem, pointed out by Cavaleri et al (2007), is the availability of the information (the characteristics of the bottom) required for the correct evaluation of the bottom friction. Within the relevance of the process for the evaluation of the wave conditions at a certain location, a detailed knowledge of the bottom characteristics of the area is a mandatory condition. This helps to decide which process can be locally relevant and, therefore, which processes need to be included in a model. However, even if the relevant processes were identified, the correct quantification of the energy involved in the processes is still a problem, as their physics itself implies that small

changes of the wave conditions can lead to an order of magnitude difference in the overall energy budget. How to deal with this problem is still an open question.

2.8 Radiation stresses

When the waves break, the wave momentum is transferred to the water column, inducing near-shore currents; this is called radiation stress, an additional term to study wave induced currents. In 1964, Longuet-Higgings and Steward published a paper where the radiation stress was discussed physically and applied to water waves. They define the radiation stress as the excess of momentum due to the presence of waves or the flux of momentum carried by the ocean waves.

Assuming a propagating wave in x-direction, and assuming that linear wave theory holds, the horizontal and vertical components of the wave velocity, u and w , respectively, may be expressed as:

$$u = \frac{H\omega}{2\sin kh}\cosh k(z+h)\cos(kx - \omega t), \text{ and} \qquad (2.3)$$

$$w = \frac{H\omega}{2\sin kh}\sinh k(z+h)\sin(kx - \omega t). \qquad (2.4)$$

where, k is the wave number, h is the water depth, z is the surface elevation, H is the wave amplitude, ω is the angular frequency.

The total flux of horizontal momentum across unit area of a vertical plane, $M(x,t),$ can be found by integrating $p + \rho u^2$ from bottom to surface:

$$M(x,t) = \int_{-h}^{\eta} (p + \rho u^2) dz \qquad (2.5)$$

The principal component of the radiation stress, S_{xx}, is defined as the mean value of $M(x,t)$ with respect to time, minus the mean flux in the absence of waves. Thus:

$$S_{xx} = \overline{\int_{-h}^{\eta} (p + \rho u^2)dz} - \int_{-h}^{\eta} p_0 dz \tag{2.6}$$

Essentially, S_{xx} consists of three main terms $S_{xx} = S_{xx}^{(1)} + S_{xx}^{(2)} + S_{xx}^{(3)}$:

$$S_{xx}^{(1)} = \overline{\int_{-h}^{\eta} \rho u^2 dz} \tag{2.7}$$

$$S_{xx}^{(2)} = \overline{\int_{-h}^{0} (p - p_0)dz} \tag{2.8}$$

$$S_{xx}^{(3)} = \overline{\int_{0}^{\eta} p\, dz} \tag{2.9}$$

where $S_{xx}^{(1)}$ is the vertically integrated Reynolds stress (or kinetic energy), $S_{xx}^{(2)}$ is the change in mean pressure with the fluid, and $S_{xx}^{(3)}$ is the potential energy density.

All the above equations have been derived using the small-amplitude approximation, hence, $S_{xx}^{(1)}$ is identical to the vertically integrated Reynolds stress $\overline{\rho u^2}$, from the bottom to the surface, in the stream-wise direction x:

$$S_{xx}^{(1)} = \overline{\int_{-h}^{\eta} \rho u^2 dz} = \int_{-h}^{0} \rho \overline{u^2} dz \tag{2.10}$$

$S_{xx}^{(2)}$ arises from the change in mean pressure within the fluid and it is assumed that there are no non-hydrostatic effects, then:

$$S_{xx}^{(2)} = \int_{-h}^{0} (\bar{p} - p_0) dz \tag{2.11}$$

From incompressibility and continuity:

$$\overline{p + \rho w^2} = -\rho g z = p_0 \tag{2.12}$$

So

$$\bar{p} - p_0 = -\rho \overline{w^2} \tag{2.13}$$

Which means that $\bar{p}$ is generally less than the hydrostatic pressure p_0 and zero, it also means that $S_{xx}^{(2)} \leq 0$. Combining equations 2.11 and 2.12 and 2.13:

$$S_{xx}^{(1)} + S_{xx}^{(2)} = \int_{-h}^{0} \rho(\overline{u^2 - w^2}) dz \geq 0 \tag{2.14}$$

After integration of equation 9, applying the velocities defined in equation 1, we have:

$$S_{xx}^{(1)} + S_{xx}^{(2)} = \frac{\rho g H^2 k h}{4 \sinh 2kh} \tag{2.15}$$

It worth mentioning that for deep water, where the particle orbits are circles, the addition of the first two terms of the radiation stress is zero (e.g. $\overline{u^2} = \overline{w^2}$), while in

shallow water u dominates (e.g. $\overline{w^2} = 0$). The sum of these first two terms is twice the kinetic energy density, that is, the total energy density of the waves.

The third term $S_{xx}^{(3)} = \overline{\int^{\eta} p dz}$ can be simplified, if we assume that the pressure at any point in the surface fluctuates in phase with the surface elevation (that is, we assume the fluid is hydrostatic):

$$p = \rho g(\eta - z) \tag{2.16}$$

Substituting 2.16 into the integral for $S_{xx}^{(3)}$, we have:

$$S_{xx}^{(3)} = \frac{\rho g \overline{\eta^2}}{2} = \frac{\rho g H^2}{16} \tag{2.17}$$

$S_{xx}^{(3)}$ is the potential energy density, that is to say, half the total energy density E,

where $E = \frac{1}{2}\rho g \eta^2$. If we express all the terms in terms of E, we find that:

$$S_{xx} = E\left(\frac{2kh}{\sinh 2kh} + \frac{1}{2}\right). \tag{2.18}$$

The ratio $\frac{2kh}{\sin 2kh}$ lies always between 0 and 1. In deep water $(kh \geq 1)$ the ration tends to 0 and so:

$$S_{xx} = \frac{1}{2}E \tag{2.19}$$

While in shallow water $(kh \leq 1)$ it tends to 1 and so:

49

$$S_{xx} = \frac{3}{2}E \qquad (2.20)$$

The transverse radiation stress S_{yy} has the same definition as S_{xx}, where v is the transverse component of velocity.

$$S_{yy} = \overline{\int_{-h}^{\eta} (p + \rho v^2)dz} - \int_{-h}^{\eta} p_0 dz \qquad (2.21)$$

In gravity waves the transverse velocity vanishes everywhere, thus,

$$S_{yy}^{(1)} = 0 \qquad (2.22)$$

where $S_{yy}^{(2)}$ and $S_{yy}^{(3)}$ are equal to $S_{xx}^{(2)}$ and $S_{xx}^{(3)}$ respectively. Following the same methodology in a similar way as for S_{xx}

$$S_{yy}^{(1)} = \overline{\int_{-h}^{\eta} \rho v^2 dz} = 0 \qquad (2.23)$$

and

$$S_{yy}^{(2)} = \overline{\int_{-h}^{\eta} \rho w^2 dz} = S_{xx}^{(2)} \qquad (2.24)$$

likewise

$$S_{yy}^{(3)} = \frac{\rho g \overline{\eta^2}}{2} = S_{xx}^{(3)} \qquad (2.25)$$

which results in

$$S_{yy} = E \frac{kh}{\sinh 2kh} \tag{2.26}$$

where the total energy density E is

$$E = \frac{1}{2}\rho g \eta^2 = \frac{\rho g H^2}{8}. \tag{2.27}$$

In deep water $S_{yy}{}^{(2)}$ cancels $S_{yy}{}^{(3)}$ and S_{yy} vanishes:

$$S_{yy} = 0. \qquad (kh \gg 1 \text{ limit}) \tag{2.28}$$

In shallow water the mean square vertical velocity $\overline{w^2}$ is small. Hence $S_{yy}{}^{(2)}$ is negligible, and

$$S_{yy} = S_{yy}{}^{(3)} = \frac{1}{2}E. \tag{2.29}$$

In the 2D case being discussed, the x-axis is aligned in the direction of wave propagation. The flow of x-momentum across the plane y = constant is given by

$$S_{xy} = \overline{\int_{-h}^{\eta} \rho uv dz} \tag{2.30}$$

There is no contribution from the mean pressure. Since $\overline{uv}$ vanishes identically,

$$S_{xy} = 0. \tag{2.31}$$

If for some reason the co-ordinate system is not orthogonal, there will be a non-zero shear stress S_{xy}.

In summary, the radiation stress tensor **S** can be calculated by the ordinary tensor transformation rules from the two-dimensional tensor **S**, which in diagonal form is given by

$$S = E \begin{pmatrix} \dfrac{2kh}{\sinh 2kh} + \dfrac{1}{2} & 0 \\ 0 & \dfrac{2kh}{\sinh 2kh} \end{pmatrix} \tag{2.32}$$

2.9 Cross-shore currents

Cross-shore currents are explained in the momentum exerted by the waves as the balance between the wave set-down and wave set-up. Wave set-down is when the water depth decreases toward the breaking point, the height of the MWL decreases and it reaches its lowest point at the breaking point. Waves incident on a shallow water region increase in amplitude and steepness, and finally break, producing a change in mean water surface level. This is caused by a change in the radiation stress (Longuet-Higgings and Steward, 1962).

Inside the surf zone, wave energy is dissipated by wave breaking, the radiation stress decreases, and setup of the mean water level occurs (Horikawa, 1986). Wave setup results in a water level which increases shoreward from the breaking point.

It is found that for the cross shore momentum balance, the change in radiation stress is quite large. However, in the case of small bottom friction, the radiation stress is balanced by the pressure force represented by the increase of mean water level. If this mean water level difference (slope) is 1/30 or larger, then this slope could drive a current if left unbalanced. On the other hand, if the two forces are balanced, there would be no forces left to create currents (Svendsen, 2006).

2.10 Long-shore currents

Radiation stress theory has been successfully used to explain the presence of long-shore currents (Bowen, 1969). Significant momentum can be transferred from waves to currents when a strong radiation stress gradient occurs due to wave breaking and to the bottom friction in the near-shore region. Radiation stress gradients are determined from the spatial gradients in the directional energy spectrum of the wave model, and the strongest gradients in radiation stress occur where depth-induced breaking happens (Mulligan et al, 2008).

To explain physically the long-shore currents or long-shore momentum variation, we have to address Svendsen's (2006) definition that relates these variations to three balancing forces or processes:

$$\underbrace{-\frac{d}{dx}S_{xy}}_{i} + \underbrace{\frac{d}{dx}\overline{\int_{-h}^{\eta}\tau_{xy}dz}}_{iii} - \underbrace{\tau_y^B}_{ii} = 0 \qquad (2.33)$$

The first term in Equation (2.33) is the cross-shore rate of variation of the long-shore radiation stress component S_{xy}, which acts as a driving force for currents; however, outside the breaker line there are no driving forces in the long-shore direction.

The second term, which is the bottom shear stress, restrains the currents but unless there is a current its value will be zero.

The rate of change of the time-averaged and depth-averaged turbulent shear stress, τ_{xy}, given by the term (iii), act as a distributing (or dispersion) mechanism that transfers $\frac{\partial S_{xy}}{\partial x}$ driving forces in the cross-shore direction. This mechanism is also called lateral mixing.

In other words, the long shore momentum is balanced by the bottom shear stress. Here the lateral mixing only distributes the forcing in the cross-shore direction. However, the long-shore component of the driving radiation stress is much smaller than the cross-shore component ($S_{xx} \ll S_{xy}$), because the incident angle $\propto_w$ of the waves relative to the normal to the shore is assumed small (Svendsen, 2006).

2.11 Nearshore circulation

Nearshore circulation is the term used for the complex nearshore currents generated by the short wave motion. These currents are determined by the depth integrated and time averaged equations of continuity and momentum (Svendsen, 2006).

The forcing available for driving currents depends on how the radiation stress gradients and the pressure gradients develop. This forcing can be expressed as the Forcing Residual R, which is defined as the vectorial sum of the two gradients

$$R_\propto = -\rho g h \frac{\partial \bar{\eta}}{\partial \propto} - \frac{\partial S_{\propto \beta}}{\partial \beta} \tag{2.34}$$

Where $\propto$ and β denote the traditional tensor notation instead of i, j. If the depth variations are such that the setup generated at two neighbouring cross-shore profiles is even moderately different we can have a situation where there is a (perhaps small) long-shore difference in the setup at the two positions. This corresponds to a long-shore gradient in $\bar{\eta}$ which can be a noticeable forcing in comparison to the other (small) long-shore forces. Therefore, as the expression for R, shows, this small gradient can drive a long-shore current, which can be strong locally. Thus in more complex situations on natural beaches it is often not a good approximation to neglect the first term in R, as we are able to do on a long straight coast. One can say: a coast only needs to deviate very

little from long and straight for the long-shore variations to be important. This also applies to the incoming waves. This can easily result in long-shore variations caused by (small) offshore depth variations that create refraction of the waves resulting in focusing or spreading of the waves near the shore (Svendsen, 2006).

In the depth-averaged equations of continuity and momentum equations, the total horizontal velocity u can be divided into two parts due to the currents and the waves a current part and a wave-part, thus, we separate them.

2.12 Sediment transport

2.12.1 Suspended sediments

Particles in suspension under the combination of waves and currents are typically associated with strong tide-induced, wind-induced or wave-induced currents, hence, the vertical mixing turbulence results in additional upward transport of particles yielding large concentrations in the upper layers. Under the combined waves and currents, the current-related transport is dominant, and can be derived from the time-averaged variables from the momentum equations (Van Rijn, 1993).

The transport of particles by rolling, sliding and saltating is called bed-load transport. The bed load can be defined as the product of particle concentration, particle velocity and layer thickness. The first bed-load formulation was presented by Meyer-Peter and Mueller (1948), for unidirectional flows. Through the years this formulation has been tested and modified.

Suspended sediment transport happens when the value of the bed shear velocity exceeds the particle fall velocity, then the lifted particles reach turbulent forces comparable to or higher than the submerged particle weight, and the particle motion becomes random or

chaotic. The suspended sediment generally is described as sediment concentration which is the solid volume per unit fluid volume (m^3/m^3) or the solid mass per unit fluid volume (kg/m^3), see as suggested by Van Rijn (1993).

Soulsby (1997) have indicated that the suspended sediment occurs when current speeds or wave motion is above the threshold of motion. At that stage, sand is entrained off the bed and into suspension, where it is carried at the same speed as the current. As a result, the proportion of the sand particles carried in suspension is much larger than that being carried as bed-load, where the suspended load is an important contribution to the total sediment transport.

2.12.2 Bed-load transport

The total load transport rate is integrated over a water depth, near the bedload layer, for the combined waves and currents, speed velocity and the sediment concentration are taken to be the mean values over a wave cycle plus a contribution of the covariance of the time varying velocities and concentrations. Soulsby (1997) studied the covariance contribution and suggests that it can be quite large, and is often in the opposite direction to the current, thus, the net sediment transport is reduced or even negative. When the waves are significant with small currents, a storm case, the covariance is greatest. There is still a gap of knowledge in the quantification of the contribution of this covariance.

In general for most models, the bedload transport is treated as a function of the near-bed velocity or bed shear stress, in 2DH models the bed shear stress follows the depth-averaged flow, whereas in 3D models it follows the near bed flow. (Roelvink & Reniers, 2012). The waves interact with the current in modifying the bed shear stress, the bed ripples, the sediment mobility and the near-bed current transporting the sediment. (Roelvink & Reniers, 2012). The total sediment transport rate is usually an important

quantity to address practical applications such as engineering works in coastal areas (Soulsby, 1997): dredging channels, morphodynamic changes by coastal structures, obstacles, and etcetera.

2.12.3   Erosion and deposition

Bedload transports are modelled in a simple way because the adjustment of the transport of sediment particles close to the bed adjusts rapidly to the new hydraulic conditions, however, suspended load transport does not have such behaviour because it takes time to transport the particles upward and downward over the depth and therefore it is necessary to model the vertical convection-diffusion process.

In an accelerating flow there is a vertical upward transport of sediment particles due to turbulence which occurs as long as the sediment transport capacity exceeds the actual transport rate. Van Rijn (1993) showed that the suspended sediment transport during decelerating flow is always larger than during accelerating flow

In an accelerating flow the suspended sediment concentration is typically lower than the equilibrium concentration, which is the concentration that would occur for stationary and uniform conditions, because the sediment has to be picked up and transported upwards by turbulent dispersion. When the flow decelerates or the waves are reduced, there is more sediment in suspension than the flow can support and sediment settles out. (Roelvink & Reniers, 2012). The large instantaneous shear stresses associated with intensified near-bed turbulence often dominate sediment resuspension and enhance bedload transport (Warner et al 2008). These processes combined have an impact on the coastal areas, thus, in the following chapters we will focus on the Wave Hub site to analyse the processes and the impact of a wave farm in the area.

To summarise the general behaviour of the sediments and the morphology, there are:

- Sand tends to go in the direction of near-bed current.

- If the current increases, the transport increases by some power greater than 1.

- On a sloping bed, sediment transport tends to be diverted downslope.

- The near-bed orbital motion of waves stirs up sediment and thus increases the transport magnitude.

- In shallow water, the wave motion becomes asymmetric in various ways, which leads to a net transport term.

2.13 Summary

Renewable energy is very important for governments, local authorities and industry, as alternative energy. The use of renewables minimise consumption of fossil resources, and thus the amount of CO_2 exerted to the atmosphere. One of the aims of the Wave Hub project is to provide and to contribute to the electricity supplied in the Southwest of England. The Wave Hub project is subdivided in multidisciplinary areas, one of them is the effect of the wave energy devices on the wave-current interaction and morphology changes, particularly in the lee side of the wave farm, which is the purpose of this research. In the nearshore coast of the Wave Hub site, there is the need to understand and to estimate the hydrodynamics and morphology in order to assess the environmental impact of the wave farm. The tides are the main driving force for the sediment transport in the Southwest coasts of England, followed by the wave action, these two driving forces are rather complicated to model at the same time, and it only can be done properly with new highly non-linear numerical models.

Numerical modelling has been applied to study the impacts of the state-of-art wave farm (Section 2.2), however, these studies lack of validation and calibration of the models to the local environment. Even, the results are mainly for the area close to the Wave Hub site. Also, there are no further studies in the near-shore area of the Wave Hub site, particularly numerical modelling systems integrating waves, currents, sediments, morphology and the wave farm.

The present study is intended to use numerical models which are capable of reproducing the hydrodynamics and morphodynamics driven by waves and tides. Thus, we need to validate the waves and tidal currents predicted by the coupled model first, and then incorporate a sediment transport model in the model system, and finally run the model with the presence of the wave farm.

In this Chapter 2 the physics behind the wave-current interaction and the sediment transport were presented. First, the tides and tidal currents have been addressed, then a look into the theory of wave-current interaction. Second, the wave induced currents through radiation stress is discussed in depth. Finally, the theory of sediment transport relating to suspended and bedload transports. In the next Chapter the wave model is validated with wave buoy observations, the tide induced currents is characterised with the presence of the wave farm. Also, the flow circulation model is validated with tide observations and parameterised waves. The coupled modelling system is validated to against measured observations.

3. The Modelling System

3.1 Introduction

As discussed in Chapter 2, the characterisation of wave resources is important for assessing the performance of the wave energy devices in a wave farm and the impacts to the surrounding environment, particularly the wave-induced currents and tide-induced currents. Also a modelling system is suggested to study these interactions; the system is composed basically by a wave model and a flow circulation model. The selection of the models was carried out among other similar models, this included type of equations, physics considered for wave-current interactions, sediment transport model characteristics, usability among other users, etc. In the end two wave models, WAM and SWAN, as well as two flow circulation models, ROMS and SHORECIRC, were reviewed.

The decision to select the wave model lies on the nature of each one; basically the scientific philosophy of SWAN is identical to that of WAM cycle 3, whereas the WAM model considers problems on oceanic scales, with SWAN the wave propagation is calculated from deep water to the surf zone. Since, WAM makes use of explicit propagation schemes in geographical and spectral spaces, it requires very small grid sizes in shallow water, and thus, it is unsuitable for applications to coastal regions. For that reason, SWAN employs implicit schemes, which are more robust and economic in shallow water than the explicit ones. Note that SWAN may be less efficient on oceanic scales than WAM (Booij et al, 2009). As a result, SWAN is selected because it can be applied to coastal areas to study wave induced currents.

The SHORECIRC model has a quasi-3D circulation mode, includes wave-induced currents, wave transformation, current-current circulation, surf modes, tidal currents, and rip currents. However, it can be applied only on small coastal areas. It has a barotropic circulation mode, the baroclinic version is adaptable. It has one way coupled system with SWAN-SHORECIRC. The sediment transport model is adaptable. The momentum balance is between horizontal radiation stress, horizontal advection, vertical viscosity and the pressure gradient, and it has depth averaged radiation stress. If the user requires help or information about this state of art model, the FAQ section in their website was last updated in 2007, and thus no users' forum. The installation might be easy; it can be run on multi-processors.

The Regional Ocean Modelling System (ROMS) is a fully 3D baroclinic circulation model which includes more physics and can be applied to include river flows, tracer advection (stratification), Coriolis forcing and can span spatially. It can be applied over large coastal areas (from shelf to coastal domains). It has modules for wave transformation, surf mode and wave breaking (adaptable). The coupling with SWAN is a two-way coupling. It has a sediment transport coupled system, and computes a depth-dependent radiation stress in 3D (vertical variation) due to momentum balance between horizontal radiation stress and the pressure gradient. The website provides full interaction with the users, even the FAQs are in real time, and all the sections are fully documented. The setup is complex and highly complicated, it requires additional netcdf and hdf5 libraries, also graphics interphase, grid creator and is run on Linux ambient. It also can be run either on shared or distributed memory. From the description of ROMS and SHORECIRC it is clear that ROMS would capture the interaction between waves and currents more accurately than SHORECIRC.

3.2 The integrated modelling system

In this study, the Simulating WAves in the Nearshore (SWAN) spectral wave model (Booij et al, 1999) and the flow circulation Regional Ocean Modelling System (ROMS) are used to form a fully two-way coupled modelling system (Warner et al, 2008). In order to validate the hydrodynamics and to assess the impact of the wave farm, the modelling system has to be accurate; this is possible if a finer grid resolution is applied. To avoid large consumption of time and computational memory, a nested modelling is required. Otherwise, we have to set up a finer grid resolution in a large scale area, which would demand large amounts of computational time. Moreover, SWAN and ROMS are coupled in a two-way online mode; this simplifies and avoids numerical errors and significant time by interpolating data in the offline one-way mode.

As shown in Figure 3.3, the SWAN model is run with three nested domains with progressively finer grid resolutions. At the finest grid (L3), SWAN is coupled with ROMS to form the coupled modelling system (SWAN+ROMS). The coupled modelling system is applied to assess the impact of waves on tidal currents and tidal currents on waves. To achieve this, a series of different cases combining spring and neap tides, high and low water levels, and high and low wave conditions, were investigated to examine the changes in wave parameters, current velocities and bottom stresses.

In the two-way coupled modelling system (see Figure 3.1 for details), the ROMS model computes surface levels, depth averaged horizontal velocity components and bottom stress based on the given sediment grain size; and the SWAN model computes wave height, wave length, wave period and wave bottom orbital velocities. Between these two models, the currents and water levels computed in ROMS are used in SWAN and the radiation stresses derived from SWAN are used to calculate the wave-induced current in

ROMS, so that the dynamic interaction between waves and tides is achieved. In addition, the wind fields, provided by the Global Forecast System model, are used as the surface forcing in SWAN model for predicting the wave field, but, the wind stress is ignored in the ROMS model due to the relatively small computational domain.
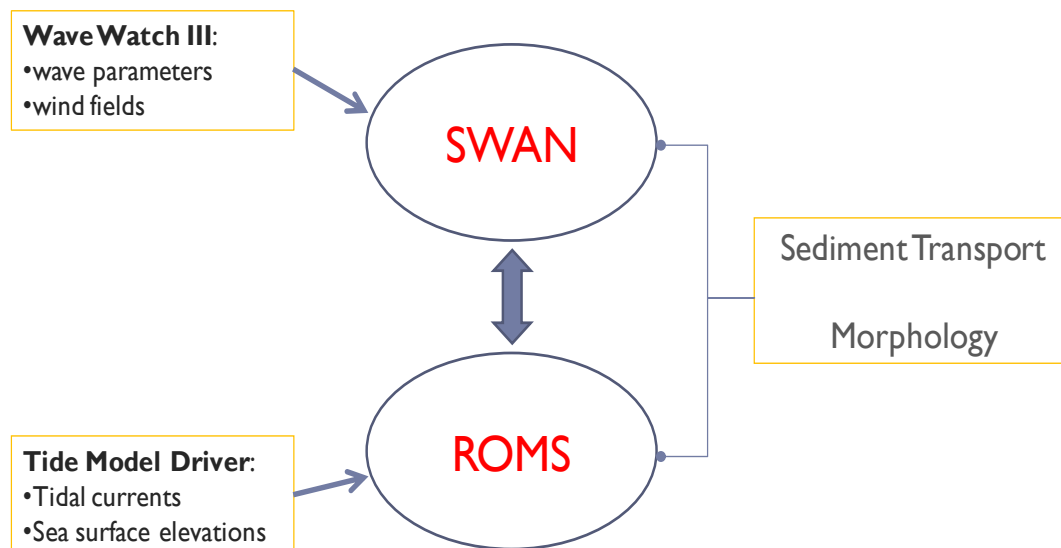
Figure 3.1 Schematic diagram of the integrated modelling system.

The coupled system is aimed to gain the most physics for the advantage of non-linear interactions such as the wave-current-sediment transport interaction, from three independent models. The two-way coupled process consists of the calculations of wave variables (SWAN) and hydrodynamic variables (ROMS) linked in the Model Coupling Toolkit (MCT) (Larson et al, 2005; Warner et al, 2008b). In other words, SWAN calculates the waves and waits until ROMS calculates the hydrodynamics, then the MCT distributes the information to the respective grids.

This process is represented in Figure 3.2, where ROMS sends to SWAN surface horizontal velocities, sea surface elevation and the bathymetry being updated every time step. SWAN sends to ROMS wave height, wave directions, wave length, horizontal

wave bottom velocity, surface wave period, bottom wave period, wave dissipation and a percentage for breaking waves.

For the vertical distribution of the wave forcing in ROMS, the wave information is sent to the surface and the bottom layers, then, the radiation stresses are calculated from Equations 3.9, 3.10, 3.11, 3.15 and 3.16. The wave energy is function of wave height and depth, thus, from hyperbolic functions (Equations 3.17 and 3.18) the wave forcing decays exponentially with depth, calculating radiation stresses every time step for every vertical grid layer.
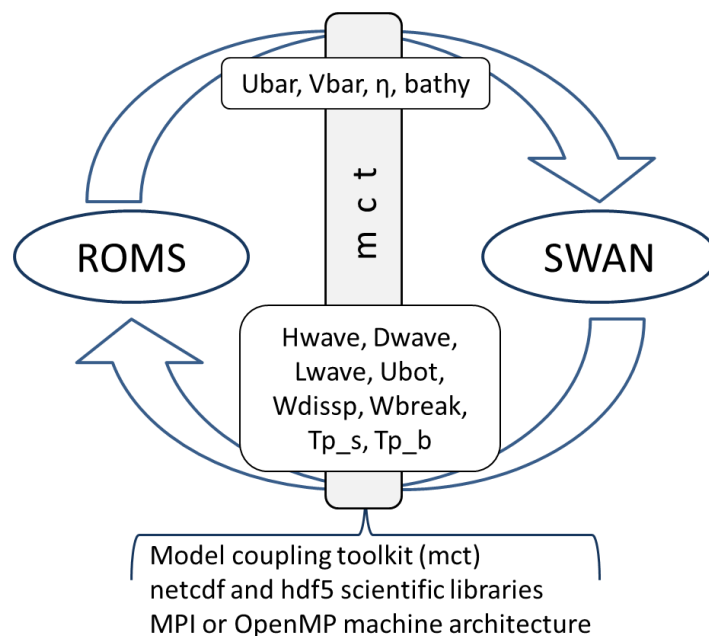
Figure 3.2 Schematic diagram of the two-way coupling with the MCT model.

In order to analyse the sediment transport due to waves and currents in the area, and assess the morphological changes in nearby beaches, a sediment transport model embedded within ROMS was incorporated in the modelling system. The Soulsby and Damgaard (2005) formulae was applied for computing bed-load transport which accounts for the combined effects of mean currents and asymmetrical waves contributions. The suspended sediment transport in the water column is computed by

solving the advection-diffusion equation, with an additional source/sink term to account for vertical settling velocity and erosion. Bottom shear stresses are used to determine re-suspension and transport, providing feedback from the sediment dynamics to the hydrodynamics (Warner et al, 2008).

3.3 Wave model

The Simulating WAves in the Nearshore (SWAN) wave model is a phase-averaged, wind wave model developed by Booij et al. (1999) that is widely used to simulate wave conditions in coastal areas. Ris et al. (1999) provided spectral verification for the model for stationary storms in coastal regions along the Netherlands coast. Ou et al. (2002) estimated cyclonic wind fields and use SWAN to simulate typhoon wave conditions over a regional domain near Taiwan, comparing model results to observed bulk wave statistics. Rogers et al. (2002) described whitecapping as the ''least understood'' wave process and investigated a fundamental problem in the form of the whitecapping term in SWAN, causing dissipation to be very sensitive to the presence of swell. Rogers et al. (2006) tested SWAN for stationary and non-stationary cases, over cascading domain scales in southern California. They found that primary contributors to model error, when compared to buoy data, were inaccuracy in the representation of wind forcing, inaccuracy in the directional distribution of wave energy at open boundaries and the relatively poor prediction of wind-sea growth/dissipation using stationary computations (Mulligan et al, 2008b).

3.3.1 Governing equations

The SWAN model (Booij et al, 1999) is a third generation shallow-water spectral wave model that includes wave propagation, refraction due to currents and depth, generation by wind, dissipation (whitecapping, bottom friction, depth-induced breaking), and

nonlinear wave-wave interactions. Longuet-Higgins and Stewart (1960, 1961, 1962) founded the theoretical description of wave-current interactions. Since then, many additional results of wave-current interactions have been published. If waves propagate in the presence of ambient current, action density is conserved whereas energy density is not. Therefore, in SWAN the action balance equation has been adopted.

SWAN is widely used to simulate wave conditions in coastal areas, where propagation, wave generation and dissipation processes are represented as: refraction and shoaling, reflection, diffraction, bottom friction, ambient currents, and depth induced breaking. The model conserves wave action density $N(\sigma, \theta)$, equal to energy density $E(\sigma, \theta)$, divided by the relative wave frequency σ. The relative wave frequency σ is related to the fixed wave frequency ω by the wave number vector $\mathbf{k}$ and mean current vector $\mathbf{u}$,

$$\sigma = \omega - \mathbf{k} \cdot \mathbf{u} \tag{3.1}$$

The evolution of the wave field in SWAN is described by the action balance equation

$$\frac{\partial}{\partial t} N + \frac{\partial}{\partial x}(c_x)N + \frac{\partial}{\partial y}(c_y)N + \frac{\partial}{\partial \sigma} c_\sigma N + \frac{\partial}{\partial \theta} c_\theta N = \frac{S_{tot}}{\sigma} \tag{3.2}$$

The left-hand side of this equation contains propagation terms in both geographical and spectral space (refraction is considered as propagation in spectral space). The right-hand side of the equation contains source terms which model the generation and dissipation of wave energy.

In Equation (3.2) $N(\sigma, \theta; x, y, t)$ is the action density as a function of intrinsic frequency σ, direction θ, horizontal coordinates x and y, and time t, all taken from the linear wave theory. The first term on the left-hand side represents the local rate of

change of action density in time, the second and third terms represent the propagation of action in geographical x, y space, respectively; and the wave's celerity c_x and c_y. The fourth term represents shifting of the relative frequency due to variations in depths and currents, with propagation velocity c_σ in σ space. The fifth term represents depth and current-induced refraction, with propagation velocity c_θ in θ space. The term $S_{tot}(\sigma, \theta; x, y, t)$ at the righ-hand side of the action balance equation is the source term representing the effects of generation, dissipation, and nonlinear wave-wave interactions (Booij et al, 1999). Radiation stresses are determined from spatial gradients in the directional energy spectrum $E(\sigma, \theta)$. The strongest gradients in radiation stress occur owing to depth-induced breaking (Mulligan et al, 2008a).

3.3.2 Source terms in SWAN

Source terms are empirical and contain empirical constants, these values are mostly based on literature and have been obtained by studying laboratory experiments or field observations. The main empirical source terms in SWAN, described below, are wind input, dissipation (surf breaking, whitecapping and bottom friction), and wave-wave interactions (Booij, 2008). Wind input consists of a linear and exponential part. The linear term is dominant only in the first stage of growth (starting from zero wave energy), thereafter the exponential term dominates.

Surf breaking or wave breaking is when the ratio of wave height and depth is exceeded (breaking and dissipation), when this happens the dissipation increases rapidly. In the whitecapping, the dissipation is proportional to the energy density and a coefficient dependent on the overall steepness of the wave field (wave height to wave length ratio). Wind input alone would make the wave height grow indefinitely, but whitecapping limits the wave height growth. Nonlinear wave-wave interactions (quadruplet

interactions) cause the average period to increase gradually and dominate the evolution of the spectrum. They transfer wave energy from the spectral peak to lower frequencies (peak frequency to lower values) and to higher frequencies (the energy is dissipated by whitecapping), as stated by Booij et al (1999).

Bottom friction and dissipation result from near-bottom orbital velocity and the shear stress on the bottom. SWAN has the capability to use formulations to vary the friction coefficient over an area (i.e. bottom roughness). As the waves propagate into shallow water the bottom friction dissipation is becoming important. This term depends mainly on the orbital motion of the waves near the bottom, and the bottom roughness. Very close to the shore surf becomes dominant. This source term depends on the ration between significant wave height and depth (Booij, 2008).

Dissipation due to bottom friction results from the near-bottom orbital velocity and the shear stress on the bottom. Both tend to 0 if the ratio of the wave length and the depth becomes small. Therefore low frequencies are more strongly dissipated than high frequencies. The bottom shear stress obviously is dependent on the properties of the bottom but the default formulation of bottom friction in SWAN does not show any dependency on bottom properties. Since bottom properties may vary over the area so that often a variable friction coefficient is usefull. The two other formulations have the possibility to enter a variable friction coefficient (Booij, 2008). Madsen et al (1988) configuration in SWAN has been used to activate the bottom friction. It also contains an equivalent roughness length scale of the bottom set as 0.05 m.

3.4 Ocean circulation model

3.4.1 Governing equations

The Regional Ocean Modeling System (ROMS) is a fully 3D baroclinic circulation model which solves the Reynolds-averaged Navier-Stokes equations using the hydrostatic and Boussinesq assumptions (Warner et al, 2008). The ROMS equations have been modified to include wave induced momentum flux (horizontal and vertical wave radiation stresses) that are important in near-shore regions by adding depth-dependent radiation stress terms in the three-dimensional momentum equations and depth-independent terms to the two-dimensional momentum equations. The governing equations in Cartesian coordinates are:

$$\frac{\partial(H_z u)}{\partial t} + \frac{\partial(u H_z u)}{\partial x} + \frac{\partial(v H_z u)}{\partial y} + \frac{\partial(\Omega H_z u)}{\partial s} - f H_z v \tag{3.3}$$

$$= -\frac{H_z}{\rho_0}\frac{\partial p}{\partial x} - H_z g \frac{\partial \eta}{\partial x} - \frac{\partial}{\partial s}\left(\overline{u'w'} - \frac{\nu}{H_z}\frac{\partial u}{\partial s}\right) - \frac{\partial(H_z S_{xx})}{\partial x}$$

$$- \frac{\partial(H_z S_{xy})}{\partial y} + \frac{\partial S_{px}}{\partial s}$$

$$\frac{\partial(H_z v)}{\partial t} + \frac{\partial(u H_z v)}{\partial x} + \frac{\partial(v H_z v)}{\partial y} + \frac{\partial(\Omega H_z v)}{\partial s} + f H_z u \tag{3.4}$$

$$= -\frac{H_z}{\rho_0}\frac{\partial p}{\partial y} - H_z g \frac{\partial \eta}{\partial y} - \frac{\partial}{\partial s}\left(\overline{v'w'} - \frac{\nu}{H_z}\frac{\partial v}{\partial s}\right) - \frac{\partial(H_z S_{xy})}{\partial x}$$

$$- \frac{\partial(H_z S_{yy})}{\partial y} + \frac{\partial S_{py}}{\partial s}$$

$$0 = -\frac{1}{\rho_0}\frac{\partial p}{\partial s} - \frac{g}{\rho_0} H_z \rho \tag{3.5}$$

with continuity as:

$$\frac{\partial \eta}{\partial t} + \frac{\partial (H_z u)}{\partial x} + \frac{\partial (H_z v)}{\partial y} + \frac{\partial (H_z \Omega)}{\partial s} = 0 \qquad (3.6)$$

and scalar transport:

$$\frac{\partial (H_z C)}{\partial t} + \frac{\partial (u H_z C)}{\partial x} + \frac{\partial (v H_z C)}{\partial y} + \frac{\partial (\Omega H_z C)}{\partial s} \qquad (3.7)$$

$$= -\frac{\partial}{\partial s}\left(\overline{c'w'} - \frac{\nu_\theta}{H_z}\frac{\partial C}{\partial s}\right) + C_{source}$$

The equations are closed by parameterizing the Reynolds stresses and turbulent tracer fluxes as:

$$\overline{u'w'} = -K_M \frac{\partial u}{\partial s}; \quad \overline{v'w'} = -K_M \frac{\partial v}{\partial s}; \quad \overline{c'w'} = -K_c \frac{\partial c}{\partial s}; \qquad (3.8)$$

where, u, v, and Ω are the mean components in the horizontal (x and y) and vertical (s) directions respectively; the vertical sigma coordinate $s = (z - \eta)/D$ ranges from s=-1 at the bottom to s=0 at the free surface; z is the vertical coordinate positive upwards with z=0 at mean sea level; η is the wave-averaged free surface elevation; D is the total water depth D=h+η; h is the depth below mean sea level of the sea floor; H_z is the grid cell thickness; f is the Coriolis parameter. An overbar represents a time average, and a prime (′) represents turbulent fluctuations. K_M, K_c are vertical eddy viscosity and diffusivity; Pressure is p; ρ and ρ_0 are total and reference densities for seawater; g is acceleration due to gravity; ν and ν_θ are molecular viscosity and diffusivity; S_{xx}, S_{xy}, S_{yy} represent horizontal radiation stress; S_{py}, S_{px} represent vertical radiation stress; C represents a tracer quantity (e.g. salt, temperature, suspended sediment); C_{source} are

71

tracer source/sink terms; and a function $\rho = f(C)$ is required to close the density relation. These equations are closed by parameterizing the Reynolds stress using one of the five options for turbulent-closure models in ROMS (Warner et al, 2008).

The vertical turbulent mixing scheme used is the Generic Length-Scale model, parameterised as κ-ε. κ-ε model is the most commonly used of all the turbulence models. It is classified as a two equation model; this denotes the fact that the transport equation is solved for two turbulent quantities κ and ε.

In Equations (3.3) and (3.4) the terms on the left hand side are: the change rate, horizontal advection and vertical advection, and the Coriolis parameter; on the right hand side: baroclinic gradient, surface pressure gradient, vertical viscosity, horizontal radiation and vertical radiation (where the surface roller term is included). Equation (3.5) represents the hydrostatic buoyancy force, Equation (3.6) represents the continuity equation and the equation (3.7) represents the scalar transport with similar terms as equations (3.3) and (3.4). The above equations neglect momentum transfer term that correlates wind-induced surface pressure fluctuations and wave slope.

The horizontal radiation stress terms (on the right hand-side of Equations 3.3 and 3.4) are:

$$S_{xx} = kE \left[\frac{k_x k_x}{k^2} F_{CS} F_{CC} + F_{CS} F_{CC} - F_{SS} F_{CS} \right] + \frac{k_x k_x}{k^2} \frac{c^2}{L} A_R R_{zn} \tag{3.9}$$

$$S_{xy} = S_{yx} = kE \left[\frac{k_x k_y}{k^2} F_{CS} F_{CC} \right] + \frac{k_x k_y}{k^2} \frac{c^2}{L} A_R R_{zn} \tag{3.10}$$

$$S_{yy} = kE\left[\frac{k_y k_y}{k^2} F_{CS}F_{CC} + F_{CS}F_{CC} - F_{SS}F_{CS}\right] + \frac{k_y k_y}{k^2}\frac{c^2}{L}A_R R_{zn} \tag{3.11}$$

where the terms in brackets are the traditional momentum flux terms due to the waves (as shown in Mellor 2003, 2005), the last term was added to account for the surface roller based on Svendsen (1984) and Svendsen et al. (2002), defined with a vertical distribution as:

$$R_{zn} = \frac{R_z}{\int R_z dz}, \qquad R_z = 1 - \tanh\left(\frac{2s}{\gamma}\right)^4 \tag{3.12}$$

where, R_z vertically distributes the additional stress term due to the roller as an exponentially decaying function with depth and γ is the ratio of wave height to water depth ($\gamma =$ H_s /D), H_s is the significant wave height, k is the wavenumber (k $=$ 2π/L where L is wavelength), k_x and k_y are the wavenumber components in the x- and y-directions and c is the wave-propagation speed, computed as:

$$c = \frac{\sigma}{k} = \sqrt{\frac{g}{k}\tanh kD} \tag{3.13}$$

where σ is the wave frequency ($\sigma = 2\pi/T$ where T is wave period). The roller area (A_R) is obtained directly from the wave model or computed from Svendsen (1984) as:

$$A_R = \frac{\alpha}{\sqrt{2}}H_s L Q_b \tag{3.14}$$

where α is a parameter with value 0.06, and Q_b is the fraction of breaking waves.

The vertical radiation-stress terms (last term on the right hand-side of Eqs. 3.3 and 3.4) are:

$$S_{px} = (F_{CC} - F_{SS}) \left[\frac{F_{SS}}{2} \frac{\partial E}{\partial x} + F_{CS}(1+s)E \frac{\partial(kD)}{\partial x} \right. \tag{3.15}$$

$$\left. - EF_{SS} \coth(kD) \frac{\partial(kD)}{\partial x} \right]$$

$$S_{py} = (F_{CC} - F_{SS}) \left[\frac{F_{SS}}{2} \frac{\partial E}{\partial y} + F_{CS}(1+s)E \frac{\partial(kD)}{\partial y} \right. \tag{3.16}$$

$$\left. - EF_{SS} \coth(kD) \frac{\partial(kD)}{\partial y} \right]$$

where the vertical structure functions in Equations (3.15) and (3.16) are:

$$F_{SS} = \frac{\sinh\big(kd(1+s)\big)}{\sinh kD} \quad, \quad F_{CS} = \frac{\cosh\big(kd(1+s)\big)}{\sinh kD} \tag{3.17}$$

$$F_{SC} = \frac{\sinh\big(kd(1+s)\big)}{\cosh kD} \quad, \quad F_{CC} = \frac{\cosh\big(kd(1+s)\big)}{\cosh kD} \tag{3.18}$$

and $E = \rho g H_s^2 / 16$ is the wave energy. These terms provide in the momentum equations wave forcing with a vertical structure that decays exponentially with depth.

The momentum expressions derived by Mellor (2003, 2005) yield equations with a mean velocity that is consistent with a Lagrangian reference frame. The Lagrangian and Eulerian reference frames are related by the Stokes velocities u_s and v_s in the x- and y-directions, computed as:

$$u_s = \frac{2k_x}{c} \frac{\cosh 2kD(1+s)}{\sinh 2kD} \left(E + \frac{DgA_R}{L} \right) \tag{3.19}$$

$$v_s = \frac{2k_y}{c} \frac{\cosh 2kD(1+s)}{\sinh 2kD} \left(E + \frac{DgA_R}{L} \right) \tag{3.20}$$

where the last terms in the parentheses are the roller contributions. Stokes velocities are subtracted from Lagrangian velocities to maintain a consistent Eulerian reference frame for the entire model dynamics.

3.4.2 Boundary conditions for ROMS

In realistic domains, open boundary conditions can be extremely difficult to get right. There can be situations where incoming flow and outgoing flow happen along the same boundary or even at the same horizontal location. The ROMS model has different vertical and horizontal open boundary conditions (OBC) including open, closed and periodic, such as, free surface, vertically integrated velocity, full three dimensional velocity fields, temperature and salinity fields. There are several options for OBC which can be combined to each other for 2D and 3D test-cases, Mori (2007) has tested the most significant OBC from the ROMS model focused on tidal inputs. For all the OBC options see Hedström (2009).

There are several combinations of open boundary condition (OBC) in the ROMS. The user can choice different OBC for free surface, vertically integrated velocity and full three dimensional velocity field. In this research study the following boundary conditions were applied in ROMS: FSCHAPMAN – free surface; M2FLATHER – vertically integrated velocity; TRADIATION – transport fields (e.g. S, T, sediments); M3GRADIENT – 3D velocity fields. Here is summarized and examined OBC in ROMS.

3.4.2.1 Gradient boundary condition

The Gradient boundary condition consists of setting the gradient of a field to zero at the edge. The outside value is set equal to the closest interior value. This boundary condition is probably too simple for realistic problems.

$$\frac{\partial \eta}{\partial x} = 0 \tag{3.21}$$

3.4.2.2 Radiation boundary condition

Orlanski (1976) proposed a radiation scheme in which a local phase velocity is computed and used to radiate things out (if it is indeed going out). This works well for a wave propagating normal to the boundary, but has problems when waves approach the boundary at an angle. Raymond and Kuo (1984) have modified the scheme to account for propagation in all three directions. In ROMS, only the two horizontal directions are accounted for:

$$\frac{\partial C}{\partial t} = -\left(C_x \frac{\partial C}{\partial \xi} + C_y \frac{\partial C}{\partial \eta} \right) \tag{3.22}$$

where:

$$C_x = \frac{F \frac{\partial C}{\partial \xi}}{\left(\frac{\partial C}{\partial \xi} \right)^2 + \left(\frac{\partial C}{\partial \eta} \right)^2} \tag{3.23}$$

$$C_y = \frac{F \frac{\partial C}{\partial \eta}}{\left(\frac{\partial C}{\partial \xi} \right)^2 + \left(\frac{\partial C}{\partial \eta} \right)^2} \tag{3.24}$$

$$F = -\frac{\partial C}{\partial t} \tag{3.25}$$

These terms are evaluated at the closest interior point in a manner consistent with the time stepping scheme used. The phase velocities are limited so that the local CFL condition is satisfied. The radiation approach is appropriate for waves leaving the domain. A check is made to see which way the phase velocity is headed. If it is entering the domain, a zero gradient condition is applied.

3.4.2.3 Chapman boundary condition

The free surface Chapman boundary condition is a combination of the Orlanski Radiation BC and a sponge with an absorbing boundary (Chapman, 1985). This OBC considers wave propagation and gives stability for the gravity wave condition.

$$\frac{\partial \eta}{\partial t} + \sqrt{g(\eta + h_0)}\frac{\partial \eta}{\partial x} = 0 \tag{3.26}$$

3.4.2.4 Clamped boundary condition

The free surface displacement is set to an externally prescribed value

$$\eta_{b\pm1} = \eta^{ext} \tag{3.27}$$

where $\eta_{b\pm1}$ indicates that elevation must be clamped one cell in from the boundary (Mellor, 2004). This continues to be apopular boundary condition for tidal simulations, due in part to the smooth spatial variation of elevation data, and readily available satellite-altimetry-derived data.

3.4.2.5 Flather boundary condition

This extension of a radiation boundary condition was originally proposed by Flather (1976). Radiation conditions are a popular class of passive OBCs, which are based on the propagation of a quantity η through a boundary. Flather condition is a combination of continuity conditions appropriated for barotropic conditions.

$$\frac{\partial \eta}{\partial t} + (gh)^{1/2} \frac{\partial \eta}{\partial x} = 0 \qquad (3.28)$$

$$\frac{\partial \eta}{\partial t} + (hu)^{1/2} \frac{\partial u}{\partial x} = 0 \qquad (3.29)$$

The Flather condition can be thought of as applying an adjustment to the externally prescribed normal velocity based on the difference between modelled and externally prescribed surface elevations, i.e. a volume error (Carter and Merrifield, 2007).

3.4.3 Bottom boundary layer

The bottom boundary layer (BBL) is important for sediment transport formulations because bottom stress determines the transport rate for bedload and the re-suspension rate for suspended sediment. BBL determines the stress exerted on the flow by the bottom, which is used in the Reynolds-averaged Navier-Stokes equations as boundary conditions for momentum in the x and y directions

$$K_M \frac{\partial u}{\partial s} = \tau_{bx}, \quad K_M \frac{\partial v}{\partial s} = \tau_{by} \qquad (3.30)$$

ROMS implements two methods for representing BBL processes: (a) simple drag-coefficient expressions, and (b) complex formulations to represent wave-current interactions over a moveable bed. The drag-coefficient methods implement formulae for linear bottom friction, quadratic bottom friction, or a logarithmic profile. The other,

more complex methods, implement some of the many wave–current BBL models (e.g., Jonsson and Carlsen, 1976; Smith, 1977; Grant and Madsen, 1979; Madsen, 1994; Styles and Glenn, 2000) and couple them with calculations of bottom roughness. ROMS offers three methods that implement slightly different combinations of algorithms for the wave–current interactions and moveable bed roughness. The first method (sg_bbl) is based on wave current algorithm and the ripple geometry and movable bed roughness of Styles and Glenn (2002); the second method (mb_bbl) uses efficient wave-current BBL computations developed by Soulsby (1995) in combination with sediment and bedform roughness estimates; the third method (ssw_bbl) implements either the wave-current BBL model of Madsen (1994) or Styles and Glenn (2000), the differences in approach among these routines are small, but they can produce significantly different results. In the present research, the ssw_bbl method is implemented along with moveable bed routines.

The BBL parameterisation implemented in ROMS requires inputs of velocities u and v at reference elevation z_r, representative wave-orbital velocity amplitude u_b, wave period T, and wave-propagation direction θ (degrees, in nautical convention). The wave parameters may be the output of a wave model such as SWAN or simpler calculations based on specified surface wave parameters and should represent the full spectrum of motion near the bed. Moreover the BBL models require bottom sediment characteristics (median grain diameter D_{50}, mean sediment density ρ_s, and representative settling velocity w_s); these are based on the composition of the uppermost active layer of the bed sediment during the previous time step.

Ripple height n_r and wavelength λ_r are calculated using information from the previous time step and the Malarkey and Davies (2003) implementation of the Wiberg and Harris

(1994) formulation, which is valid for wave dominated conditions. They approximate ripple wavelength as $535D_{50}$ and ripple steepness as:

$$\frac{n_r}{\lambda_r} = exp\left[-0.095\left(ln\left(\frac{d_0}{n_r}\right)\right)^2 + 0.442\left(ln\left(\frac{d_0}{n_r}\right)\right) - 2.28\right] \tag{3.31}$$

where $d_0 = u_b T/\pi$ is the wave orbital diameter.

Roughness lengths associated with grain roughness z_{0N}, sediment transport z_{0ST}, and bedform roughness length (ripples) z_{0BF} are estimated as:

$$z_{ON} = 2.5D_{50}/30\,, \quad z_{OST} = \alpha D_{50}a_1\frac{T_*}{1+a_2 T_*}\,, \quad z_{OBF} = a_r\eta_r^2/\lambda_r \tag{3.32}$$

where the sediment-transport coefficients are $\alpha = 0.056$, $a_1 = 0.068$, and $a_2 = 0.0204\,ln(100D_{50}^2) + 0.0719\,ln(100D_{50})$ with the bedform roughness D_{50} expressed in meters, $a_r = 0.267$ is a coefficient suggested by Nielsen (1992). The roughness lengths are additive, so subsequent BBL calculations use $z_0 = max[z_{0N} + z_{0ST} + z_{0BF}, z_{0MIN}]$, where $z_{0MIN} = 5e^{-5}\,m$. and allows setting a lower limit on bottom drag.

The pure currents and pure wave limits are used as initial estimates for calculations towards consistent profiles for eddy viscosity and velocity between z0 and zr, using either the model of Madsen (1994) or Styles and Glenn (2000). Both of these models assume eddy viscosity profiles scaled by $u_{*wc} = \sqrt{\tau_{wc}}$ in the wave-boundary layer (WBL) and $u_{*c} = \sqrt{\tau_b}$ in the current boundary layer, calculated as:

$$K_M = \begin{cases} ku_{*wc}z, & z < \delta_{wbl} \\ ku_{*c}z, & z > \delta_{wbl} \end{cases} \tag{3.33}$$

where δ_{wbl} is the thickness of the WBL, which scales as $u_{*wc}T/(2\pi)$. τ_{wc} represents the maximum vector sum of wave- and current-induced stress, but the τ_b is influenced by the elevated eddy viscosity in the WBL, and must be determined through an iterative process. The parameter τ_b is the mean bed shear stress over many wave periods and is used as the bottom-boundary condition in the momentum equations, and τ_{wc} is the maximum instantaneous stress exerted over the bottom by representative waves and currents. These stresses directly influence flow near the bottom and act as agents for sediment re-suspension and bedload transport.

3.5 Sediment transport model

The sediment transport model, which is embedded in ROMS, has been incorporated in the modelling system for computing sediment transport for beach morphological changes. The Soulsby and Damgaard (2005) formulae is applied for computing bedload transport which accounts for the combined effects of mean currents and asymmetrical waves on bedload flux. The bed model accounts for changes in sea floor elevation resulting from convergence or divergence in sediment fluxes. These morphological changes can have an impact on flow transport when they are larger (Warner et al, 2008).

The sediment transport model represents an unlimited number of user-defined sediment classes. Each class has fixed attributes of grain diameter, density, settling velocity, critical shear stress for erosion and erodability constant. Two main classes of sediments are included: non-cohesive and cohesive.

3.5.1 Mobile bed

The mobile bed is represented by three-dimensional arrays, constant number of layers, each with initial thickness, sediment-class distribution, porosity, and age. The mass of each sediment class in each cell can be determined from these values and the grain density. The attributes of the sediment classes and descriptions of the subgrid-scale morphology (ripple height and wavelength) are used to estimate bed roughness in the bottom stress calculations. Bottom stresses are used to determine re-suspension and transport, providing feedback from the sediment dynamics to the hydrodynamics (Warner et al, 2008).

Bed layers are modified each time-step to account for erosion, deposition and track stratigraphy. Every time step an active-layer z_a thickness is calculated based on the relation of Harris and Wiberg (1997):

$$z_a = max\left[k_1\left(\tau_{sf} - \overline{\tau_{ce}}\right)\rho_0, 0\right] + k_2 D_{50} \tag{3.34}$$

where τ_{sf} is bottom skin-friction stress due to combined maximum wave-current interaction; τ_{ce} is the critical stress for erosion, the overbar indicates that is averaged over all sediment classes; D_{50} is the median grain diameter of surface sediment; and k_1, k_2 are empirical constants with values of 0.0007 and 6.0 respectively.

Suspended-sediment that is deposited, or bedload that is transported into a computational cell, is added to the top bed layer. If continuous deposition results in a top layer thicker than a user-defined threshold, a new layer is provided to begin accumulation of depositing mass. The bottom two layers are then combined to conserve the number of layers. After calculating erosion and deposition, the active-layer thickness is recalculated and bed layers readjusted to accommodate it.

3.5.2 Suspended sediment transport

Sediment suspended in the water column is transported by solving the advection-diffusion equation (3.7), as well as the temperature and salinity. For a suspended-sediment an additional source/sink term is added for vertical settling and exchange with the bed as:

$$C_{source,m} = -\frac{\partial w_{s,m} C_m}{\partial s} + E_{s,m} \tag{3.35}$$

Where $w_{s,m}$ is the vertical-settling velocity (positive upwards), $E_{s,m}$ is the erosion source, and m equals one through the number of classes. The model solves each term of Equation (3.7) independently, in the sequence: vertical settling, source/sink, horizontal advection, vertical advection, vertical diffusion, and horizontal diffusion.

The vertical advection algorithm includes a parabolic method proposed by Colella and Woodward (1984), and a weighted essential non-oscillatory scheme proposed by Liu et al (1994). This method integrates depositional flux over multiple grid cells, so is not constrained by the CFL criterion. Zero-flux boundary conditions are imposed at the surface and bottom in the vertical diffusion equation. The source or sink term in the advection equation represents the net of downward settling and upward flux of eroded material and is only applied to the bottom computational cell.

3.5.3 Sediment density effects

The model can simulate processes where sediment density influences hydrodynamics, such as density stratification and gravitationally driven flows. Suspended sediment effects on the density field are included with terms for weight of each sediment class in the equation of state for sea water density as:

$$\rho = \rho_{water} + \sum_{m=1}^{Nsed} \frac{C_m}{\rho_{s,m}} (\rho_{s,m} - \rho_{water}) \tag{3.36}$$

3.5.4 Bedload transport

ROMS implements two methods for computational bedload transport, which depends on the characteristics of individual sediment classes, including size D, density, specific density in water, and critical shear stress. Method 1: the Meyer-Peter Mueller (1948) formulation for unidirectional flow; and, Method 2: Soulsby and Daamgard (2005) formulae that accounts for combined effects of currents and waves, the Soulsby and Damgaard's formulations have been used as the sediment transport calculations in this research.

Non-dimensional transport rate function Φ is calculated for each sediment class and converted to dimensional bed-load transport rates q_{bl} applying horizontal vector quantities with directions that correspond to the combined bed-stress vectors.

$$q_{bl} = \Phi \sqrt{(s-1)gD_{50}^3 \rho_s} \qquad (3.37)$$

To determine the sediment transport rate function Φ, the Soulsby and Damgaard's formulations are commonly used.

3.5.4.1 Soulsby and Damgaard's bedload transport

The Soulsby and Damgaard's formulations are based on numerical integration, over a wave cycle of non-dimensional transport equation:

$$\vec{\Phi} = max\left[A_2 \theta^{0.5}(\theta_{sf} - \theta_c)\frac{\overrightarrow{\theta_{sf}}}{\theta_c}, 0\right] \qquad (3.38)$$

where $\vec{\Phi}$ and $\overrightarrow{\theta_{sf}}$ are vectors with components in the direction of the mean current and in the direction perpendicular to the current: $\vec{\Phi} = (\Phi_\parallel, \Phi_\perp), \overrightarrow{\theta_{sf}} = (\theta_{sf\parallel}, \theta_{sf\perp})$.

θ_{sf} is the non-dimensional Shields parameter for skin stress, $A_2 = 12$ is a semi-empirical coefficient.

$$\theta_{sf} = \frac{\tau_{sf}}{(s-1)gD_{50}} \qquad (3.39)$$

$\theta_c = 0.047$ is the critical Shields parameter, τ_{sf} is the magnitude of total skin-friction component of bottom stress

$$\tau_{sf} = \left(\tau_{bx}^2 + \tau_{by}^2\right)^{0.5} \qquad (3.40)$$

τ_{bx} and τ_{by} are the skin-friction components of bed stress, from currents alone or the maximum wave-current combined stress, in the x and y directions.

The implementation of the Soulsby and Daamgard (2005) formulae requires computation of transport rates in the directions parallel and perpendicular to the currents as $\vec{\Phi} = (\Phi_{\parallel}, \Phi_{\perp})$:

$$\Phi_{\parallel} = max[\Phi_{\parallel 1}, \Phi_{\parallel 2}] \tag{3.41}$$

$$\Phi_{\perp} = A_2 \frac{0.1907\theta_w^2}{\theta_w^{3/2} + 1.5\theta_m^{0.5}}(\theta_m \sin 2\phi + 1.2\gamma_w\theta_w \sin\phi) \tag{3.42}$$

where:

$$\Phi_{\parallel 1} = A_2\theta_m^{0.5}(\theta_m - \theta_c) \tag{3.43}$$

$$\Phi_{\parallel 2} = A_2(0.9534 + 0.1907 \cos 2\phi)\theta_w^{0.5}\theta_m \tag{3.44}$$
$$+ A_2(0.229\gamma_w\theta_w^{0.5}\cos\phi)$$

$\theta_m = \frac{\tau_m}{(s-1)dD_{50}}$ is the mean Shield parameter, $\tau_m = \tau_c\left(1 + 1.2\left(\frac{\tau_w}{\tau_w+\tau_c}\right)^{1.5}\right)$

τ_c is the bottom stress from currents only, τ_w is the bottom stress from waves only calculated in the bottom-boundary layer routines, the asymmetry factor γ_w is the ratio between the amplitude of the second harmonic and the amplitude of the first harmonic oscillatory wave stress. The asymmetry factor is estimated using the theory of Stokes second-order making it less than 0.2. the non-dimensional fluxes (Equations 3.41 and 3.42) are partitioned into x and y components using the directions for mean current and

waves, then they are dimensionalised with Equation (3.37) to yield values for q_{blx} and q_{bly} for each sediment class.

3.5.5 Bed slope effect

Computed bedload rates are modified to account for local bed slope following Lesser et al. (2004) with a bed slope term:

$$q_{bl\_slope} = \frac{\tan \varphi_m}{(\tan \varphi_m - \tan \beta) \cos \beta} \tag{3.45}$$

Where the local bed slope $\beta = \tan^{-1}(dz/dx_\alpha)$ is evaluated for each direction of transport with a positive value of dz/dx_α in the downslope direction, and where $\varphi_m = 33°$ is the friction angle of the sediment. The bedload magnitudes are multiplied by q_{bl_slope} .

3.5.6 Morphology

As detailed in Warner et al (2008), morphological changes on the bed model account by equating the bottom boundary condition of the vertical velocity to the rate of change of elevation of the sea floor. Bedload fluxes, erosion and deposition rates are multiplied by a scale factor. The morphological scale factor method works well for systems with unlimited sediment in the bed. When the amount of sediment to be eroded is limited by the amount available and application of the morphological scale factor cannot remove the scaled amount of sediment from the bed, the scale factor method can generate extra sediment in systems with unlimited supplies of bed sediment. Subsequent deposition does place a scaled amount of sediment on the bed thus creating new mass in the bed.

3.6 Model setup

The wave model SWAN has been nested from coarse to fine grid resolutions. The largest area (L1), shown in Figure 3.3, covers part of the North Atlantic ocean, the second grid domain (L2) covers the Southwest of England, and the finest grid covers the region where the Wave Hub is located as well as its adjacent coast. The modelling system (SWAN+ROMS) has been coupled at the finer grid domain L3 (Figure 3.3), it's worth a mention that this first test validation has a coarse resolution, thus predictions of overestimated waves and current velocities are expected. The wave model is driven by a global wave model, which in turn is driven by the wind fields provided by a global atmospheric model. Also, a global tide model drives the circulation model that is coupled with the wave model.
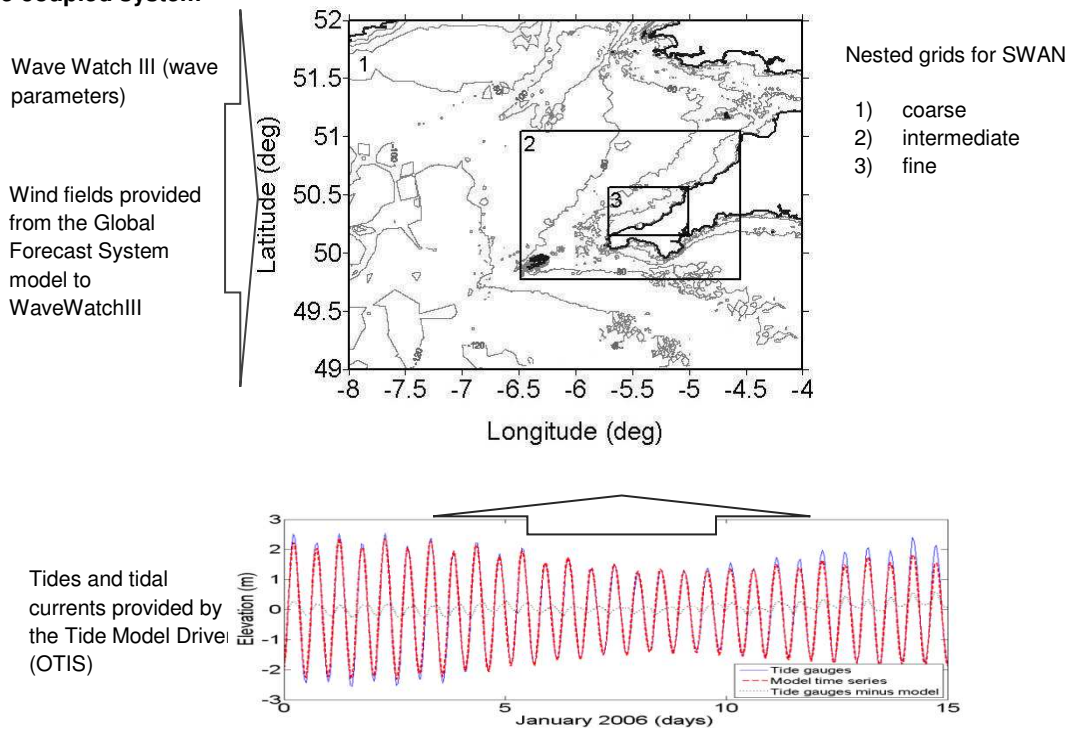
Figure 3.3 Model boundary conditions and nested grid domains.

3.6.1 The SWAN model

The wave model is run and coupled in the L3 grid (see Figure 3.3) with a 52 x 40 grid domain, cells are about 500 meters in both x and y directions; wave boundary conditions are imposed at the northern and western boundaries, they come from the upper nested levels as spectral wave conditions; wind fields are imposed at every 3 hours for the entire domain; the wave model runs in third-generation mode with wind-input, quadruplet interactions and whitecapping. The bottom friction is given by the Madsen et al. (1988) approximation, and it varies over the computational region, which is computed within ROMS model; the triad wave-wave interaction is also activated; the numerical propagations uses the BSBT method.

The computational spectral grid is defined for swell winds with a spectral directional resolution of 10 degrees, the grid resolution interval in frequency-space is 36, even, the directional spread of the waves (directional spreading coefficient), that drives the incoming wave directions, is set as 17.1 for a reasonably surfing swell, discrete frequencies varies between the minimum 0.05 and the maximum 0.95 frequencies.

As shown in Figure 3.3, the wave model exports fields of wave heights, wave period, wave directions, wave particle velocities at the top and bottom, and forces as radiation stresses for the wave contribution in the circulation model. Fields of water elevation, water depth and velocity currents, as well as, bottom friction come from the two-way coupled circulation model ROMS.

The SWAN model is a spectral wave model based on linear wave theory. When apply such a model to wave energy devices, the details of wave-structure interaction are not possibly resolved by the model. The consequence of that would be errors in wave heights, directions in adjacent to the structure. So broadly speaking, the SWAN is good

at far-field modelling, i.e. km away from the devices, not reliable close to the devices (M. Li – personal communication).

3.6.2 The ROMS model

The ROMS model has been run in baroclinic mode with 5 terrain-following (sigma) layers in the vertical; the numerical grid has 52 grid cells in the longitude direction, which extends from -7.77W to -4.0W. Along the latitude direction the grid has 40 grid cells and the domain extends from 50.16N to 50.58N. The coordinates for both, the wave and flow models are in curvilinear coordinates. Salinity and temperature remain constant, S_o= 30 psu and T_o = 10 Celsius.

Boundary conditions for tidal forcing were derived from the OTIS model (Egbert and Erofeeva, 2002; Padman and Erofeeva, 2004), tidal elevations and tidal currents were interpolated to the boundaries of the computational grid in ROMS.

In section 3.4.2 the available boundary conditions within the flow model ROMS were defined. For barotropic currents, the Flather boundary condition (Flather, 1976) is set, which allows the free propagation of the barotropic currents through the four boundaries. For the free surface, the Chapman boundary condition (Chapman, 1985) is applied because it allows and includes wave propagation and also gives stability for the gravity wave conditions. In general, most of the physical default parameters were held constant (e.g. harmonic/biharmonic horizontal and vertical mixing, surface turbulent kinetic energy flux, momentum stress, density and linear equation of state parameters).

To perform the wave-current interaction, data exchange between the wave and flow models is necessary. The first requirement to exchange data is to agree on the units of the parameters (e.g. m/s^2 or N/m^2) and the exact definition (e.g. H_{m0} or H_{rms}). Then, a

central grid to interpolate between grids is adopted. Generally, the flow model grid is chosen as the central grid, which is the same for transports and morphological changes.

In ROMS the baroclinic time step is set as 30 s and a barotropic time step of 20 s. In SWAN, for this coarse grid, the time step is 1200 s. An exchange rate of data between ROMS and SWAN is every 1200 s. The test case simulation is from 1st of December 2005 to 31st of January 2006. For the boundary conditions of the wave and flow models, the data was extracted from the global models: OTIS, WAVEWATCH III and Global Forecast System.

The SWAN prediction is fed into ROMS to produce the wave-induced properties such as current speed, bottom shear stresses and sediment transport, in the presence of WECs. Thus, in ROMS there is no explicit representation of WECs. The ROMS model is based on shallow water equation system, the pressure distribution across the water depth is assumed to be linear. So again close to the devices, the model would not be able to resolve the details of the flow changes. But far from the structure, where the flow is dominated by the wave-tides again, the model would be reasonable (M. Li – personal communication).

In appendix A the forcing sources, tidal and wave forcing, to initialise the modelling system are described. Also, the characteristics of the high performance computer used in this research are discussed.

3.6.3 Wave farms impact on wave climate

Venugopal and Smith (2007), studied the effect of hypothetical wave devices on wave climate. They present wave disturbance coefficients related to wave heights, to show the variations in wave absorption by the devices affecting the wave energy transmission and reflection around the devices. This is an important contribution because the work shows

a reduction of the wave height between 13-69% by the devices. Palha et al (2010), tested several configurations of wave farms studying the impact of wave energy devices (Pelamis) on the wave climate along the nearshore coast. They conclude that the extracted wave energy from the wave farms ranges between 9.3-23%, also they observed an affected length of coast up to 26 km by the wave farms. Beels et al (2010), tested overtopping wave energy devices studying the reflection and energy transmission of the wave climate, they developed a methodology to estimate the wave absorption by overtopping devices and the impact on the surrounding areas. Reeve et al (2011), make significant contributions to the Wave Hub project, studying the available wave power for future climate scenarios. They show an increase and decrease of the wave power, depending on the climate conditions based on the IPCC reports, suggesting that wave heights will have wider spread due to impacts of climate change, traducing it in longer periods of generation loss and potential benefits for wave farm developers.

3.6.4 Wave energy transmission

Addressing the above knowledge about wave energy transmission through wave farms, in this study the wave farm was represented in the wave model SWAN as an array of wave energy converters (WECs) at the Wave Hub site. The array is a 4km partially transmitting obstacle, aligning approximately parallel to the incoming wave crests. The energy transmission has been fixed as the average from several wave energy converters previously examined by Millar et al (2007) and Babarit and Hals (2011).

Millar et al (2007), tested in the wave model SWAN different energy transmission coefficients by an obstacle set at 0%, 40%, 70% and 90%. These energy transmission percentages were set for specific reasons: 0%—Represents complete absorption of all incoming wave energy at the obstacle—an unachievable scenario. 70%—Represents an

array of densely spaced, high efficiency WECs. This would be an optimistic target for a wave farm developer to achieve. 90%—Represents lower efficiency, widely spaced WECs, a more realistic scenario at the Wave Hub site. 40%—Included in the study to enable the establishment of trends, although it is extremely improbable that this could be attained in reality. They concluded that an energy transmission coefficient of 90% produces an average change in significant wave height at the shoreline.

Babarit and Hals (2011) have provided an extensive list of the capture width ratio η_1, which is used for assessing the wave energy absorption from WECs. The width ratio is defined as the ratio between the absorbed power P_{abs} (W) and the available wave power resource P_{wave} (W/m) per meter of wave front times a relevant dimension B (m).

$$\eta_1 = \frac{P_{abs}}{P_{wave}B} \tag{3.46}$$

The list of WECs clusters four main categories: Oscillating water column devices, Overtopping devices, Wave activated bodies, and others. The purpose of the Wave Hub project is to have the less impact of WECs on the near-shore due to recreation and environment policies. Hence, oscillating water column and wave activated devices are taking into account for this research. Between these two categories an average of wave energy absorption of 25% was identified.

Therefore, the energy transmission percentage in this study is set as 75% which represents a densely-spaced array of high-efficiency WECs.

3.7 Summary

In this chapter the modelling system has been described in full as a tool to assess the wave farm impacts on the hydrodynamics and morphology, from the selection of the wave and flow circulation models, to the setup of the whole system. The wave SWAN model has been defined as a 3rd generation spectral wave model for regional and coastal areas. As described by ASR (2007), these models represent the spatial waves as real life conditions where the patterns of waves in the sea is made up of large and small waves moving in many directions. The basic architecture of SWAN is based on the action balance equation, which defines the propagation terms in both geographical and spectral space (refraction is considered as propagation in spectral space), and the source terms which model the generation and dissipation of wave energy.

The circulation ROMS model has been analysed in a similar way. Based on the Reynolds-averaged Navier-Stokes equations, where the motion terms like the change rate, horizontal advection and vertical advection, and the Coriolis parameter, are described. On the other hand, the mixing terms like baroclinic gradient, surface pressure gradient, vertical viscosity, horizontal radiation and vertical radiation are described. Additional equations are also described in the ROMS model like the hydrostatic buoyancy force, the continuity equation and scalar transports. Moreover, initial and boundary conditions have been described. In addition, the sediment transport model embedded in ROMS has been described to estimate the change in the sea-bed (bathymetry) through bedload transport rates, suspended transport rates and sediment concentrations.

And finally, the setup of the modelling system has been addressed. Properties of grid domains, physical parameters, coefficients for specific variables, for each model were

sketched. Also, the presence of the wave farm in the wave model has been described as an obstacle transmission in arrays of WECs at the Wave Hub site. Even, the source models that feed the coupled modelling system are shown. The tide model provides water elevations and tidal currents to the ROMS model in the boundaries. The global wave model provides spectral wave boundary conditions to the SWAN model, also the Global Forecast System model provides wind forcing, the main driver for the SWAN model.

The way the model has been setup is to have the farm represented in SWAN, but not in ROMS, which means inevitably the error in the current field will affect the sediment transport, i.e. the additional mixing and perturbation from the devices are not simulated for sediment suspension and transport in the water in comparison with the none-structure situation. It is therefore expected that the sediment suspension is underestimated close to the farm site (M. Li – personal communication).

4. Model Validation

4.1 Introduction

As mentioned before, this research project applies the spectral wave model SWAN (Booij et al, 1999) and the flow circulation model ROMS to form a fully two-way coupled modelling system (Warner et al, 2008). As shown in Figure 4.1, the SWAN model is run with three nested domains with progressively finer grid resolutions. At the finest grid (L3), the SWAN is coupled with the ROMS model to form the coupled modelling system (SWAN+ROMS). The SWAN model input is provided by the output of the global wave spectral model WAVEWATCH III, in turn driven by the wind fields from the Global Forecast System (GFS) model. The global tidal model OTPS (Egbert et al, 2002; Padman and Erofeeva, 2004) provides tidal currents and water elevations as boundary conditions for the ROMS model. The wave model results can be affected by both water elevations and tidal currents; hence, the tidal information obtained from the ROMS model is used in the wave model.
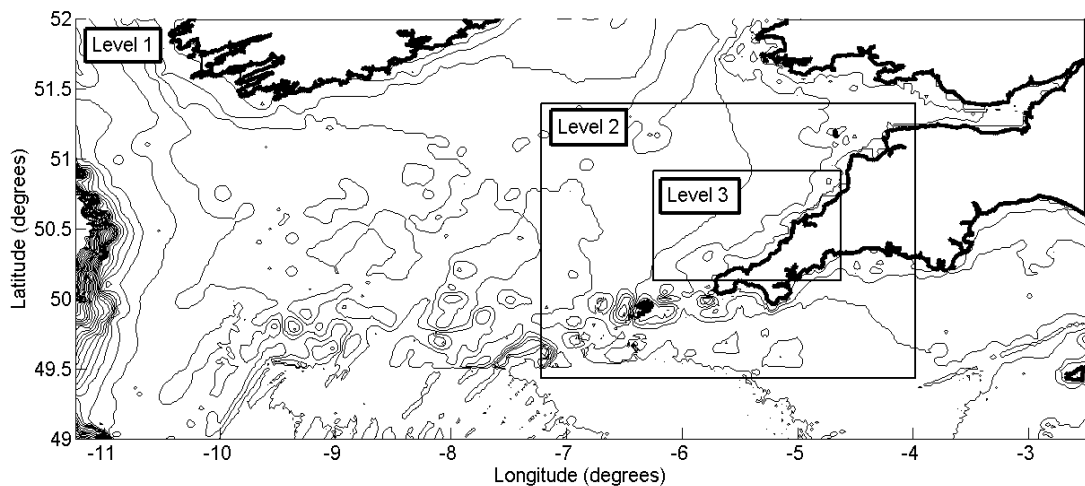
Figure 4.1 Nested computational domains for SWAN and ROMS.

In order to assess the impact of waves on tidal currents and tidal currents on waves, the coupled modelling system (SWAN+ROMS) was applied to a series of different cases combining spring and neap tides, high and low water levels, and high and low wave conditions. These cases were investigated to examine the changes in wave conditions, current velocities and bottom stresses in and around the Wave Hub site.

4.1.1 Modelling system setup

The SWAN model is forced at the boundaries by the output of the global wave spectral model WAVEWATCH III, the grid resolution is 1.25 degree horizontal x 1 degree vertical, the data output is every 3 hours for both wave parameters and wind fields. Bathymetry for the coarser grid is taken from GEBCO08 data; for intermediate and finer grids the Digimap2010 database was used. The SWAN model has been run with some default input parameters, the computational spectral grid was defined with a low frequency value of 0.05 and a high frequency value of 0.95, and the number of subdivisions of the spectral directional resolution is 36. The parameterisation of some physical variables have been described in Booij et al (1999) like the wind is assumed to cause exponential Komen growth of the waves and the characterisation of the wind wave spectra is set as spectral directional resolution for wind sea as 10. The western boundary has been forced as parametric spectra input, thus, the shape of the wave spectrum at the boundaries is assumed to satisfy the JONSWAP spectrum.

4.1.2 Tide model calibration

Data from four tide gauge stations were downloaded from POL-BODC, and analysed (Newlyn, St Marys, Milford, Ilfracombe, approx. 1989 − 2007) as time series. A least-square method was performed to obtain amplitude and phase for each station. In order to get the five main constituents (M_2, N_2, S_2, O_1, K_1), the Atlas of Tidal Elevations and Currents (Howarth, 1990) was consulted.
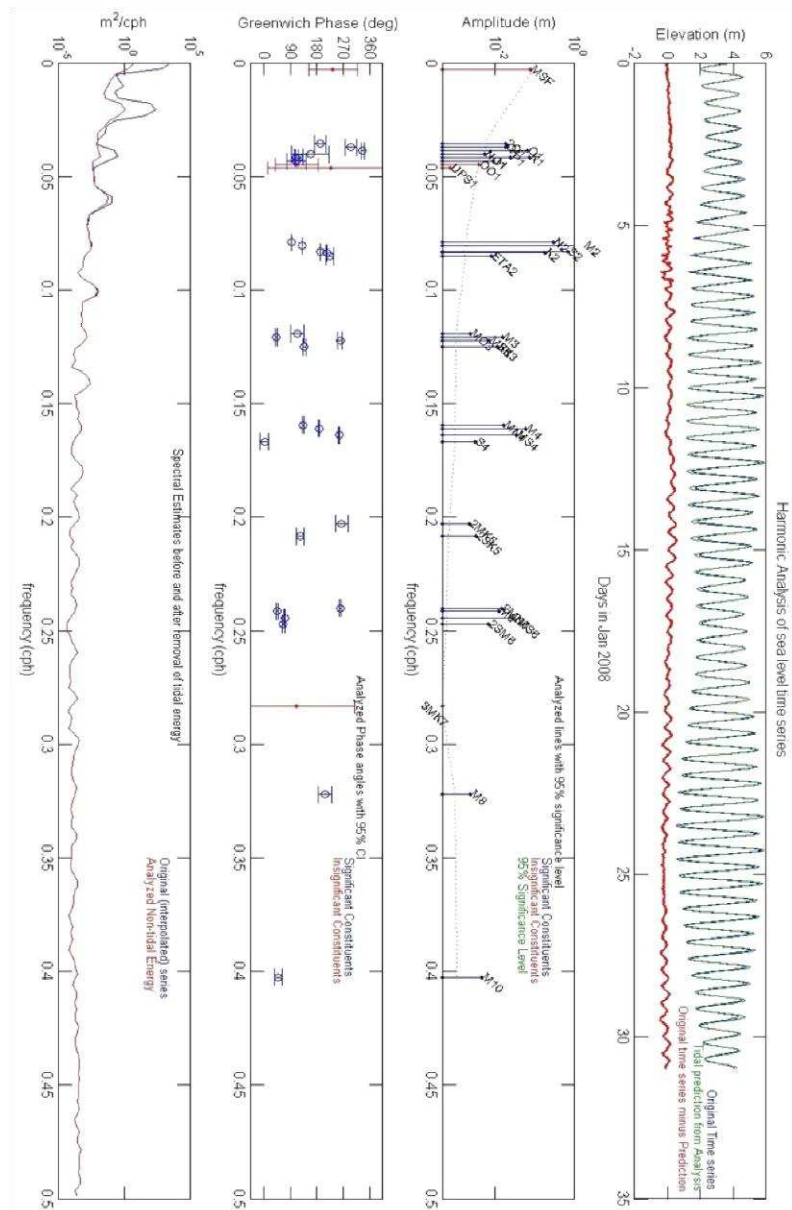
Figure 4.2 Analysis of predicted time series for the St. Marys station on January 2008, applying the Pawlowicz (2002) model. (1st top) Predicted time series with residual, (2nd) List of constituents used, frequency of tidal constituents (cycles/hr) this is the amplitude of all analysed components with 95% significance level. Note frequency dependence. (3rd) Phase of significant constituents (degrees relative to Greenwich) with 95% confidence interval. (4th bottom) Spectral estimates before and after removal of tidal energy.

Figure 4.2 shows an analysis for tides and their harmonic constituents. Predictions show great accuracy from both the tidal model and the modelling system. To analyse the predicted time series more in depth, the Pawlowicz's (2002) model was applied to analyse and compare the predicted and the original time series, Again, a high correlation between the predicted and the observed tidal elevations was found. The Figure 4.2 shows that the main constituent is the M_2 for a semi-diurnal tide, also the orientations and frequency for every constituent.

Then, the OTIS model was applied to get water elevations at specific sites, and thus compare results with the tide gauges. Figure 4.3 shows the comparison between the model and observations, three tide gauges (St. Marys, Newlyn and Ilfracombe) at different sites and along the Southwest of England, have been compared. The model shows very good accuracy in both phase and amplitude. Also, it can be observed a slightly reduction in amplitude around the second spring tide group, particularly for the St. Marys gauge which is an offshore station, this under-predicted result might be because a storminess period (high waves) is detected (see Figure 4.2), modifying the tide gauges.
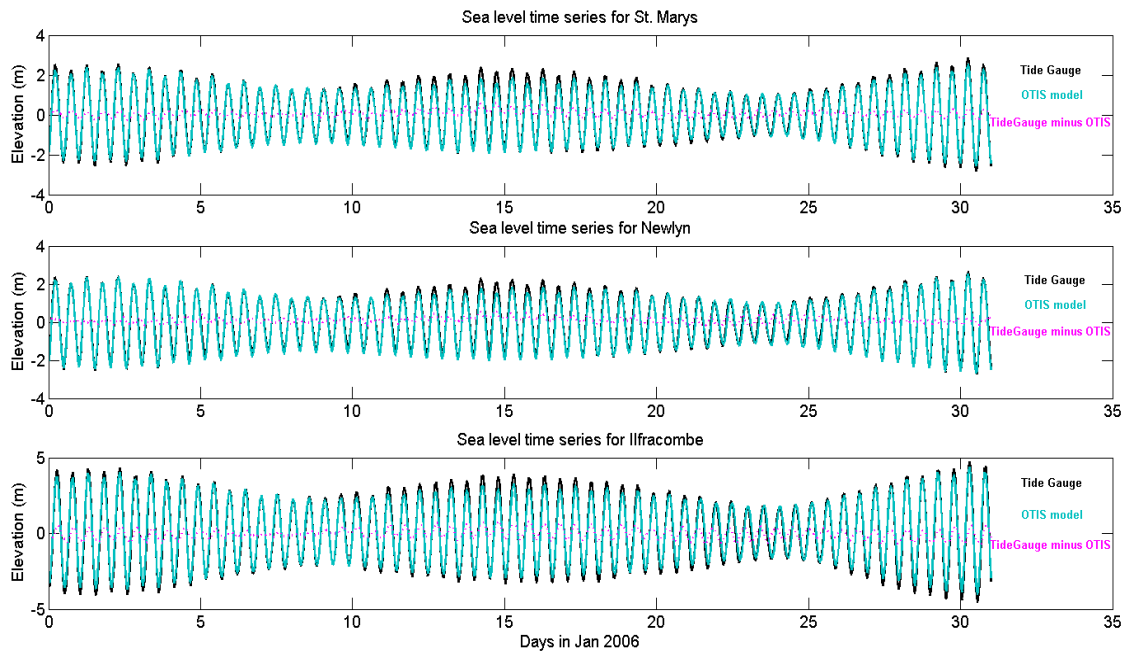
Figure 4.3 Comparison of computed tidal levels with measurements from tide gauges at St. Marys (top), Newlyn (middle) and Ilfracombe (bottom).

4.2 Parametric test cases

This section is to test the SWAN model parametrically, this means making assumptions on wave properties and hydrodynamics. In particular, to study the effect of waves on currents and currents on waves for calm and extreme wave conditions. The assumptions include forcing the domain in one boundary with constant wave properties (e.g. height, direction, period), including or not variation on water elevations and tidal currents. Also in the ROMS model, some assumptions of constant wave parameters are tested, showing the importance of coupling wave-current interactions.

4.2.1 Parametric tidal currents on waves

For boundary conditions the model was forced at the west boundary throughout the parametric spectral parameter, from the nested coarse grid, along each side of the boundaries the directional spectral distribution varies according the parametric data, the

wind fields were every 6 hrs, tidal currents were obtained from the OTIS model, as well as water elevations. Propagation, wave generation and dissipation processes are represented as: refraction and shoaling, reflection, and diffraction, bottom friction, ambient currents, and depth-induced breaking. Focused on the effects of currents and water elevations on waves, stationary and non-stationary (time varying) tests cases were performed. The tests were run with different case scenarios (Diagram 4.1). When the effect of the wind is not taken into account, wind-driven processes are not taken into account within the model, these wind-driven processes include quadruplet wave-wave interactions, and whitecapping.

Non-stationary model tests were first carried out with the SWAN model, setting conditions of variation of tidal levels, tidal currents and constant wind. It was observed that normal conditions have a quicker numerical stabilisation rather than the extreme conditions; also a non-steady state produced by currents and water elevations was observed. The first coarse non-stationary case has been forced at the western boundary with $H_s = 1.6$ m, $T_m = 5.4$ sec and dir $= 200°$, for normal conditions, and for extreme conditions $H_s = 4$ m, $T_m = 14$ sec, dir$= 210°$, taken from SWRDA (2006). However, Millar et al (2006) proposed an offshore reference wave state of $H_s = 3.3$ m, $T_m = 11$ sec, dir$= 1°$, where H_s is the significant wave height, T_m is the mean wave period, and dir is the wave direction.

Figure 4.4 shows the effect of tidal currents on spatial wave heights for the fine grid domain for spring tides at high tidal level (top) and low tidal level (bottom). With tidal currents, the computed significant wave heights at the Wave Hub are higher by approximately 20% larger than the wave heights computed without tidal currents at high water level. However, at the low tidal level, the magnitude of the increase is smaller, in a range of about 10% of increase in wave heights due to tides. This increase is related to

the water depth as water levels increase, high tide, the wave dissipation due to the

bottom friction is less rather than at low tide.
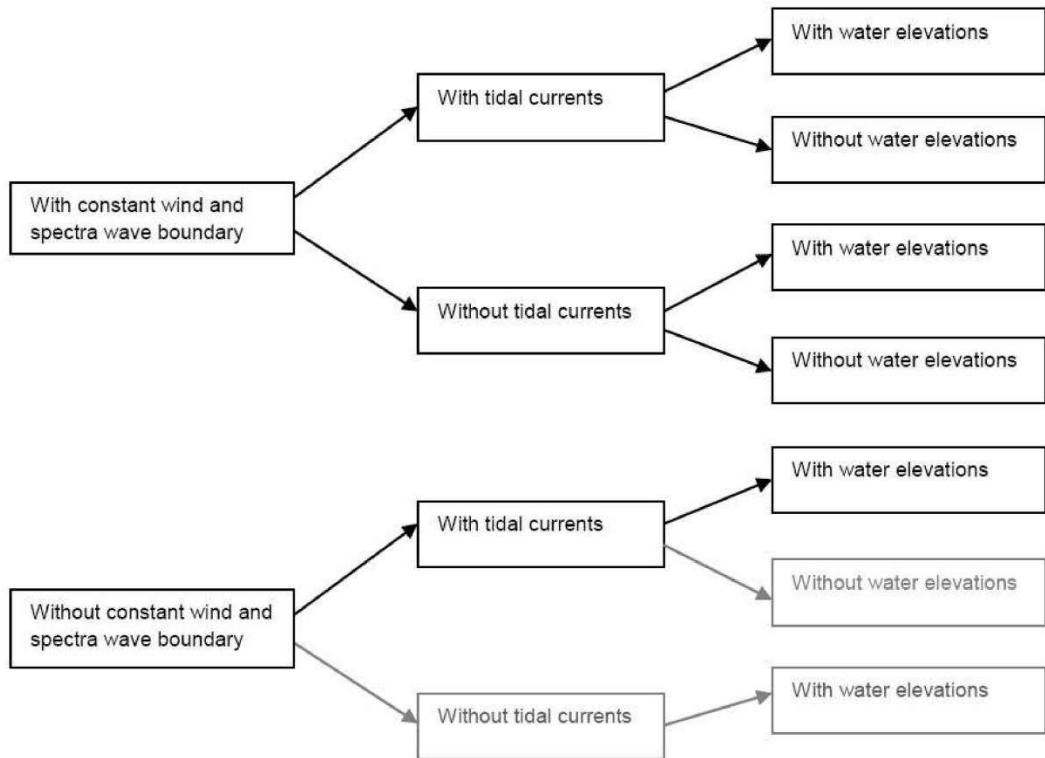
Diagram 4.1 Different case scenarios tested for both normal and extreme conditions.

4.2.2 Parametric waves on tidal currents

The next test-cases take into account analytical waves which were provided to the circulation model to interact with the tidal currents. Analytical conditions mean forcing the boundaries with constant wave parameters (e.g. Hs, Tp, dir). Three main cases of wave and current interactions have been tested: first, tidal currents only; second, tidal currents and constant waves and; third, currents and waves, evolving due to constant surface stress (wind induced stress).
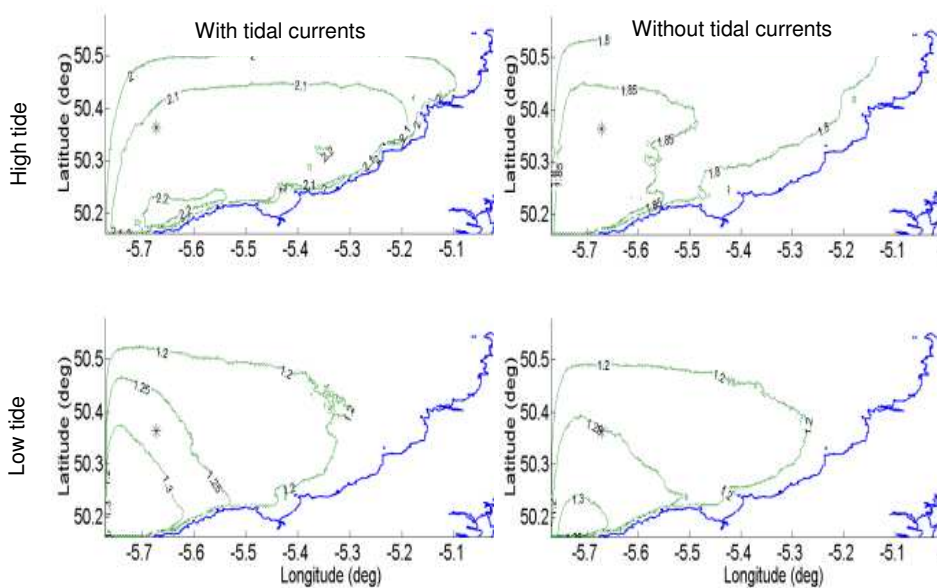
Figure 4.4 Snapshots of contours of the computed significant wave height (m) with (left) and without (right) currents within the fine nested grid at at high and low spring tides. (*) Wave Hub site.

For the sake of clarity, the computed current velocities have been decomposed into long-shore and cross-shore directions based on the main direction of the shoreline at the Wave Hub site, and neglecting the vertical structure of the horizontal velocities. These components are shown in Figure 4.5, the depth-averaged long-shore component at the top panel and the cross-shore component at the bottom panel. This test shows that long-shore results are larger rather than cross-shore results, showing the importance of wave-

induced currents by radiation stress gradients, long-shore currents (Longuet-Higgins and Stewart, 1962).
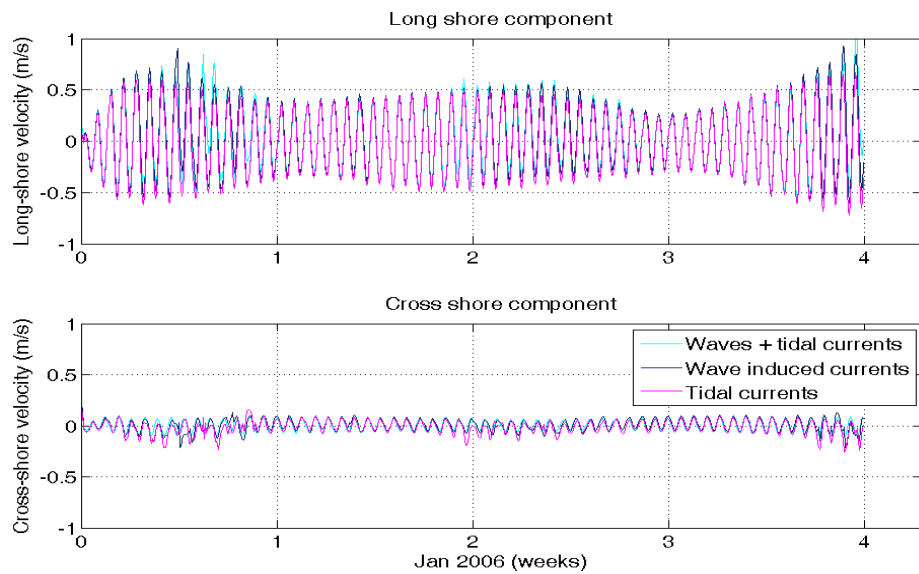
Figure 4.5 The long-shore and cross-shore components of the current velocities at the Wave Hub site. The legend at the bottom panel applies for the two panels.

As shown in Figure 4.5, the velocities computed for tide only and combined tide and wave without wave-current interaction are found to be almost identical. However, when the wave-current interaction is included, the computed velocities are clearly enhanced, particularly for the long shore component. By removing the underlying tidal velocity, the impact of wave-current interaction on the computed current velocities at the Wave Hub is clear, as illustrated in Figure 4.6 during spring tides. The anomalies of the currents shown in Figure 4.5 were calculated using a least square method (harmonic analysis), so that the regular tidal variation can be removed.

Figure 4.7 shows the kinematic bottom stresses at spring tides at the Wave Hub. In comparison to the velocities, the impact of the wave-induced current on the bottom shear stress is larger in the long-shore than in the cross-shore direction.
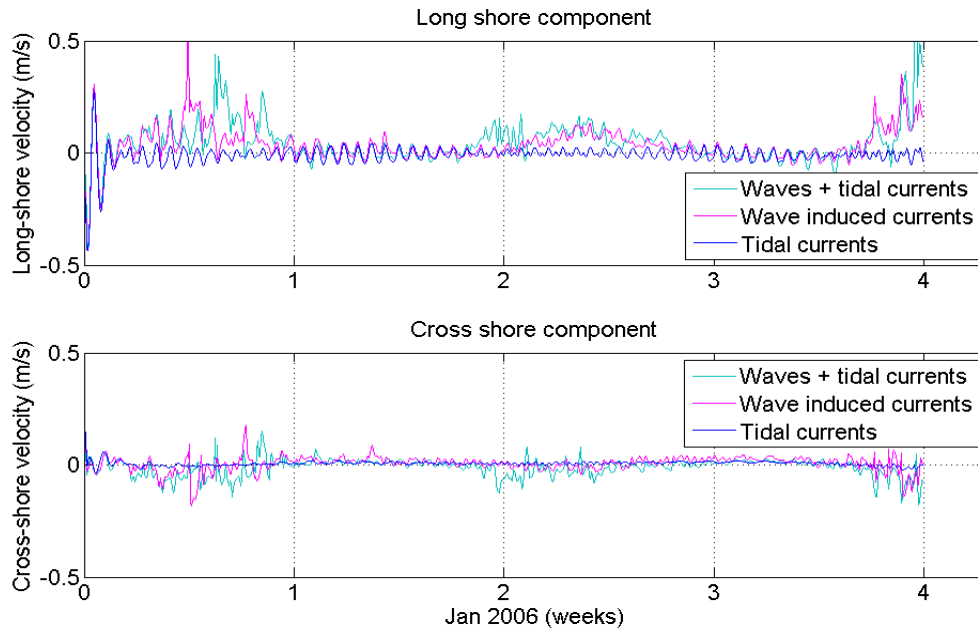
Figure 4.6 Anomalies of the current velocities for long-shore and cross-shore components, at the Wave Hub site.
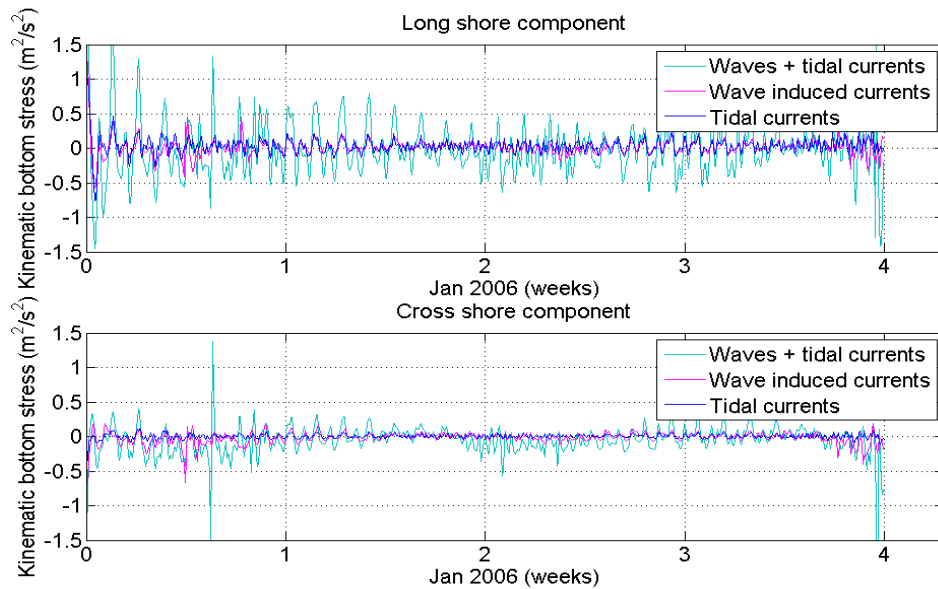
Figure 4.7 long-shore (top) and cross-shore (bottom) component of the bottom shear stress at the Wave Hub site.

4.2.3 Wave radiation stress influence

In order to study the wave-tide interactions the concept of radiation stress is included, which is the flux of momentum carried by the ocean waves. When these waves break, the wave momentum is transferred to the water column, inducing near-shore currents. Radiation stress theory has been successfully used to explain the presence of long-shore currents (Bowen, 1969). Significant momentum can be transferred from waves to currents when a strong radiation stress gradient occurs due to wave breaking and to the bottom friction in the near-shore region. Radiation stress gradients are determined from the spatial gradients in the directional energy spectrum of the wave model and the strongest gradients in radiation stress occur where depth-induced breaking happens (Mulligan et al, 2008a).

Figure 4.8 Computed currents with and without waves (✳ – the Wave Hub).

The waves influence on currents through the following physical mechanisms: i) surface shear stress, the effect of surface waves on the drag coefficient is included in ROMS (Warner et al, 2008); ii) bottom stress, waves enhance the turbulent mixing, therefore, waves modify the bottom stresses caused by currents (Grant & Madsen, 1979; Zou, 2004); and iii) radiation stress which represent the excessive momentum flux within the circulation due to the presence of waves (Longuet-Higgins and Stewart, 1964).

Figure 4.8 shows a snapshot of surface current speed with (left) and without (right) the radiation stress influence. Again, the long-shore component has more impact on the general circulation of the area of study. It is worth mentioning that for these cases the surface stress has been idealised as constant over the whole domain.

4.2.4 Wave effects on hydrodynamics

To assess the impact of waves on tidal currents a series of different cases combining spring and neap tides, high and low waters, high and low wave conditions, were tested to obtain bottom current velocities and bottom stresses. In Figure 4.9 the significant wave height at the Wave Hub is plotted, as predicted or measured, for a number of cases: with SWAN only (black line); with SWAN and ROMS (pink line); difference in predictions with the two models (blue line); water elevation measurements (green line); and wave buoy data (cyan line). The figure shows variations of wave heights when the tidal forcing is included. In general, the wave height is enhanced when coupling SWAN and ROMS, improving the wave-current prediction, however, the comparison against buoy observations is not crucial for this particular figure as these are parametric test cases which imply assumptions, constant values, in wave parameters and tide conditions.
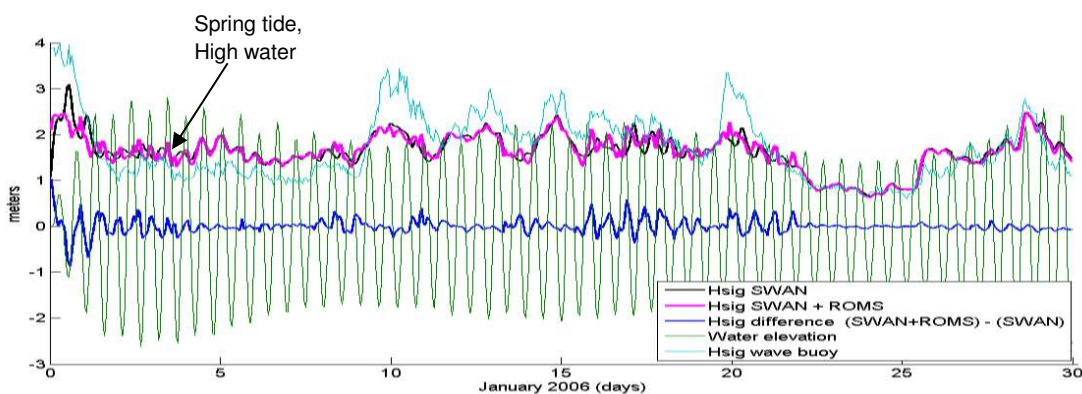
Figure 4.9 Significant wave heights with (pink) and without (black) tidal currents. The difference between the two, the water elevations (green) and the waves measured by the wave buoy at the site (cyan) are also shown.
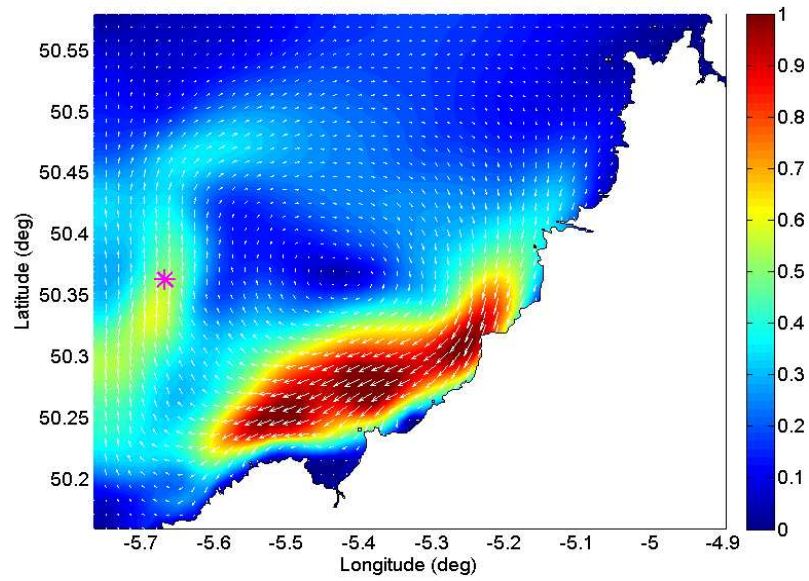
Figure 4.10 Differences of flow currents between ROMS+SWAN and ROMS only at the point indicated by an arrow in Figure 4.8.
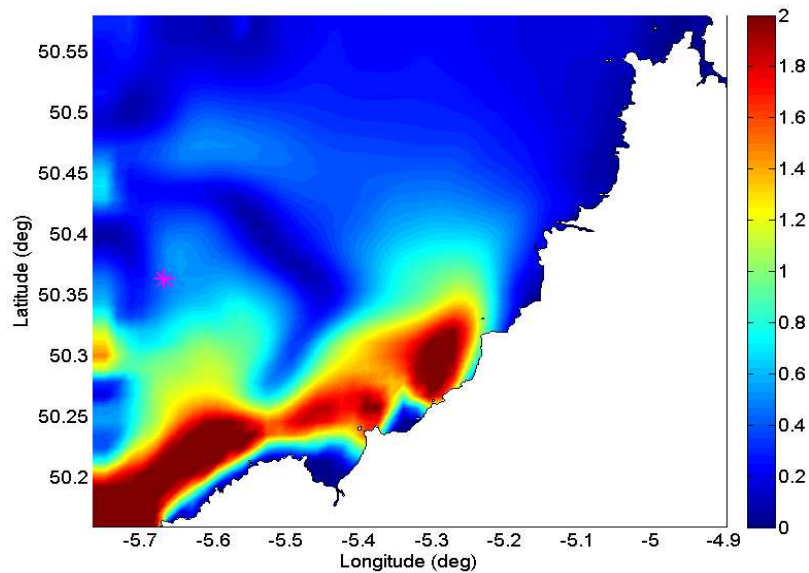
Figure 4.11 Differences of the bottom stress (N/m^2) between ROMS+SWAN and ROMS only at the point indicated by an arrow in Figure 4.8.

In order to see the effects of waves on tidal currents, the change of currents on the magnitude of the velocity differences with and without the wave influence, the following formulation was applied to the velocity field:

$$V_{diff} = \sqrt{\left(U_{wy} - U_{wn}\right)^2 + \left(V_{wy} - V_{wn}\right)^2}$$ (4.1)

where, U_{wy} and U_{wn} are the x-horizontal velocity components with wave interaction and without wave interaction, respectively. V_{wy} and V_{wn} similarly for y-horizontal velocity components.

Figure 4.10 shows the magnitude of the current velocity differences. Notice that in the near-shore region waves have a major impact on the current velocities because the velocity differences are close to 1m/s. Similarly, the bottom stress difference, plotted in Figure 4.11, shows that the waves have greatest impact on the bottom shear stress at the point in Figure 4.9 indicated by the arrow. These figures show that there is a change in magnitude for current speed and bottom shear stress with the presence of the wave farm for calm conditions, the change is qualitatively taken because these are parametric test cases. This is a significant finding on the wave-current interaction study due to a wave farm, because it shows that in the lee side of the wave farm the current speed and bottom shear stress are affected significantly. If the bottom shear stress is affected by the wave farm this would imply also a change in sediment transport with the presence of the wave farm.

4.3 Model validation

The modelling system was run for two months, from 1st December 2005 to 31st January 2006, corresponding to a period when wave buoy data was also available. Three test cases were selected to examine the space distribution of wave-tide interactions through the tidal cycle (Figure 4.12). These test cases are selected at the peak of the storm and during spring tide: Case (a) Middle water level and high current velocities; Case (b) Low water level and low current velocities; and Case (c) High water level and low current velocities.
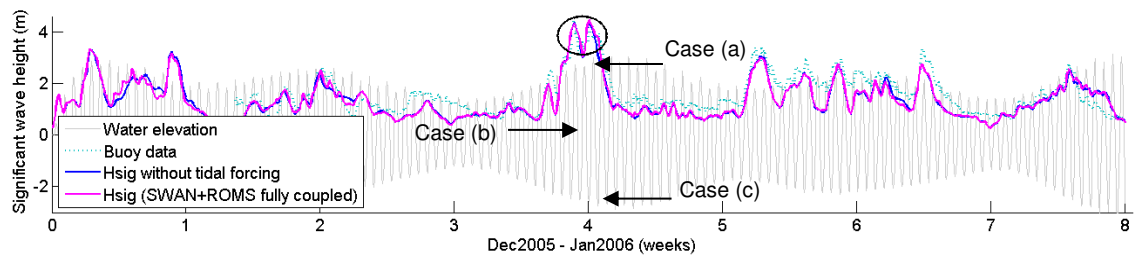
Figure 4.12 Significant wave heights with/without tidal influence. Circle represents maximum wave heights at spring tide. Three main cases have been analysed at the peak of the storm event indicated by the circle: at high water elevation and low current velocity (Case a); at middle water level and high current velocity (Case b); and at low water elevation and low current velocity (Case c).

In Figure 4.13 the predicted tidal currents are shown within the studied area, also the comparison due to time series of the St. Marys tide-gauge station is shown in Figure 4.14. This figure shows high accuracy from the tide model because amplitude and phase are highly correlated to the tide gauge, even the difference between these two time series show minor changes, this could be related to storm conditions affecting the astronomical tide elevation.
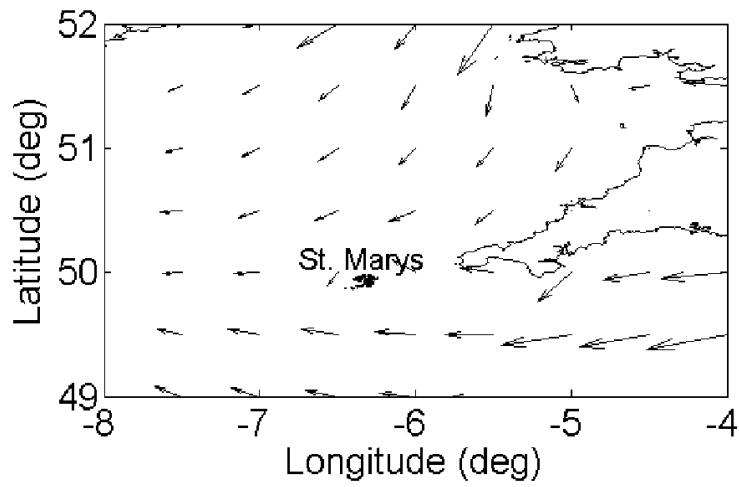
Figure 4.13 Tidal currents from the Tide Model Driver, sample snapshot is for the coarse grid, at the middle of the grid there is the St. Marys station.
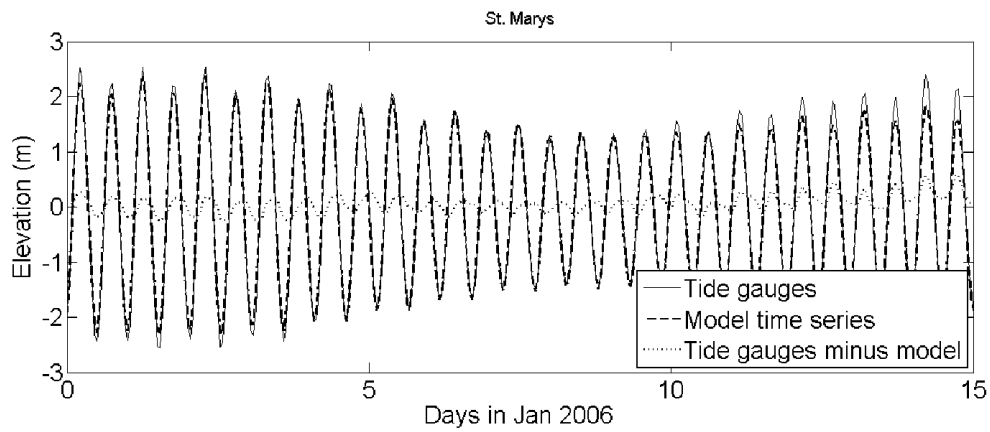
Figure 4.14 Time series comparison between the predicted and the measured from the tide gauge at St. Mary.

4.3.1 Wave-current interaction analysis

Figure 4.15 shows the influence of tidal currents and tidal elevations on the significant wave heights at the Wave Hub site predicted by the coupled system, compared with buoy measurements. Figure 4.16 shows the differences, with and without tidal currents, of the significant wave height and wave direction for the cases indicated above within the L3 domain (see Figure 4.1). Three reference sites shown in this figure for further comparisons are the Wave Hub site, St Ives Bay and St Agnes. This figure shows the difference between the coupled modelling system and the wave model only for the significant wave height and wave direction, but mostly the strong correlation of wave height, wave direction and wind velocity, suggesting that wind waves play an important role on the long-shore currents and therefore on the sediment transport. The wave direction oriented more along the shore would produce stronger along-shore currents, for example during the low water level case. When tidal currents are included, the wave direction is modified by less than 10 degrees during high waves, but about 20 degrees during low waves, in overall. As the waves propagate towards the coast, the wave propagation speed and direction may be modified by tidal currents due to refraction. In general, the main changes of wave direction are found during low wave heights and high tidal currents.

Comparisons between surface current velocities at the Wave Hub site from the coupled modelling system (SWAN+ROMS) and the circulation model (ROMS) were carried out in section 4.2.4. The comparisons indicated that the impact of wave-current interactions on the computed current velocities is significant during the spring tides. Similar to the current velocities, both components of the current-induced bottom stress in a spring tide are significantly affected by the waves.
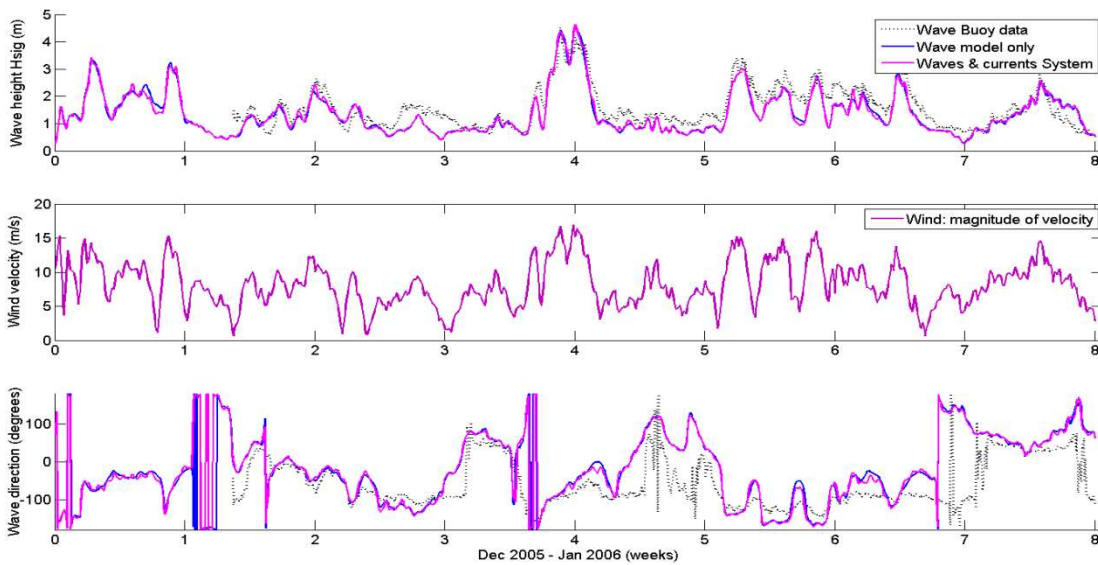
Figure 4.15 Time series of the significant wave height (top), magnitude of wind velocity (middle), and wave direction (bottom), for the wave-current interaction and waves only at the Wave Hub site. Note the strong correlation between the wind, the significant wave height, and the wave direction.

Once the underlying tidal velocities have been removed from the velocity field, applying harmonic analysis and the least square method (see Appendix 1.A.2 and 1.A.3 for details). The impact of wave-current interactions on the computed current velocities may be analysed. This impact is clearly illustrated in Figure 4.17 during spring tides. The components of the current induced bottom stress, shown in Figure 4.18 during a spring tide, are also significantly affected by the waves.

Figure 4.17 shows the contribution of wave induced currents. It should be noted that the computed current velocities have been decomposed into long-shore and cross-shore directions based on the main direction of the shoreline at the site. The velocities at the coast, of the fully coupled system, are clearly enhanced by the wave forcing, particularly in the long-shore direction. This enhancement is significant in St Ives Bay

and St Agnes). In fact, it was found that at the Wave Hub site the current magnitudes, after removing the tidal signal, are smaller than those at St Ives Bay and St Agnes. At St Agnes, the long-shore currents vary from -0.5 to 0.5 m/s, and at St Ives Bay, long-shore currents vary from -0.5 to 1.1 m/s. Figures 4.17 and 4.18 show that the magnitudes of current speed and bottom stress for both long-shore and cross-shore are quite similar, respectively. This is the result of the direction of wave propagation relative to the shoreline at this site.
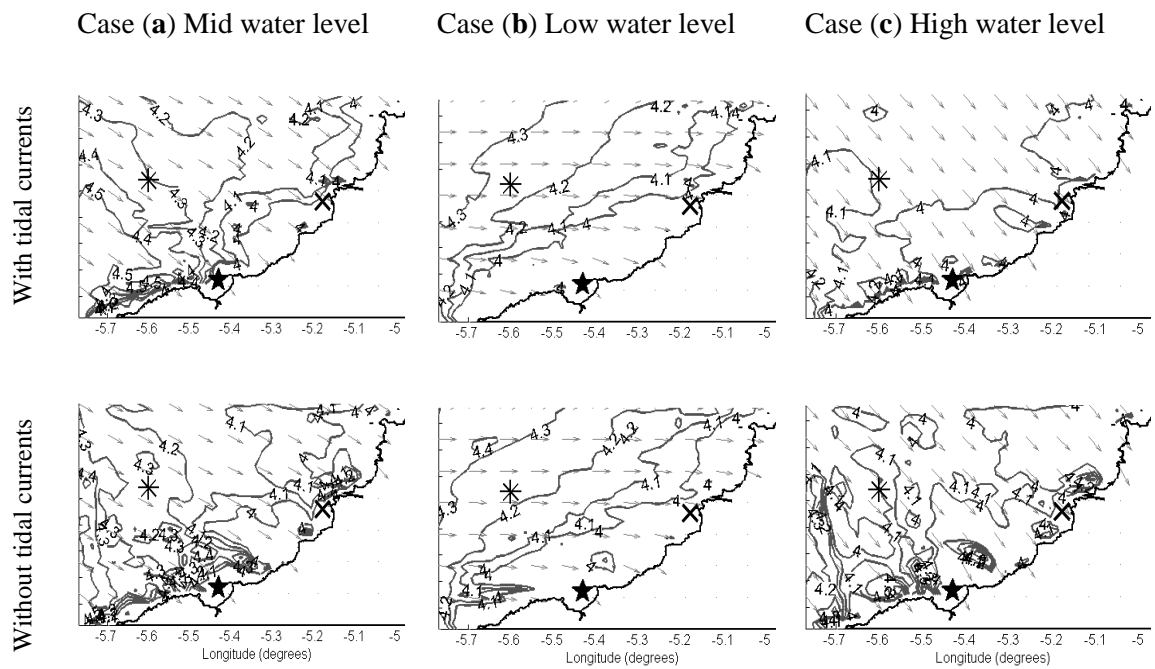
Figure 4.16 Significant wave height (contours, in m), and wave direction (arrows), with tidal currents (top panels) and without tidal currents (bottom panels), for the cases indicated in Figure 4.12. Three reference sites are selected for further comparisons: Wave Hub site (*), St Ives Bay (★) and St Agnes (×).
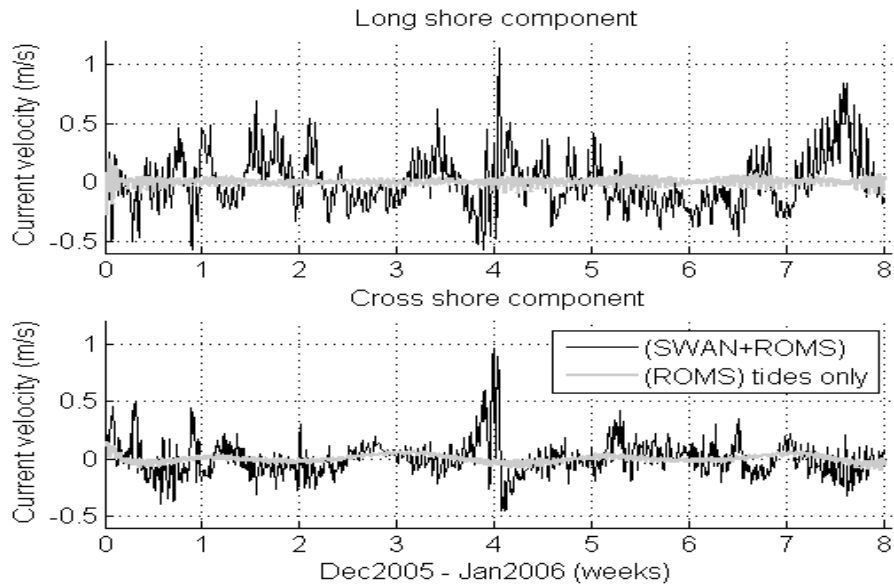
Figure 4.17 Long-shore and cross-shore components of current velocities, after removing the tidal signal, at St Ives Bay.
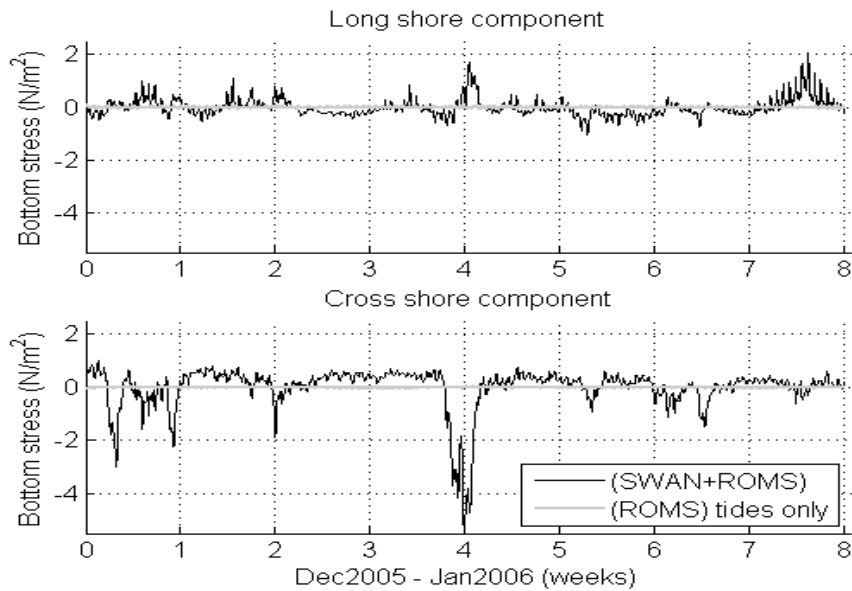
Figure 4.18 Long-shore and cross-shore components of bottom stress, after removing the tidal signal, at St Ives Bay.

When tidal currents and wave-induced currents are coupled, the strength of the current field at the Wave Hub site increases significantly, compared with the results when there is no wave-current interaction. The total current is dominated by the tidal currents which are more uniform away from the coast. However, along the shoreline, currents are enhanced by the wave action through radiation stresses. This means that wave induced currents are significant in this zone, even though the tidal currents are the main force for the general circulation.

Figure 4.19 shows the bottom current speed difference with and without the wave forcing; it is shown the importance of wave-induced currents, especially in shallow waters. It can be observed that the current field is similar at the Wave Hub site with and without wave forcing. On the other hand, at St Ives Bay and St Agnes, the currents are enhanced significantly by the waves, especially at the peak of the storm around week 4 where velocities are up to 2 m/s. At St Ives Bay the wave effect is the largest.

As waves propagate towards the coast, the wave propagation speed and direction may be modified by tidal currents due to refraction. In general, the main changes of wave direction are found during low waves and high tidal currents. The velocities near the coast, predicted by the fully coupled modelling system, are clearly enhanced by the wave forcing, particularly in the long-shore direction. In St Ives Bay, this effect is the most significant (Figure 4.19).
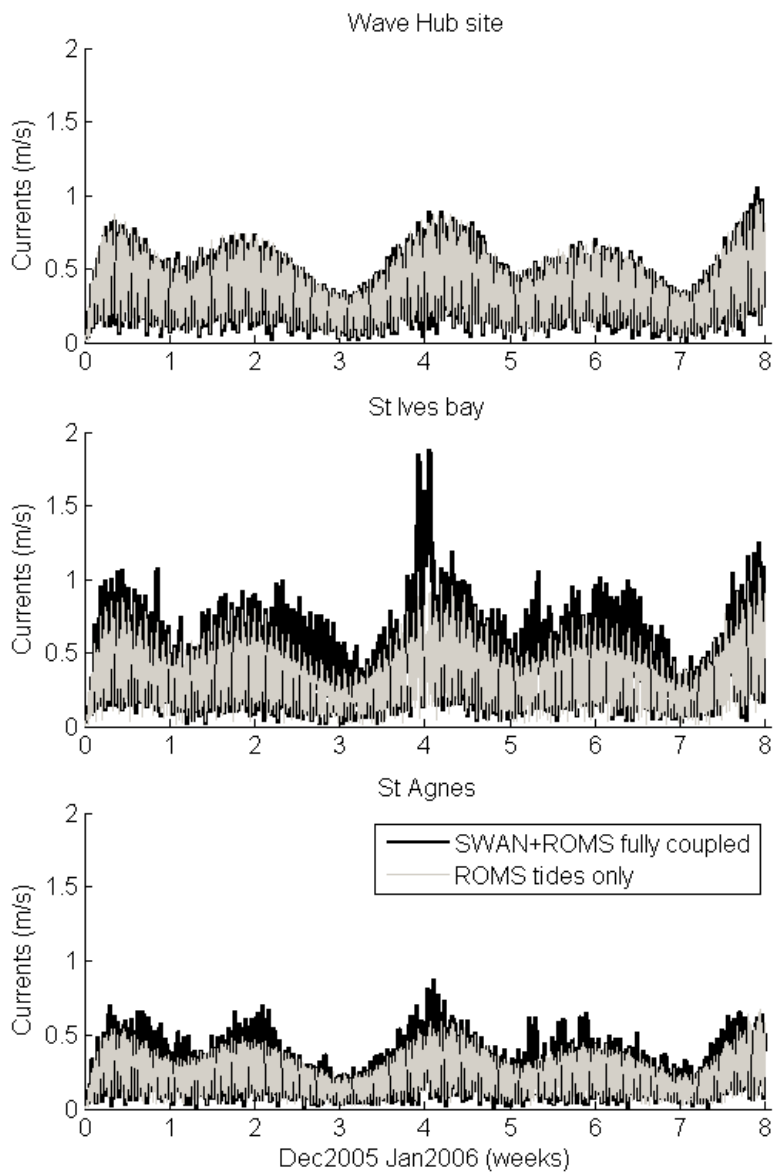
Figure 4.19 Magnitude of currents (m/s) at St. Agnes coast (top), St. Ives Bay (middle)

and Wave Hub site (bottom) with and without wave contributions (dark and gray lines)

over 8 weeks. (Positions of these locations are shown in Figure 4.13).
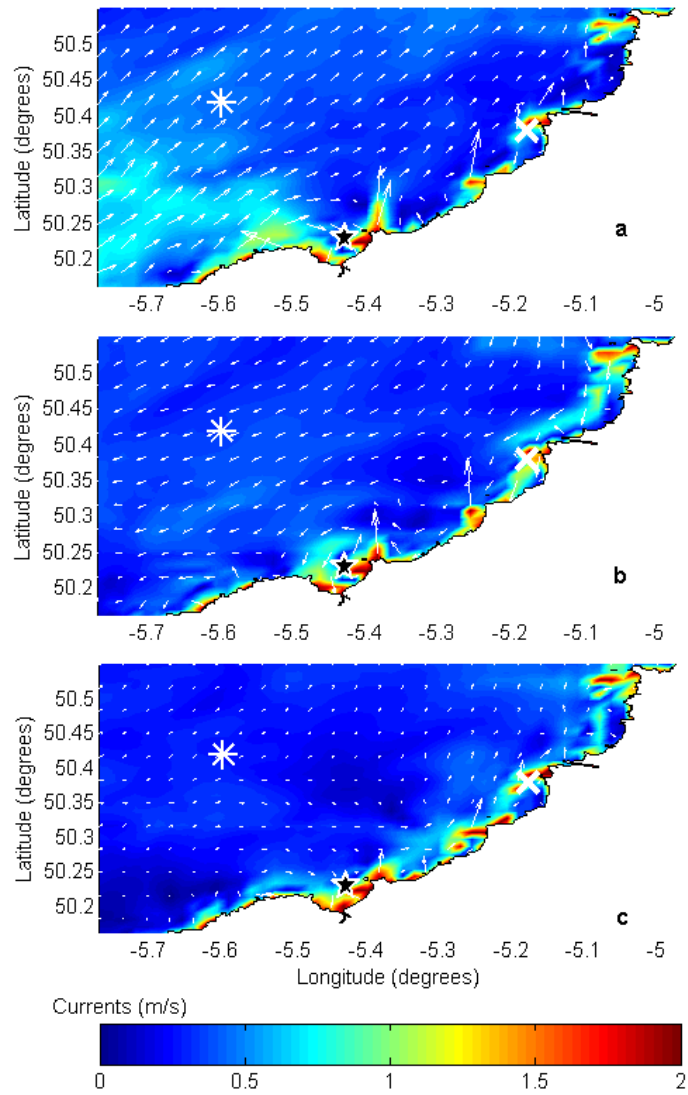
Figure 4.20 Spatial distribution of current velocities (ROMS+SWAN fully coupled) for the cases indicated in Figure 4.11: (a) mid water elevation; (b) low water elevation; (c) high water elevation. Wave Hub site (*), St Ives bay (★) and St Agnes (×).

The spatial distribution of the wave influence on currents is shown in Figure 4.20 where larger velocities and eddies are observed along the coast. In Case (a) for middle water level, when the tidal current speed is at its maximum, the total current velocity field is uniform in the offshore zone and increases in magnitude in the nearshore zone where the significant wave heights are high. In Case (b), when water elevations and tidal currents are at a minimum, the region with significant wave induced currents is extended in the offshore direction due to decreasing water depth. In Case (c), when water elevation is high but tidal currents are low, the region with significant wave induced currents is confined to the coast.

Figure 4.21 shows the combined wave-current bottom stress at different water levels during the tidal cycle. The bottom stress is affected by the local water depth as shown in Figure 4.20 for Cases (a) to (c). Case (b) shows maximum bottom stress along the coast because of lower water elevation, Case (c) shows smaller bottom stress because of the high water elevation.

Figure 4.22 shows the bottom stress contribution by waves (left) and by tides (right) for the tidal cycle cases. The wave contribution on the bottom stress is large compared to tides only, driving the sediment transport at the most and during the storm peak. The bottom stress is also correlated with the currents field for Cases (a) to (c) and is affected by the local water depth. The region with significant bottom stress is confined to the shallow water region and moves towards/away from the coast when the water level decreases/increases during the tidal cycle. Case (c) shows maximum bottom stress along the coast because of lower water elevation, Case (a) shows smaller bottom stress because of the high water elevation.

Figure 4.21 Combined wave-current bottom stress (N/m^2) with tidal currents for the cases indicated in Figure 4.11: (a) mid water elevation; (b) low water elevation; (c) high water elevation. Wave Hub site ($*$), St Ives Bay ($\bigstar$) and St Agnes ($\times$).
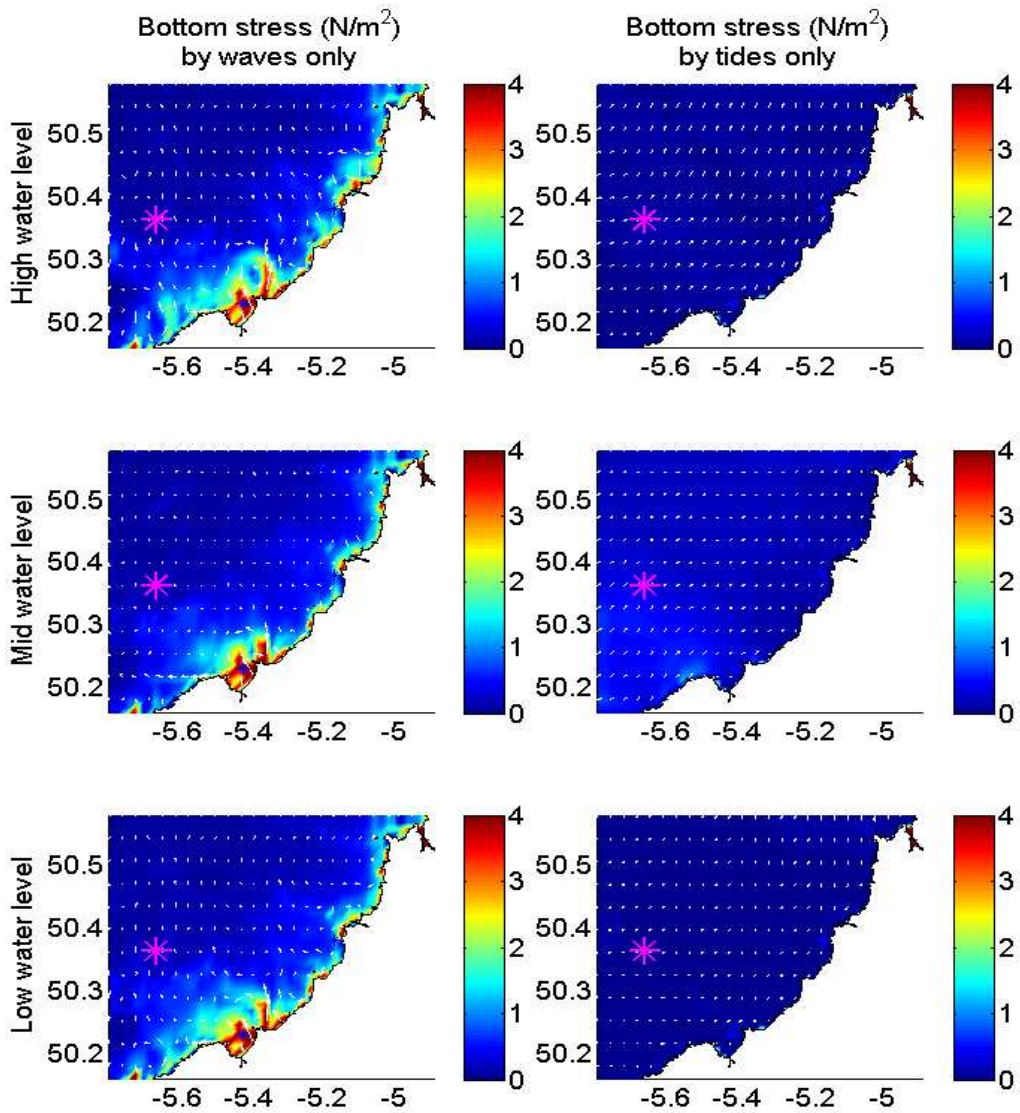
Figure 4.22 Bottom stress comparisons by waves (left) and by tides (right) only, and velocity vectors (arrows) for the tidal cycle cases. Wave Hub site ($*$).

4.4 Discussion

The wave model has uses a nested grid from coarse to fine domains, it has been forced by spectral wave boundaries and wind fields from global models. Model results have been compared against tide gauges and wave buoy observations with reasonable agreement. The circulation model has been forced by the tide model and wave parameters as radiation stress from the wave model. Also wind induced waves have been tested to improve the wave-current effect on the bed shear stress and velocity current fields.

The tidal elevation and tidal currents have a significant effect on the wave height predictions, tidal currents and wind waves have a significant effect on the bed shear-stress, relevant to sediment transport.

Waves via radiation stresses have an important effect on the long-shore and cross-shore velocity components, particularly during spring tides. Waves can impact on the bottom boundary layer and the mixing in the water column.

Significant wave heights are better predicted by the model when the coupled modelling system is implemented. Also velocity currents and bed shear stresses show the significant influence from waves via radiation stress.

Interaction between waves and tides at the Wave Hub site is important when modelling sediment transport influenced by wave energy devices. The addition of wind fields on the circulation model is compulsory to determine the effect of surface stresses on waves and currents.

The results of this study will help the wave energy resource assessment and potential environment impact of the wave farm. Model results will be validated against the wave and current measurements by HF RADAR, ADCP and Directional Waverider buoys during the on-going Wave Hub projects.

5. Effects of the wave farm on hydrodynamics

5.1 Introduction

After the model validation on hydrodynamics (see Chapter 4), the model is now applied to the period in the winter of 2010 (October to December 2010) for further examining the wave-current interaction when the wave and tide observations are available. Figure 5.1 shows the locations of the nearshore wave buoys and tide gauges. It worth mentioning that the morphological module was setup to compute the sediment transport and the resulting bathymetry changes affected by the wave farm, (see Chapter 6). The model results of wave and current distribution with and without the presence of the wave farm are used to assess the effect of wave farm on hydrodynamics in the near-by region.

The new test case was first run for 72 days of simulation (from 20 October to 31 December 2010). This period was selected because during winter time many extreme events are observed. Within this winter time a shorter period was identified when particularly energetic storms were observed (from 01 to 16 of November). Comparisons between these two periods showed that the most significant changes in the hydrodynamics and morphodynamics occurred between 1st and 16th of November 2010.

Following the methodology to setup the wave-current modelling system, described in Section 3.6, the SWAN wave model is driven by the global WAVEWATCH III wave model and the global GFS atmospheric model that provides the wind fields. Also, the

global OTIS tide model drives the ROMS circulation model that is coupled with the wave model.
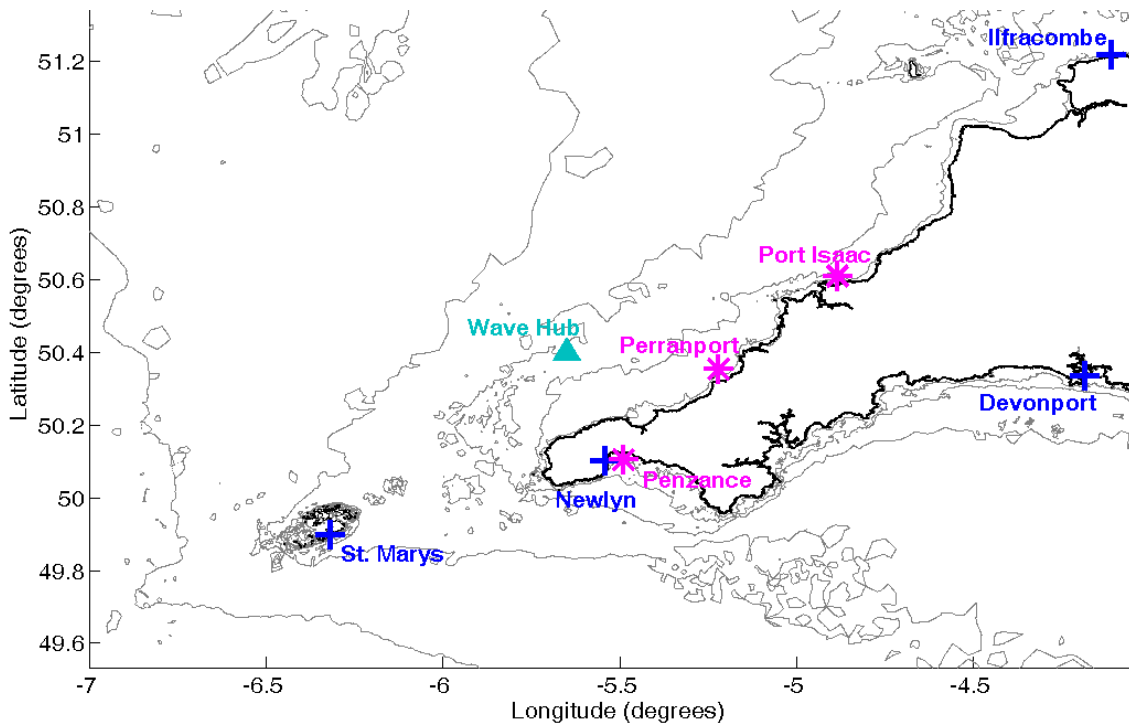
Figure 5.1 Level 2 grid domain of nested wave modelling (L2) of the Southwest of England shown in Figure 4.1. Locations of wave buoys (*), tide gauges (+) and the Wave Hub site (▲)

The model system setup is similar to the one described in Section 3.6, however there are some changes for the new refined grid domain. The wave model is run in a 270 x 170 grid domain, cells are about 300 meters in x and y directions; boundary conditions, in the four sides, come from the upper nested level as spectral wave conditions; wind fields are every 3 hours for the entire domain. The wave model exports fields of wave heights, wave period, wave directions, wave particle velocities at the top and bottom,

126

and forces as radiation stresses for the wave contribution in the circulation model. Fields of water elevation, water depth and velocity currents, as well as, bottom friction come from the two-way coupled circulation model ROMS.

The wave farm is set as an obstacle transmission in arrays of WECs at the Wave Hub site, suggested by Millar et al (2007), represented as a 4km partially transmitting obstacle, aligning approximately parallel to the incoming wave crests. The energy transmission percentage was set as 75% which represents an array of densely spaced, high-efficiency WECs.
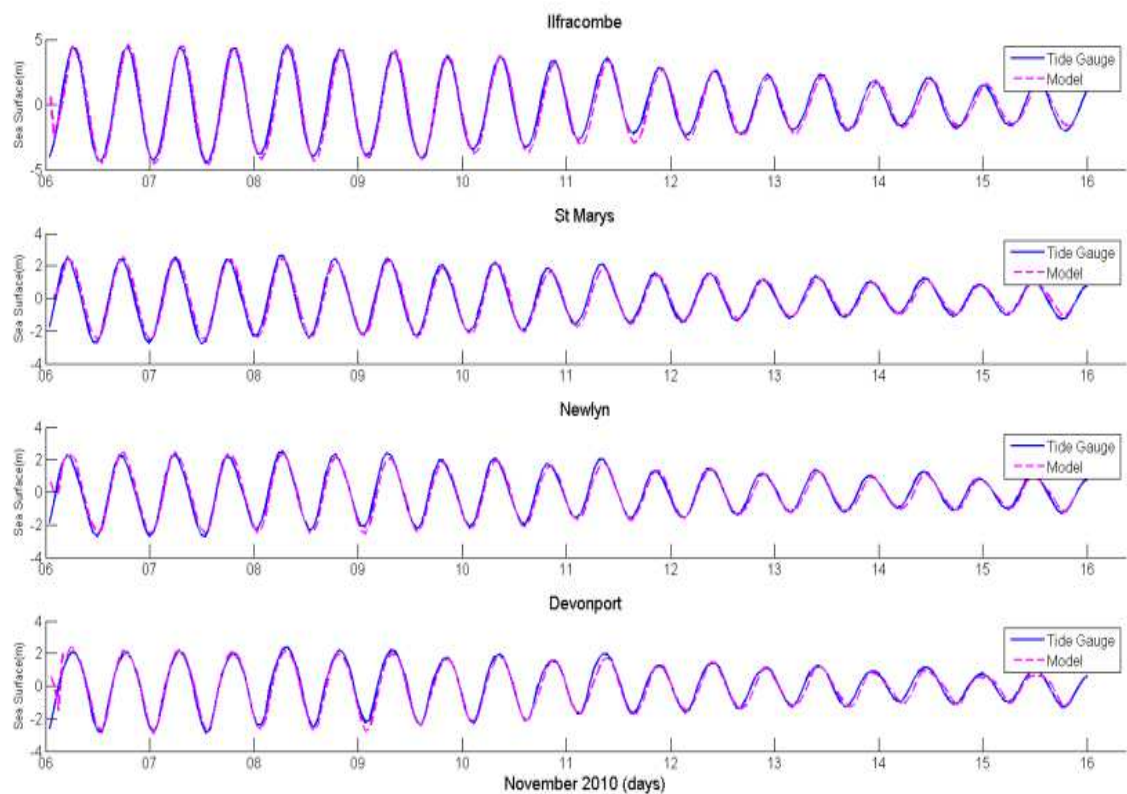
Figure 5.2 Model surface elevations comparison against tide gauges along the coast in the Southwest of England (see Fig 5.1 for locations).

The ROMS model has been run in fully 3D baroclinic mode with 5 terrain-following (sigma) layers in the vertical; the numerical grid has 270 grid cells in the longitude direction, which extends from -7.000830 to -4.007289. Along the latitude direction the grid has 170 grid cells and the domain extends from 49.532940 to 51.432068. Boundary conditions for tidal forcing were derived from the OTIS model (Egbert and Erofeeva, 2002; Padman and Erofeeva, 2004), tidal elevations and tidal currents were interpolated to the boundaries of the computational grid in ROMS.

The test case simulation is from 1st to 16th of November 2010, in ROMS the baroclinic time step is set as 30 s and a mode-splitting ratio of 30 s. In SWAN, for this semi-coarse grid, the time step is 600 s. An exchange rate of data between ROMS and SWAN is every 1200 s. Due to the new field data being available, further comparisons of the computed tidal levels and nearshore waves with the measurements are made to re-ensure the accuracy of the modelling system.

5.2 Nearshore surface elevations

Predicted time series of sea surface elevation from the modelling system are compared against four tide gauges along the southwest of England. Figure 5.1 shows the four locations of the gauge stations for Ilfracombe, St. Marys, Newlyn and Devonport. The four tide stations are along the coast in the Southwest of England, Ilfracombe is at the north of Devon, this site is where the largest tidal range is present, around 10 m of difference. St. Marys station is an offshore tide gauge in the St Marys isles. Newlyn is at the south of Cornwall in a protected area. Devonport is in Plymouth. Figure 5.2 gives a comprehensive impression of the accuracy of the modelling system in terms of tidal elevations, the four modelled locations show high correlation with observations.

5.3 Nearshore waves

For comparison purposes of wave parameters, three sites (Perranporth, Port Isaac and Penzance) have been selected along the Southwest of England, as mentioned before, these sites are due to the available information from wave buoys from the Coastal Observatory. Here the three storm events, around 3rd, 9th, and 12th of November, are presented. In this chapter, model-data comparisons are carried out at these locations to validate the model or study the wave farm effects on these sites. Perranporth and Port Isaac are close to the lee of the wave farm, however, Perranpoth is the closest which makes it a good candidate to examine the effects of the wave farm, Penzance is further away from the effects of the wave farm but has been used to validate the modelling system.

Figure 5.3 shows wave comparisons at Perranporth, where the significant wave height (mid panel) between the modelled and the observed are compared. Wave direction (bottom panel) is compared as well with good agreement, this shows that offshore wind-waves play an important role in the propagation of nearshore waves. The magnitude of wind speed (top panel) also has a close correlation to the peaks observed in the significant wave height. Similarly, Figure 5.4 shows wave comparisons at Port Isaac, and Figure 5.5 shows wave comparisons at Penzance. It worth mention that the waves come from swell winds from a global wave model, and this is a result of a nesting modelling performance, thus, at these three sites the predicted significant wave heights have an acceptable accuracy.

In general the predicted wave heights closely correlated with the wind speed as indicated in the figures (top panels), and the storms are reproduced reasonably well. In comparison with observations, it can be seen that the storm peak was slightly under-

predicted at Perranporth, where water depth is relatively shallow. As waves propagate towards the coast, their propagation speed and direction may be modified by the ambient tidal currents causing wave refraction. Therefore, wave refraction can have a significant impact on the wave-current interaction.

Based on the wave height in Figure 5.3 (mid panel) three storm peaks are observed, and will be used for further analyses. We will next focus on between 8th and 9th of November where the highest wave conditions and spring tides are present.
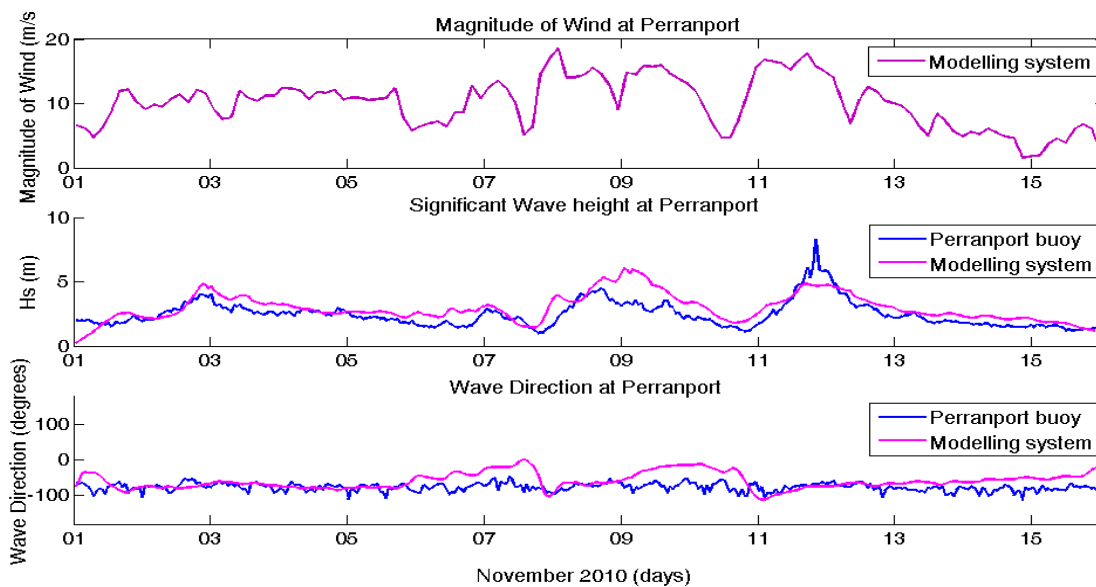
Figure 5.3 Comparison of wave parameters between the modelling system and wave buoy at Perranporth (see Fig 5.1 for location).
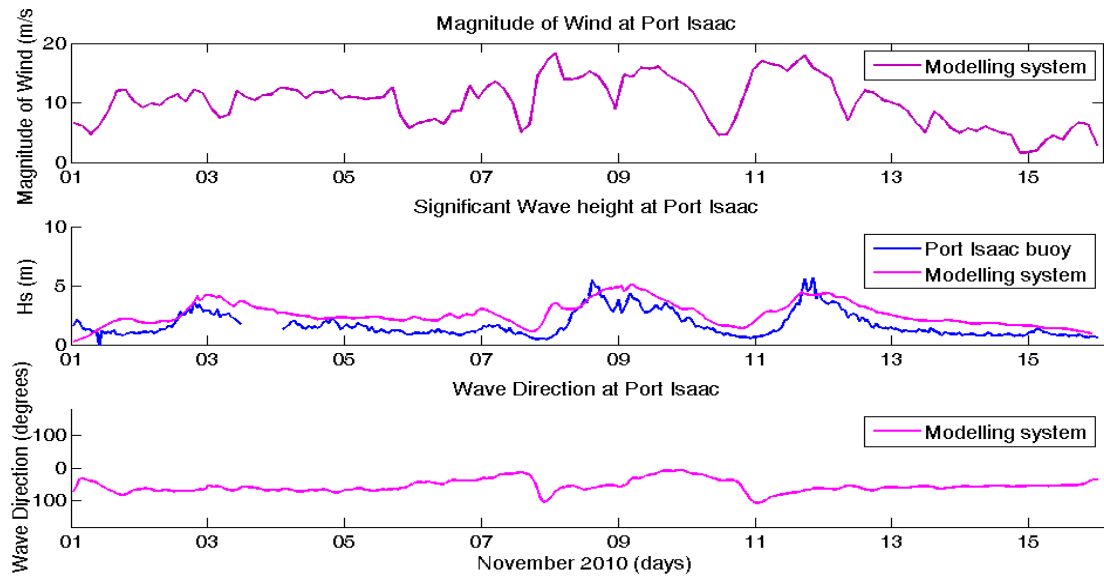
Figure 5.4 Comparison of wind and wave parameters between the modelling system and wave buoy at Port Isaac (see Fig 5.1 for location).
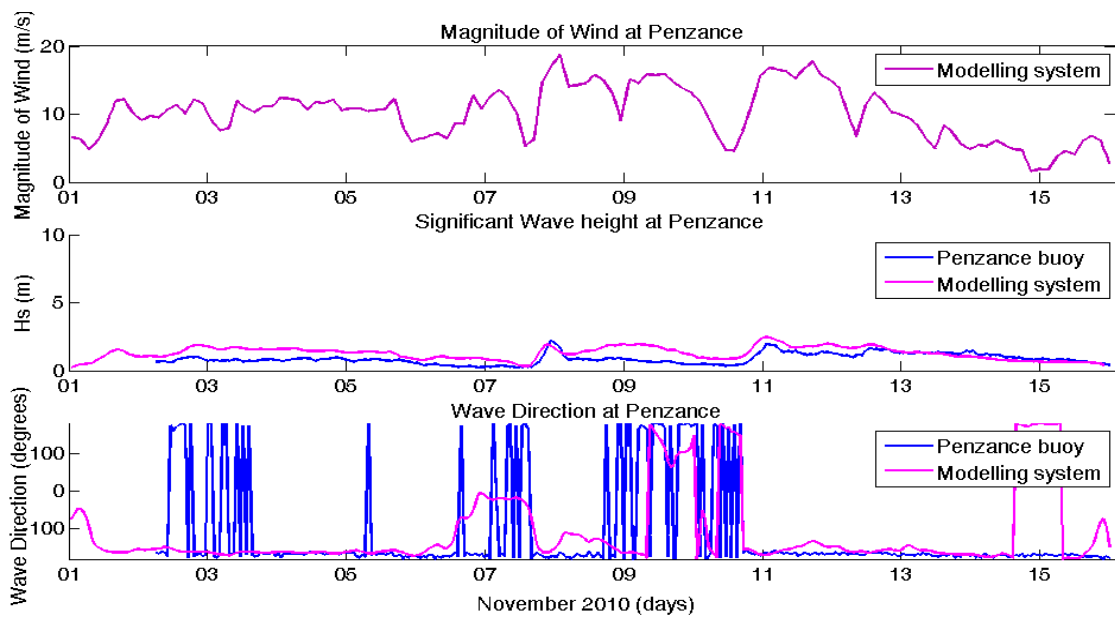
Figure 5.5 Comparison of wind and wave parameters between the modelling system and wave buoy at Penzance (see Fig 5.1 for location).

Figure 5.6 shows significant wave height (colours) and wave direction (vectors) for the storm case and for the tidal cycle cases. In this figure the difference between the wave-current interaction against the wave-current and wave farm interaction is shown. The change of the wave height with and without the wave farm is between 5cm and 10 cm at the nearshore zone, and the maximum extension affected by the wave farm is about 26km from St. Ives Bay to upwards for the high water level case which is the most significant in terms of wave height variations.

5.4 Wave-current model results

The Southwest of England has a continuous wave activity, either from high-energy Atlantic swell, or from waves generated locally by the prevailing westerly to southwesterly winds. The usual high-energy conditions, coupled with a gentle slope generally leads to the development of a wide surf zone. The mean tidal range in the nearshore area of the Wave Hub site is 5.5m, with maximum values over 7m during spring tides (Marino-Tapia, 2003).

One of the purposes of this chapter is the analysis of waves and currents at the storm peak of November 2010 in the Southwest of England and more specifically, in the Wave Hub site. Since this period differs from the model validation study in Chapter 4 (December 2005), further model validations were carried out for this period. Water elevations were compared against tide gauges at four locations (shown in Figure 5.1), and wave heights were compared with the wave buoy data at three locations, namely Port Isaac, Perranporth and Penzance (also shown in Figure 5.1). In Chapter 4 the contribution of waves to the general circulation was analysed. It was observed that during spring tides the highest current speed occurred in most of the nearshore area,

even at the isoline where the Wave Hub is deployed, also was observed that the wave

contribution during the storm peak enhances the nearshore current speed.
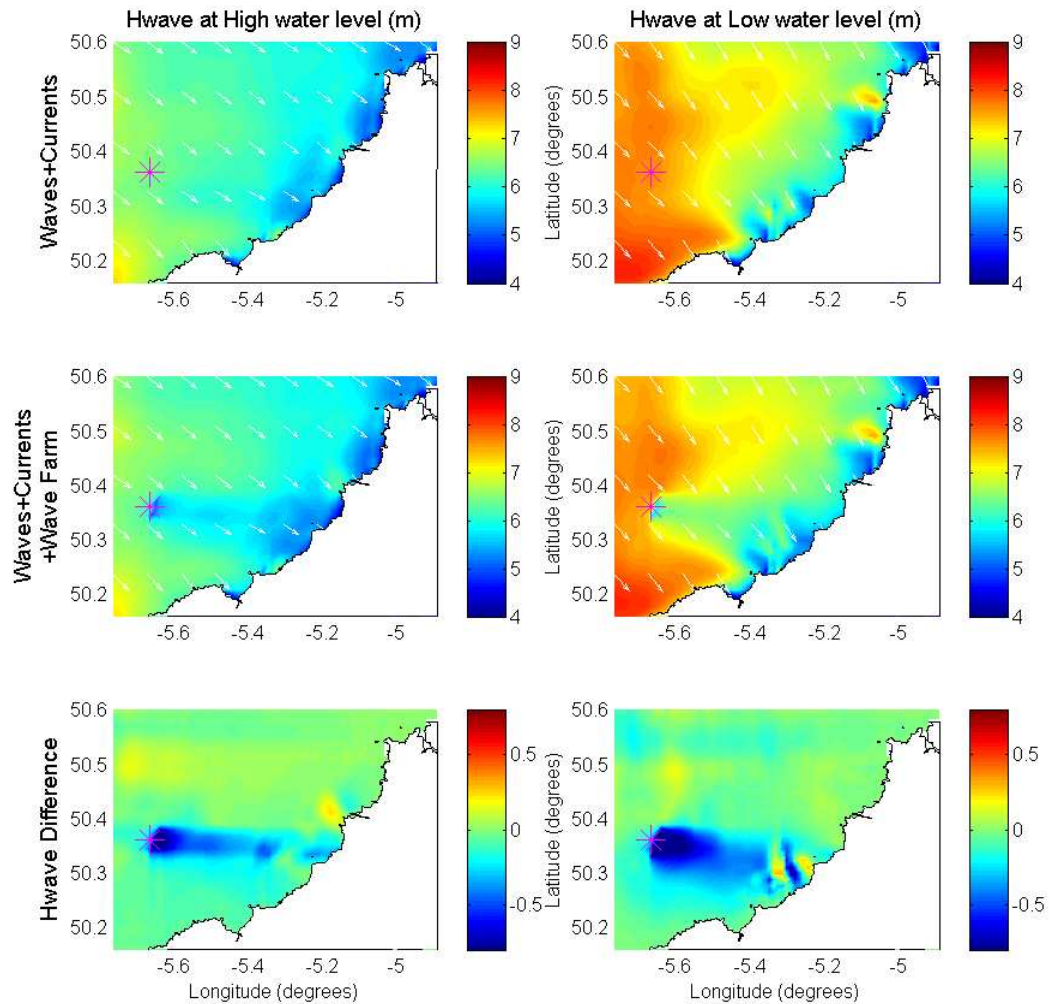
Figure 5.6 Effects of the wave farm on the wave heights under low and high water

elevations: (top) computed wave height without wave farm; (middle) computed wave

height with wave farm; (bottom) the difference of the computed wave height with and

without wave farm. (Vectors are the wave directions; * - Wave Hub)

In Figure 5.6 the significant wave height is decreased because the wave energy is decreased, thus negative values are expected in the lee side of the wave farm. Bottom shear stresses are the combined wave-induced and current-induced stresses that are related to wave radiation stress gradients driven the wave-induced currents. In other words, as the wave height decreases, the current speed may decrease or increase, depending on the gradients of radiation stresses and bottom shear stresses. This means that the wave height is not necessary in conflict with the bottom shear stresses.

5.4.1 Surface currents

The contribution of waves over the tidal forcing can be analysed through averaged tidal cycles. The tidal elevations have been split in two main components, namely flood and ebb tides. Here both the averaged flood and ebb tidal elevations are considered. The mean flood and ebb tides were taken from the highest significant wave conditions along the sixteen days of simulation, corresponding to the extracted period around 8th and 9th of November of 2010 (see Figure 5.3 for details), in result there are forty-eight hours of storminess, from which, the mean flood and mean ebb results are analysed. To assess the dominant tidal case during the storm, a control index has been applied to estimate the dominant flux contributions in the different physical parameters like speed currents, bottom stresses, sediment concentrations, etc.

As mentioned, forty-eight hours of storminess are averaged as mean flood, this was performed taking as reference the tidal cycle from the trough to the crest, and extracting the magnitude of the currents for every cell of the domain through the 48 hours. In a similar way, the magnitudes of currents were extracted as mean ebb speed, from the crest to the trough of the tidal cycle. In result the averaged tidal cases for current speed

are represented in Equation 5.1 for the mean flood tide and Equation 5.2 for the mean ebb tide.

$$|\overline{u_f}| = \frac{1}{n}\sum_{i=1}^{n} \sqrt{u_i{}^2 + v_i{}^2} \tag{5.1}$$

$$|\overline{u_e}| = \frac{1}{n}\sum_{i=1}^{n} \sqrt{u_i{}^2 + v_i{}^2} \tag{5.2}$$

Figure 5.7a shows the surface for current speed at the mean flood tide, vectors show the direction and magnitude of the current speed. In spite of the strength of the wave action the vectors show the direction is dominated by the tidal forcing, which is one order of magnitude higher than the wave forcing. However, the storm has an impact on the direction and speed of the currents in the nearshore area. In average, the current speed along the coast is around 1 m/s, nevertheless, there is an area where the speed increases up to 2 m/s. This area corresponds to a shallow depth where similar magnitudes of velocity are identified in the wave-current interaction analysis in Chapter 4. Also, the Figure 5.7a shows that during high waves and flood conditions, the surface velocities are enhanced, nearly uniformly, along the coast and nearshore areas.

Figure 5.7b shows the mean ebb current speed for the storm case. Contrary to flood conditions, the mean ebb direction of the vectors is southward, driven by the tidal forcing. Surface current speeds are not uniform along the coast because the main direction is southwards and the speed is higher in the south in both nearshore and offshore areas. The highest velocities are found in the same area presented for flood conditions, up to 2 m/s, which is analysed in the following sections.
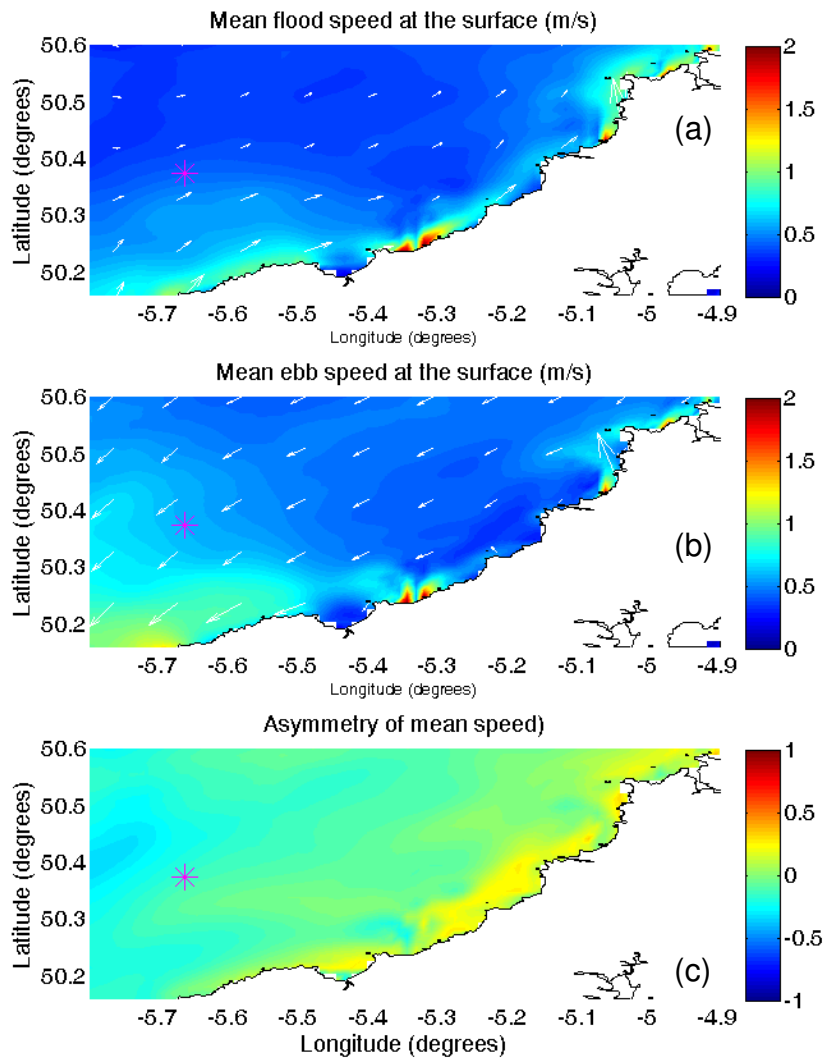
Figure 5.7 Mean flood (top) and mean ebb (middle) current speeds at the storm peak, vectors are the mean direction of the current speed, asymmetry index (bottom) to weight between flood and ebb. (*) The wave farm.

5.4.1.1 Asymmetry index for surface currents

In order to quantify the dominant conditions that drive the nearshore processes during storminess and to compare the magnitude between flood and ebb, an asymmetric control index is applied, this is because current speeds for flood and ebb have similar magnitudes, even that the tidal currents are one order of magnitude higher than the wave induced currents.

The asymmetry index A_I for the mean current speeds is defined as

$$A_I = \frac{|\overline{u_f}| - |\overline{u_e}|}{|\overline{u_f}| + |\overline{u_e}|} \tag{5.3}$$

Where, $|\overline{u_f}|$ is the averaged magnitude of the current speed for flooding during the storm conditions, $|\overline{u_e}|$ is the averaged magnitude of the current speed for ebb conditions during the storm. The control index can vary from -1 to +1. It is negative when $|\overline{u_f}| < |\overline{u_e}|$ and positive when $|\overline{u_f}| > |\overline{u_e}|$.

In Figure 5.7c the control index for flood and ebb conditions is shown. Positive values mean that flood conditions are dominant, this is observed along the coastline and nearshore areas. Dominance index shows values ranging from -0.5 to 0.5, suggesting that ebb conditions have similar magnitudes to flood conditions.

The applied methodology in Section 5.4.1 is similar to Wu et al (2011), they are interested in the study of fine particles at the surface, applying a flow circulation model only. In this study we are focused on surface and near-bed currents affected by the wave farm and the wave-current interaction.

5.4.2 Surface currents affected by the wave farm

To observe the impact of the wave farm in terms of flood and ebb conditions and during storminess, the same methodology to extract mean flood and ebb speeds was applied, but now with the inclusion of the wave farm. At first sight, both comparisons with and without the wave farm look similar.

Equation 5.4 shows a simple deduction to see the difference in magnitude between mean current speed with the wave farm and mean current speed without the wave farm. This equation can be applied to both flood and ebb conditions to analyse the differences.

$$|\bar{u}|_{diff} = [(\bar{u}_{with} - \bar{u}_{without})^2 + (\bar{v}_{with} - \bar{v}_{without})^2]^{\frac{1}{2}} \qquad (5.4)$$

where $\bar{u}_{with}$ and $\bar{u}_{without}$ are the mean current speed components in the x-direction, with the wave farm and without the wave farm, respectively. $\bar{v}_{with}$ and $\bar{v}_{without}$ are the mean current speed components in the y-direction, respectively.

Figure 5.8a shows the mean flood speed difference at the surface, after applying the Equation 5.4. It can be observed that in the lee of the wave farm the speed has a difference of about 0.15 m/s, this is due to a reduction in the mean current speed. In the same way and close to the nearshore in the leeside of the wave farm, the mean flood current speed is decreased as well, also an area where the mean current speed is decreased for flood conditions is highlighted. The vectors show the mean direction of the current speed for flood conditions during the storm. It is worth mentioning that during the storm test case the bottom morphological changes have been considered. If the bathymetry varies over the time, it is expected that the velocities are modified by the variation of the bottom. This will be discussed in Section 5.4.3.

Figure 5.8b shows that the mean ebb current speed is reduced by the wave farm, compared to flood conditions (Figure 5.8a). In the nearshore area affected by the wave farm, the reduction of the mean speed is more towards the coast comparing with the flood conditions. It seems that the impact of the wave farm to the immediate adjacent area during ebb conditions is enhanced by the storm event, this can be seen in the lee side of the wave farm, and is extended along the coast. On the other hand, during flood conditions the impact of the wave farm to the coast is smaller suggesting that the magnitude of the tidal current is greater towards offshore rather than wave-induced currents during ebb conditions, and also the reduction in the mean speed in the nearshore is focused in a specific area where wave heights are reduced by the wave farm effects (see Section 4.7.1). The changes in wave induced current are caused by the incident wave height and the local wave height change from flood to ebb conditions.

Following the above methodology and applying Equation 5.3 the asymmetry index with the presence of the wave farm was used. In order to estimate the asymmetry index difference for mean speeds at the surface a subtraction of both indexes, with-without the wave farm, was performed. Figure 5.8c shows the asymmetry difference of mean speed where a clear dominance during flood conditions is observed, this is in the lee and along the nearshore coast, suggesting that at high water levels and during the storm event the wave farm has more impact in the lee and close to the nearshore. Also, there is an area where ebb condition dominate, suggesting an increase in velocity by tidal currents and low water level, causing erosion in the bottom. Index difference shows dominance for ebbing in the lee where higher velocities are present.

Figure 5.8 Mean flood (top) and mean ebb (middle) current speeds at the storm peak.

Asymmetry index (bottom) to weight between flood and ebb. (*) The wave farm.

5.4.3 Near-bed currents

The spatial distribution of the wave influence on bottom currents is shown in Figure 5.9 where larger velocities and eddies are observed along the coast which are up to 2 m/s. In Case (a), when the water elevation is high, but with low tidal currents, the region with significant wave induced currents is more confined to the coast. In Case (b) for middle water level, tidal currents are at its maximum, and the total current velocity field is uniform in the offshore zone and increases in magnitude in the nearshore zone where the significant wave height is high. In Case (c), when water elevations and tidal currents are both at the minimum, the region with significant wave induced currents is extended in the offshore direction due to decreasing water depth. The current velocities near the coast, predicted by the fully coupled modelling system, are clearly enhanced by the wave forcing, particularly in the longshore direction. In St Ives bay, this effect is the most apparent.

When tidal currents and wave-induced currents are coupled, the total currents at the Wave Hub site are most significantly enhanced. Away from the shoreline, the resultant flow is dominated by the tidal currents which are more uniform. However, along the shoreline, currents are enhanced by the wave action through radiation stress gradients which become stronger. This means that wave-induced currents are significant in this zone, even though the tidal currents remain as the main force for the general circulation.

The impact of waves on tidal forcing can be observed in changes of the current velocity, in particular in changes in the bottom as mean current speed during a storm event. Figure 5.10a shows similar characteristics in magnitude and direction to the surface mean current speed, a significant difference is observed where higher magnitudes are concentrated for both upper and bottom layers. At the surface a mean speed is up to 2

m/s while at the bottom the magnitude is about 1 m/s, which suggests that in the nearshore and during storminess there are places where the mean speed at the bottom drops half of its surface speed. Compared to the surface mean speed, the bottom mean speed is decreased in the nearshore for both flood and ebb conditions.

In Figure 5.10b the mean current speed during ebb flux is presented, a similar difference is observed as mentioned above. It worth mention that the mean current speed at the bottom is enhanced in offshore areas whereas in flood conditions the higher current speed is confined mostly at the nearshore. In Figure 5.10c the asymmetry index between flood and ebb at the bottom shows dominance of flooding conditions along the coast, however, the area where the highest velocities are presented, ebb conditions might dominate.

These current results have to be compared to bottom stress results to see whether flooding and ebbing have significant contribution to the bedload rate and sediment transport, therefore, a further analysis of the long term influence of the wave farm might be required.
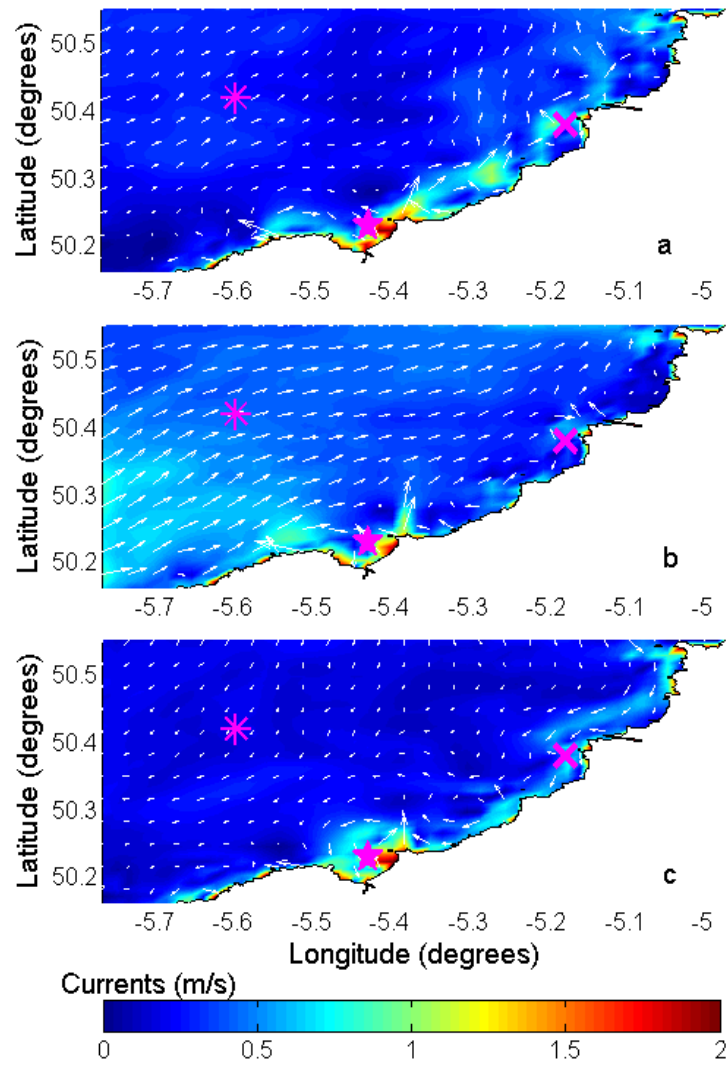
Figure 5.9 Spatial distribution of bottom current velocities (with ROMS+SWAN fully coupled) for (a) high water elevation; (b) mid water elevation; and (c) low water elevation. Wave Hub site (*), St Ives Bay (★) and St Agnes (×).
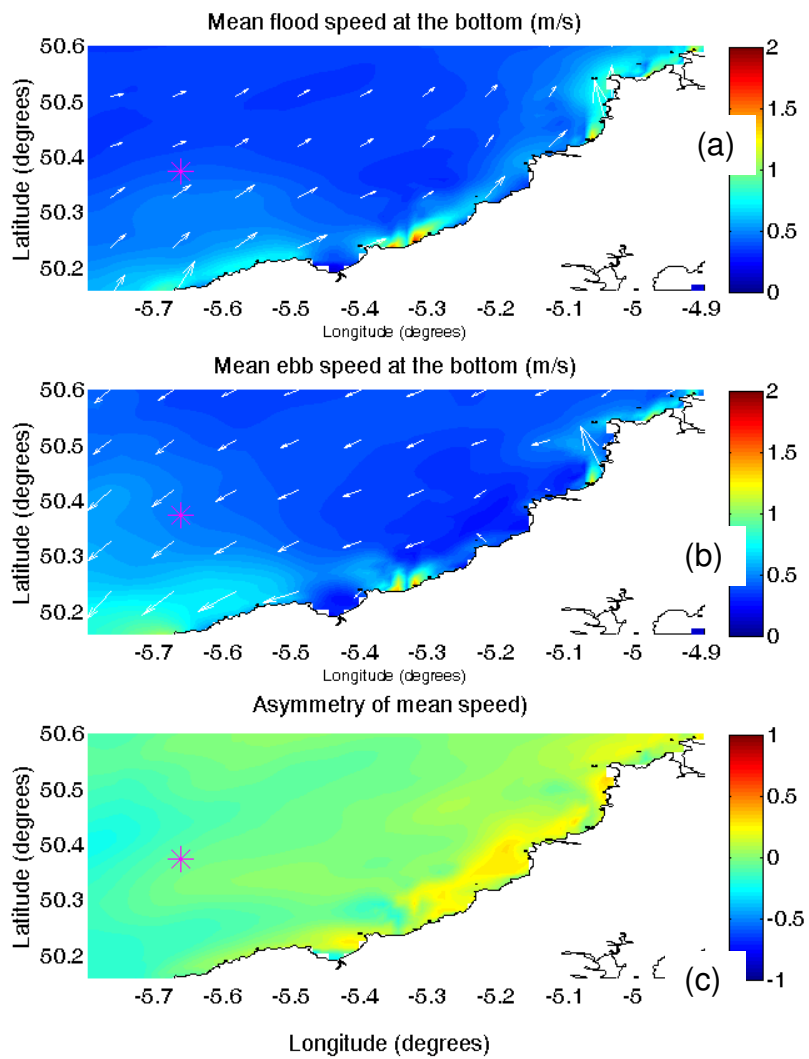
Figure 5.10 Mean flood (top) and ebb (middle) current speeds at the storm peak. Asymmetry index (bottom) to weight between flood and ebb. (*) The wave farm.

5.4.4 Near-bed currents affected by the wave farm

Figure 5.11 shows the bottom current speed during the storm peak (left panels) and its wave farm effects (right panels) at high and low water levels. This figure confirms that the bottom shear stresses are related to both waves and currents. In Fig 9 the significant wave height is decreased because the wave energy is decreased, thus negative values are expected in the lee side of the wave farm. In other words, as the wave height decreases, the current speed may decrease or increase, depending on the gradients of radiation stresses and bottom shear stresses. Bottom shear stresses are the combined wave-induced and current-induced stresses that are related to wave radiation stress gradients driving the wave-induced currents.
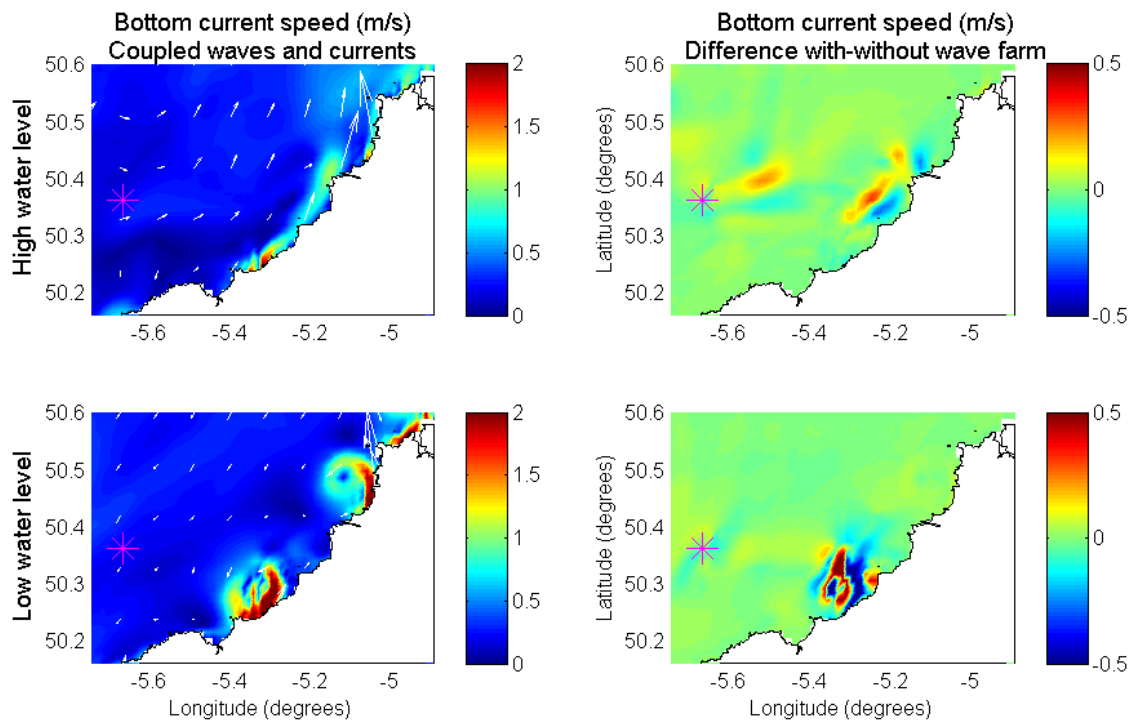
Figure 5.11 Effects of wave farm on bottom current speed at high and low tides. (Vectors are magnitude and direction of the current speed, colour indicates the magnitude, * – Wave Hub)

To observe the impact of the wave farm in terms of flood and ebb conditions and during storminess, the same methodology to extract mean flood and ebb speeds was applied (Equations 5.1 and 5.2). Effects of the wave farm on the mean speed at the bottom can be observed in Figure 5.12. Figure 5.12a shows the magnitude difference with and without the wave farm, after applying Equation 5.4, for flood conditions. In a similar result as Figure 5.8a, an area of higher magnitude of mean speed is exposed around the coordinates -5.3 longitude and 50.35 latitude, that indicates a change in the mean speed by the wave farm and presumably a reduction in the mean speed, which it has been discussed above.

Figure 5.12b shows the mean speed for ebbing, similar shape in magnitude as Figure 5.8b, but less magnitude. For ebb conditions or low water levels, mean speeds change in the lee and the nearshore areas by the wave farm, assuming a slightly reduction in the magnitude but uniform speeds along the area.

Following the above methodology and applying Equation 5.3, the asymmetry index with the presence of the wave farm shows almost no change for flooding or ebbing during a storm event. Figure 5.12c shows the difference of the control index with and without the wave farm. In the lee of the wave farm and close to the shoreline there is an area where flood dominates. Ebb conditions dominate in a small area beneath the flood dominance. Flood dominance by the wave farm coincides with the change in mean speed as shown in Figure 5.12a. This suggests that the wave farm changes significantly the mean speed during flood and storm conditions.

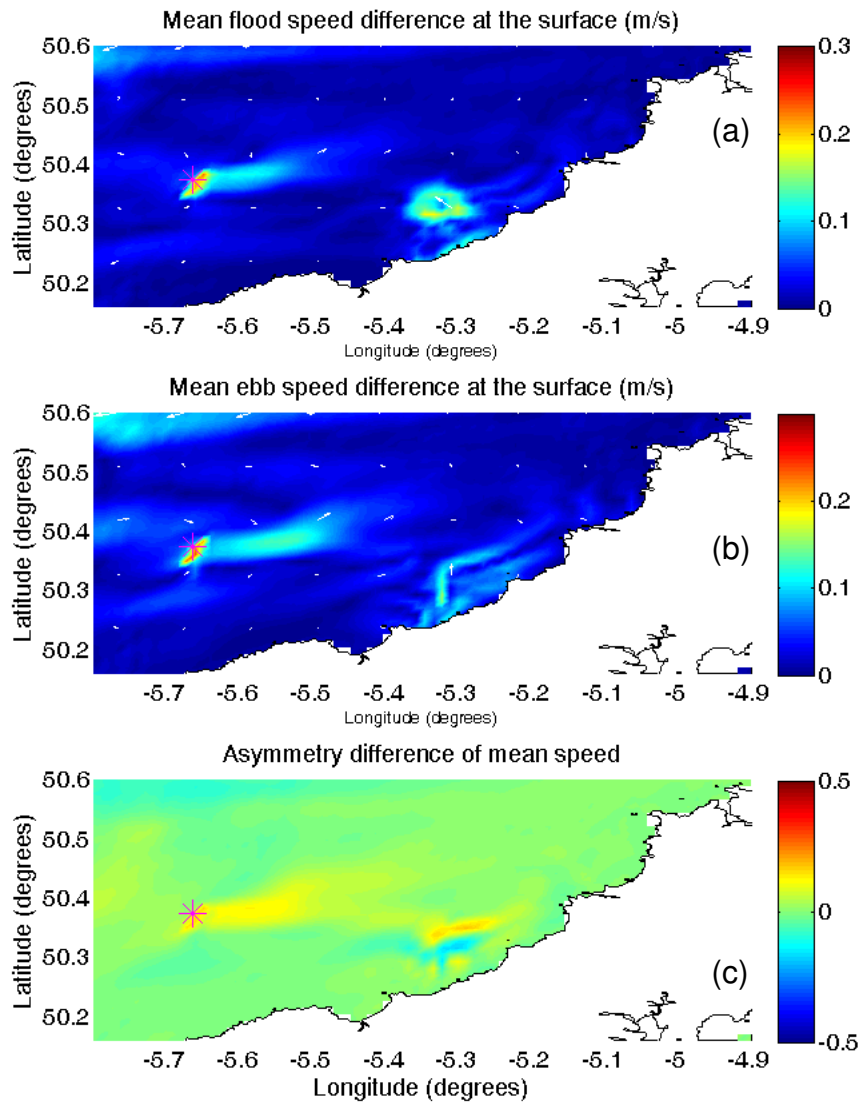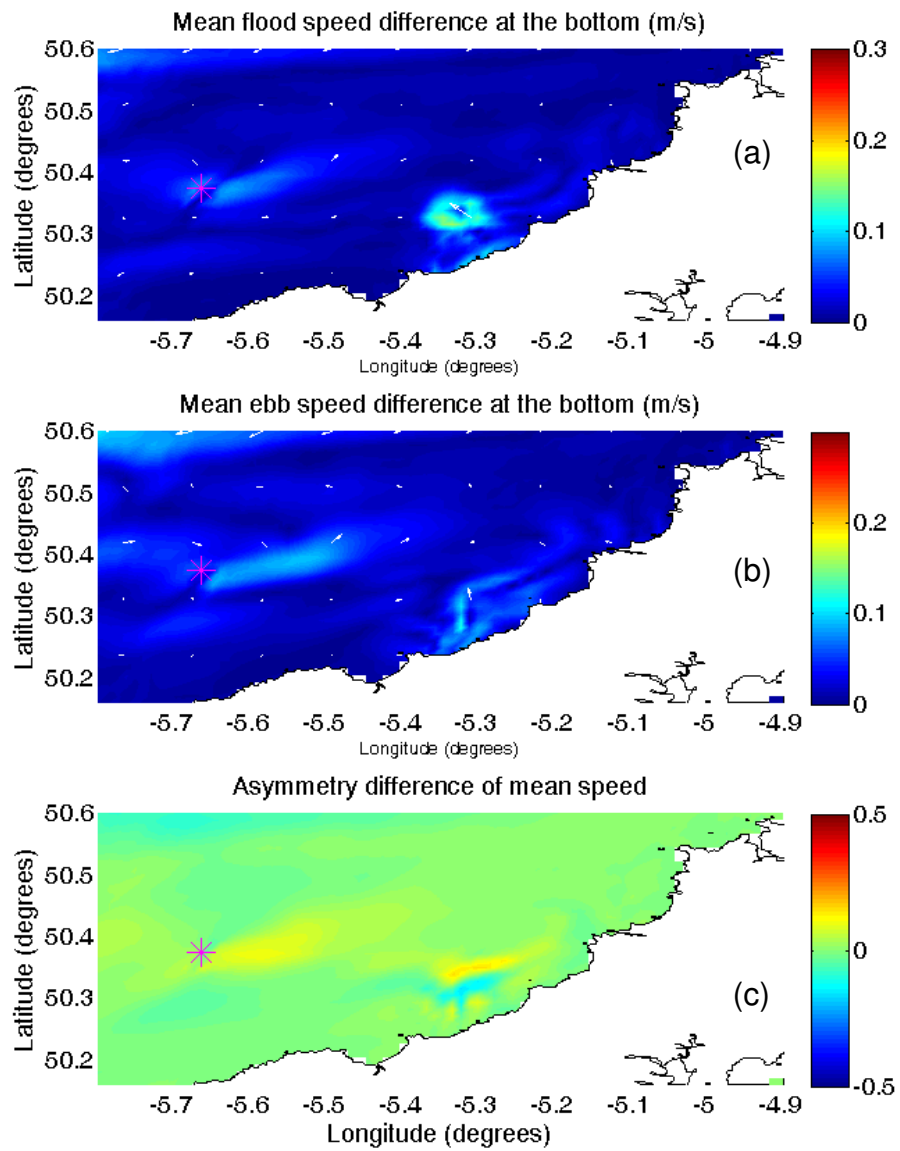Figure 5.12 Mean flood (top) and ebb (middle) current speeds at the storm peak. Asymmetry index (bottom) to weight between flood and ebb. (*) The wave farm.

5.4.5 Bottom stress

Figure 5.13 shows the bottom shear stress, at the high, mid and low water levels. The wave contribution on the bottom stress is large compared to tides only, driving the sediment transport at the most, particularly during the storm peak. This was discussed in Section 4.7.2, where bottom stress comparisons were carried out, showing the significant effects of the wave action, especially through the radiation stress. The bottom shear stress in Figure 5.13 is also found to correlate with the currents field.

Figure 5.14 shows the bottom shear stress for flooding and ebbing conditions, for both cases it is quite similar with an increase in the bottom stress by wave action in the nearshore areas. This is because the waves contribute more to the bottom stress than tidal currents. Figure 5.14a shows the mean flood bottom stress, up to 5 N/m^2, is higher in the nearshore areas rather than for mean ebb conditions, this can be observed around the upper bay of St. Ives and at the top right corner of the plot. These areas, where the wave energy is concentrated, there are major impacts on bottom friction and sediment transport. Vectors show the mean direction and magnitude of the bottom stress.

Mean ebbing results for bottom stress (Figure 5.14b) show and increase towards offshore and southwards where the bathymetry is relatively shallow. As for mean flood conditions, higher values, up to 5 N/m^2, are observed around the St. Ives bay. Ebb conditions show less uniform bottom stress along the coast, upwards from St. Ives bay, different from flood conditions. However, higher values of bottom stress are more uniform towards the south coast, mainly for shallow waters. Vectors show the mean direction and magnitude of the bottom stress.

Normally the asymmetric index ranges from -1 to 1, comparing flood and ebb conditions. However, for display purposes, in Figure 5.14c, the index has values from -0.5 to 0.5. This means that in terms of intensity both flood and ebb conditions can be similar. Assessing the control index, it is clear that the mean flood tide has a more significant impact on the bottom stress than the ebb tide. Again, the mean flood dominates over the mean ebb conditions, close to nearshore areas, however, there is a small area upwards from St. Ives bay where ebb conditions dominate, this might be highly correlated by change in the bottom by the morphological model.

The asymmetry index difference for bottom stress, shown in Figure 5.15c, confirms that mean flood conditions dominate over ebb conditions, even the wave farm reduces the bottom stress significantly. It worth mention that most of the significant changes in mean ebb bottom stress, by the wave farm, are correlated with the ebb dominance of the difference in mean flood speed.
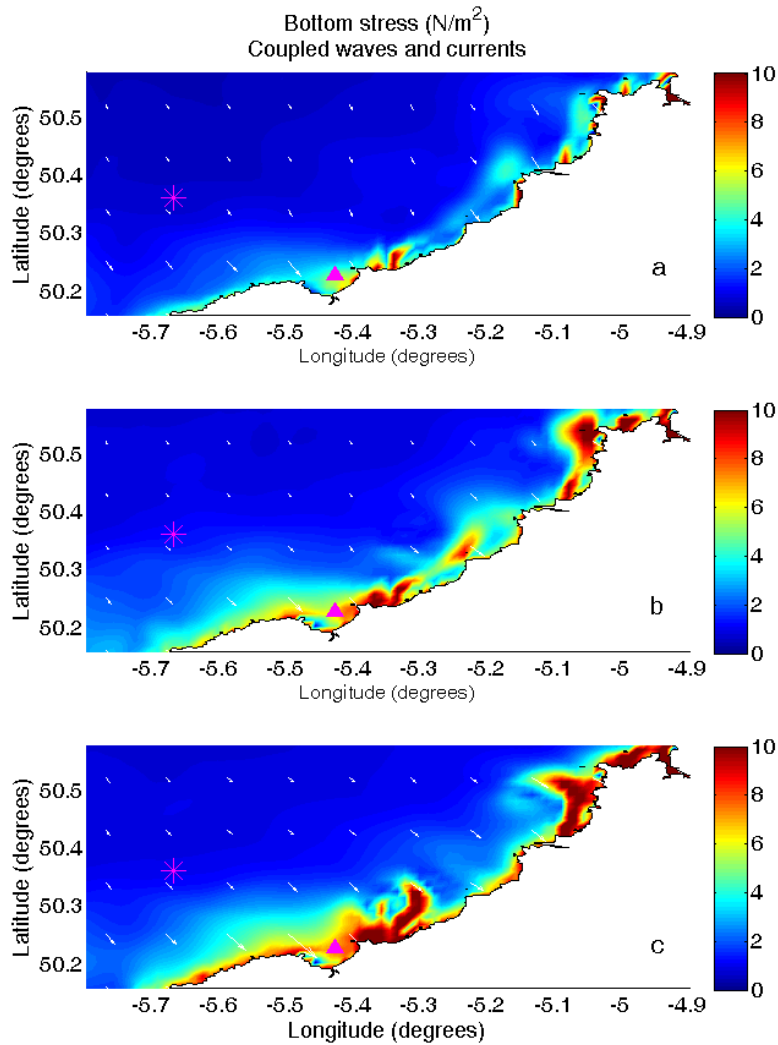
Figure 5.13 Bottom stress for the full wave-current interaction and bottom stress vectors (arrows), at high (a), mid (b) and low (c) water elevations. The figure indicates the location of St. Ives Bay (▲), and the Wave Hub site (*).
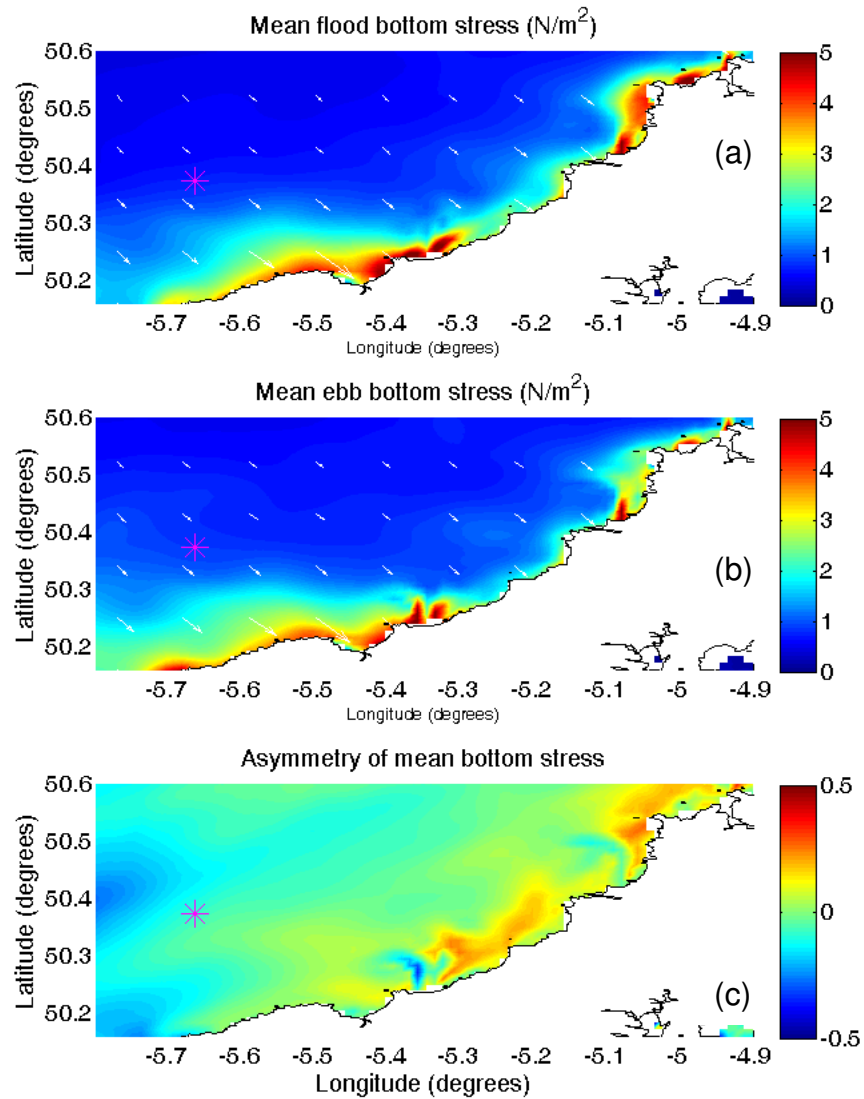
Figure 5.14 Mean flood tide for bottom stress during the storminess (a), mean ebb tide for bottom stress (b), the asymmetric relationship between the mean flood bottom stress and mean ebb bottom stress (c). Vectors are the mean direction for flood/ebb bottom stress. The wave farm (*).

5.4.6 Bottom stresses affected by the wave farm

In Figure 5.15 it can be observed that the bottom stress, especially in the leeside of the wave farm, is affected significantly by the wave farm. Also, the regions where the bottom stress is significantly affected are the shallow water regions and the nearshore areas. The wave farm impact on the bottom stress is maximum at low water level, which is strongly correlated to the currents field, waves and depth.

The bottom boundary layer (BBL) is very important for sediment transport formulations because the bottom shear stress gradient determines the sediment transport rate, which modifies the bed into ripples and other forms (Warner et al, 2008). The BBL determines the stress exerted on the flow by the bottom, entering to the Reynolds-averaged Navier-Stokes equations as boundary conditions for momentum in the x and y directions, these BBLs are represented in complex formulations (sections 3.4 and 3.5) to represent wave-current interactions over a moveable bed.

In chapter 4 and 5 it was observed that the physical variables for the wave-current interaction, the order of magnitude of waves, tides and bottom stress look according to the literature. Tidal current speeds, for the coupled system, show enhanced currents at spring tides and at high waves, weak currents are present due to neap tides and low wave heights.

Bottom shear stress is a controlling factor for the sediment transport. It directly controls the intensity and pathway of the bed load transport. For suspended load, it dominates suspended concentration in an indirect way through its effects on the entrainment processes between the seabed and water column. (Wu et al, 2011).
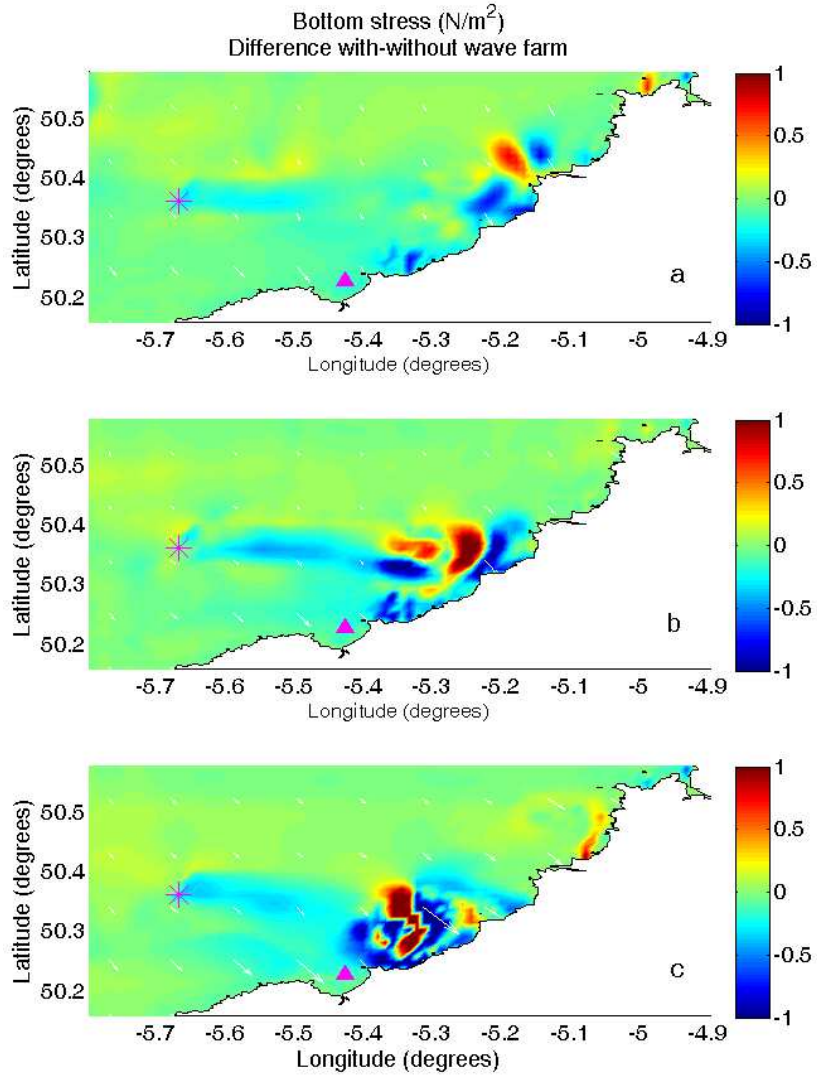
Figure 5.15 Bottom stress differences, for high (a), mid (b) and low (c) water elevations, with and without the wave farm and bottom stress vectors (arrows). Note that for the case of low water level, the wave farm has a significant effect on the bottom stress. St. Ives Bay (▲), Wave Hub site (*).

The described methodology in Sections 5.4.1 and 5.4.2 is applied to the test case that includes the wave farm. Results for the bottom stresses show similar values for both flooding and ebbing as the ones without the wave farm, to contrast both cases Equation 5.4 was applied to see the difference, with-without the wave farm.

The magnitude difference, shown in Figure 5.16a, indicates that for flooding conditions there is an impact on the lee and along the nearshore zone of the wave farm up to 0.5 N/m^2. Bottom shear stress alterations by the wave farm are mainly in these areas and show that the influence of the wave farm reaches a wider area from St. Ives bay to upwards, and this influence is mainly in the nearshore area, in general, it can be observed that in the lee and nearshore areas of the wave farm there is a reduction in bottom stress due to a decrease in the wave energy transmitted.

Figure 5.16b shows the mean ebb difference of bottom stress, because the water level is lower, the magnitude difference is more significant than flooding. This is observed in the lee of the wave farm with higher effects during the ebb period. In the nearshore, the magnitude difference of bottom stress shows significant changes where significant magnitudes of mean current speed where detected (Figures 5.8 and 5.10), suggesting a major reduction in bottom stress by the wave farm during ebb conditions.

The asymmetry index difference for bottom stress, shown in Figure 5.16c, confirms that ebb conditions dominate over flood conditions, even the wave farm reduces the bottom stress significantly. It worth mention that most of the significant changes in bottom stress, by the wave farm, this ebb dominance is correlated to the difference in mean flood speed.
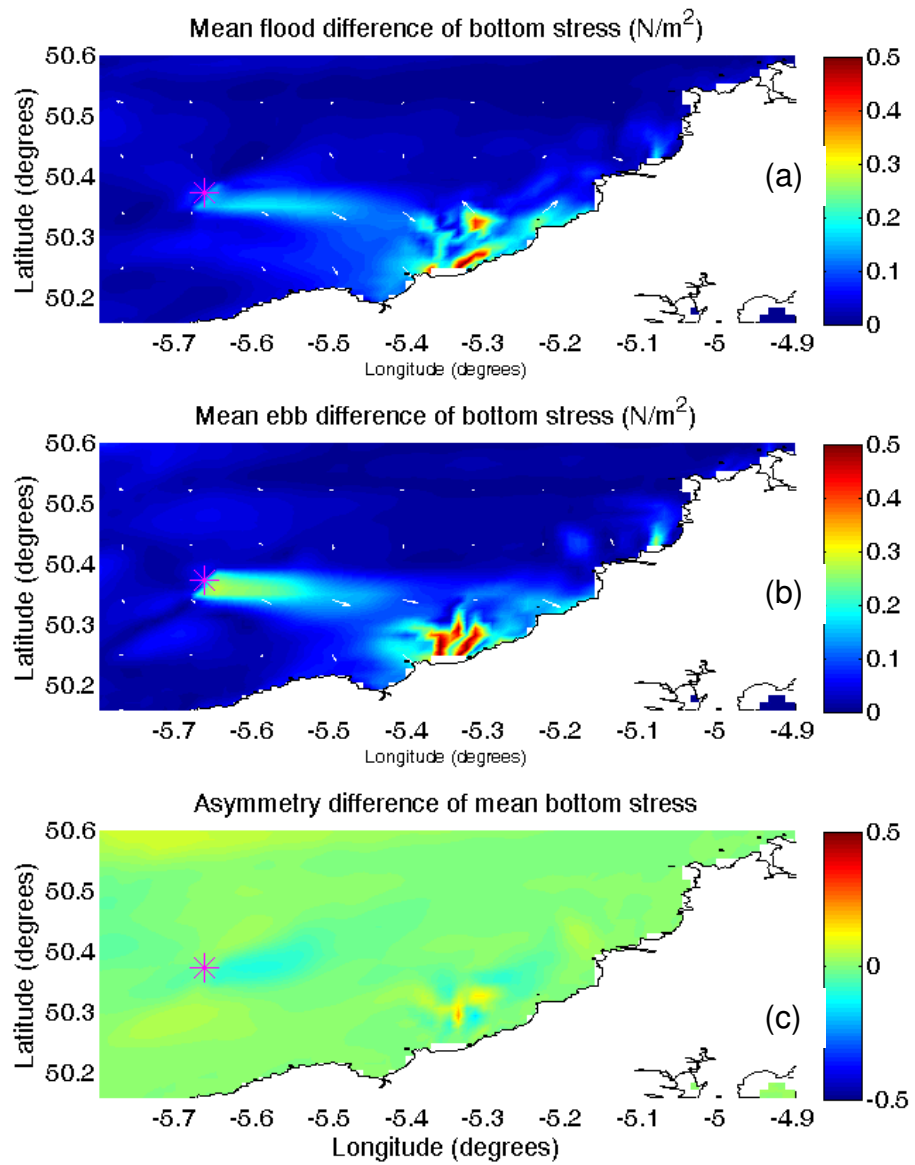
Figure 5.16 The difference of with and without the wave farm for mean flood bottoms stress (a), the difference for mean ebb bottom stress (b), and the difference of asymmetric indexes for bottom stresses (c). Vectors are the mean direction difference for flood/ebb bottom stress. The wave farm (*).

5.5 Discussion

Wave-current interaction has been analysed and validated in the presence of the wave farm (see Chapter 4). Wave induced currents are through a combination of stresses in the water column, especially in the surf zone where waves break. Waves and currents are coupled through physical interactions or processes like surface shear stresses that transmit the stress to the water column affecting shallow waters; bottom stresses enhanced by the action of waves modifying the water column; and radiation stresses produced by breaking waves increasing the turbulence mixing, driving long-shore and cross-shore currents.

Since this period differs from the previous period for model validation (see Section 4.3), additional model validations were carried out for November 2010. Water elevations were compared against tide gauges at four locations and wave heights were compared with the wave buoy data at three locations. The comparisons between computed water elevations and the measurements from four tidal gauges around the study area show good agreements. The same is true for computed wave heights and wave buoys measurement comparisons. In general, the predicted wave heights closely follow the wind speed, and the storm events are reproduced reasonably well. In comparison with the measurements, the storm peak was slightly under-predicted in areas where water depths were relatively shallow.

In this chapter a new testing period has been applied due to the available data observations, also a refined nesting approach has been setup to improve the modelling performance. Results show acceptable comparisons and accuracy in terms of sea surface level and significant wave height, as well as, wave period and direction. Three main storm events are observed during the new test case. The maximum storm event has been

analysed to observe the effect of the waves and the wave farm on the tidal circulation. The tidal circulation is split into a flood and ebb periods. Bottom stresses and currents are significant during the flooding tide than during the ebbing tide. Also, wave farm effects have a significant impact on the tidal currents and wave parameters, even the bottoms stress experiences substantial changes by the wave action in nearshore areas, during the flood tide.

Analysis of averaged flood and averaged ebb cases show that, in general, flood conditions dominate over ebb ones. For averaged current speeds ebb conditions dominate, especially where low water depths are present. With the presence of the wave farm, the current speed is reduced in lee side of the wave farm. Also, significant changes in the current speed by the wave farm are observed during flood conditions.

Averaged flood and ebb conditions of bottom stress show a significant dominance of the flood over ebb cases during the storminess, even, the bottom stress is reduced with the presence of the wave farm, particularly in its lee side. The bottom stress shows a significant change by the wave farm for flood conditions, this is observed in the dominant index for the bottom stress.

Further analyses are needed to study the wave-current interactions, by refining the domain to study a particular site, because along the coast of the Southwest of England the bathymetry and sediment properties vary, thus, the wave farm impact would also vary along the coast.

6. Effects of the wave farm on morphodynamics

6.1 Introduction

To study the effects of the wave farm on the sediment transport and morphological changes, a similar analysis as in Chapter 5, is carried out for the wave farm effect on the sediment transport and morphological changes in the adjacent coastal region. After the model validation on hydrodynamics, the morphological modules were implemented to compute the sediment transport and bathymetry changes for the cases with and without the presence of the wave farm. The analysis is aimed for the same period of simulation, as in Chapter 5, of 48 hours of storminess during November 2010, where three storm events at the Wave Hub site were observed (see Figure 5.3 for details).

In order to assess the morphology changes due to the wave farm, a morphology analysis is performed to correlate the sediment transport during and after the storminess period. Bedload transport rates show a reduction in magnitude when the wave farm is present, reducing the erosion of the sea bed, thus deposition of sediments is observed in the lee side of the wave farm. This can be observed in the final bottom bed or bathymetry, after the storminess period of simulation. An asymmetric coefficient to assess the dominant tide half cycles (averaged flood or averaged ebb conditions) is discussed. In general, the averaged flood cases are dominant over the averaged ebb cases. However, ebb conditions dominate towards offshore in the lee side of the wave farm, when the wave farm is present. Significant morphology changes are observed in the lee side of the wave farm and in the nearshore coastal areas during and after the storm. Although, the

modelling system may over-estimate the morphological changes, the model predictions are qualitatively acceptable.

6.2 Suspended sediment concentration

In the coupled modelling system, bedload transport rates are calculated by the Soulsby and Damgaard (2005) formulae, which accounts for the combined effects of waves and currents on bedload flux. The suspended load is transported in the water column by solving the diffusion-advection equation, with an additional source/sink term added accounting for vertical settling velocity and erosion. In this section suspended sediments are analysed due to the wave farm effects. First, analyses of the impact of the wave farm on the sediment concentration by varying the water elevations or tidal cycles, as seen in Chapter 4. Then, the analysis of the effects of tidal cycles averaged as flood and ebb cases to assess the impact of the wave farm on the suspended sediments.

Figure 6.1 shows a snap shot of the suspended sediment concentration field during the peak of the storm (see Figure 5.3), with the plots corresponding to the fully coupled wave-current model. It is worth mentioning that at low tide (bottom panel) the sediment concentration is increased near the coast, this is because storm waves enhance the bottom stress in spite of low tidal currents, and thus, the sediment transport and erosion rates occur with more intensity. When tidal currents speed are maximum (mid panel) the bottom stress produces a uniform concentration along the coast, with major concentrations occurring where erosion is taking place (red areas). At high water and low tidal currents (upper panel) the impact of the storm has its minimum (compared to the other two cases).

In Sections 5.4.4 and 5.4.6 the effects of the wave farm on hydrodynamics and bottom stresses at high, mid and low water elevations were discussed and compared. Here, a similar analysis is presented, but for the case of storminess during November 2010.
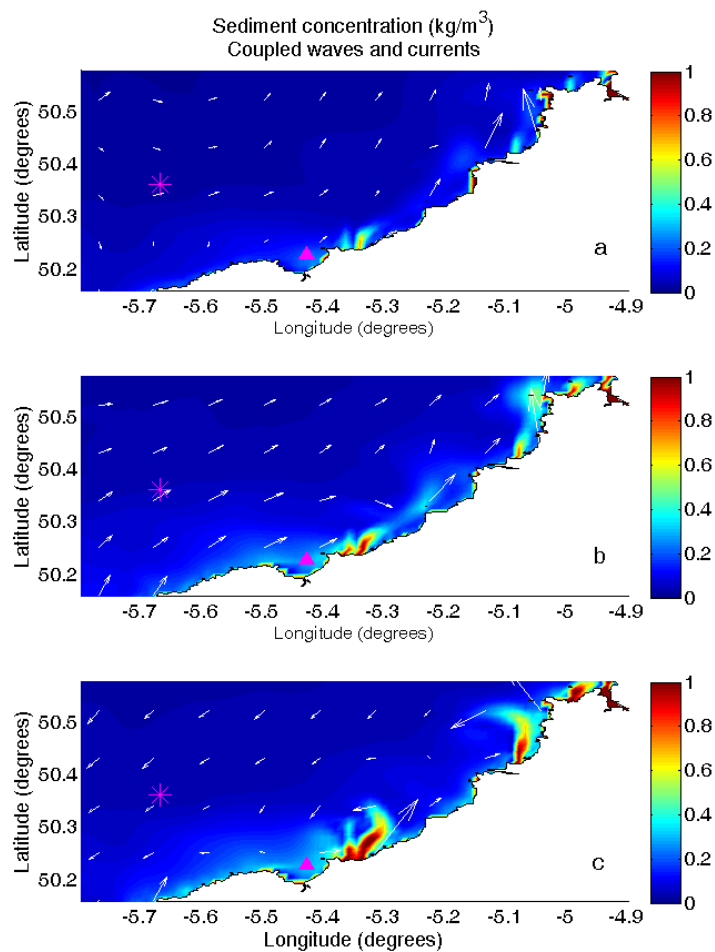
Figure 6.1 Effects of the wave farm on suspended sediment concentration under high (a), mid (b) and low (c) water levels. Vectors are magnitude and direction of current speed, colour indicates the magnitude. St. Ives Bay (▲), Wave Hub site (*).

The results show that sediment concentrations are large at low tides along the coastline during the storm peak. As expected, the bottom stress distribution (shown in Figure 5.13) has a strong correlation with the sediment concentration distribution (shown in Figure 6.1). When the tidal currents are close to zero, as is the case at high and low tide (top and bottom panels, respectively), wave farm impacts on sediment transport distribution is mainly due to the waves. The maximum changes in sediment concentration by the wave farm are from -0.1 to 0.1 kg/m^3 during the tidal cycle and occur at the lee of the wave farm and near the coast north of St. Ives Bay. During the tidal cycle, the sediment concentration affected by the wave farm extends about 26 km upwards from St. Ives Bay at high tide. On the other hand, at the low tide, the sediment concentration moves slightly offshore, mainly in the lee side of the wave farm, presenting the highest concentrations.

Figure 6.2 shows the difference between Figures 6.1, without the wave farm, and the case where the wave farm is included. For high water level (upper panel) the sediment concentration difference shows the largest wave farm impact occurs on the leeside of the wave farm and in the nearshore area. Also in the upper panel it is observed that when the tidal currents are small, wind waves or storms have the largest impact on the change of sediment transport. Three main areas where impacts are large, are observed; these areas have sediment concentrations of less than 0.05 kg/m^3. For the case of mid water level (mid panel) the wave farm causes an increase in sediment concentration at two well-defined nearshore areas. A major concentration change in the lee of the farm was also detected, presumably due to a decrease in wave height and water level. For the case of low water level, as expected, the sediment concentration is enhanced in the area where the bottom shear stress is decreased. Also in Figure 6.2 it is observed an increase of sediment concentration by the wave farm as the water level is reduced at the peak of

the November 2010 storms, implying that even during storms the wave farm causes significant changes in sediment transport.

In general, the following phenomena have been observed in both, theory (Van Rijn, 1993) and model results (Figure 6.1):

- Increase of sediment concentrations due to increase of wave height.

- In combined waves and currents, sediment transport is dominated by mixing processes. Mixing effects are small for weak currents and large for strong currents.

- Near-bed sediment concentrations are mostly influenced by wave-induced currents.

- Wave direction might be a minor influence on the suspended sediment concentration.

- The boundary layer theory is limited by its basis (e.g. sinusoidal waves, etc).

- Wave-induced transport is not included in the current modelling system (e.g. wave stir up, sediment and current transport).
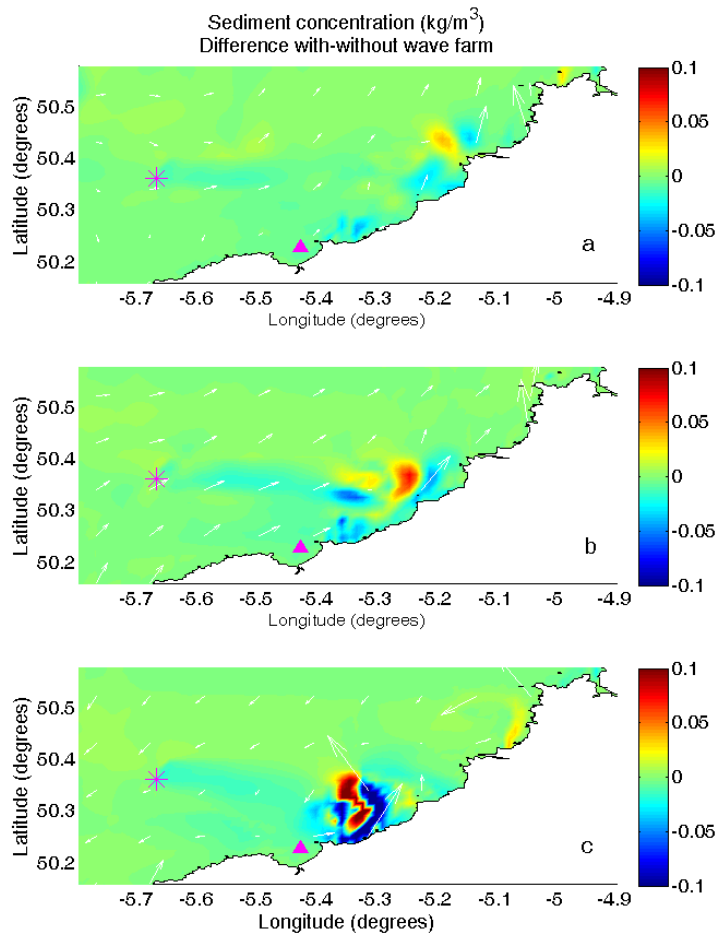
Figure 6.2 Sediment concentration difference with and without the wave farm (colours) and velocity vectors (arrows), at high (a), mid (b) and low tide (c). St. Ives Bay (▲), Wave Hub site (*).

In Section 5.4 forty-eight hours of storminess were averaged as mean flood and mean ebb cases, taking as reference the tidal cycle from the trough to the crest and vice-versa, and extracting the magnitude of the currents for every cell of the domain through the forty-eight hours. Here the same method is applied to analyse the suspended sediments and subsequently in the following sections the bedload transport rate. Applying the same methodology as in Section 5.4.1, the averaged tidal cases for sediment concentrations are represented in Equation 5.1 for the mean flood tide and Equation 5.2 for the mean ebb tide.

Figures 6.3a and 6.3b correspond for mean flood and mean ebb suspended sediment concentrations, respectively. Figure 6.3a shows the mean flood sediment concentration with the highest values, up to 0.3 kg/m^3, close to the nearshore areas, this can be observed around the upper bay of St. Ives and at the top right corner of the plot. These areas, where the wave energy is concentrated, there are major impacts by the wave action on bottom friction, bottom stress, and thus, the sediment transport concentration. Vectors show the mean direction and magnitude of the current speed.

Mean ebbing results for sediment concentration (Figure 6.3b) show and increase towards offshore and southwards where the bathymetry is relatively shallow than deep depths. As for mean flood conditions, higher values, up to 0.3 kg/m^3, are observed around the St. Ives bay. Ebb conditions show less uniform bottom stress along the coast, upwards from St. Ives bay, rather than flood conditions. However, higher concentrations of sediment concentration are more uniform towards the south coast, mainly for shallow waters. Vectors show the mean direction and magnitude of the current speed.
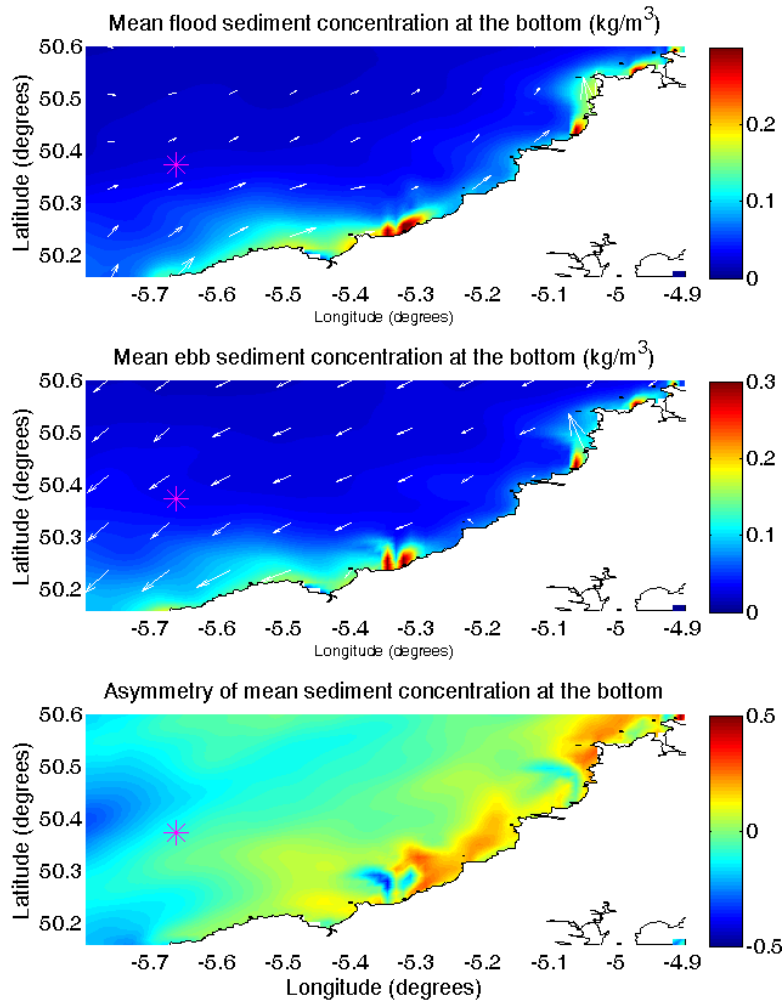
Figure 6.3 Mean flood tide for sediment concentration during the storminess (a), mean ebb tide for sediment concentration (b), the asymmetric relationship between the mean flood sediment concentration and mean ebb sediment concentration (c). Vectors are the mean direction for flood and ebb bottom current speeds. The wave farm (*).

In a similar way, Equation 5.3 is applied to obtain the asymmetry index to quantify the dominant conditions that drive the nearshore processes during storms and to compare the suspended sediment transport between the mean flood and mean ebb conditions. The asymmetry index is applied to distinguish between the magnitude of sediments for flood and sediments for ebb conditions.

Normally the asymmetric index ranges from -1 to 1, comparing flood vs ebb conditions for the sediment concentration the index has values from -0.5 to 0.5, this means that in terms of intensity both flood and ebb cases can be similar. Evaluating the control index, it is clear that flood tide have a more significant impact on the sediment concentration than ebb tide. The mean flood dominates over the mean ebb case, close to nearshore areas, however, there is a small area upwards from St. Ives bay where ebb conditions dominate, this might be highly correlated by the change in the bed by the morphological model.

6.3 Suspended sediment concentration affected by the wave farm

Results for suspended sediment concentrations, with the presence of the wave farm, show similar values for both flooding and ebbing as the ones without the wave farm, to contrast both cases Equation 5.4 was applied to see the difference, with-without the wave farm.

The magnitude difference, shown in Figure 6.4a, indicates that for flooding conditions there is an impact on the leeside and along the nearshore zone of the wave farm up to 0.03 kg/m^3. The sediment concentration changes by the wave farm are mainly in these areas and show that the influence of the wave farm reaches a wider area than for ebb periods from St. Ives bay to upwards, and this influence is mainly in the nearshore area,

in general, it can be observed that in the lee and nearshore areas of the wave farm there is a reduction in sediment concentration due to a decrease in the wave energy transmitted.

Figure 6.4b shows the mean ebb difference of sediment concentration, because the water level is lower, the magnitude difference is more significant than flooding. This is observed in the lee of the wave farm with higher effects during the ebb period. In the nearshore, the magnitude difference of sediment concentration shows significant changes where significant magnitudes of mean current speeds were detected (Figures 5.8 and 5.11), suggesting an increase in sediment concentration by the wave farm during ebb conditions.

The littoral transport in the lee of the wave farm decreases due to the attenuated wave and long-shore currents in the area sheltered by the wave farm. This causes trapping of sand in the lee, depending on the hydrodynamic conditions, as the wave farm reflects and dissipates the incoming wave energy, thus, it reduces wave heights and shore erosion in the shadowed area of the wave farm. Moreover, the littoral transport of sediments is deposited in the lower wave energy region. The diversion of the long-shore currents will cause the development of local erosion close to the heads of the obstacle or the wave farm. The wave farm, represented by an obstacle in this study, traps sand under all circumstances, hence, its long-term impacts on the coastline are expected to be significant.

The asymmetric index was applied to quantify the dominant conditions that lead the nearshore processes of sediment concentrations during storminess. The asymmetry index difference for the sediment concentration, shown in Figure 6.4c, confirms that flood conditions dominate over ebb conditions, even when the wave farm increases the

sediment concentration. It worth mention that most of the significant changes in sediment concentration by the wave farm, the mean flood case dominance is correlated to the similar analysis observed for mean flood bottom stress (Figure 5.15).
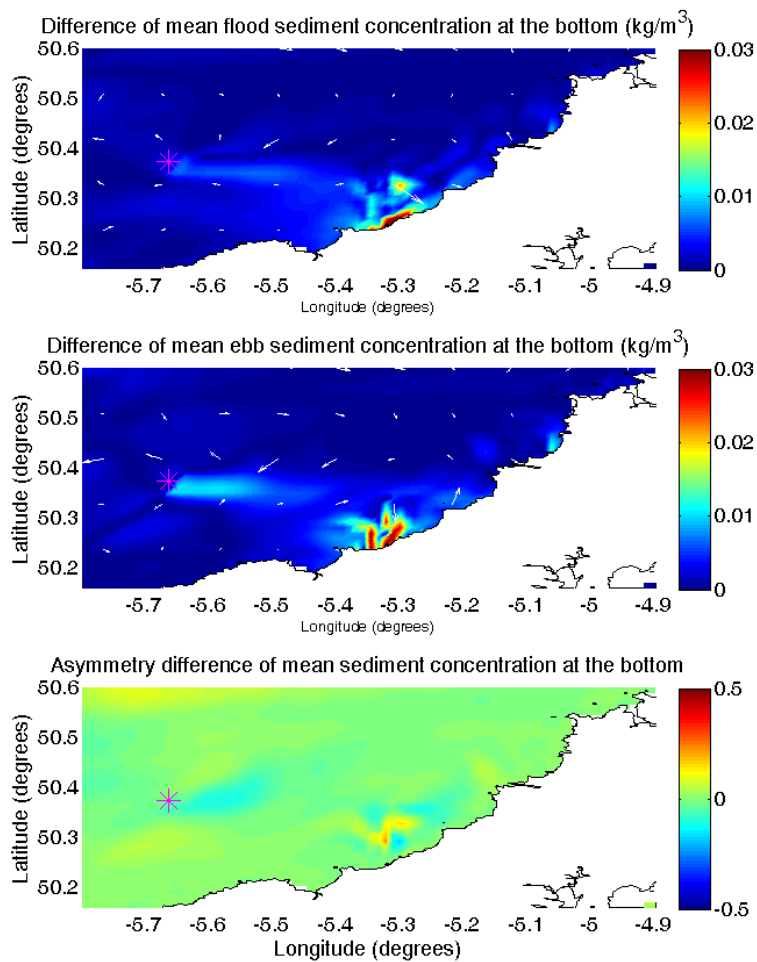
Figure 6.4 The difference of with and without the wave farm for mean flood sediment concentration (a), the difference for mean ebb sediment concentration (b), and the difference of asymmetric indexes for sediment concentration (c). Vectors are the mean direction difference for flood and ebb current speeds. The wave farm (*).

6.4 Bed-load transport rate

The bed load layer is considered as a layer in which the mixing due to turbulence is so small that it cannot influence the sediment particles, thus, suspension of particles is impossible in the bed load layer. In general for most models, the bedload transport is treated as a function of the near-bed velocity or bed shear stress, in 2DH models the bed shear stress follows the depth-averaged flow, whereas in 3D models it follows the near bed flow. Also, the waves interact with the current in modifying bed shear stress, bed ripples, sediment mobility and the near-bed current, transporting the sediment (Roelvink & Reniers, 2012). The total sediment transport rate is usually an important quantity to address practical applications such as engineering works in coastal areas (Soulsby, 1997): dredging channels, morphodynamic changes by coastal structures, obstacles, etcetera.

The changes of the seabed are calculated from the convergence or divergence in sediment fluxes, which are the sum of suspended and bed load transport (Warner et al, 2008). Bed load transport vectors are partitioned into x and y components, q_x and q_y, based on the magnitude of the bed shear stresses of waves and currents. Figure 6.5 shows the horizontal components of bed load transport rate for the two hot spots of erosion (A) and deposition (B) due to the presence of wave farm shown in Figure 6.10. The bed load transport at B is about one order of magnitude larger than that at A. It is evident from the bottom panel of Figure 6.5 that the peak of wave height is closely correlated with the peaks of bed load rates.

Figure 6.6 shows the comparison of bed load rates with and without the wave farm at locations A and B in Figure 6.10 in a similar way, the bed load rate (left panels) is one order of magnitude larger at B than that at A. Figure 6.6 also shows that, bed load rates

are markedly reduced by the presence of the wave farm during the storm peaks, where the peak sediment transport is weakened and dispersed.

The under-predicted wave height by the wave model implies significant influence by local wind-waves as the model is being forced from swell (offshore) waves, also the resolution of the horizontal grid size (~300 m) is quite coarse to be compared to a single point, and the minimum depth in the near-shore is around 5 m.

With regards to the effect of these under-predicted hydrodynamic conditions on the morphology changes, Amoudry and Souza (2012) have analysed several sediment transport and morphology models. They show that even the most advanced model to date has higher uncertainties about the results. This is due to strong amplification of any small errors in the hydrodynamics, which is explained by the power-law dependence of the sediment transport rates on the flow velocities, introduced by Soulsby and Damgaard in 2005 for combined waves and currents. The amplification of hydrodynamics on sediments is as follow: Power = 3 is for the bed-load transport and Power > 3 for suspended load. They conclude that present sediment transport models rely on the specification of physical parameters which themselves exhibit large variability and uncertainty.
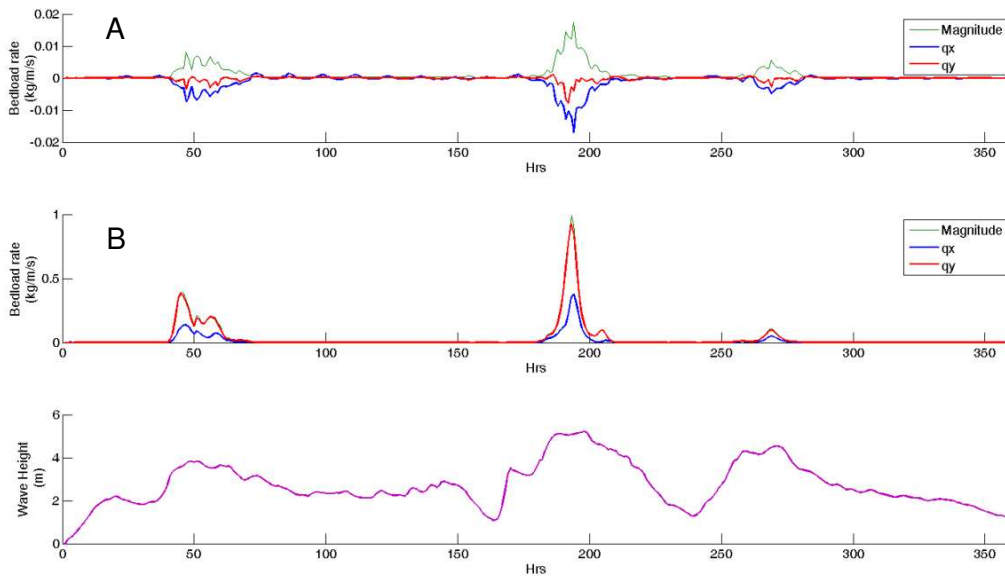
Figure 6.5 Time evolution of magnitude, x- and y- components of bed load transport rate at location A and B indicated in Figure 6.10.
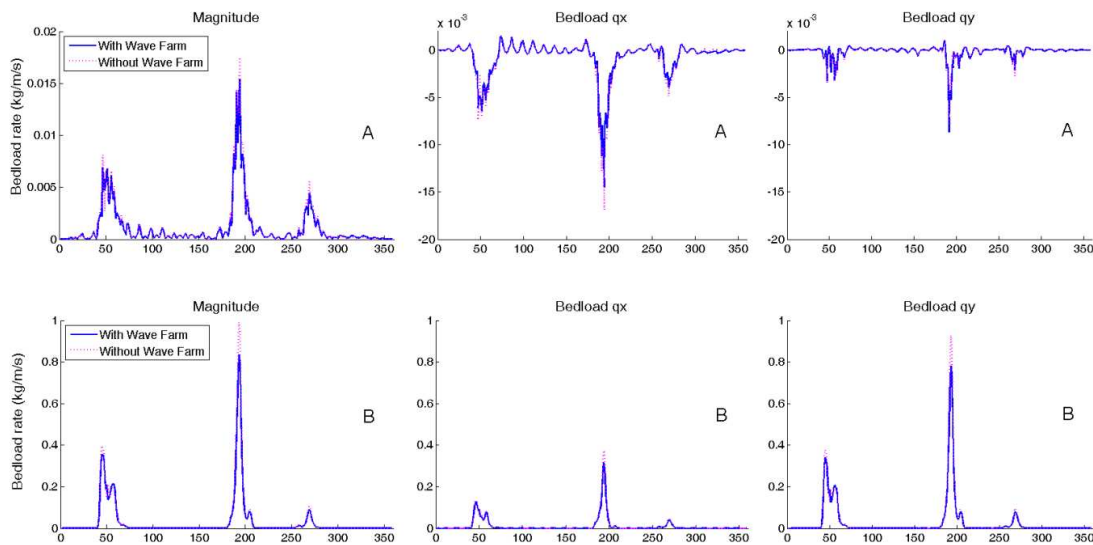
Figure 6.6 Time evolution of the bed load rate difference with and without wave farm at locations A and B indicated in Figure 6.10. Magnitude (left panels); x-components (middle); y-components (right panels).

In a similar analysis of the Section 6.2 and applying equations 5.1 and 5.2, the bed-load transport rate has been separated as mean flood and mean ebb cases during forty-eight hours of storminess (see Figure 5.3 for maximum wave heights).

Figures 6.7a and 6.7b show the mean flood and mean ebb cases, respectively, during the storm for the bedload rate transports. In both cases the same area between St Ives and Perranporth is highlighted. The rate for the mean flood case is more confined on nearshore areas, especially towards the northeastern part of St. Ives Bay where higher transport rates are observed. Mean ebb tide shows an extended bedload rate towards the offshore with similar bedload rates as the mean flood tide. Around the Wave Hub site the bedload rate transport is negligible. Values of bedload transport rates for both, flood and ebb cases, are up to 0.02 kg/m/s.

To assess the dominant tidal cycle condition during the highest storm event, the well applied asymmetry index, it has been applied to the bedload transport rates. Applying the equation 5.3, Figure 6.7c shows the asymmetric difference between flood and ebb conditions. During the storminess event it is observed that flood have dominance over ebb conditions along the coast and nearshore zones. However, in the area north-eastwards of St. Ives Bay, and more specifically in offshore zones, ebb conditions have dominance over flood conditions, it is also observed where higher bedload rates are detected, suggesting that in shallow depths ebb conditions might dominate over the flood cases.
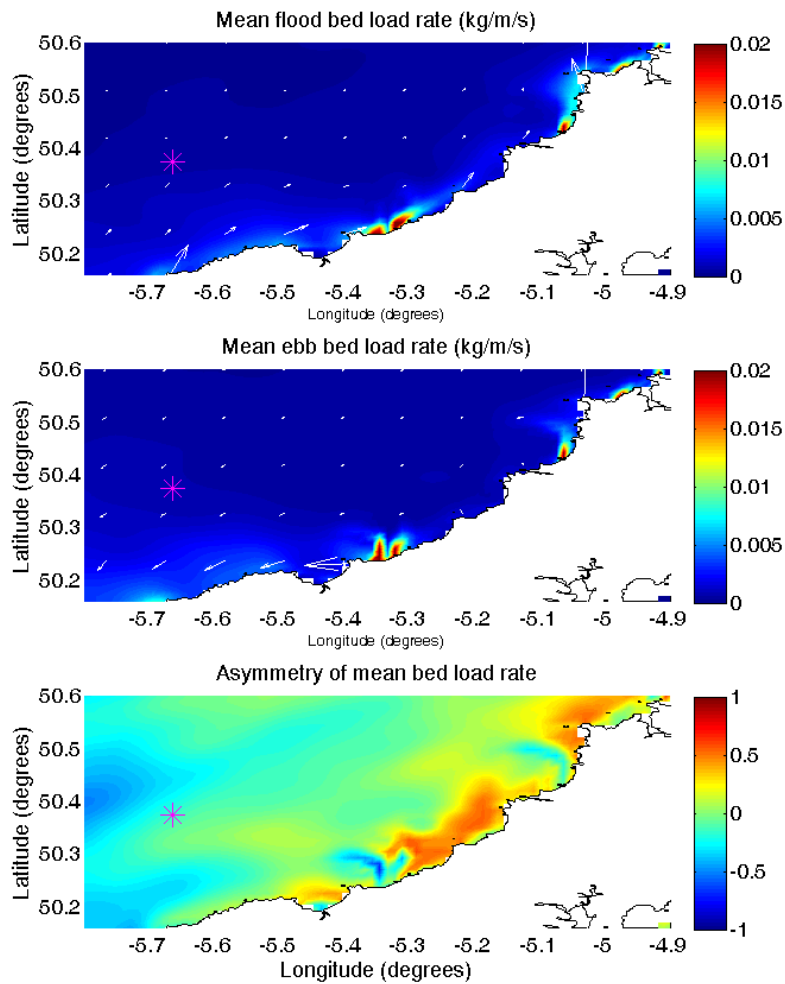
Figure 6.7 Mean flood tide for bed-load during the storminess (a), mean ebb tide for bed-load (b), the asymmetric relationship between the mean flood bed-load and mean ebb bed-load (c). Vectors are the mean direction for flood and ebb bed-load transport rates. The wave farm (*).

6.5 Bed-load transport rate affected by the wave farm

Analysing the bedload transport rates with the presence of the wave farm, Equations 5.1 and 5.2 have been applied again during the storminess detected in Figure 5.3. Figure 6.8a shows the difference between the mean flood cases for bedload transport rate without the wave farm and with the wave farm, applying the Equation 5.4. Similarly, Figure 6.8b shows this difference but for mean ebb cases. Comparing these two snapshots for storm conditions, it can be observed that the wave farm has a significant impact on the magnitude of bedload rate for the mean ebb case, and this impact is noticeable towards nearshore. These bedload differences by the wave farm suggest a reduction in erosion rates producing more deposition of the sediments in these areas, particularly on the lee side of the eave farm and its nearshore zone. However, the impact by the wave farm, for the mean flood case, is smaller and more spreadable, not only along the coast but also towards the offshore areas.

Finally and applying Equations 5.3 and 5.4, the asymmetry index difference in the Figure 6.8c indicates that the wave farm has more impact on mean ebb conditions, particularly at the northeast of St. Ives Bay and outside the nearshore area, where higher rates are observed. On the other hand, bedload transports affected by the wave farm for the averaged flood conditions might dominate in a wider area of nearshore zones, suggesting also a reduction of the erosion rates. According to the asymmetry index, the mean flood case is dominant in the lee side of the wave farm, however, mean ebb cases are relatively dominant is shallower areas.
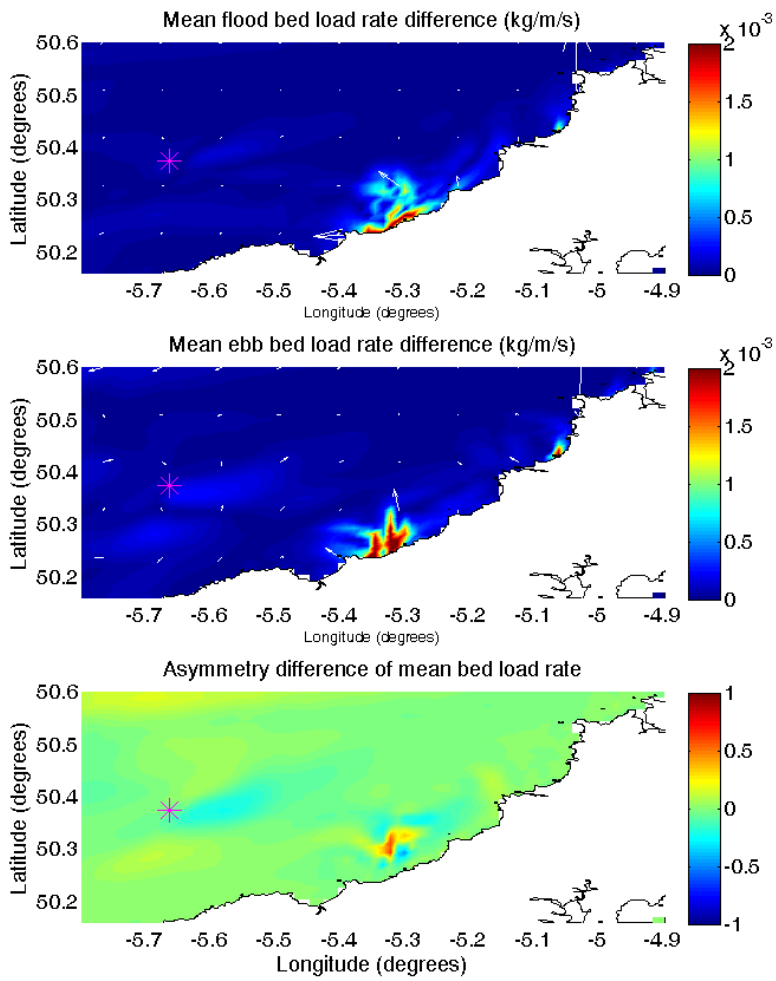
Figure 6.8 The difference of with and without the wave farm for mean flood bed-load (a), the difference for mean ebb bed-load (b), and the difference of asymmetric indexes for bed-load transport rates (c). Vectors are the mean direction difference for flood and ebb bed-loads. The wave farm (*).

6.6 Effects of the wave farm on morphological changes

Due to the use of the coupled modelling system, the effect of morphological changes on flow and sediment transport is dynamically incorporated in the model. Figure 6.9 shows the bed level changes over a 16-day simulation. This simulation covers the period of three storms occurring in November 2010. Figure 6.9(a) shows the bed level changes when there is no wave farm, and Figure 6.9(b) shows the bed level changes where there is a the wave farm at the Wave Hub site. The general patterns of erosion and deposition appear to be similar in both cases: the most significant morphological changes are found in three bays along the coast, and the range of the change is from -1 m to 1 m. The difference of the morphological changes with and without the wave farm is shown in Figure 6.10.

The overall impact of the wave farm is found to shift the sediment transport from the westerly in St Ives Bay, resulting in the eastern area being more eroded rather than the western area being less eroded, however, the area near the shore is being accreted. To further examine the bed load transport in this area, two locations where the most deposition and erosion occurred are identified, A and B in Figure 6.10. These locations correspond to the maximum wave farm effects on bed shear stress (see Figures 6.5 and 6.6, respectively) and sediment concentration are observed. At the end of the simulation both erosion and deposition occur, with bathymetry differences between -2 and 2 meters caused by the presence of the wave farm.

The results show that the area near St. Ives Bay is the area most affected by the wave farm. As before, this is expected as this area is located in the leeside of the wave farm and the predominant waves are north-easterly. The presence of the wave farm is found

to cause more deposition in the south-west area and more erosion in the north-east area close to the St. Ives Bay, where most bed changes are taking place.
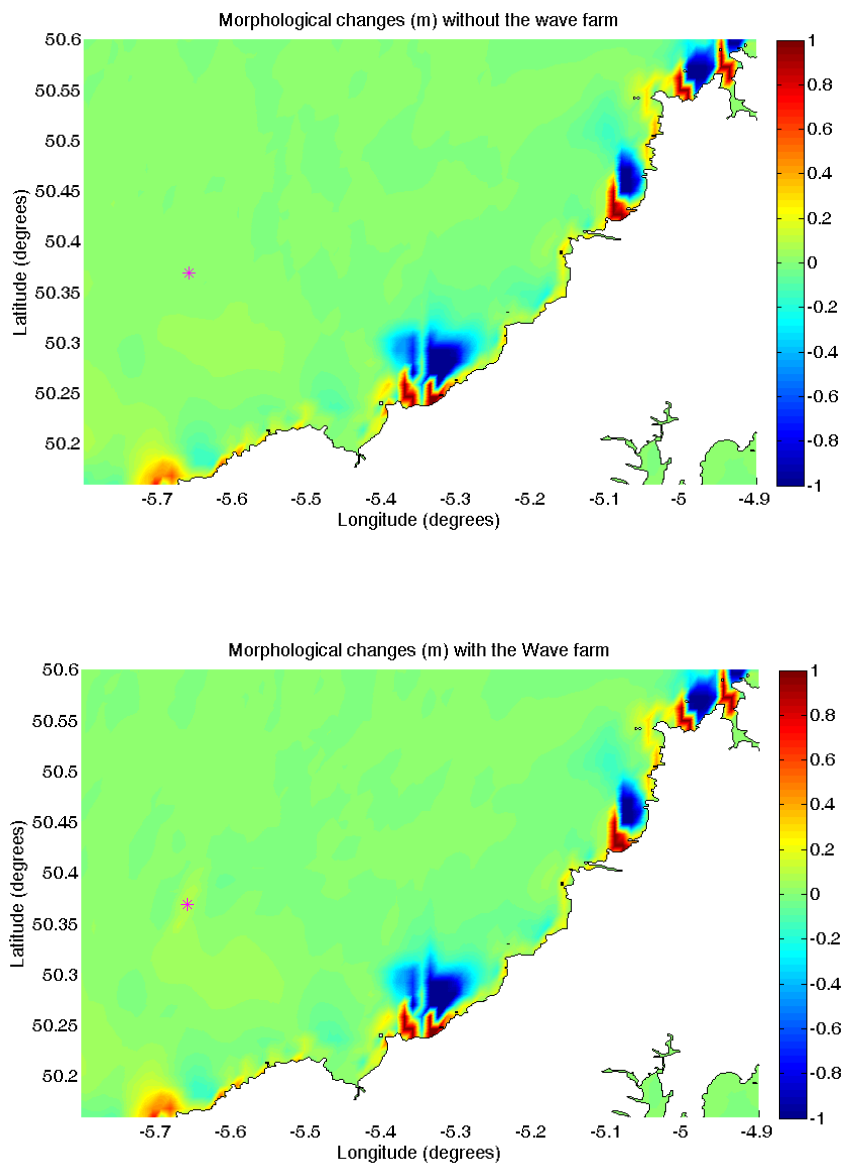
Figure 6.9 Morphological changes after 16 days of simulation without the wave farm (top) and with the wave farm (bottom).
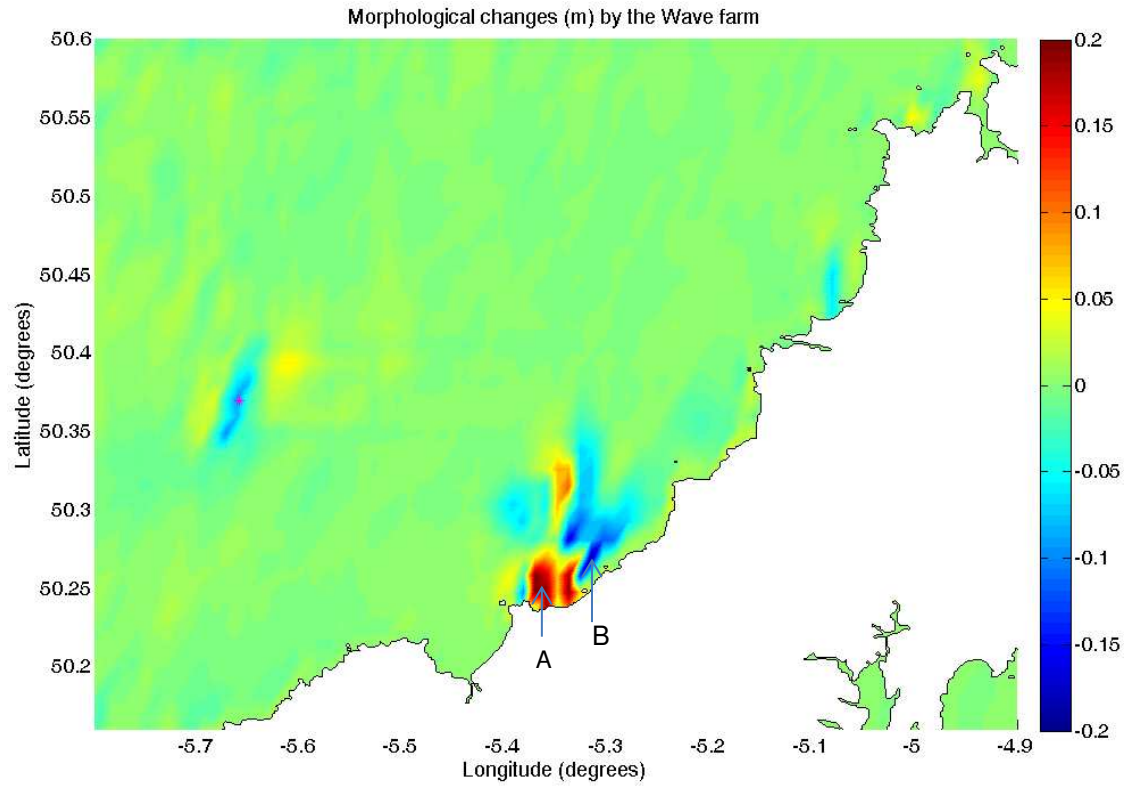
Figure 6.10 Difference in morphological change with and without the wave farm after 16 days of simulation. Red area shows erosion at point A, Blue area shows deposition at point B

6.7 Discussion

In the Southwest of England, the tides are the main force that drives the nearshore circulation and therefore the sediment transport along the coast. However, wind waves play an important role driving long-shore and cross-shore currents and sediments within the near shore region, especially during storm events when most of the sediments are transported.

The bottom stress becomes larger at low tide and high wave, and also at mid-tide and high wave. This change occurs not only in the nearshore zone but also in some parts of the offshore area, which suggests that the sediment transport changes significantly during the tidal cycle and storm peak. The bottom stress difference with and without the wave farm shows significant variations at the low water level case, strongly correlated to the wave contribution through radiation stresses, which is enhance at relatively shallow water

During the storminess simulation period three storm events were presented (see Figure 5.3 for details), significant changes near the shoreline are found by the presence of wave farm. Significant changes on the final bathymetry affected by the wave farm are also observed. In general, erosion occurs towards the coast from isolines 10 to 30, this is correlated with the direction of bottom stress vectors distribution, also a small accretion is presented in the northeast of St Ives bay. The significant impacts of the wave farm on the morphological changes are again found in the coastal area near St. Ives Bay, as well as in immediate lee side of the wave farm. The bed changes indicate a northward shift of erosion and deposition pattern due to the wave diffraction caused by the wave farm.

The maximum changes in sediment concentration with and without the wave farm are from -0.1 to 0.1 kg/m3 at low tide and occur at the lee of the wave farm, the changes are much more profound in the nearshore area north of St Ives Bay. From low tide to high tide, the sediment concentration extends about 26 km upwards from St. Ives Bay along the coast. At the low tide, the sediment concentration moves in slightly offshore. These results are closely correlated to the bottom stress results. The bedload rate flux is considerable reduced when the wave farm is positioned in the study area, also it is shown that at the peak of the three storm events, the bedload rate flux is decreased.

The effect of the wave farm was also examined at two locations A and B, where stronger deposition and erosion of 0.2 m occurs, respectively. These locations are at the lee of the wave farm and near the coast slightly north of St Ives Bay, where maximum impact of wave farm on sediment concentration and bed shear stress are predicted by our model. We also found that the bed load transport at these areas is considerably reduced when the wave farm is positioned in the study area, suggesting deposition of sediments in the lee side of the wave farm and its nearshore zones.

In general, averaged flood conditions dominate over the averaged ebb cases during the storminess period, as shown for the suspended sediment concentrations and bedload transport rates. The mean ebb cases showed dominance on shallower depths, which are in the nearshore area. The wave farm impacts on sediments and bedload transports for mean flood conditions extend not only in the lee side but also in a wider area close to the nearshore, whereas the wave farm effects for mean ebb conditions are more consistent and significant in the lee side.

7. Conclusions

This research is to study the impact of a wave farm on the wave-current interaction at its nearshore area in the Southwest of England, particularly its interaction with the sediment transport and coastal morphology, using an integrated modelling system. The modelling system consists of SWAN and ROMS to take account for the impacts from the wave farm and for the wave-current interaction, with the wave farm incorporated. The built-in morphodynamic modules also enable the sediment transport at the study site to be simulated, as well as, the impacts of the wave farm on morphological changes.

The highly complex modelling system was set up at the Wave Hub site at the Southwest of the UK and validated comprehensively with the field data available to the study, with the multi-layer nested grids, driven by wave boundary conditions from the WAVEWATCH III model and wind fields from the GFS model, as well as the tidal boundary conditions from the global tidal model OTIS. The modelling simulations were carried out on the High Performance Computing clusters at both Plymouth and Exeter Universities, supported by the Peninsula Research Institute for Marine Renewable Energy (PRIMaRE).

7.1 Main findings

The main findings from this study can be summarised as the following:

1. Model validation shows the model results are in good agreement with the measurements by tide gauges and wave buoy.

2. Significant wave heights are better predicted by the model when the coupled modelling system is implemented, indicating significant effect of current on

waves. Wave effects on bottom stress are isolated by removing the tidal signals from current velocity and bottom stress. The tidal currents and wind waves have a significant effect on the bed shear-stress, relevant to sediment transport. The contribution from wave dominant over tide during storm events.

3. Model results at high, mid and low tides during the peak of a storm, occurring between 1st of December 2005 and 31st January 2006, were presented to show tidal effects on waves, current velocities and bottom stresses, during spring tides. It is found that the wave height increases with the tidal elevation, and the wave direction is modified by the change of direction of tidal currents. It was also found that the tidal current effect on waves is maximum when the tidal current is at its peak and the tidal elevation change has a significant effect on wave directions. The tidal current effect on wave direction is relatively small when wave height is large. In order to improve the accuracy of the model results, a refinement of the grid domain was required.

4. In Chapter 4 results, the finer grid has a resolution of about 500 meters in the x and y directions, and 3 layers in the vertical. In the Chapters 5 and 6, a grid resolution of 300 m was used and 5 layers in the vertical. The new grid domain was tested with a new testing period due to the availability of observations to validate the modelling system, which shows acceptable comparisons and accuracy with the water elevations and wave properties.

5. The change of the wave height, with and without the wave farm, varies between 5 cm and 10 cm at the nearshore area, and the maximum extension affected by the wave farm is about 26 km from St. Ives Bay to upwards at the high water level case.

6. The bottom stress becomes larger at high waves combined with low and middle tidal levels. This change occurs not only in the nearshore zone but also in some parts of the offshore area, which suggest that sediment transport changes significantly during the tidal cycle and storm peak.

7. The analysis of the mean flood and mean ebb tidal conditions during a storminess period indicates that current speed, bottom stress, suspended sediment concentrations and bed-load transport rates are affected by the wave farm with the reduction of current velocities and bottom stresses in the lee side of the wave farm, resulting in deposition of sediments.

8. The sediment transport model was incorporated to estimate the non-cohesive concentration and morphology changes affected by waves, tides and the wave farm.

9. It was found that the suspended sediment concentration is higher at the lee of the wave farm, presumably because the longshore current is partially blocked by the circulation currents (in the lee), so that some of the longshore currents are diverted outside the wave farm.

10. The littoral transport in the lee of the wave farm decreases due to the attenuated wave and longshore currents in the area sheltered by the wave farm. This causes the trapping of sand in the lee, depending on the hydrodynamic conditions, as the wave farm reflects and dissipates some of the incoming wave energy, thus, it reduces wave heights and shore erosion in the shadowed area of the wave farm. Moreover, the littoral transport of sediments is deposited in the lower wave energy region. The diversion of the longshore currents will cause the development of local erosion close to the heads of the obstacle or the wave farm.

An obstacle, in this case the wave farm, traps sand under all circumstances, hence, there will be a coastal impact in any circumstance.

11. Suspended sediment concentrations show a similar pattern to the bed-load transport. However, the sediment concentration reaches large scales along the coast during the flood and ebb tidal cycles. The dominance of the mean flood case during a storm event for sediment concentrations suggests that the significant changes in the sediments are produced not only by the storm but also by the tidal currents along the coast.

12. The sediment concentration with the presence of the wave farm shows similar patterns for the mean flood and the mean ebb cases, in the asymmetry index, mean flood and mean ebb sediment concentrations are similar in magnitude, suggesting that the wave farm has significant changes in its leeside towards the coast.

13. Bedload transport rates during mean flood conditions show dominance over those of during mean ebb conditions. The mean flood conditions are confined to the nearshore area along the upstream coast, whereas the mean ebb conditions are extended towards offshore areas, particularly in shallower areas. Bedload transport rates with the presence of the wave farm show a significant increase in the magnitude, particularly on nearshore areas in the lee side of the wave farm. For the mean flood case, the bed-load rate is not only confined to the coast but also along the coast. For the mean ebb case, the increase of bed-load rate by the wave farm presents higher magnitudes than the mean ebb case, also the difference is noticed towards offshore as mentioned above.

14. The morphology changes by the wave farm suggest that the area near St. Ives Bay is the most affected by the wave farm. Because it is in the lee side of the wave farm and the predominant waves are north-easterly. The presence of the wave farm is found to cause more deposition in the south-west area and more erosion in the north-east area close to the St. Ives Bay, where most bed changes are taking place.

15. Erosion is present because the bottom shear stress is the dominant force that drives the sediments, when this force is reduced, the bedload transport rate is reduced as well.

The results of this study provide important and useful information for further studies in assessing the resources of wave energy and the impacts of the wave farm on the local and nearshore environment. Model results will be further examined for longer term impacts of the WEC operations.

The interaction between waves and tides at the Wave Hub site is important when modelling sediment transport influenced by the wave energy devices. The addition of wind fields on the circulation model is compulsory to determine the effect of surface stresses on waves and currents. The analysis on sediment transport shows that the largest impact on sediment transport due to the wave farm occurs near the coast rather than at the Wave Hub site.

7.2 Recommendations for future research

The integrated modelling system is capable to predict hydrodynamic and morphological changes during storm and normal conditions, affected by the deployment of wave energy devices. The modelling system under-estimates the wave parameters, which can be improved in a nested and finer grid resolution, this will improve the comparison of model results against data observations. Underestimate peak wave is typical. Finer resolution not necessarily solves the problem. Need to discuss other source of error of SWAN such as error in wind inputs, storm track.

Different sediment diameters can be set in the ROMS, for this research only one D_{50}=0.35 mm was used, representing the averaged sediment size diameter around the Wave Hub site. However, this does not represent all the sediment classes along the coast, even the main composition of most of the beaches is rock. Therefore, there is the need for the study of small nearshore areas, covering different sediment classes. The use of coarse grid resolutions brings uncertainty when validating the model against a single point. Therefore, it is recommended to use finer resolutions through the two-way coupled nested parent and child grid domains for best results. With a refined modelling system, well calibrated, will help to better understand the impacts of wave energy devices on nearshore coastal areas, which is still at its infancy.

With regards to the impacts of the wave farm on hydrodynamics and morphology changes, the analysis of these physical variables presented in this research were focused during short periods of storminess. Hence, there is a need to continue the study over longer-term, covering summer and winter seasons.

References

Amoudry, L.O. and A. Souza. 2011. Deterministic coastal morphological and sediment transport modelling: a review and discussion. Reviews of Geophysics 49, RG2002/2011, 2010RG000341.

Babarit, A. and Hals Jorgen. 2011. On the maximum and actual capture width ratio of wave energy converters. Proceedings: European Wave and Tidal Energy Conference.

Babtie Group Ltd. 2002. Hayle Harbour hydrodynamics modelling report. in South West of England Development Agency (2006). Wave Hub Development and Design Phase, Coastal Processes Study Report. http://www.wavehub.co.uk/.

Beels C., P. Troch, G. Backer, M. Vantorre, J. Rouck. 2010. Coastal Engineering. 57, 471-492.

Bertin Xavier, Anabela Oliveira, André B. Fortunato 2008, Simulating morphodynamics with unstructured grids: Description and validation 3 of a modeling system for coastal applications, Ocean Modelling, doi:10.1016/j.ocemod.2008.11.001.

Bolanos R. J. Wolf, J. Brown, P. Osuna, J. Monbaliu, A. Sanchez-Arcilla. 2008. Comparison of wave-current interaction formulation using the polcoms-wam wave-current model. International Conference of Coastal Engineering.

Booij, N., Ris, R.C., Holthuijsen, L.H. 1999. A third generation wave model for coastal regions, part I, model description and validation. Journal of Geophysical Research 104 (C4), 7649-7666.

Booij, N. 2008. SWAN Demo Course, Digital Hydraulics Holland BV, www.digital-hydraulics.com/download

Bowen, A. J. 1969. The generation of longshore currents on a plane beach, J. Mar. Res., 27, 206–214.

Bowen, A.J. D.L. Inman and V.P. Simmonds. 1968. Wave 'set down' and set-up. J. Geosphys. Res., 73, 2569-2577.

Buscombe D.D. & Scott T.M. 2008. The Coastal Geomorphology of North Cornwall, Wave Hub Impact on Seabed and Shoreline Processes – Report, http://www.research.plymouth.ac.uk/whissp/index.html

de Boer G.J. 2008. On the interaction between tides and stratification in the Rhine Region of Freshwater Influence, Phd Thesis, Technische Universiteit Delft.

Carter G.S. and Merrifield M.A. 2007. Open boundary conditions for tidal simulations, Ocean Modelling 18, 194-207.

Cavaleri L. The WISE Group L., J.-H.G.M. Alves, F. Ardhuin, A. Babanin, M. Banner, K. Belibassakis, M. Benoit, M. Donelan, J. Groeneweg, T.H.C. Herbers, P. Hwang, P.A.E.M. Janssen, T. Janssen, I.V. Lavrenov, R. Magne, J. Monbaliu,M. Onorato, V. Polnikov, D. Resio, W.E. Rogers, A. Sheremet, J. McKee Smith, H.L. Tolman, G. van Vledder, J. Wolf, I. Young. 2007. Wave modelling – The state of the art, Progress in Oceanography 75, 603–674.

Chapman D. 1985. Numerical treament of cross-shelf open boundaries in a barotropic coastal ocean model, JPO, 15, 1060-1075.

Chen, Q. and I.A. Svendsen. 2003. Effects of cross-shore boundary condition errors in nearshore circulation modelling. Coast. Engrg., 48, 243-256.

Cox, D.T., N. Kobayashi, and A. Okayasu. 1995. Experimental and numerical modelling of surfzone hydrodynamcis. Res. Rep. No. CACR 95-07, University of Delaware. pp293.

Cruz J. 2008. Ocean Wave Energy, Green Energy and Technology – current status and future perspectives. Springer, pp. 427.

Dean R. G. 1991. Water wave mechanics for engineers and scientists, World Scientific Publishing, 353 pp.

Dyke P. 2007. Modelling Coastal and Offshore processes, Imperial College Press, Cambridge., 400 pp.

Egbert, Gary D., Svetlana Y. Erofeeva. 2002. Efficient Inverse Modeling of Barotropic Ocean Tides. J. Atmos. Oceanic Technol., 19, 183–204.

Engquist, B and Majda. 1977. Absorving boundary conditions for the numerical simulations of waves. Math. Comp., 31, 139, 629-651.

Flather, R.A. 1976. A tidal model of the north-west European continental shelf. Memoires de la Societe Royale des Sciences de Liege 6 (10), 141–164.

Fredoe, J. and R. Deigaard. 1992. Mechanics of coastal sediment transport. World Scientific, Singapore, 369pp.

Galvin, C.J. and P.S. Eagleson. 1965. Experimental studyof longshore currents on a plane beach. U.S. Army Corps of ewng. Res. Center, Tech. Mem. 10, 1-80.

Givoli, D. 1991. Non-reflective boundary conditions. J. Comp. Phys., 94, 1-29.

Goda Yoshimi. 2008. Wave setup and longshore currents induced by directional spectral waves: prediction formulas based on numerical computation results, Coastal Engineering Journal, vol. 50, 397-440.

Grant, W.D., Madsen, O.S. 1979. Combined wave and current interaction with a rough bottom. Journal of Geophysical Research 84 (C4), 1797-1808.

Grant, W.D., Madsen, O.S. 1986. The continental shelf bottom boundary layer. Ann Rev. Fluid Mech., 18, 265-305.

Greenberg, M.D. 1988. Advanced engineering mathematics. Prentice Hall, Eaglewood Cliffs, New Jersey 07632. pp 946.

Haas K.A., Warner J.C. 2009. Comparing a quasi-3D to a full 3D nearshore circulation model: SHORECIRC and ROMS, Ocean Modelling 26, 91-103.

Hamilton, D.G. and B.A. Ebersole. 2001. Establishing uniform longshore currents in a large-scale sediment transport facility. Coastal Engineering, 42, 199-218.

Hansen, J.B. 1990. Periodic waves in the surf zone: Analysis of experimental data. Coast. Eng., 14, 14-41.

Hansen, J.B. and I.A. Svendsen. 1979. Regular waves in shoaling water experimental data. Inst. Hydrodyn. Hydraul. Eng., Tech. Univ. Denmark, Lyngby, Ser. Pap., 21.

Hedström K. S. 2009. Technical Manual for a Coupled Sea-Ice/Ocean Circulation Model (Version 3). U.S. Department of the Interior, Minerals Management Service, Anchorage, Alaska, Contract No. M07PC13368.

Higdon, R.L. 1986. Absorving boundary conditions for difference approximations to the multidimensional wave-equation. Math. Comp., 47, 176, 437-459.

Higdon, R.L. 1987. Numerical absorving boundary conditions for the wave equation. Math. Comp., 49, 179, 65-90.

Horikawa K. 1987. Nearshore dynamics and coastal processes. University of Tokyo Press. 522 pp.

Howarth, M. J. 1982. Tidal currents of the continental shelf, pp. 10-26, in Offshore Tidal Sands (ed. A. H. Stride). London: Chapman & Hall, 222 pp.

Howarth M.J. 1990. Atlas of tidal elevations and currents around the British Isles. Proudman Oceanographic Laboratory, UK.

Jonsson, I.G. 1966. Wave boundary layers and friction factors. 10th Int'l. Coast. Eng. Conf., Tokyo.

Jonsson, I.G. and N.A. Carlsen. 1976. Experimental and theoretical investigations in an oscillatory rough turbulent boundary layer. J. Hydr. Res., 14, 1, 45-60.

Kamphuis, J.W. 1975. Friction factor under oscillatory waves. ASCE J. Wtrway. Harbors Coast. Engrg. 101, 2, 135-144.

Kantha L.H., Clayson C.A. 2000. Numerical models of oceans and oceanic processes. Academic Press, International Geophysics Series, Volume 66, pp. 981.

Kemp, P.H. and R.R. Simons .1983. The interaction of waves and a turbulent current: Waves propagating against the current. J. Fluid Mech., 130, 73-89.

Kobayashi, N., A.K. Otta and I. Roy. 1987. Wave reflection and runup on rough beaches. ASCE J. Waterw. Port, Coast. and Oc. Engrg., 113, 3, 282-298.

Larson J., Jacob R., Ong E. 2005. The model coupling toolkit: A new Fortran90 toolkit for building multiphysics parallel coupled models. International Journal of High Performance Computing Applications 19, 277-292.

Le Roux J. P. 2002. Wave friction factor as related to the Shields parameter for steady currents, Sedimentary Geology Volume 155, Issues 1-2, 10 January 2003, Pages 37-43.

Lesser, G.R., Roelvink, J.A., van Kester, J.A.T.M., Stelling, G.S. 2004. Development and validation of a three-dimensional morphological model. Coastal Engineering 51, 883–915.

Lewis, A., S. Estefen, J. Huckerby, W. Musial, T. Pontes, J. Torres-Martinez. 2011. Ocean Energy. In IPCC Special Report on Renewable Energy Sources and Climate Change Mitigation [O. Edenhofer, R. Pichs-Madruga, Y. Sokona, K. Seyboth, P. Matschoss, S. Kadner, T. Zwickel, P. Eickemeier, G. Hansen, S. Schlömer, C. von Stechow (eds)], Cambridge University Press, Cambridge, United Kingdom and New York, NY, USA.

Li M. 2013. University of Liverpool, School of Engineering, UK – personal communication.

Liu, P. L. and R.A. Dalrymple. 1978. Bottom frictional stresses and longshore currents due to waves with large angles of incidence. J. Marine Res., 36, 357-375.

Longuet-Higgins, M. S. and Stewart, R. W. 1962. Radiation stress and mass transport in gravity waves, with application to 'surf beats', Journal of Fluid Mechanics 13 (4):481–504.

Longuet-Higgins, M. S. and Stewart, R. W. 1963. A note on wave set-up. J. Marine Research, 21, 4-10.

Longuet-Higgins, M. S. and Stewart, R. W. 1964. Radiation stress in water waves, a physical discussion with application. Deep Sea Research, 11, 529-563.

Lundgren, H. 1963. Wave thrust and wave energy level. IAHR Proc. 10th Int. Congr. Assoc. Hydr. Res. London, 1, paper 1.20, 147-151.

Marino-Tapia I. J. 2003. Cross-shore sediment transport processes on natural beaches and their relation to sand bar migration patterns. PhD Thesis, University of Plymouth.

Mei, C.C. 1983. The applied dynamics of ocean surface waves. John Wiley and Sons, Inc., 740pp.

Mellor, G.L. 2004. User's guide for a three-dimensional, primitive equation, numerical ocean model. Program in Atmospheric and Oceanic Sciences, Princeton University, Princeton, NJ 08544-0710.

Millar D.L., Smith H.C.M., Reeve D.E. 2007. Modelling analysis of the sensitive of shoreline change to a wave farm. Ocean Engineering 34, 884-901.

Moon J. 2005. Impact of a coupled ocean wave-tide-circulation system on coastal modelling, Ocean Modelling 8, 203-236.

Mori N. 2007. ROMS memoramdum - open boundary condition, Osaka City University.

Moomaw, W., F. Yamba, M. Kamimoto, L. Maurice, J. Nyboer, K. Urama, T. Weir. 2011. Introduction. In IPCC Special Report on Renewable Energy Sources and Climate Change Mitigation [O. Edenhofer, R. Pichs-Madruga, Y. Sokona, K. Seyboth, P. Matschoss, S. Kadner, T. Zwickel, P. Eickemeier, G. Hansen, S. Schlömer, C.von Stechow (eds)], Cambridge University Press, Cambridge, United Kingdom and New York, NY, USA.

Mulligan, R. P., A. E. Hay, and A. J. Bowen. 2008b. Wave-driven circulation in a coastal bay during the landfall of a hurricane, J. Geophys. Res., 113, C05026, doi:10.1029/2007JC004500.

Mulligan, R. P., A. J. Bowen, A. E. Hay, A. J. van der Westhuysen, and J. A. Battjes. 2008a. Whitecapping and wave field evolution in a coastal bay, J. Geophys. Res., 113, C03008, doi:10.1029/2007JC004382.

Munk W. H. 1950. Origin and generation of waves. Proceedings 1st International Conference on Coastal Engineering, Long Beach, California. ASCE, pp. 1-4.

Niclansen B.A. 2006. An operational wave model for the Faroe Shelf. PhD Thesis, University of the Faroe Islands.

Nielsen, P. 1993. Coastal bottom boundary layers and sediment transport. World Scientific. Singapore, 324pp.

196

NOAA Wavewatch III. NOAA/NCEP Operational Wave Models [online]. Available from: http://polar.ncep.noaa.gov/waves

Olabarrieta M., Warner J.C., Kumar N. 2011. Wave-Current interaction in Willapa Bay, Journal of Geophysical Research, Vol. 116, C12012.

Orlanski I. 1976. A simple boundary condition for unbounded hyperbolic flows. J. Comp. Phys., 21(3):251–269.

Ou, S., J. Liau, T. Hsu, and S. Tzang. 2002. Simulating typhoon waves by SWAN wave model in coastal waters of Taiwan, Ocean Eng., 29, 947 – 971.

Padman L. and Erofeeva S. 2004. A barotropic inverse tidal model for the Artic Ocean, Geophysical Research Letters, vol. 31.

Palha A., L. Mendes, C. Fortes, A. Brito-Melo, A. Sarmento. 2010. The impact of wave energy farms in the shoreline wave climate: Portuguese pilot zone case study using Pelamis energy wave devices. Renewable Energy, 35, 62-77.

Pawlowicz Rich, Beardsley Bob, Lentz Steve. 2002. Classical tidal harmonic analysis including error estimates in MATLAB using T TIDE, Computers & Geosciences 28, 929–937.

Peregrine, D.H. 1976. Interaction of wave s and Currents. Adv. Appl. Mech., 16, 9-117.

Peregrine, D.H. and I.J. Johnson. 1983. Interaction of waves and currents. U.S. Army Corps of Engineers Rws. Center, Misc. Rep. No. 83-6.

Phillips, O.M. 1977. Dynamics of the upper ocean. Cambridge University Press.

Pleskachevsky et al. 2009. Interaction of waves, currents and tides, and wave-energy impact on the beach area of Sylt Island, Ocean Dynamics 59, 451 – 461.

Pradeep C. Fernando, Pengzhi Lin & Junke Guo. 2011. Wave–current interaction at an angle 2: theory, Journal of Hydraulic Research, 49:4, 437-449.

Prandle, D. 1997. The influence of bed friction and vertical eddy viscosity on tidal propagation. Continental Shelf Research 17 _11., 1367–1374.

Pugh, D.T. 1987. Tides, Surges and Mean Sea Level: a handbook for engineers and scientists. Chichester, John Wiley & Sons, 472 pp.

Putrevu, U. and I.A. Svendsen. 1991. Wave induced nearshore currents: A study of the forcing, mixing and stability characteristics. Res. Rep. CARC-91-11, Center for Applied Coastal Res. Univ. of Delaware, 242pp.

Raymond W. H. and Kuo H. L. 1984. A radiation boundary condition for multi-dimensional flows. Quart. J. R. Met. Soc., 110:535–551.

Reeve D.E., Y. Chen, S. Pan, V. Magar, D.J. Simmonds, A. Zacharioudaki. 2011. An investigation of the impacts of climate change on wave energy. Renewable Energy. 36, 2404-2413.

Ris, R., L. Holthuijsen, and N. Booij. 1999. A third-generation wave model for coastal regions: 2. Verification, J. Geophys. Res., 104, 7667 – 7681.

Rogers, W., P. Hwang, and D. Wang. 2002. Investigation of wave growth and decay in the SWAN model: three regional-scale applications, J. Phys. Oceanogr., 33, 366 – 389.

Rogers, W., J. Kaihatu, L. Hsu, R. Jensen, J. Dykes, and K. Holland. 2006. Forecasting and hindcasting waves with the SWAN model in the Southern California Bight, Coastal Eng., 54, 1 – 15.

Roelvink D. & Reniers Ad. 2012. A guide to modelling coastal morphology. Advances in coastal and ocean engineering, vol. 12, World Scientific, pp 274.

Sathaye, J., O. Lucon, A. Rahman, J. Christensen, F. Denton, J. Fujino, G. Heath, S. Kadner, M. Mirza, H. Rudnick, A. Schlaepfer, A. Shmakin. 2011. Renewable Energy in the Context of Sustainable Development. In IPCC Special Report on Renewable Energy Sources and Climate Change Mitigation [O. Edenhofer, R. Pichs-Madruga, Y. Sokona, K. Seyboth, P. Matschoss, S. Kadner, T. Zwickel, P. Eickemeier, G. Hansen, S. Schlömer, C. von Stechow (eds)], Cambridge University Press, Cambridge, United Kingdom and New York, NY, USA.

Scott, T.M., Russell, P.E., Masselink,G., Wooler, A., Short, A.D. 2007. Beach rescue statistics and their relation to near shore morphology and hazards: a case study for Southwest England. Journal of Coastal Research, SI 50,1–6.

Sleath, J. 1984. Sea bed mechanics. John Wiley and Son, New York.

Soulsby, R. L., L. Hamm, G. Klopman, D. Myrhaug, R.R. Simons, and G.P. Thomas. 1993. Wave-current interaction within and outside the bottom boundary layer. Coastal Eng., 21, 41-70.

Soulsby R. 1997. Dynamics of marine sands, HR Wallingford, Thomas Telford Publications, pp 250.

South West of England Development Agency – SWRDA. 2006. Wave Hub Development and Design Phase, SWRDA Group Limited, Coastal Processes Study Report. http://www.wavehub.co.uk/.

Stive, M.J.F. and H.G. Wind. 1986. Cross-shore mean flow in the surf zone. Coast., Engrg. 10, 325-340.

Styles, R. and S.M. Glenn. 2000. Modeling stratified wave and current bottom boundary layers in the continental shelf, JGR, 105, 24119-24139.

Svendsen, I.A. 2006. Intorduction to nearshore hydrodynamics. Advanced series on ocean engineering, Vol 24, World Scientific Publishing Co. Re. Ltd. 722 pp.

SWAN Cycle III version 40.72ABCDEF. 2010. Scientific and Technical Documentation, Delft University of Technology, pp. 119.

Thomas , G.P. 1981. Wave current interactions: An experimental and numerical study. Part 1. Linear waves. J. Fluid Mech., 110, 457-474.

Thorton, E.B. 1970. Variation of longshore current across the surf zone, Proc., 12th Coast. Engrg. Conf., ASCE, Washington, D.C., 291-308.

Ting, F.C.K. and J.T. Kirby. 1994. Observation of undertow and turbulence in a laboratory surfzone. Coastal Engrg., 24, 51-80.

Ting, F.C.K. and J.T. Kirby. 1995. Dynamics of surf-zone turbulence in a strong plunging breaker. Coastal Engrg, 24, 177-204.

Trowbridge, J. and O.S. Madsen. 1984. Turbulent boundary layers, Parts I and II, J. Geophys. Res., 89, C5, 7989-8007.

Van Dongeren, A.R. and I.A. Svendsen. 1977. Absorving-generating boundary conditions for shallow water models. ASCE J. Waterwaves, Port, Coastal, and Ocean Engrg., 123, 6, 303-313.

Van Rijn L. C. 1993. Principles of sediment transport in rivers, estuaries and coastal seas. Aqua publications. 690 pp.

Venugopal, V. Smith, G.H. 2007. Wave climate investigation for an array of wave power devices. Paper presented at the 7th European Wave and Tidal Energy Conference, Porto, Portugal.

Verboom, G.K., G.S. Stelling, and M.J. Officer. 1981. Boundary conditions for the shallow water equations. In: Engineering applications of computational hydraulics (eds. M.B. Abbot and J.A. Cunge), Pitman Publishing, Ltd., London. 230-262.

Warner J.C., Sherwood C.R., Signell R.P., Harris C.K., Arango H.G. 2008a. Development of a three dimensional, regional, coupled wave, current, and sediment transport model. Computers & Geosciences 34, 1284-1306.

Warner J.C., Perlin N., Skyllingstad E.D. 2008a. Using the model coupling toolkit to couple earth system models. Environmental Modeling & Software 23, 1240-1249.

Wolf J., Prandle D. 1999. Some observations of wave-current interaction, Coastal Engineering 37, 471 – 485.

Wu, Y., Chaffey J., Greenberg D.A., Colbo K., Smith P.C. 2011. Tidally-induced sediment transport patterns in the upper Bay of Fundy: A numerical study. Continental Shelf Research doi:10.1016/j.csr.2011.10.009

Zou, Q.P. 2004. A simple model for random wave bottom friction and dissipation. Journal of Physical Oceanography 34 (6), 1459-1467.

Zou, Q.-P., A. J. Bowen & A. E. Hay. 2006. The vertical distribution of wave shear stress in variable water depth: theory and field observations. J. Geophys. Res., 111 (C09032), doi:10.1029/2005JC003300

Zou, Q.P. 2004. A simple model for random wave bottom friction and dissipation. Journal of Physical Oceanography 34 (6), 1459-1467.

Zou, Q.-P., A. J. Bowen & A. E. Hay. 2006. The vertical distribution of wave shear stress in variable water depth: theory and field observations. J. Geophys. Res., 111 (C09032), doi:10.1029/2005JC003300

Appendices

A1. Model forcing

The coupled modelling system has been forced with other global models at the boundaries. The wave SWAN model has been forced by the global model WAVEWATCH III model and the global GFS model for wind fields. The ROMS circulation model has been forced by the global OTIS tide model

1.A.1   Tidal forcing

In order to provide the boundary conditions to the ROMS model, the tide model provided by the Oregon State University Tidal Inversion Software (OTIS) based on the TOPEX/POSEIDON altimeter data (Egbert and Erofeeva, 2002; Padman and Erofeeva, 2004), was used. Predictions of tidal currents and water elevations from eleven harmonic constituents (M_2, N_2, S_2, K_2, O_1, K_1, P_1, Q_1, M_4, MS_4, MN_4) for the studied area were carried out. The high-resolution data assimilation model AOTIM, which is the foundation of the OTIS, fits the available tide height data and also best represents tidal currents. This has been validated since the inverse model is consistent with the shallow-water wave equations to within the assumed accuracy of the bathymetry-based and dissipation terms (Padman and Erofeeva, 2004).

The OTIS model is based on the linear shallow water dynamic equations as follow:

$$\frac{\partial U}{\partial t} + f\hat{z} \times U + g \cdot H\nabla(\zeta - \zeta_{sal}) + F = f_0 \qquad (A.1)$$

$$\frac{\partial \zeta}{\partial t} = -\nabla \cdot U \qquad (A.2)$$

Here ζ is the elevation of the sea surface; U is the volume transport vector, equal to velocity times water depth H; f is the Coriolis parameter, $\hat{z}$ is oriented to the local vertical and F is the frictional or dissipative stress; the astronomical tide generating force with allowance for Earth's body tides is denoted by f_0 (Egbert and Erofeeva, 2002).

Altimeter data was processed using TOPEX/POSEIDON altimeter data for the inversion. Firstly the PATHFINDER database was filtered with a low-pass filter along each ground track, thereafter the TPXO.3 model to obtain the solid Earth tide was applied, these databases are included in a complex solution to correct the solid Earth tides and to eliminate geoid errors. For Topex/Poseidon, time series at most locations are long enough to separate all major constituents, then, it is possible to estimate the vectors of harmonic constants by least-squares method (Egbert and Erofeeva, 2002).

1.A.2   Harmonic analysis

Tide gauge wave-averaged sea level (ζ) measurements can be studied as a sum of three separate time-dependant components: tides, meteorological-induced surge (non-tidal residual) and mean sea level (Pugh, 1987), represented as:

$$\zeta(t) = Z_0(t) + X(t) + Y(t) + XY(t) \tag{A.3}$$

where $Z_0(t)$ is the mean sea level, $X(t)$ the tidal component, $Y(t)$ the meteorological non-tidal residual and $XY(t)$ represents the interaction between tidal and non-tidal levels, which is usually only significant in extensive shallow water areas. This statistical approach of sea level is explained by the relative independence of the physical forces which produce the different components (Pugh, 1987).

The basis of harmonic analysis is the assumption that the tidal variations can be represented by a finite number N, of harmonic terms of the form:

$$H_n cos(\sigma_n t - g_n) \tag{A.4}$$

When H_n is an amplitude, g_n is a phase lag on the equilibrium tide at Greenwich, and σ_n is an angular speed, which should be expressed in radians. The angular speed in degrees per mean solar hour is denoted by $\sigma_n = 360\omega_n/2\pi$. The angular speeds ω_n are determined by an expansion of the Equilibrium Tide into a similar harmonic term (Pugh, 1987).

1.A.3   Least-squares method

The aim of least-squares analysis is to estimate the tidal harmonic constituent amplitudes and phases which can then be used for long-term tidal predictions (Emery and Thomsom, 1997). The least-squares fitting procedure involves matrix algebra, but the equations are very similar to

$$[observed\ level] = [Equilibrium\ tide][empirical\ constants]$$

$$[known] \qquad [known] \qquad [unknown]$$

The tidal variation function is represented by a finite number of N harmonic constituents, depending on the length and quality of the observed data. In the harmonic analysis by least-squares the tidal function is fitted as follows:

$$T(t) = Z_0 + \sum_N H_n f_n cos[\sigma_n t - g_n + (V_n + u_n)] \tag{A.5}$$

Where the unknown parameters are Z_0 and the series (H_n, g_n). The fitting is adjusted so that $\sum S^2(t)$ is the square of the difference between the observed and computed tidal

206

levels $S(t) = O(t) - T(t)$. The f_n and u_n are the nodal adjustments and the terms $\sigma_n t$ and V_n together determine the phase angle of the Equilibrium constituent. V_n is the Equilibrium phase angle for the constituent at the arbitrary time origin. The accepted convection is to take V_n as for the Greenwich Meridian and t in the local time of the station concerned (Pugh, 1987).

1.A.4   Wave forcing

- The SWAN model requires initial and spectral boundary conditions, also wind fields to force the surface layer. The NOAA WAVEWATCH III operational wave model is a 3rd generation (spectral) global wave model. It consists of a set of five wave models, based on version 2.22 of WAVEWATCH III. All models use the default settings of WAVEWATCH III unless specified differently. These models have available online data, either historic or forecast data. In this research, the regional Western North Atlantic (WNA) model is applied.

Regional wave models within the WAVEWATCH III:

- The regional Alaskan Waters (AKW) model

- The regional Western North Atlantic (WNA) model

- The regional North Atlantic Hurricane (NAH) model

- The regional Eastern North Pacific (ENP) model

- The regional North Pacific Hurricane (NPH) model

In the WAVEWATCH III online website the user can obtain information from the regional wave models as follows: All regional models obtain hourly boundary data from

the global model, they are run on the 00z, 06z, 12z and 18z model cycles, and start with a 6h hindcast to assure continuity of swell. The models provide 126 hour forecasts, with the exception of the NAH model (72 hour forecast), and also they are based on shallow water physics without mean currents. No wave data assimilation is performed.

1.A.5 WAVEWATCH III

Winds from the operational Global Data Assimilation Scheme (GDAS) and the aviation cycle of the Medium Range Forecast model (Kanamitsu 1989, Kanamitsu et al. 1991, Derber et al., 1991, Caplan et al., 1997). This forecast/analysis system is now called the Global Forecast System or GFS. The winds are converted to 10m height assuming neutral stability. The wind fields are available at 3h intervals (using analyses and 3h forecasts in the hindcast part of the wave model run). For the NAH and NPH models, the above wind fields are blended with GFDL hurricane winds when possible. These wind fields are available hourly. Ice concentrations are obtained from NCEP's automated passive microwave sea ice concentration analysis (Grumbine 1996) and are updated daily. Sea Surface Temperatures as needed in the stability correction for wave growth are obtained taken from the GDAS. Boundary data for the regional models are obtained from the global model and are updated hourly.

Graphical and binary model output is available. The operational wave models use a combination of bathymetric and obstruction grids. Bathymetric grid files contain an array of water depth values or land flags (zero depth) at the wave model resolution, whereas obstruction grids consist of two arrays representing the degree of meridional and zonal blocking of wave energy propagation due to subgrid topographic features (Tolman, 2003).

1.A.6   High Performance Computing

The modelling system has been run at the Plymouth University High Performance Computing Centre, and at the University of Exeter Supercomputer facilities.

In Plymouth two supercomputers has been used with the following characteristics:

A distributed-memory cluster with a 3U Head & Storage Node (HS316i) and 82 compute nodes (HX2224i) equipped with Dual Intel Xeon E5420 (Quad Core 2.50Ghz) processors and 8 GB of memory per motherboard, connected by an RJ45 Cat 6 network accessible 12 TB parallel file system. The whole system is supported using IPMI (KVM over LAN) Technology. The latest addition are 808 cores using Intel Xeon E5650 (Six Core 2.66GHz, 6.40GT/s QPI) Processors.

A.2 Publications

MODELLING OF THE IMPACT OF A WAVE FARM ON NEARSHORE SEDIMENT TRANSPORT

Raúl González-Santamaría[1], Qingping Zou[2] and Shunqi Pan[3]

This paper presents the results from an integrated modelling system investigating the effects of a wave farm on nearshore sediment transport. Wave Hub project is a large scale demonstration site for the development of the operation of arrays of wave energy generation devices located at the southwest coast of the UK where multiple field measurements took place. The two-way coupled SWAN and ROMS models with nested modelling system were set up at the Wave Hub site and run with and without a wave farm. The model results show that the presence of the wave farm has significant impacts on the nearshore circulation, bed shear stresses and sediment transport. The morphological changes are also altered by the wave farm. The study is the key element for the wave resource characterization and environmental impact assessment of the wave farm.

Keywords: wave-current interaction, renewable energy, ROMS, SWAN, sediment transport, Wave Hub

INTRODUCTION

Located at the southwest coast of England, the Wave Hub project aimed to create one of the world's largest wave farms for demonstration and testing wave energy converter devices. Recent studies at the Wave Hub site suggest that wave induced currents are important in controlling sediment movement (SWRDA, 2006). Better understanding of tidal effects on waves and sand transport is crucial to wave resource characterization and environmental impact assessment of the wave farm at the Wave Hub site. A numerical study carried out by SWRDA (2006) suggested that the wave energy converters (WECs) installed at the Wave Hub site would cause a reduction between 3% - 5% of wave height in the adjacent coast of the Wave Hub, as well as changes in tidal currents and bathymetry. However, in their study the hydrodynamic model, Flow3D, was forced by four tidal constituents during a storm to assess the impact of the deployed WECs on tidal currents and sediment transport. Tidal currents recorded maximum current velocity of 1.2 m/s, in comparison of the admiralty pilot reported tidal currents between 0.5 and 1.0 m/s on the north coast of Cornwall during spring tides. To assess the WECs effect on the studied area, wave dragon devices were used. Model results suggest that sediment transport for this case study changes significantly at the Wave Hub site, but the impact of the wave farm on the adjacent nearshore zone remains an unresolved issue.

Millar et al (2007) carried out a study at the Wave Hub site to estimate the impact of WECs on the nearshore wave climate by analysing the wave energy transmitted through the WECs to the adjacent nearshore region. By comparing the SWAN model results with field observations from wave buoys, they concluded that assuming a 90% transmission rate, the average reduction in significant wave height was of the order of 1 cm, and that the stretch of the coast most likely to be affected was between Godrevy and Towan Heads that are close to the Wave Hub site.

Buscombe and Scott (2008) have addressed that sand transport due to tides is believed to be weak and not well quantified in this region, and the volume of sand involved is limited in comparison with other sectors of the English coasts. Also it was found that wave induced currents are believed to be more important in controlling sediment movement, not only from the prevailing southerly and westerly winds, but also the easterly winds can produce significant movement of sediment. Although storm events may cause movement of sand on the inner shelf, their effects are greater in the nearshore zone where significant cross- and long-shore sediment transport takes place.

Therefore, there is currently a lack of studies in the nearshore and shoreline areas in the lee side of the wave farm. Following the previous studies of wave-tide interactions at this area (Gonzalez-Santamaria et al, 2011; Gonzalez-Santamaria et al, 2012), the aim of the present study is to investigate the effect of a wave farm on the wave field, bed shear stresses, sediment transport and morphological changes, particularly along the shoreline behind the wave farm. We use the integrated and fully coupled wave-current numerical modelling system, extended with the sediment transport modules to gain insight into how the wave farm affects the current and bottom friction at the Wave Hub site, as well as sediment transport and the resulting morphological changes.

---

[1] School of Marine Science and Eng, Plymouth University, Plymouth, PL4 8AA, UK
[2] Department of Civil and Environmental Engineering, University of Maine, USA
[3] School of Engineering, Cardiff University, Cardiff, CF24 3AA, UK

METHODOLOGY

In this study, the spectral wave model SWAN (Booij et al, 1999) and the ocean circulation model ROMS are used to form a fully two-way coupled modelling system (Warner et al, 2008). The schematic diagram of the modelling system is shown in Figure 1. In order to include the far-field effects for waves, the SWAN model is run with three nested domains with progressively finer grid resolutions, as shown in Figure 2. At the finest grid (L3), the SWAN is coupled with the ROMS model to form the coupled modelling system (SWAN+ROMS). The SWAN model is fed by the output of the global wave spectral model Wave Watch III (NOAA: http://polar.ncep.noaa.gov) driven by the wind fields from the Global Forecast System (GFS) model. The global tidal model OTPS (Egbert et al, 2002; Padman and Erofeeva, 2004) provides tidal currents and water elevations as boundary conditions for the ROMS model. The wave model results can be affected by both water elevations and tidal currents, hence, the tidal information obtained from the ROMS model is used in the wave model.
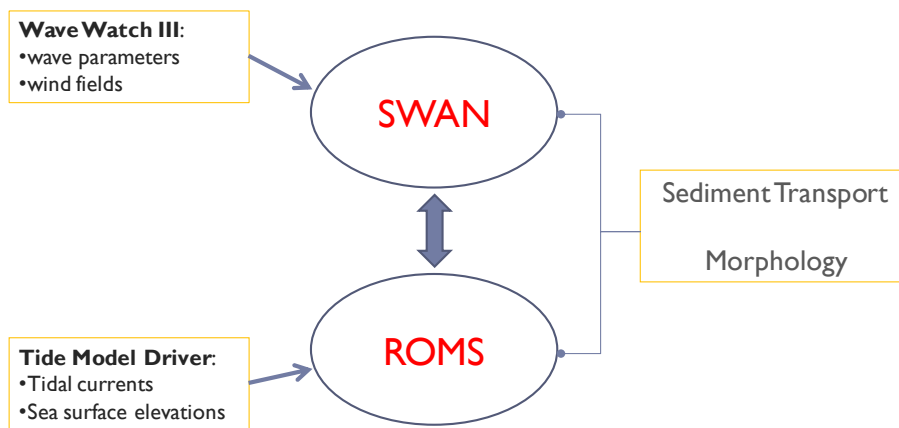
Figure 1. Schematic diagram of the integrated modeling system.
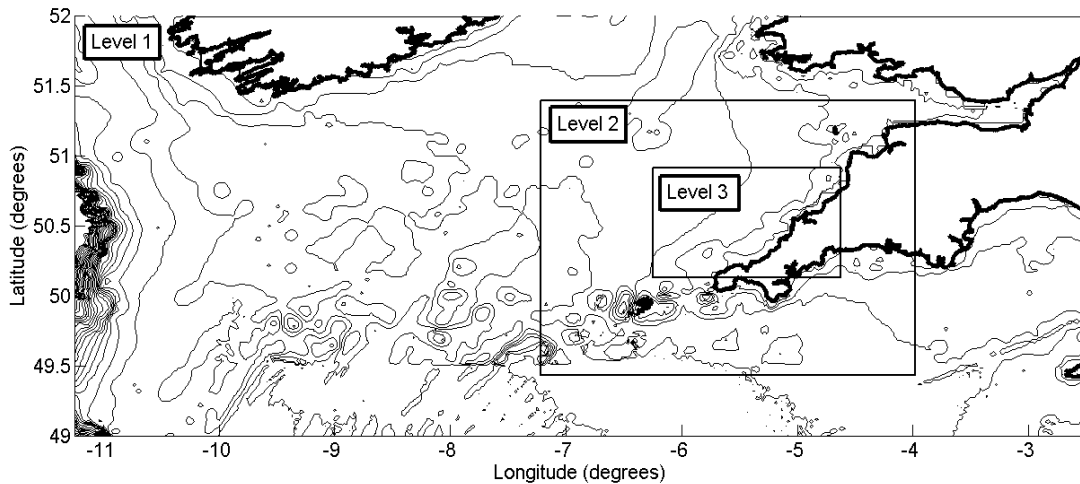
Figure 2. Nested computational domains for SWAN and ROMS.

The Oregon State University Tidal Prediction Software (OTPS/TPXO) based on the TOPEX/POSEIDON altimeter data (Egbert et al, 2002; Padman and Erofeeva, 2004), was used to predict tidal currents and water elevations from eleven harmonic constituents (M_2, S_2, N_2, K_2, K_1, O_1, P_1, Q_1, M_4, MS_4, MN_4). We found that the predicted water elevations are in a good agreement with the measurements from tide gauges near the Wave Hub site. In addition, a sediment transport model embedded in ROMS was incorporated in the modelling system for computing sediment transport and nearshore morphological changes. The Soulsby and Damgaard (2005) formulae is applied for computing bedload transport which accounts for the combined effects of mean currents and

asymmetrical waves on bedload flux. Suspended load is transported in the water column by solving the diffusion-advection equation, additional a source/sink term is added in exchange with the bed for vertical settling velocity and erosion. Erosion depends linearly on the bottom shear stress. The bed model accounts for changes in sea floor elevation resulting from convergence or divergence in sediment fluxes. These morphological changes can have an impact on flow transport when they are larger (Warner et al, 2008).

The two-way coupled modelling system consists of two models which are linked with shared information: the ROMS model, which computes sea surface levels, depth averaged horizontal velocity components and bottom stress based on the given sediment grain size; and the SWAN model, which computes wave height, wave length, wave period and wave bottom orbital velocities. Between these two models, the currents and water levels computed in ROMS are used in SWAN and the radiation stresses derived from the SWAN are used to calculate the wave induced current in ROMS, so that the dynamic interaction between waves and tides is realized. In addition, wind fields are used as the surface forcing in the SWAN model for predicting the wave field, but, the wind stress is ignored in the ROMS model due to the relatively small computational domain.

The coupled modelling system (SWAN+ROMS) was first applied to assess the impact of waves on currents and currents on waves. To achieve this, a series of different cases combining spring and neap tides, high and low water levels, high and low wave conditions, were investigated to examine the changes in waves, currents and bottom stresses. Then, the calibrated modelling system was implemented with a wave farm and applied to a storm period to investigate the effects of the wave farm on wave field predictions, bed shear stresses under combined wave and current conditions, sediment transport and the resulting morphological changes, with particular focus on the nearshore area in the lee side of the wave farm.

RESULTS

Wave-current interaction

For investigating the wave-current interaction, the modelling system was run for two months, from 1st December 2005 to 31st January 2006 in order to match the availability of wave buoy data. Three test cases were selected to examine the space distribution of wave-current interactions through the tidal cycle. These test cases are selected at the peak of the storm and during spring tide: high water level and low current velocities; middle water level and high current velocities; and low water level and low current velocities.

Comparisons between surface current velocities at the Wave Hub site from the coupled modelling system (SWAN+ROMS) and the ROMS (only) model were carried out in Gonzalez-Santamaria et al (2011), where the influence of tidal currents and tidal elevations on the significant wave heights at the Wave Hub site predicted by the coupled system, are compared with the buoy measurements. The model results indicate that the impact of wave-current interactions on the computed current velocities is significant during the spring tides. Similar to the current velocities, the current-induced bottom stresses in a spring tide are significantly affected by the waves. As waves propagate towards the coast, the wave propagation speed and direction may be modified by tidal currents due to refraction. In general, the main changes of wave direction are found during low wave heights and high tidal currents. In the same study three reference locations were compared. It was found that at the Wave Hub site the current magnitudes, after removing the tidal signal, are smaller than those at the nearshore area where the wave action enhances the current significantly. For example, at two nearshore points, the longshore currents vary, at one point from -0.5 to 0.5 m/s, and at the other point from -0.5 to 1.1 m/s, as a clear indication of the impact of change of wave direction on the current.

In studying the wave-tide interactions, analysis also includes the wave radiation stress, which is the flux of momentum carried by the ocean waves. When waves disperse in nearshore areas, the wave momentum is transferred to the water column, generating the near-shore currents (Bowen, 1969). Significant momentum can be transferred from waves to currents when a strong radiation stress gradient and radiation stress gradients are determined from the spatial gradients in the directional energy spectrum of the wave model and the strongest gradients in radiation stress occur where depth-induced breaking happens (Mulligan et al, 2008).

Within the fully coupled modelling system, the following physical mechanisms contribute to the wave-current interactions: i) surface shear stress, the effect of surface waves on the drag coefficient is included in ROMS (Warner et al, 2008); ii) bottom stress, waves enhance the turbulent mixing, therefore, waves modify the bottom stress experience by currents (Grant & Madsen, 1979; Zou, 2004); and iii) radiation stress which represents the excessive momentum flux within the circulation due to the

presence of waves (Longuet-Higgins and Stewart, 1964; Zou et al, 2006). For a hypothetic wave coming from the western boundary, a comparison with and without the wave effect, shown in Figure 3, illustrate the radiation stress influence on the circulation system. This figure shows the transferred momentum from waves to currents in the nearshore region, it worth mention that tidal currents are one order of magnitude higher and, in this case, the surface stress has been idealized over the whole domain. When tidal currents and wave induced currents are combined, the currents at the Wave Hub site are significantly enhanced, compared with the results when the waves are not included. The resultant flow is dominated by the tidal currents which are more uniform away from the coast. However, along the shoreline, currents are enhanced by the wave action through radiation stress gradients. This means that wave induced currents are significant in this zone, even though the tidal currents are the main force for the general circulation.
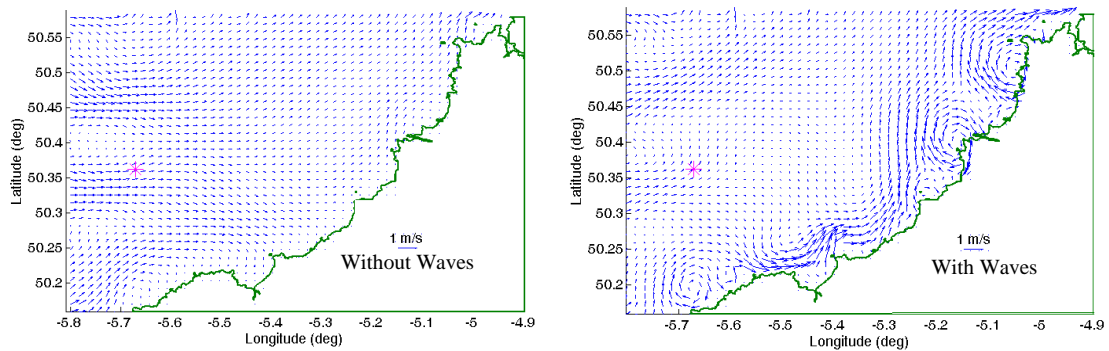

Figure 3. Computed currents with and without waves (✳ – the Wave Hub).

While during neap tides, the tidal influence on waves is insignificant, during spring tides, the difference becomes more noticeable, this is observed in Gonzalez-Santamaria et al, (2011), where the differences in significant wave height and wave direction and with-without tidal currents are shown, particularly for the cases indicated above within the L3 domain (see Figure 2). Moreover, the difference between the coupled modelling system and the wave model only for the significant wave height and wave direction showed strong correlation of wave height, wave direction and wind velocity, suggesting that wind waves play an important role on the longshore currents, which will affect the sediment transport. It is also found that when tidal currents are included, the wave direction is modified by around 10 degrees during high waves, but about 20 degrees during low waves. The change in wave direction to further align the shore is also an important factor, as this will produce stronger alongshore currents, particularly, during the low water level case.

As shown in Gonzalez-Santamaria et al (2012), the spatial distribution of the wave influence on bottom currents showed larger velocities and eddies along the coast up to 2 m/s. At high tide and low tidal currents, the region with significant wave induced currents is more confined to the coast. At mid tide, tidal currents are at its maximum, and the total current velocity field is uniform in the offshore zone and increases in magnitude in the nearshore zone where the significant wave height is high. At low tide, tidal currents are at the minimum, the region with significant wave induced currents is extended in the offshore direction due to decreasing water depth. The velocities near the coast are clearly enhanced by the wave forcing, particularly in the longshore direction.

Effects of the wave farm on wave height and bed shear stress

The wave farm was incorporated in the SWAN model following Millar et al (2007) and arrays of WECs at the Wave Hub site was represented as a 4 km partially transmitting obstacle, aligning approximately parallel to the prevailing incoming wave crests. The energy transmission percentage was set as 75% which represents an array of densely spaced, high-efficiency WECs. Figure 4 shows significant wave height (colours) and wave direction (vectors) for the storm case and for the water elevations, even, the difference between with and without the wave farm is shown. The change of the wave height with and without the wave farm is between 5 cm and 10 cm at the nearshore line, and the maximum extension affected by the wave farm is about 26 km northwards St. Ives Bay (south of L3) for the high water level case when the most significant wave farm impact on wave height occurs.
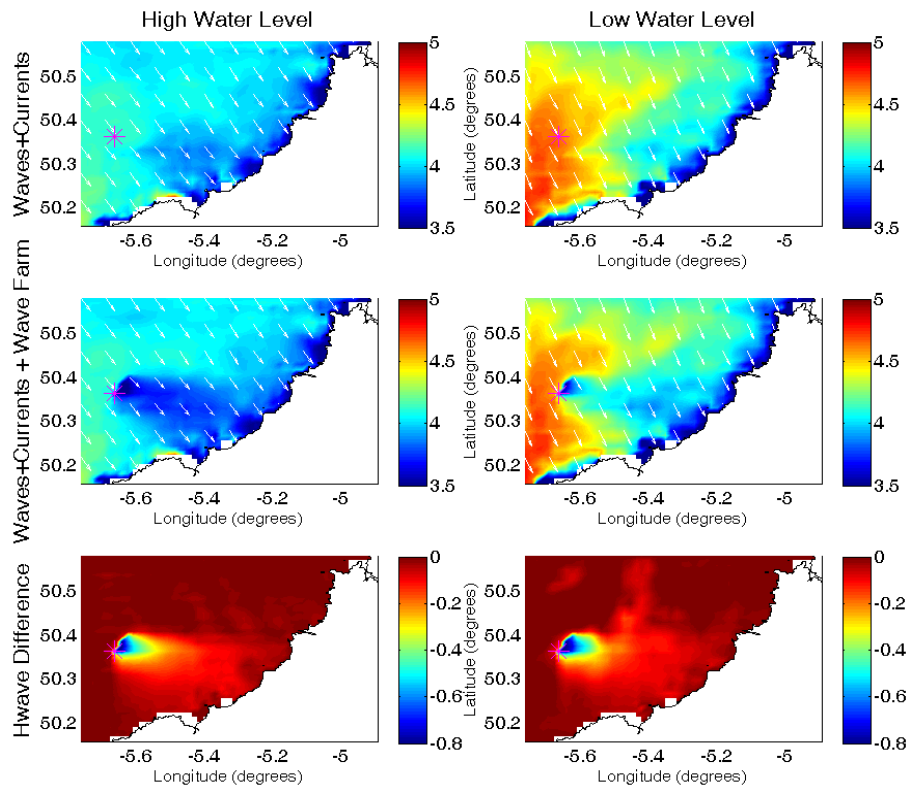
Figure 4. Effects of the wave farm on the wave heights under low and high water elevations: (top) computed wave height without wave farm; (middle) computed wave height with wave farm; (bottom) the difference of the computed wave height with and without wave farm. (Vectors are the wave directions; ✳ – Wave Hub)

Figure 5 shows the bottom stress contribution for the coupled modelling system, with and without the wave farm, at the high and low water levels. The wave contribution on the bottom stress is large compared to tides only (not shown here), driving the sediment transport at the most, particularly during the storm peak. The bottom stress is also found to correlate with the currents field and is affected by the local water depth. As shown in Figure 4, the wave field, especially in the leeside of the wave farm, is affected significantly by the wave farm, it can be seen that the regions where significant bottom stress is affected are in the shallow water regions and the nearshore areas. The results also indicate the the water depth is an important factors to influence the bottom shear stresses. The maximum changes in bottom stress along the coast are found at the lower water elevation, and smaller bottom stress at the higher water elevation. Wave farm impact, on the bottom stress (right panels), is maximum at low water level, which is strongly correlated to the currents field, waves and depth.

Effects of the wave farm on sediment transport

After the model validation on hydrodynamics, the morphological modules were implemented to compute the sediment transport and the resulting bathymetry changes for cases with and without the presence of the wave farm. Due to the availability of wave buoys, the model was run for November 2010, when three storm events were observed at the Wave Hub site.

To study the effects of the wave farm on the sediment transport and morphological changes, we will focus on the analysis at the maximum storm peak, where further field measurements are available. Since this period differs from the previous period for model validation in Gonzalez-Santamaria et al, (2011), further model validations were carried out for this period. Water elevations were compared against tide gauges at four locations (not shown here) and wave heights were compared with the wave buoy data at three locations. The computed water elevations and the measurements from four tidal gauges around the study area show a good agreement, so do the computed wave heights and measurements by the wave buoys deployed at three locations close to the study site. In general the predicted wave heights closely follow the wind speed, and the storms are reproduced reasonably well. In comparison with the measurements, the storm peak was slightly under-predicted where water depths were relatively shallow.
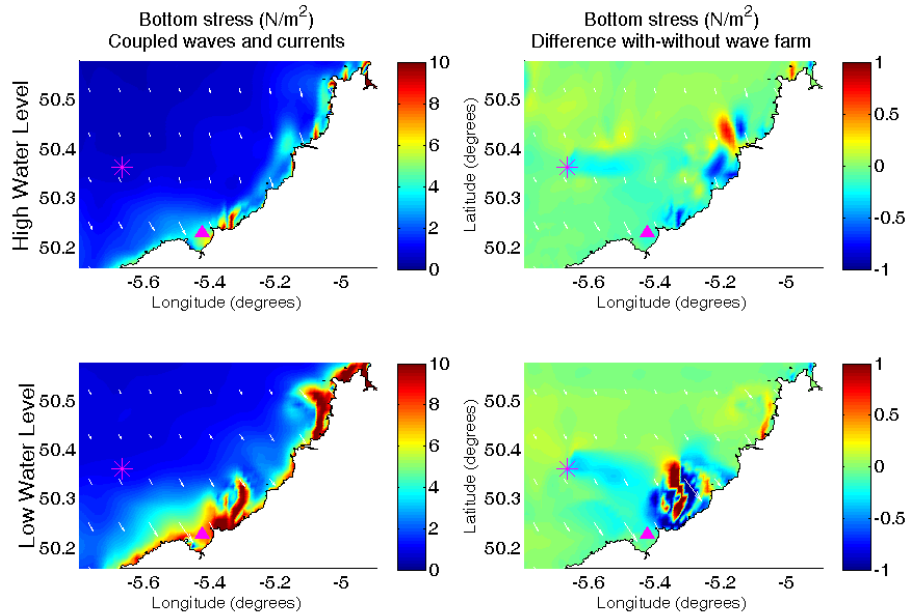
Figure 5. Effects of wave farm on bottom shear stresses at high and low tide. (Vectors are magnitude and direction of bottoms stresses, color indicates the magnitude, ▲ – St. Ives Bay, ✷ – Wave Hub)

In the coupled modelling system, bedload transport rates are calculated by the Soulsby and Damgaard (2005) formulae, which accounts for the combined effects of waves and currents on bedload flux. The suspended load is transported in the water column by solving the diffusion-advection equation, with additional a source/sink term added in exchange with the bed for vertical settling velocity and erosion. Erosion depends linearly on the bottom shear stress (Warner et al, 2008). Figure 6 shows the non-cohesive sediment (sand) concentration (kg/m^3) for without wave farm (left panels) and the difference with and without the wave farm effect (right panels). We found strong sediment concentration at low tides along the coastline during the storm peak. As expected, the bottom stress distribution shown in Figure 5 has a strong correlation with the sediment concentration distribution in Figure 6. When the tidal currents are close to zero at high and low tide (top and bottom panels), the wave farm effect on the sediment distribution is mainly due to wave contribution. The maximum changes in sediment concentration with and without the wave farm are from -0.1 to 0.1 kg/m^3 during the tidal cycle and occur at the lee of the wave farm and near the coast north of St. Ives Bay. During the tidal cycle, the sediment concentration affected by the wave farm extends about 26 km northwards from St. Ives Bay at high tide. On the other hand, at the low tide, the sediment concentration moves slightly offshore, mainly in the lee of the wave farm, but with the maximum concentrations.

Effects of the wave farm on morphological changes

The changes of the sea bed are calculated from the convergence or divergence in sediment fluxes which are the sum of suspended and bedload transports (Warner et al, 2008). Due to the use of the coupled modelling system, the effect of morphological changes on flow and sediment transport is dynamically incorporated in the model.

Figure 7 shows the bed level changes over a 16-day duration of simulation, which includes three storm events. Figure 7(a) and (b) shows the bed level changes without and with wave farm, respectively. The general patterns of erosion and deposition are similar in both cases, where the most significant morphological changes are found in three bays along the coast, between -1 m and 1 m. The difference of the morphological changes with and without the wave farm is shown in Figure 7(c). The results show that the area near St. Ives Bay is most affected by the wave farm. This is expected as this area is located in the leeside of the wave farm and the predominant waves are north-easterly. The overall impact of the wave farm is found to cause more deposition in the south-west area and more erosion in the north-east area close to the St. Ives Bay where most bed changes are taking place.

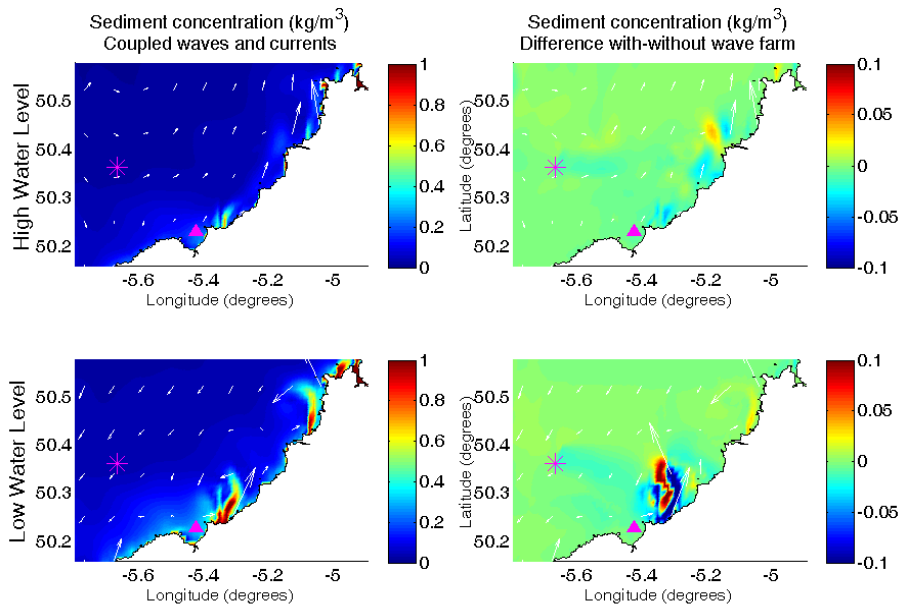**Figure 6. Effects of wave farm on sediment concentration under low and high water levels. (Vectors are magnitude and direction of current speed, color indicates the magnitude, ▲ – St. Ives Bay, ✳ – Wave Hub)**
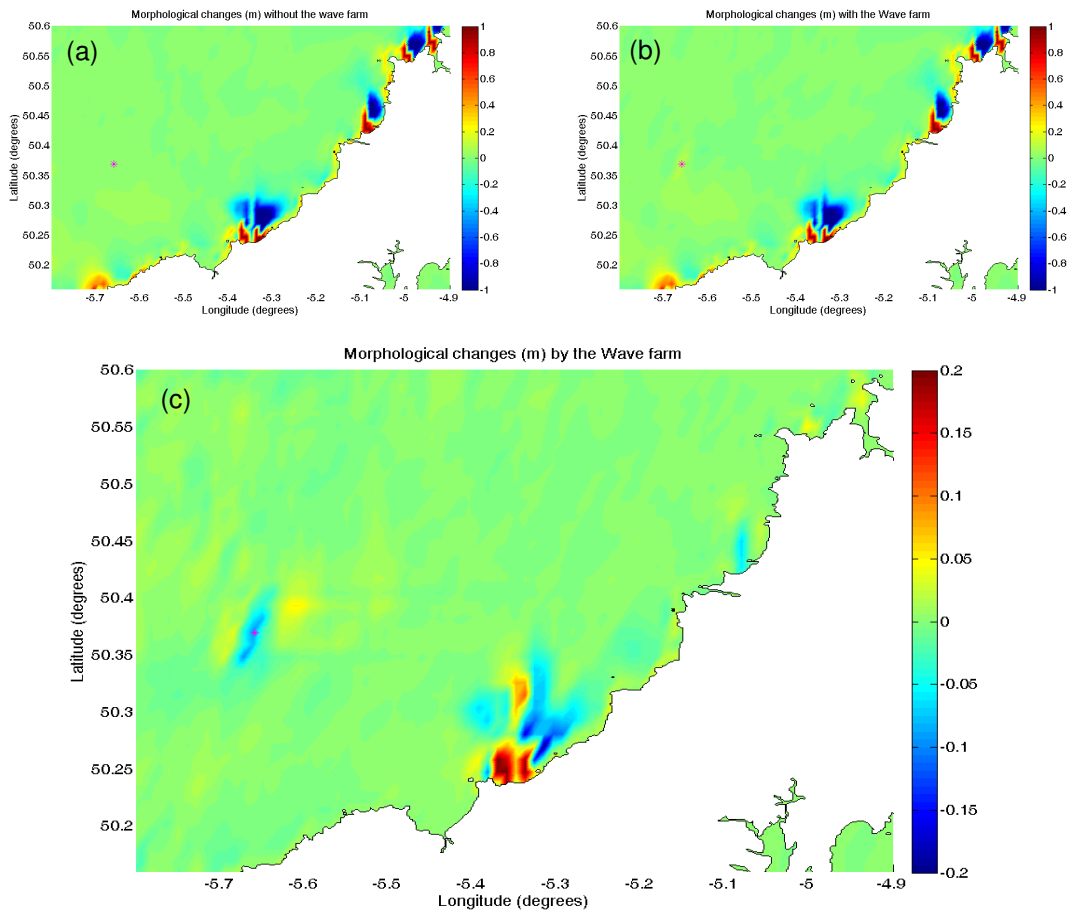
Figure 7. Effects of the wave farm on morphologic changes: (a) bed level changes without wave farm; (b) bed level changes with wave farm; and (c) difference of the bed level changes between (a) and (b). (✳– Wave Hub)

CONCLUSIONS & DISCUSSIONS

A two-way coupled modelling system with SWAN and ROMS models implemented with sediment transport modules has been used to study the impact of a wave farm at the Wave Hub site in the South West of England on nearshore morphodynamics. The modelling system was calibrated against various field measurements, showing a good agreement.

It was found that the sediment concentration is higher at the lee of the wave farm, presumably because the longshore current is partially blocked by the circulation currents (in the lee), producing some of the longshore currents to be diverted outside the wave farm. The littoral transport in the lee of the wave farm decreases due to the attenuated wave and longshore currents in the area sheltered by the wave farm. This causes the trapping of sand in the lee, depending on the hydrodynamic conditions, as the wave farm reflects and dissipates some of the incoming wave energy, thus, it reduces wave heights and shore erosion in the shadowed area of the wave farm. Moreover, the littoral transport of sediments is deposited in the lower wave energy region. The diversion of the longshore currents will cause the development of local erosion close to the heads of the obstacle or wave farm. An obstacle, in this case the wave farm, traps sand under all circumstances, hence, there will be a coastal impact in any circumstance.

The maximum changes in sediment concentration with and without the wave farm are from -0.1 to 0.1 kg/m^3 at low tide and occur at the lee of the wave farm, the changes are much more profound in the nearshore area north of St Ives Bay. From low tide to high tide, the sediment concentration extends about 26 km upwards from St. Ives Bay along the coast. At the low tide, the sediment concentration moves in slightly offshore. These results are closely correlated to the bottom stress results. The bedload rate flux is considerable reduced when the wave farm is positioned in the study area, also it is shown that at the peak of the three storm events, the bedload rate flux is decreased.

The significant impacts of the wave farm on the morphological changes are again found in the coastal area near St. Ives Bay, as well as in immediate lee side of the wave farm. The bed changes indicate a northward shift of erosion and deposition pattern due to the wave diffraction caused by the wave farm.

ACKNOWLEDGMENTS

REFERENCES

Booij N., Ris R.C., Holthuijsen L.H. 1999. A third generation wave model for coastal regions, part I, model description and validation, Journal of Geophysical Research 104 (C4), 7649-7666.
Bowen A. J., 1969.The generation of longshore currents on a plane beach, Journal of Marine Research, 27, 206–214.
Buscombe D.D., Scott T.M. 2008. The coastal geomorphology of north Cornwall, Wave Hub impact on seabed and shoreline processes – report [online]. Available: http://www.research.plymouth.ac.uk-/whissp/index.html/
Egbert G. D., Erofeeva S. Y. 2002. Efficient inverse modeling of barotropic ocean tides, Journal of Atmospheric and Oceanic Technology, 19, 183–204.
Gonzalez-Santamaria R., Zou Q.-P. and Pan S. 2011. Two-way coupled wave and tide modelling of a wave farm, Journal of Coastal Research, SI 64, 1038–1042, ISSN 0749-0208.
Gonzalez-Santamaria R., Zou Q.-P. and Pan S. 2012. Impacts of a wave farm on waves, currents and coastal morphology, Journal of Estuaries and Coasts, SI: Renewable Ocean Energy. (under review).
Grant W.D., Madsen O.S. 1979. Combined wave and current interaction with a rough bottom, Journal of Geophysical Research, 84 (C4), 1797-1808.
Longuet-Higgins M. S., Stewart R. W. 1962. Radiation stress and mass transport in gravity waves, with application to 'surf beats', Journal of Fluid Mechanics 13 (4):481–504.
Millar D.L., Smith H.C.M., Reeve D.E. 2007. Modelling analysis of the sensitive of shoreline change to a wave farm, Ocean Engineering, 34, 884-901.

Mulligan R. P., Hay A. E., and Bowen A. J. 2008. Wave-driven circulation in a coastal bay during the landfall of a hurricane, Journal of Geophysical Research, 113, C05026, doi:10.1029/2007JC004500.

NOAA Wavewatch III. NOAA/NCEP Operational wave models. [online]. Available: http://polar.ncep.noaa.gov/waves.

Padman L. and Erofeeva S. 2004. A barotropic inverse tidal model for the Arctic Ocean, Geophysical Research Letters, vol. 31.

Soulsby R.L., Damgaard J.S. 2005. Bedload sediment transport in coastal waters, Journal of Coastal Engineering, 52 (8), 673-689.

SWRDA - South West of England Development Agency, Wave Hub development and design phase, SWRDA Group Limited, coastal processes study report. [online]. Available: http://www.wavehub.co.uk/

Warner J.C., Sherwood C.R., Signell R.P., Harris C.K., Arango H.G. 2008. Development of a three dimensional, regional, coupled wave, current, and sediment transport model, Journal of Computers & Geosciences, 34, 1284-1306.

Zou Q.P. 2004. A simple model for random wave bottom friction and dissipation, Journal of Physical Oceanography, 34 (6), 1459-1467.

Zou, Q.-P., Bowen A. J. & Hay A. E. 2006. The vertical distribution of wave shear stress in variable water depth: theory and field observations. Journal of Geophysical Research, 111 (C09032), doi:10.1029/2005JC003300.

Two-way coupled wave and tide modelling of a wave farm

R. Gonzalez-Santamaria†, Q.-P. Zou‡ and S. Pan∞
† ‡ ∞ University of Plymouth, School of Marine Science and
Engineering, Drake Circus, PL4 8AA, Plymouth, United Kingdom
† raul.gonzalez@plymouth.ac.uk
‡ qingping.zou@plymouth.ac.uk
∞ shunqi.pan@plymouth.ac.uk

ABSTRACT

Gonzalez-Santamaria R., Zou Q.-P., and Pan S., 2011. Two-way coupled wave and tide modelling of a wave farm. Journal of Coastal Research, SI 64 (Proceedings of the 11th International Coastal Symposium), pg – pg. Szczecin, Poland, ISSN 0749-0208

This study investigates the interactions of waves and tides at a wave farm in the southwest of England, in particular their effects on radiation stress, bottom stress, and consequently the effects on the sediment transport and the coast adjacent to the Wave Hub, the wave-farm. In this study, an integrated complex numerical modelling system is setup at the Wave Hub site and is used to study the effect of wave-current interaction on current circulation, bottom shear stress, as well as the impacts in the nearshore zone. Results show that tidal elevation and tidal currents have a significant effect on the wave height and direction predictions; tidal forcing and wind waves have a significant effect on the bed shear-stress, relevant to sediment transport; waves via radiation stresses have an important effect on the longshore and cross-shore velocity components, particularly during the spring tides. Waves can impact on bottom boundary layer and the mixing in the water column. Interactions between waves and tides at the Wave Hub site are important when modelling coastal morphology influenced by wave energy devices.

ADDITIONAL INDEX WORDS: Wave Hub, wave-tide interaction, SWAN, ROMS.

INTRODUCTION

The Wave Hub project aims to create one of the world's largest wave farms for demonstration and testing wave energy converter devices, located at the southwest coast of England, as shown in Figure 1. Recent studies at the Wave Hub site suggest that wave induced currents are important in controlling sediment movement (SWRDA, 2006). Better understanding of tidal effects on waves and sand transport is crucial to wave resource characterization and environmental impact assessment of the wave farm at the Wave Hub site.

A study by SWRDA (2006) based on numerical modelling suggests that the wave energy converters (WECs) installed at Wave Hub would cause a reduction between 3% - 5% of wave height in the near coast of the Wave Hub, as well as changes in tidal currents and bathymetry. In that study the hydrodynamic model applied, Flow3D, was forced by four tidal constituents during a storm to assess the impact of the deployed WECs on tidal currents and sediment transport. Wave buoy data from 3 to 14 Feb 2005 was used in the model calibration. Tidal currents recorded maximum current velocities of 1.2 m/s. The admiralty pilot reports tidal currents between 0.5 and 1.0 m/s on the north coast of Cornwall during spring tides. The wave dragons were used as the worst case scenarios WECs in this study. Model results show that sediment transport for the worst case scenario changes significantly at the Wave Hub site, but the impact of the wave farm on the adjacent nearshore zone remains an unresolved issue.

Millar et al (2006) carried out a study at the Wave Hub site to estimate the impact of WECs on the nearshore wave climate by analysing the wave energy transmitted through the WECs to the adjacent nearshore region. By comparing the SWAN model results with field observations from wave buoys, they concluded that assuming a 90% transmission rate, the average reduction in significant wave height was of the order of 1cm, and that the

stretch of the coast most likely to be affected was between Godrevy and Towan Heads that are close to the Wave Hub site.

From the perspective of the impact on this stretch of coast, the tidal control on sand transport is weak and uncertain in this region, and the volume of sand involved are limited in comparison with other sectors of the English coasts. Therefore, wave induced currents are more important in controlling sediment movement. The prevailing winds are from the South and West, but easterly winds can also produce significant movement of sediment. Although storm events may cause movement of sand on the inner shelf, their effects are greater in the nearshore zone where significant cross- and long- shore sediment transport takes place (Buscombe & Scott, 2008).

Clearly, there is a lack of studies in the nearshore and shoreline areas on the lee side of the wave farm, thus, the aim of this study is to investigate the wave-tide interactions, in particular their effects on sediment transport along the coast behind the wave-
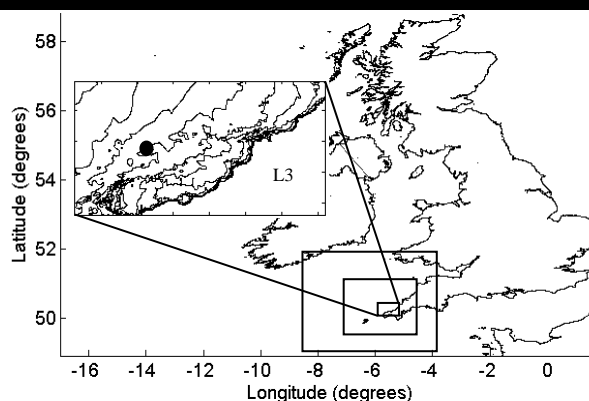

Figure 1. SWAN nested grids (squares); SWAN+ROMS coupled system domain (L3), Wave Hub site (●).

farm. We examine the tidal effects on wave, wave-induced currents, radiation stresses and bottom stresses, using a complex wave-current coupled numerical modelling system to gain insight into how wind waves and tidal currents affect the current and bottom friction at the Wave Hub site and the adjacent nearshore zone.

THE MODELLING SYSTEM

In this study, the spectral wave model SWAN (Booij et al, 1999) and the circulation ROMS model are used to form a fully two way coupled modelling system (Warner et al, 2008). As shown in Figure 1, the SWAN model is run with three nested domains with progressively finer grid resolutions. At the finest grid (L3), the SWAN is coupled with the ROMS model to form the coupled modelling system (SWAN+ROMS). The SWAN model is fed by the output of the global wave spectral model Wave Watch III (NOAA http://polar.ncep.noaa.gov) driven by the wind fields from the Global Forecast System (GFS) model. The global tidal model OTPS (Egbert et al, 2002; Padman and Erofeeva, 2004) provides tidal currents and water elevations as boundary conditions for the ROMS model. The wave model results can be affected by both water elevations and tidal currents, hence, the tidal information is obtained from the ROMS model to be used in the wave model. In addition, a sediment transport model was incorporated in the modelling system for computing bottom roughness and beach morphological changes, the results of which, however, are not discussed in this paper.

The tidal model used is the Oregon State University Tidal Prediction Software (OTPS/TPXO) based on the TOPEX/POSEIDON altimeter data (Egbert et al, 2002; Padman and Erofeeva, 2004), which was used to obtain predictions of tidal currents and water elevations from eleven harmonic constituents (M_2, S_2, N_2, K_2, K_1, O_1, P_1, Q_1, M_4, MS_4, MN_4). We found that the predicted water elevations are in a good agreement with the measurements from tide gauges near to the Wave Hub site.

The coupled modelling system (SWAN+ROMS) was applied to assess the impact of waves on tidal currents and tidal currents on waves. To achieve this, a series of different cases combining spring and neap tides, high and low water levels, high and low wave conditions, were investigated to examine the changes in wave parameters, current velocities and bottom stresses.

The two-way coupled modelling system consists of sharing information: the ROMS model, which computes sea surface levels, depth averaged horizontal velocity components and bottom stress based on the given sediment grain size; and the SWAN model, which computes wave height, wave length, wave period and wave bottom orbital velocities. Between these two models, the currents and water levels computed in ROMS are used in SWAN and the radiation stresses derived from the SWAN are used to calculate the wave induced current in ROMS, so that dynamic interaction between waves and tides are realised. In addition, wind fields are used as the surface forcing in the SWAN model for predicting the wave field, but, the wind stress is ignored in the ROMS model due to the relatively small computational domain.

RESULTS

The modelling system was run for two months, from 1st December 2005 to 31st January 2006 due to the availability of wave buoy data. Three test cases were selected to examine the space distribution of wave-tide interactions through the tidal cycle. These test cases are selected at the peak of the storm and during spring tide: Case (a) Middle water level and high current velocities; Case (b) Low water level and low current velocities; and Case (c) High water level and low current velocities.

Figure 2 shows the influence of tidal currents and tidal elevations on the significant wave heights at the Wave Hub site predicted by the coupled system, compared with buoy measurements. Figure 3 shows the differences, with and without tidal currents, of significant wave height and wave direction for the cases indicated above within the L3 domain (see Figure 1). Three reference sites shown in this figure for further comparisons are the Wave Hub site, St Ives bay and St Agnes. When tidal currents are included, the wave direction is modified by less than 10 degrees during high waves, but about 20-30 degrees during low waves.

As waves propagate towards the coast, the wave propagation speed and direction may be modified by tidal currents due to refraction. In general, the main changes of wave direction are found during low wave heights and high tidal currents.

In order to study the wave-tide interactions the concept of radiation stress is included, which is the flux of momentum carried by the ocean waves. When these waves break, the wave momentum is transferred to the water column, inducing near-shore currents. Radiation stress theory has been successfully used to explain the presence of long-shore currents (Bowen, 1969). Significant momentum can be transferred from waves to currents when a strong radiation stress gradient occurs due to wave breaking and to the bottom friction in the near-shore region. Radiation stress gradients are determined from the spatial gradients in the directional energy spectrum of the wave model and the strongest gradients in radiation stress occur where depth-induced breaking happens (Mulligan et al, 2008).

The results of the surface current velocities at the Wave Hub site from the coupled modelling system (SWAN+ROMS) were compared against those of running the circulation model (ROMS) only. Figure 4 shows the contribution of wave induced currents. It should be noted that the computed current velocities have been decomposed into longshore and cross-shore directions based on the main direction of the shoreline at the site.
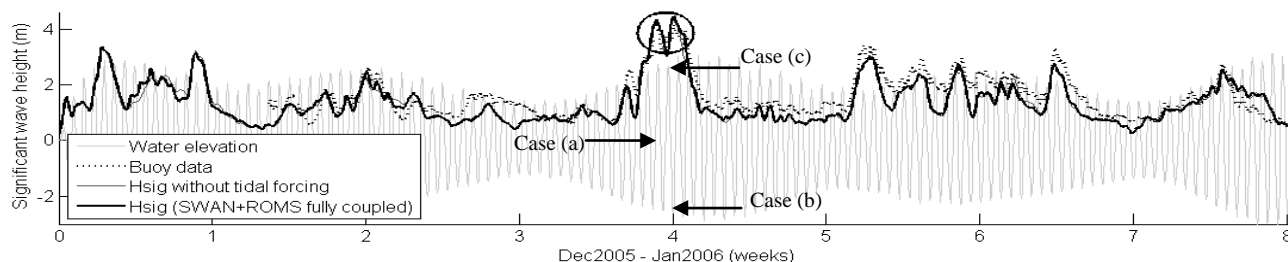

Figure 2. Significant wave heights with/without tidal influence. Circle represents maximum storm Hsig at spring tide. Three main cases have been analysed at the peak of the storm event indicated by the circle: at mid water level and high current velocities (Case a); Low water elevation and low current velocity (Case b); High water elevation and low current velocity (Case c).
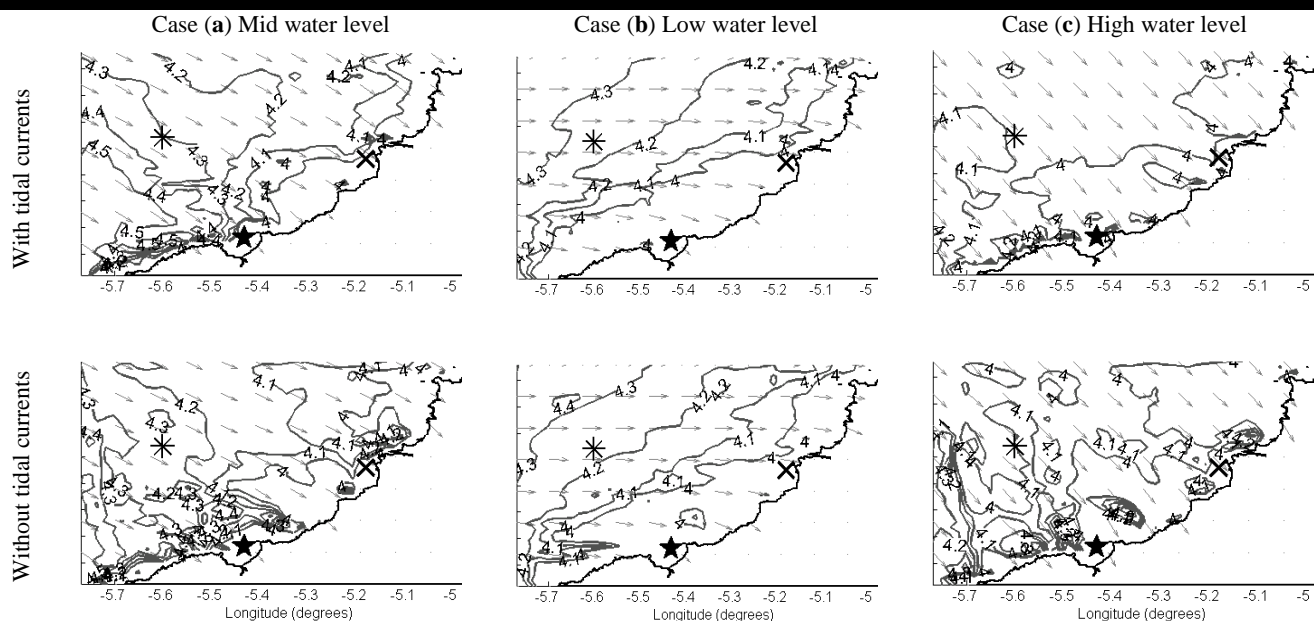
Figure 3. Significant wave height in m (contours), and wave direction (arrows), with tidal currents (top panels) and without tidal currents (bottom panels), for the cases indicated in Figure 2. Three reference sites are selected for further comparisons: Wave Hub site (*), St Ives bay (★) and St Agnes (×).

Removing the underlying tidal velocity (by using harmonic analysis), the impact of wave-current interactions on the computed current velocities is clearly illustrated during the spring tides. Similar to the current velocities, the both components of the current induced bottom stress in a spring tide are significantly affected by the waves (Figure 5).

The velocities at the coast, of the fully coupled system, are clearly enhanced by the wave forcing, particularly in the longshore direction. In St Ives bay, such effect is the most significant (Figure 4). We found that at the Wave Hub site the current magnitudes, after removing the tidal signal, are smaller than those at St Ives bay and St Agnes where the wave action enhances the current significantly. At St Agnes, the longshore currents vary from -0.5 to 0.5 m/s, and at St Ives bay, longshore currents vary from -0.5 to 1.1 m/s. Figure 4 and 5 show that magnitudes of both longshore and cross-shore currents and bottom stress are quite similar. This

is the result of wave propagation direction relative to the shoreline at this site.

Waves and currents are coupled through the following physical mechanisms: i) surface shear stress, the effect of surface waves on the drag coefficient is included in ROMS (Warner et al, 2008); ii) bottom stress, waves enhance the turbulent mixing, therefore, waves modify the bottom stress experience by currents (Grant & Madsen, 1979; Zou, 2004); and iii) radiation stress which represent the excessive momentum flux within the circulation due to the presence of waves (Longuet-Higgins and Stewart, 1964).

When tidal currents and wave induced currents are coupled the currents field at the Wave Hub site increases significantly, compared with the results when there is no wave interaction. The total current is dominated by the tidal currents which are more uniform away from the coast. However, along the shoreline, currents are enhanced by the wave action through radiation stress.
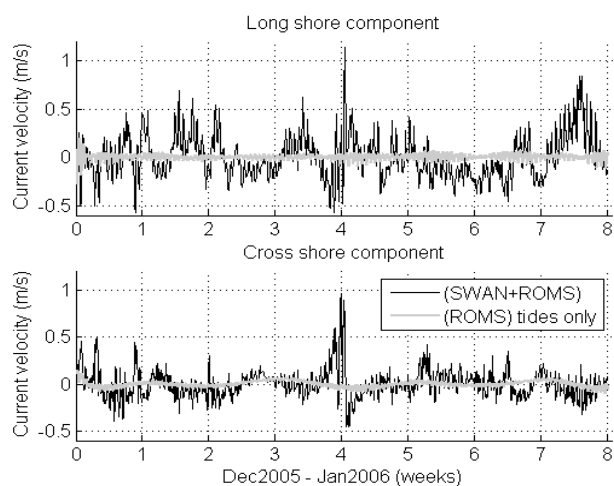

Figure 4. Longshore and cross-shore components of current velocities, after removing the tidal signal, at St Ives bay.
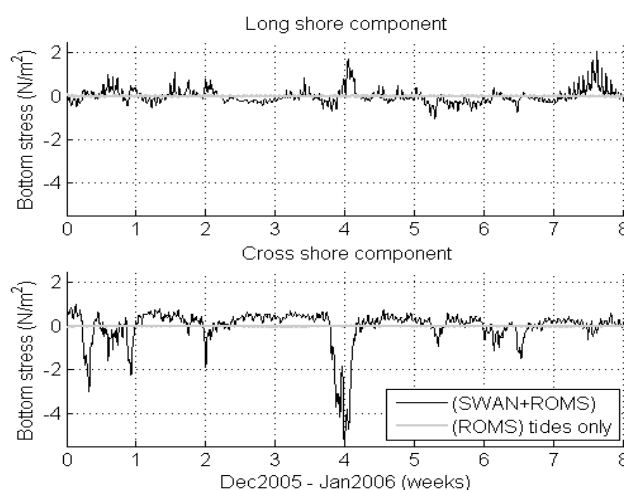

Figure 5. Longshore and cross-shore components of bottom stress, after removing the tidal signal, at St Ives bay.

This means that wave induced currents are significant in this zone, even though the tidal currents are the main force for the general circulation.

Figure 6 shows that the current field is similar at the Wave Hub site with and without wave forcing. On the other hand, at St Ives bay and St Agnes, the currents are enhanced significantly by the waves, especially at the peak of the storm around week 4 where velocities are up to 2 m/s. At St Ives bay the wave effect is the largest.

The spatial distribution of the wave influence on currents is shown in Figure 7 where larger velocities and eddies are observed along the coast. In Case (a) for middle water level, tidal currents are at its maximum, the total current velocity field is uniform in the offshore zone and increases in magnitude in the nearshore zone where the Hsig is high. In Case (b), water elevations and tidal currents are minimum, the region with significant wave induced currents is extended in the offshore direction due to decreasing water depth. In Case (c), the water elevation is high but low tidal currents, the region with significant wave induced currents is more confined to the coast. Figure 8 shows the combined wave-current bottom stress at different water levels during the tidal cycle. The bottom stress is correlated with the currents field in Figure 7 for Cases (a) to (c) and is affected by the local water depth. The region with significant bottom stress is confined to the shallow water region and moves towards/away from the coast when the water level decreases/increases during the tidal cycle. Case (b) shows maximum bottom stress along the

Figure 7. Spatial distribution of current velocities (ROMS+SWAN fully coupled) for the cases indicated in Figure 2: (a) mid water elevation; (b) low water elevation; (c) high water elevation.

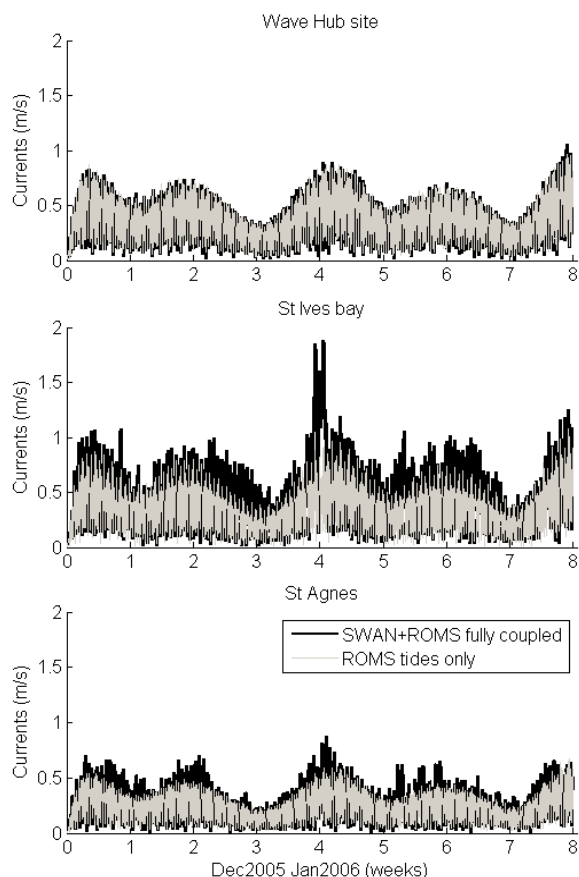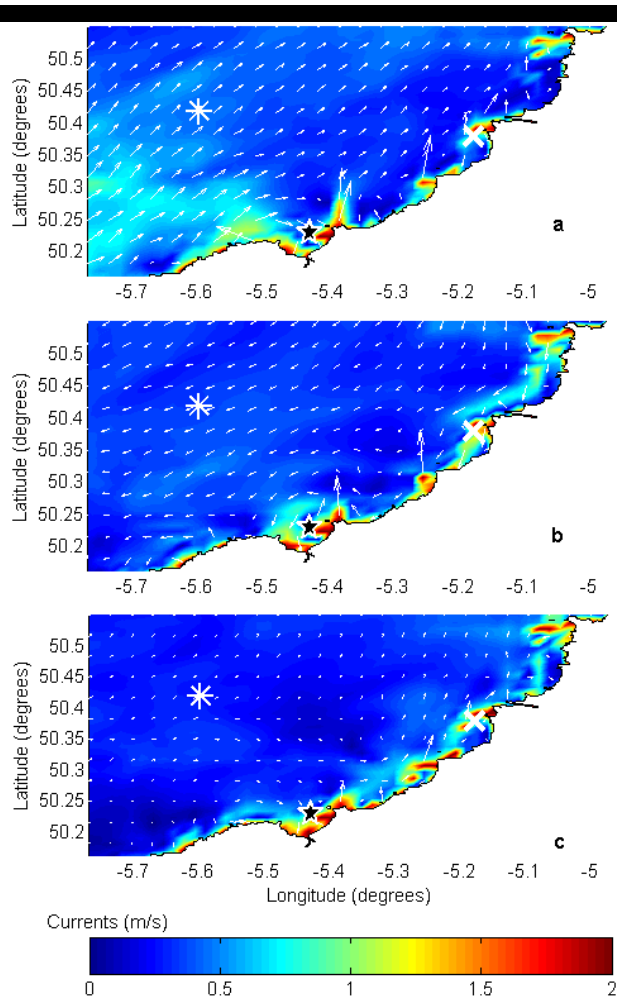Wave Hub site (*), St Ives bay (★) and St Agnes (×).

Figure 6. Magnitude of currents (m/s) at St. Agnes coast (top), St. Ives Bay (middle) and Wave Hub site (bottom) with and without wave contributions (dark and gray lines) over 8 weeks. (Positions of these locations are shown in Figure 3).

coast because of lower water elevation, Case (c) shows smaller bottom stress because of the high water elevation.

CONCLUSIONS

In this study, a two-way coupled modelling system with the SWAN and ROMS models has been used to study the wave-current interactions at the Wave Hub site, a wave farm in the South West of England. The wave model, SWAN, was nested from coarse to fine grids, forced by the spectral wave model Wave Watch III and wind fields from the GFS model. The circulation model, ROMS, was forced by the tide outputs from the global tidal model OTPS (Egbert et al, 2002; Padman and Erofeeva, 2004) and by the wave forcing from the SWAN model on the fine grid. Model results are in good agreement with the measurements by tide gauges and wave buoy.

Model results at high, mid and low tides during the peak of a storm, were presented to show tidal effects on waves, current velocities and bottom stresses, during spring tides. It is found that the wave height increases with the tidal elevation, and the wave direction is modified by the change of direction of tidal currents. We also found that the tidal current effect on waves is maximum at mid and low tide when the tidal current is at its peak and the
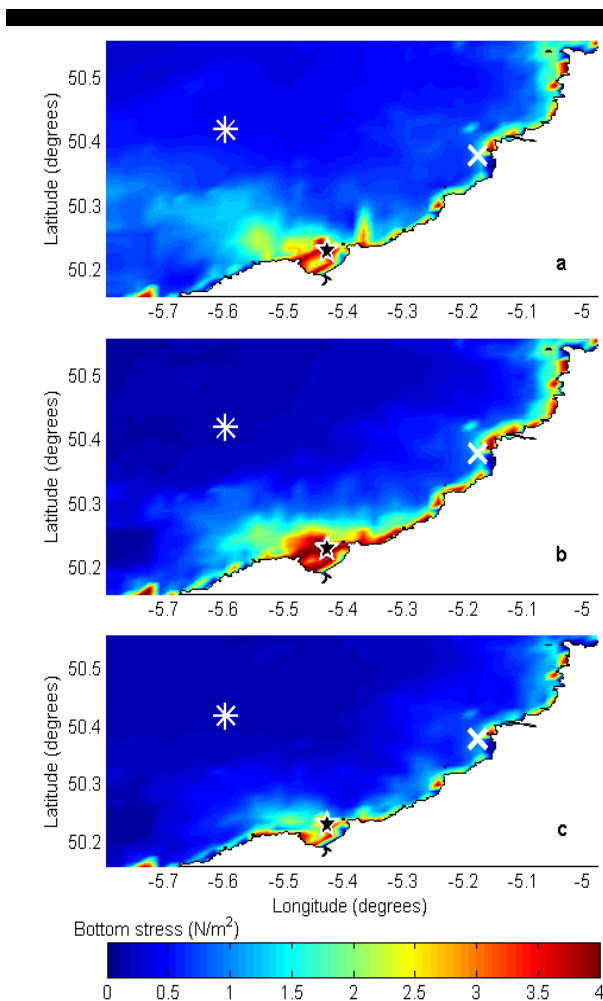
and Directional Waverider buoys taken during the on-going Wave Hub project.

Figure 8. Combined wave-current bottom stress (N/m^2) with tidal currents for the cases indicated in Figure 2: (a) mid water elevation; (b) low water elevation; (c) high water elevation. Wave Hub site (∗), St Ives bay (★) and St Agnes (×).

tidal elevation change has a significant effect on wave directions. The tidal current effect on wave direction is relatively small when wave height is large.

Wave effects on currents are isolated by removing the tidal signal from current velocity and bottom stress. Model results show significant cross- and long-shore wave induced currents along the shoreline, which is at its peak at mid-tide with maximum tidal currents and at peak wave heights. Wave induced current is negligible at the Wave Hub site. Uniform current field at the Wave Hub site are observed with and without wave forcing.

The bottom stress becomes larger at low tide and high wave, and also at mid-tide and high wave. This change occurs not only in the nearshore zone but also in some parts of the offshore area, which suggest that sediment transport changes significantly during the tidal cycle and storm peak.

The results of this study provides important and useful information for further studies in assessing the resources of wave energy and the impacts of the wave farm on the local and nearshore environment. Model results will be further validated against wave and current measurements by HF RADAR, ADCP

LITERATURE CITED

Booij, N., Ris, R.C., Holthuijsen, L.H., 1999. A third generation wave model for coastal regions, part I, model description and validation. Journal of Geophysical Research 104 (C4), 7649-7666.

Bowen, A. J. (1969), The generation of longshore currents on a plane beach, J. Mar. Res., 27, 206–214.

Buscombe D.D. & Scott T.M., 2008. The coastal geomorphology of north Cornwall, Wave Hub impact on seabed and shoreline processes – report, http://www.research.plymouth.ac.uk/whissp/index.html

Egbert, Gary D., Svetlana Y. Erofeeva, 2002. Efficient inverse modeling of barotropic ocean tides. J. Atmos. Oceanic Technol., 19, 183–204.

Grant, W.D., Madsen, O.S., 1979. Combined wave and current interaction with a rough bottom. Journal of Geophysical Research 84 (C4), 1797-1808.

Longuet-Higgins, M. S. and Stewart, R. W. 1962: Radiation stress and mass transport in gravity waves, with application to 'surf beats', Journal of Fluid Mechanics 13 (4):481–504.

Millar D.L., Smith H.C.M., Reeve D.E., 2007. Modelling analysis of the sensitive of shoreline change to a wave farm. Ocean Engineering 34, 884-901.

Mulligan, R. P., A. E. Hay, and A. J. Bowen, 2008. Wave-driven circulation in a coastal bay during the landfall of a hurricane, J. Geophys. Res., 113, C05026, doi:10.1029/2007JC004500.

NOAA Wavewatch III. NOAA/NCEP Operational wave models [online]. Available from: http://polar.ncep.noaa.gov/waves.

Padman L. and Erofeeva S., 2004. A barotropic inverse tidal model for the Artic Ocean, Geophysical Research Letters, vol. 31.

SWRDA - South West of England Development Agency, 2006. Wave Hub development and design phase, SWRDA Group Limited, coastal processes study report. http://www.wavehub.co.uk/.

Warner J.C., Sherwood C.R., Signell R.P., Harris C.K., Arango H.G., 2008. Development of a three dimensional, regional, coupled wave, current, and sediment transport model. Computers & Geosciences 34, 1284-1306.

Wolf J., Prandle D., 1999. Some observations of wave-current interaction, Coastal Engineering 37, 471 – 485.

Zou, Q.P., 2004. A simple model for random wave bottom friction and dissipation. Journal of Physical Oceanography 34 (6), 1459-1467.

ACKNOWLEDGMENTS

The impact of a wave farm on large scale sediment transport

R. Gonzalez-Santamaria[#1], Q.-P. Zou[*2] and S. Pan[#3]

[#] Plymouth University, School of Marine Science and Engineering,

Drake Circus, PL4 8AA, Plymouth, United Kingdom

[1]raul.gonzalez@plymouth.ac.uk   [3]shunqi.pan@plymouth.ac.uk

[*]Department of Civil and Environmental Engineering,

University of Maine, Orono, Maine 04469, USA

[2]qingping.zou@maine.edu

Abstract— **This study investigates the interactions of waves and tides at a wave farm in the southwest of England, in particular their effects on radiation stress, bottom stress, and consequently on the sediment transport and the coast adjacent to the wave-farm (the Wave Hub). In this study, an integrated complex numerical modelling system is setup at the Wave Hub site and is used to compute the wave and current fields by taking into account the wave-current interaction, as well as the sediment transport. Results show that tidal elevation and tidal currents have a significant effect on the wave height and direction predictions; tidal forcing and wind waves have a significant effect on the bed shear-stress, relevant to sediment transport; waves via radiation stresses have an important effect on the longshore and cross-shore velocity components, particularly during the spring tides. Waves can impact on bottom boundary layer and mixing in the water column. The results highlight the importance of the interactions between waves and tides when modelling coastal morphology with presence of wave energy devices.**

Keywords— **Wave Hub, Wave-tide interaction, Sediment transport, SWAN, ROMS**

I. INTRODUCTION

The Wave Hub project aims to create one of the world's largest wave farms for demonstration and testing wave energy converter devices, located at the southwest coast of England, as shown in Fig. 1. Recent studies at the Wave Hub site suggest that wave induced currents are important in controlling sediment movement (SWRDA, 2006). Better understanding of tidal effects on waves and sand transport is crucial to wave resource characterization and environmental impact assessment of the wave farm at the Wave Hub site. A study by SWRDA (2006) based on numerical modelling suggests that the wave energy converters (WECs) installed at Wave Hub would cause a reduction between 3% - 5% of wave height in the near coast of the Wave Hub, as well as changes in tidal currents and bathymetry. In their study the hydrodynamic model, Flow3D, was forced by four tidal constituents during a storm to assess the impact of the deployed WECs on tidal currents and sediment transport. Wave buoy data from 3 to 14 Feb 2005 was used in the model calibration. Tidal currents recorded maximum current
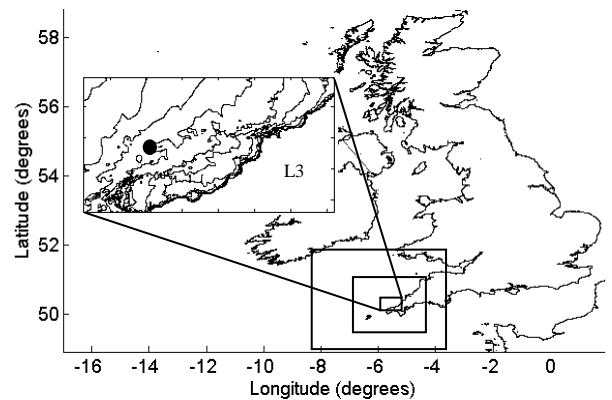

Fig. 1 SWAN nested grids (squares); SWAN+ROMS coupled system domain (L3), Wave Hub site (●).

velocities of 1.2 m/s. The admiralty pilot reports tidal currents between 0.5 and 1.0 m/s on the north coast of Cornwall during spring tides. To assess the WECs effect on the studied area, wave dragon devices were used as the worst case scenarios. Model results show that sediment transport for the worst case scenario changes significantly at the Wave Hub site, but the impact of the wave farm on the adjacent nearshore zone remains an unresolved issue. Millar et al (2007) carried out a study at the Wave Hub site to estimate the impact of WECs on the nearshore wave climate by analysing the wave energy transmitted through the WECs to the adjacent nearshore region. By comparing the SWAN model results with field observations from wave buoys, they concluded that assuming a 90% transmission rate, the average reduction in significant wave height was of the order of 1cm, and that the stretch of the coast most likely to be affected was between Godrevy and Towan Heads that are close to the Wave Hub site.

From the perspective of the impact on this stretch of coast, the sand transport due to tides is believed to be weak and unquantified in this region, and the volume of sand involved is limited in comparison with other sectors of the English coasts. Therefore, wave induced currents are more important in controlling sediment movement. The prevailing winds are from the South and West, but easterly winds can also produce significant movement of sediment. Although storm events
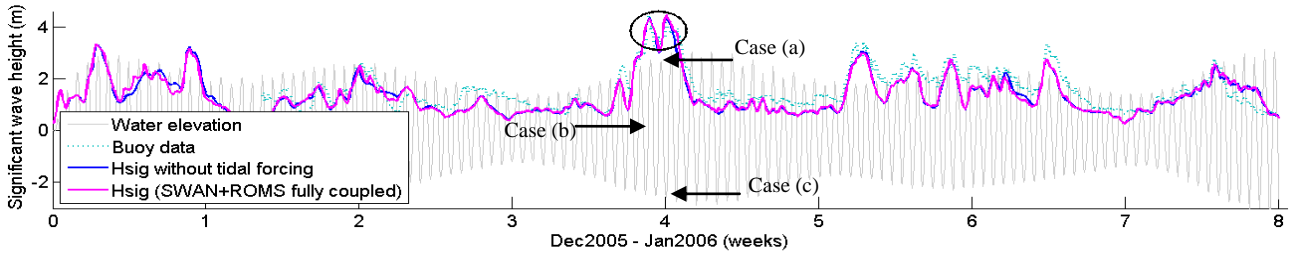
Fig. 2 Significant wave heights with/without tidal influence. Circle represents maximum storm Hsig at spring tide. Three main cases have been analysed at the peak of the storm event indicated by the circle: at high water elevation and low current velocity (Case a); at middle water level and high current velocity (Case b); and at low water elevation and low current velocity (Case c).

may cause movement of sand on the inner shelf, their effects are greater in the nearshore zone where significant cross- and long-shore sediment transport takes place (Buscombe and Scott, 2008). Clearly, there is a lack of studies in the nearshore and shoreline areas in the lee side of the wave farm, thus, the aim of this study is to investigate the wave-tide interactions, in particular their effects on sediment transport along the coast behind the wave-farm. We examine the tidal effects on wave, wave-induced currents, radiation stresses and bottom stresses, using a complex wave-current coupled numerical modelling system to gain insight into how wind waves and tidal currents affect the current and bottom friction at the Wave Hub site and the adjacent nearshore zone.

II. THE MODELLING SYSTEM

In this study, the spectral wave model SWAN (Booij et al, 1999) and the flow circulation model ROMS are used to form a fully two-way coupled modelling system (Warner et al, 2008). As shown in Fig. 1, the SWAN model is run with three nested domains with progressively finer grid resolutions. At the finest grid (L3), the SWAN is coupled with the ROMS model to form the coupled modelling system (SWAN+ROMS). The SWAN model is fed by the output of the global wave spectral model Wave Watch III (NOAA:

http://polar.ncep.noaa.gov) driven by the wind fields from the Global Forecast System (GFS) model. The global tidal model OTPS (Egbert et al, 2002; Padman and Erofeeva, 2004) provides tidal currents and water elevations as boundary conditions for the ROMS model. The wave model results can be affected by both water elevations and tidal currents, hence, the tidal information obtained from the ROMS model is used in the wave model.

The tidal model used is the Oregon State University Tidal Prediction Software (OTPS/TPXO) based on the TOPEX/POSEIDON altimeter data (Egbert et al, 2002; Padman and Erofeeva, 2004), which was used to obtain predictions of tidal currents and water elevations from eleven harmonic constituents (M_2, S_2, N_2, K_2, K_1, O_1, P_1, Q_1, M_4, MS_4, MN_4). We found that the predicted water elevations are in a good agreement with the measurements from tide gauges near to the Wave Hub site.

In addition, a sediment transport model embedded in ROMS was incorporated in the modelling system for computing sediment transport for beach morphologicaL changes. The Soulsby and Damgaard (2005) formulae is applied for computing bedload transport which accounts for the combined effects of mean currents and asymmetrical waves on bedload flux. The bed model accounts for changes
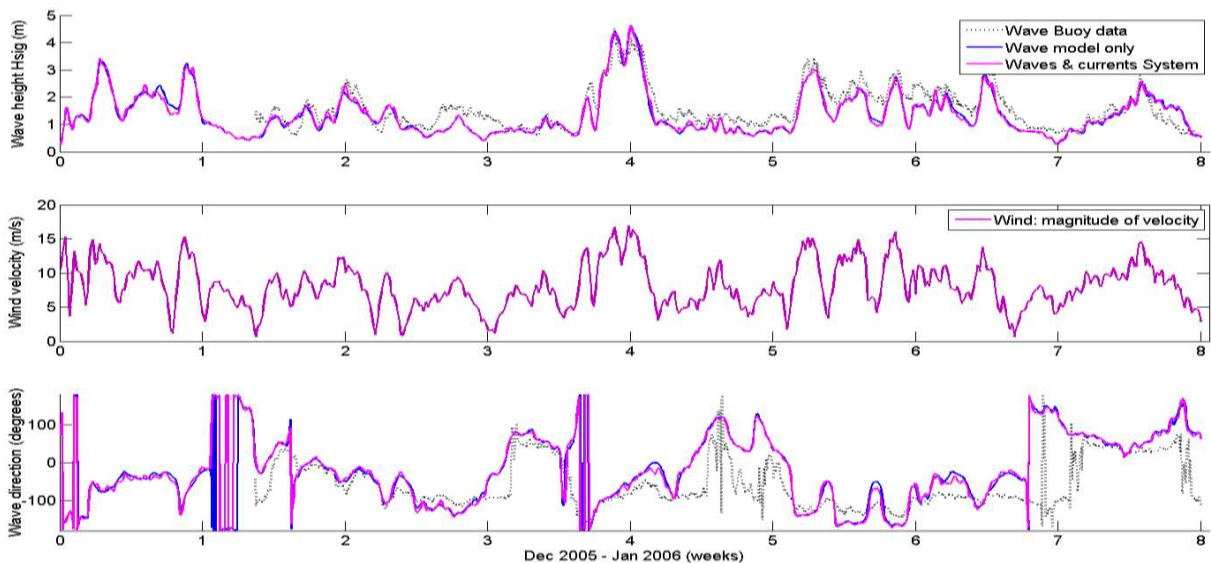

Fig. 3 Time series at the Wave Hub site of significant wave height (top), magnitude of wind velocity (middle), and wave direction (bottom), for the wave-current interaction and waves only. Note the strong correlation between the wind, the significant wave height, and the wave direction.

in sea floor elevation resulting from convergence or divergence in sediment fluxes. These morphological changes can have an impact on flow transport when they are larger (Warner et al, 2008).

The coupled modelling system (SWAN+ROMS) was applied to assess the impact of waves on tidal currents and tidal currents on waves. To achieve this, a series of different cases combining spring and neap tides, high and low water levels, high and low wave conditions, were investigated to examine the changes in wave parameters, current velocities and bottom stresses.

The two-way coupled modelling system consists of two models which are linked with shared information: the ROMS model, which computes sea surface levels, depth averaged horizontal velocity components and bottom stress based on the given sediment grain size; and the SWAN model, which computes wave height, wave length, wave period and wave bottom orbital velocities. Between these two models, the currents and water levels computed in ROMS are used in SWAN and the radiation stresses derived from the SWAN are used to calculate the wave induced current in ROMS, so that the dynamic interaction between waves and tides is realised. In addition, wind fields are used as the surface forcing in the SWAN model for predicting the wave field, but, the wind stress is ignored in the ROMS model due to the relatively small computational domain.

III. RESULTS

A. Wave-tide interaction

The modelling system was run for two months, from 1st December 2005 to 31st January 2006 due to the availability of wave buoy data. Three test cases were selected to examine the space distribution of wave-tide interactions through the tidal cycle. These test cases are selected at the peak of the storm and during spring tide: Case (a) High water level and low current velocities; Case (b) Middle water level and high current velocities; Case (c) Low water level and low current velocities.

Fig. 2 shows the influence of tidal currents and tidal elevations on the significant wave heights at the Wave Hub site predicted by the coupled system, compared with buoy measurements. Fig. 3 shows the differences, with and without tidal currents, of the significant wave height and wave direction for the cases indicated above within the L3 domain (see Fig. 1). This figure shows the difference between the coupled modelling system and the wave model only for the significant wave height and wave direction, but mostly the strong correlation of wave height, wave direction and wind velocity, suggesting that wind waves play an important role on the longshore currents and therefore on the sediment transport. The wave direction oriented more along the shore would produce stronger alongshore currents, for example during the low water level case. When tidal currents are included, the wave direction is modified by less than 10 degrees during high waves, but about 20 degrees during low waves.

In order to study the wave-tide interactions, the concept of radiation stress is included, which is the flux of momentum carried by the ocean waves. When these waves break, the wave momentum is transferred to the water column, inducing near-shore currents. Radiation stress theory has been successfully used to explain the presence of long-shore currents (Bowen, 1969). Significant momentum can be transferred from waves to currents when a strong radiation stress gradient occurs due to wave breaking and to the bottom friction in the near-shore region. Radiation stress gradients are determined from the spatial gradients in the directional energy spectrum of the wave model and the strongest gradients in radiation stress occur where depth-induced breaking happens (Mulligan et al, 2008).

Waves and currents are coupled through the following physical mechanisms: i) surface shear stress, the effect of surface waves on the drag coefficient is included in ROMS (Warner et al, 2008); ii) bottom stress, waves enhance the turbulent mixing, therefore, waves modify the bottom stress experience by currents (Grant & Madsen, 1979; Zou, 2004); and iii) radiation stress which represents the excessive momentum flux within the circulation due to the presence of waves (Longuet-Higgins and Stewart, 1964).

Comparisons between surface current velocities at the Wave Hub site from the coupled modelling system (SWAN+ROMS) and the circulation model (ROMS) were carried out. These comparisons are shown in Gonzalez-Santamaria et al (2011), the results indicate that the impact of wave-current interactions on the computed current velocities is significant during the spring tides. Similar to the current velocities, both
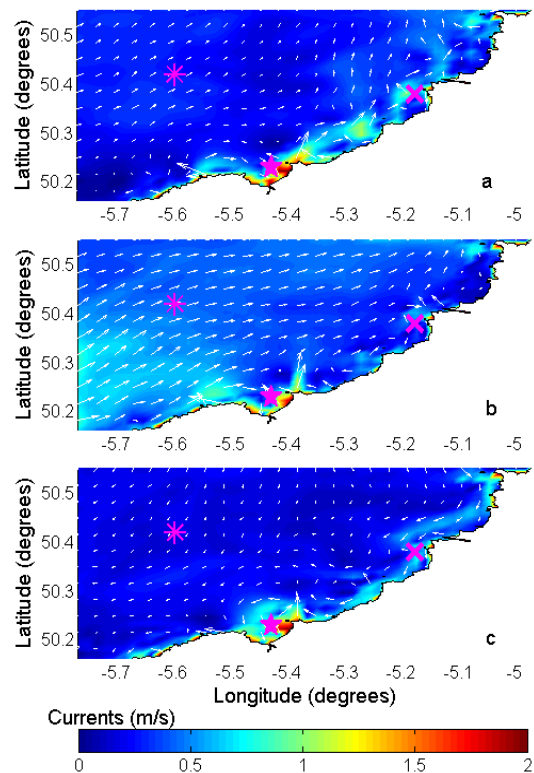

Fig. 4 Spatial distribution of bottom current velocities (ROMS+SWAN fully coupled) for the cases indicated in Fig. 2: high water elevation (a); mid water elevation (b); low water elevation (c).

Wave Hub site (*), St Ives bay (★) and St Agnes (×).

components of the current-induced bottom stress in a spring tide are significantly affected by the waves. As waves propagate towards the coast, the wave propagation speed and direction may be modified by tidal currents due to refraction. In general, the main changes of wave direction are found during low wave heights and high tidal currents. Three reference sites shown in Fig. 4 for further comparisons are the Wave Hub site, St Ives bay and St Agnes. It was found that at the Wave Hub site the current magnitudes, after removing the tidal signal, are smaller than those at St Ives bay and St Agnes where the wave action enhances the current significantly. At St Agnes, the longshore currents vary from -0.5 to 0.5 m/s, and at St Ives bay, longshore currents vary from -0.5 to 1.1 m/s. This is the result of wave propagation direction relative to the shoreline at this site.

The spatial distribution of the wave influence on bottom currents is shown in Fig. 4 where larger velocities and eddies are observed along the coast which are up to 2 m/s. In Case (a), when the water elevation is high but with low tidal currents, the region with significant wave induced currents is more confined to the coast. In Case (b) for middle water level, tidal currents are at its maximum, and the total current velocity field is uniform in the offshore zone and increases in magnitude in the nearshore zone where the significant wave height is high. In Case (c), water elevations and tidal currents are both in minimum, the region with significant wave induced currents is extended in the offshore direction due to decreasing water depth.

The velocities near the coast, predicted by the fully coupled modelling system, are clearly enhanced by the wave forcing, particularly in the longshore direction. In St Ives bay, this effect is the most significant (Fig. 4).

When tidal currents and wave induced currents are coupled,

the currents field at the Wave Hub site increases significantly, compared with the results when there is no wave interaction. The total current is dominated by the tidal currents which are more uniform away from the coast. However, along the shoreline, currents are enhanced by the wave action through radiation stress. This means that wave induced currents are significant in this zone, even though the tidal currents are the main force for the general circulation.

B. Wave farm effects

The wave farm was set in the SWAN model as suggested in Millar et al (2007), arrays of WECs at the Wave Hub site represented as a 4km partially transmitting obstacle, aligning approximately parallel to the incoming wave crests. The energy transmission percentage was set as 75% which represents an array of densely spaced, high-efficiency WECs.

Fig. 5 shows significant wave height (colours) and wave direction (vectors) for the storm case and for the tidal cycle cases. In this figure the difference between the wave-current interaction against the wave-current and wave farm interaction is shown. The change of the wave height with and without the wave farm is between 5cm and 10 cm at the nearshore line, and the maximum extension affected by the wave farm is about 26km from St. Ives Bay to upwards for the high water level case which is the most significant in terms of wave height variations.

Fig. 6 shows the bottom stress contribution by waves (left) and by tides (right) for the tidal cycle cases. The wave contribution on the bottom stress is large compared to tides only, driving the sediment transport at the most and during the storm peak.

Fig. 7 shows the combined wave-current bottom stress (left panels) at different water levels during the tidal cycle, as well
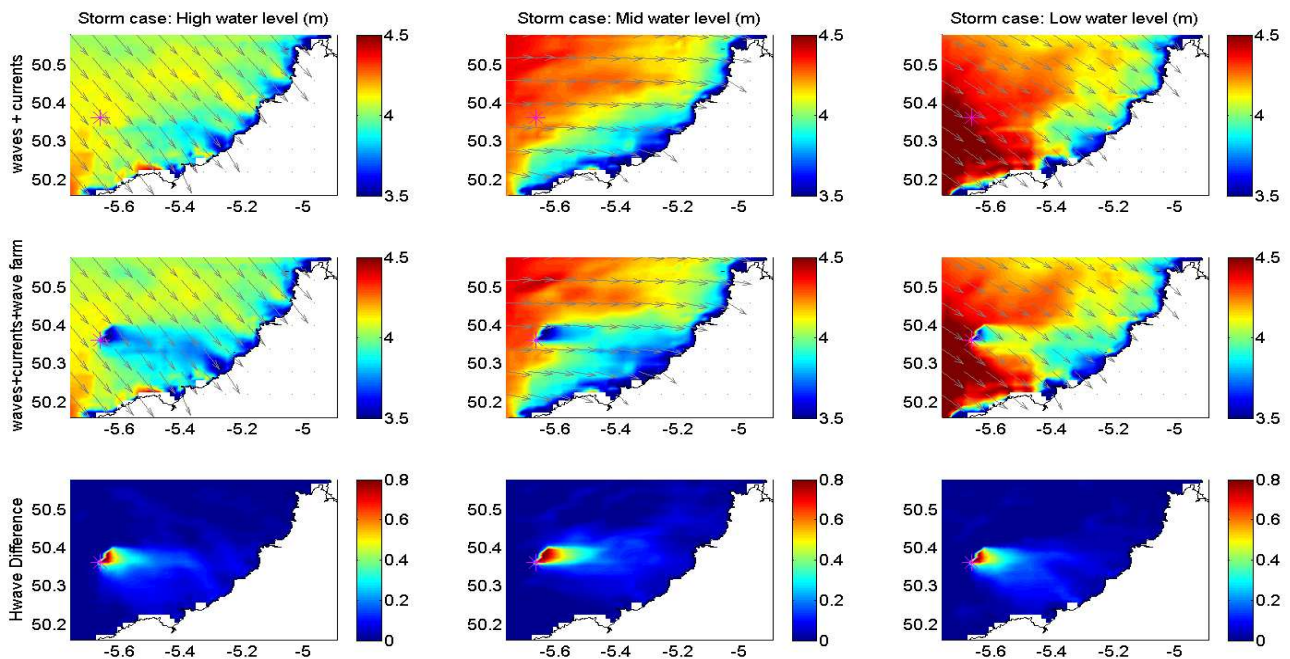

Fig. 5 Significant wave height (colours) and wave direction (vectors) for the storm case and for the tidal cycle cases. In this figure is shown the difference (bottom panels) between the wave-current interaction (top panels) and the wave-current & wave farm interaction (middle panels). Wave Hub site (*).

as the velocity vectors because both magnitude and direction are important when correlating wave induced currents. The bottom stress is also correlated with the currents field for Cases (a) to (c) and is affected by the local water depth. The region with significant bottom stress is confined to the shallow water region and moves towards/away from the coast when the water level decreases/increases during the tidal cycle. Case (c) shows maximum bottom stress along the coast because of lower water elevation, Case (a) shows smaller bottom stress because of the high water elevation. The bottom stress difference with and without the wave farm (right panels) shows the most significant variation for the low water level case, which is strongly correlated to the currents field, waves and depth.

C. Sediment transport distribution

Fig. 8 shows the non-cohesive sediment (sand) concentration (kg/m^3) for the fully coupled system (left panels) and the difference with and without the wave farm effect (right panels). Here the Case (c) is the most significant as the sediment transport changes as the tidal cycle varies during the storm peak. As expected, the bottom stress has a strong correlation with the sediment distribution, for the low water level case; however, when the velocity current is close to zero (top and bottom panels) the wave farm has an effect on the sediment distribution and this is directly correlated to the wave contribution. The wave contribution is driven mainly by the wind. The observed changes in sediment concentration with and without the wave farm are up to 0.002 kg/m^3 at St. Ives Bay for the variation of the tidal cycle. As

Fig. 6 Bottom stress comparisons by waves (left) and by tides (right) only, and velocity vectors (arrows) for the tidal cycle cases. Wave Hub site (*).
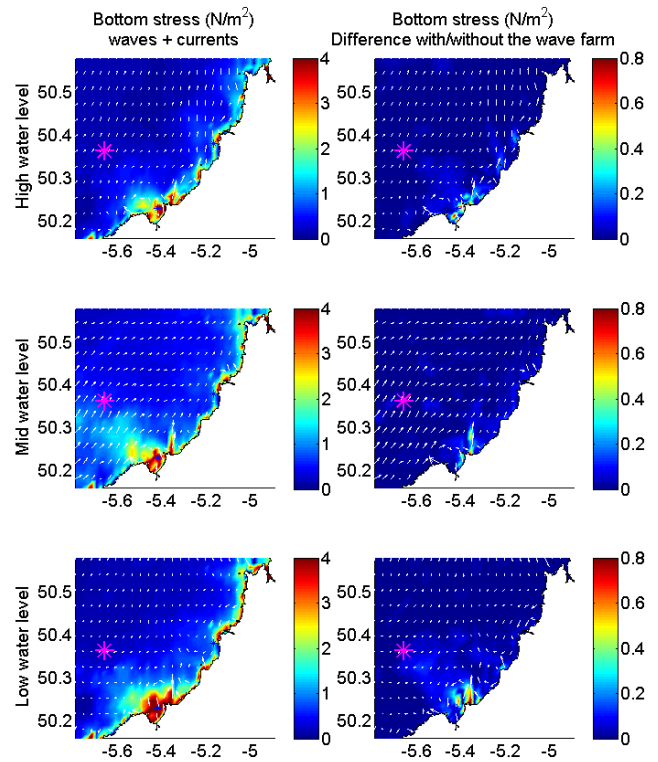

Fig. 7 Bottom stress differences, for the full wave-current interaction, with and without the wave farm and velocity vectors (arrows). Note that for the case of low water level, the wave farm has a significant effect on the bottom stress. Wave Hub site (*).

the tidal cycle varies the sediment concentration extends about 26 km upwards from St. Ives Bay for the high water level case which has larger effects. On the other hand, at the low water level case, the sediment concentration moves in some offshore areas, mainly in the lee of the wave farm.

IV. CONCLUSIONS

In this study, a two-way coupled modelling system with the SWAN and ROMS models has been used to study the wave-current interaction and the impact of the Wave Hub site on the nearshore area, a wave farm in the South West of England. The wave model, SWAN, was nested from coarse to fine grids, forced by the spectral wave model Wave Watch III and wind fields from the GFS model. The circulation model, ROMS, was forced by the tide outputs from the global tidal model OTPS and by the wave forcing from the SWAN model on the fine grid. The sediment transport model was incorporated to estimate the non-cohesive concentration affected by waves, tides and the wave farm. Model results are in good agreement with the measurements by tide gauges and wave buoy.

Model results at high, middle and low tidal levels during the peak of a storm were presented to show tidal effects on waves, current velocities and bottom stresses, during spring tides. It is found that the wave height increases with the tidal elevation, and the wave direction is modified by the change of direction of tidal currents. We also found that the tidal current effect on waves is at maximum at middle and low
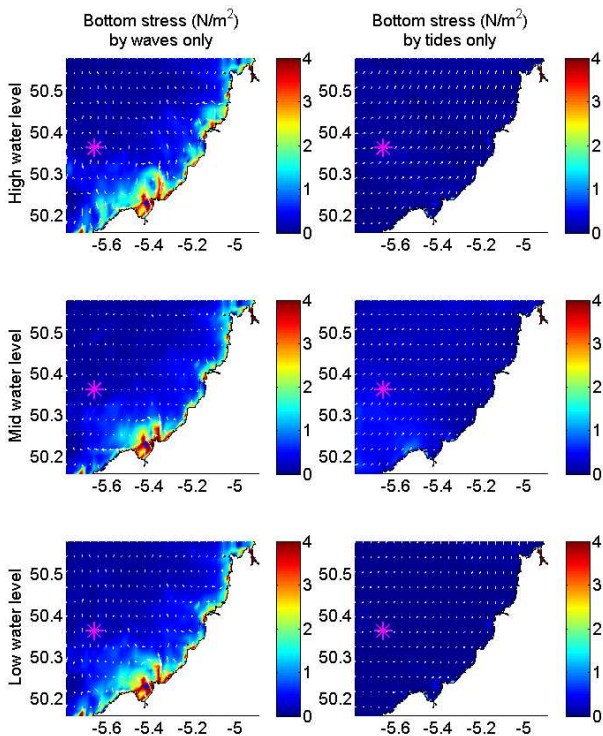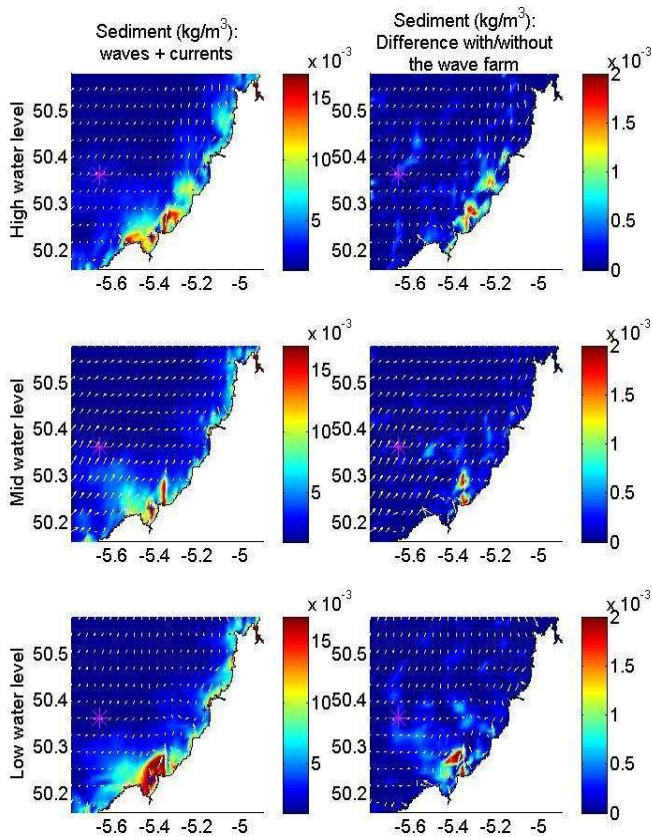
Fig. 8 Sediment transport distribution (colours) and velocity vectors (arrows) for the tidal cycle cases (left panels), and the difference with and without the wave farm (right panels). Wave Hub site (*).

tides when the tidal current is at its peak and the tidal elevation change has a significant effect on wave directions. The tidal current effect on wave direction is relatively small when wave height is large.

Wave effects on currents are isolated by removing the tidal signals from current velocity and bottom stress. Model results show significant cross- and long-shore wave induced currents along the shoreline, which is at its peak at mid-tide with maximum tidal currents and at peak wave heights. Wave induced current is negligible at the Wave Hub site. Uniform current field at the Wave Hub site are observed with and without wave forcing.

The bottom stress becomes larger at low tide and high wave, and also at mid-tide and high wave. This change occurs not only in the nearshore zone but also in some parts of the offshore area, which suggest that sediment transport changes significantly during the tidal cycle and storm peak.

The change of the wave height with and without the wave farm varies between 5cm and 10 cm at the nearshore area, and the maximum extension affected by the wave farm is about 26km from St. Ives Bay to upwards at the high water level case.

The bottom stress difference with and without the wave farm shows significant variations at the low water level case, strongly correlated to the wave contribution through radiation stresses.

The observed changes in sediment concentration with and without the wave farm are up to 0.002 kg/m^3 at St. Ives Bay. As the tidal cycle varies the sediment concentration has larger effects at the high water level case, with maximum extension of 26 km upwards from St. Ives Bay. At the low water level case the sediment concentration moves in some offshore areas, this effect is closely correlated to the bottom stress results.

The results of this study provide important and useful information for further studies in assessing the resources of wave energy and the impacts of the wave farm on the local and nearshore environment. Model results will be further validated against wave and current measurements by HF RADAR, ADCP and Directional Waverider buoys taken during the on-going Wave Hub project.

REFERENCES

[1] N. Booij, R.C. Ris, L.H. Holthuijsen. "A third generation wave model for coastal regions, part I, model description and validation," Journal of Geophysical Research 104 (C4), 7649-7666. 1999.

[2] A. J. Bowen, "The generation of longshore currents on a plane beach," J. Mar. Res., 27, 206–214. 1969.

[3] D.D. Buscombe, T.M. Scott, "The coastal geomorphology of north Cornwall, Wave Hub impact on seabed and shoreline processes – report," [online]. Available: http://www.research.plymouth.ac.uk-/whissp/index.html/

[4] G. D. Egbert, S. Y. Erofeeva, "Efficient inverse modeling of barotropic ocean tides," J. Atmos. Oceanic Technol., 19, 183–204. 2002.

[5] R. Gonzalez-Santamaria, Q.-P. Zou and S. Pan, "Two-way coupled wave and tide modelling of a wave farm," Journal of Coastal Research, SI 64 (Proceedings of the 11th International Coastal Symposium), 1038–1042, Szczecin, Poland, ISSN 0749-0208. 2011.

[6] W.D. Grant, O.S. Madsen, "Combined wave and current interaction with a rough bottom," Journal of Geophysical Research 84 (C4), 1797-1808. 1979.

[7] M. S. Longuet-Higgins, R. W. Stewart, "Radiation stress and mass transport in gravity waves, with application to 'surf beats'," Journal of Fluid Mechanics 13 (4):481–504. 1962.

[8] D.L. Millar, H.C.M. Smith, D.E. Reeve, "Modelling analysis of the sensitive of shoreline change to a wave farm," Ocean Engineering 34, 884-901. 2007.

[9] R. P. Mulligan, A. E. Hay, and A. J. Bowen, "Wave-driven circulation in a coastal bay during the landfall of a hurricane," J. Geophys. Res., 113, C05026, doi:10.1029/2007JC004500. 2008.

[10] NOAA Wavewatch III. NOAA/NCEP Operational wave models. [online]. Available: http://polar.ncep.noaa.gov/waves.

[11] L. Padman and S. Erofeeva, "A barotropic inverse tidal model for the Artic Ocean," Geophysical Research Letters, vol. 31. 2004.

[12] R.L. Soulsby, J.S. Damgaard, "Bedload sediment transport in coastal waters," Coastal Engineering 52 (8), 673-689. 2005.

[13] SWRDA - South West of England Development Agency, Wave Hub development and design phase, SWRDA Group Limited, coastal processes study report. [online]. Available: http://www.wavehub.co.uk/

[14] J.C. Warner, C.R. Sherwood, R.P. Signell, C.K. Harris, H.G. Arango, "Development of a three dimensional, regional, coupled wave, current, and sediment transport model," Computers & Geosciences 34, 1284-1306. 2008.

[15] Q.P. Zou, "A simple model for random wave bottom friction and dissipation," J. of Physical Oceanography 34 (6), 1459-1467. 2004.

MODELLING WAVE-TIDE INTERACTIONS AT A WAVE FARM
IN THE SOUTHWEST OF ENGLAND

Raúl González-Santamaría[1], Qingping Zou[1], Shunqi Pan[1], Roberto Padilla-Hernandez[2]

The Wave Hub project will create the world's largest wave farm off the coast of Cornwall, Southwest England. This study is to investigate wave and tide interactions, in particular their effects on bottom friction and sediment transport at the wave-farm coast. This is an ambitious project research which includes the use of a very complex numerical modelling system. The main question to answer is how waves, tidal currents and winds affect the bottom friction at the Wave Hub site and the near-shore zone, as well as their impact on the sediment transport. Results show that tidal elevation and tidal currents have a significant effect on the wave height predictions; tidal forcing and wind waves have a significant effect on the bed shear-stress, relevant to sediment transport; waves via radiation stresses have an important effect on the long-shore and cross-shore velocity components, particularly during the spring tides. Waves can impact on bottom boundary layer and the mixing in the water column. Interactions between waves and tides at the Wave Hub site is important when modelling coastal morphology influenced by wave energy devices. This open-source modelling system tool will help the study of physical impacts on the Wave Hub farm area.

Keywords: Wave Hub; marine renewable energy; wave-current interaction; wave-tide interaction; SWAN; ROMS.

INTRODUCTION

The Wave Hub project aims to create the world's largest wave farm for demonstration and proving of operation of arrays of wave energy converter devices, located at the southwest coast of England (Figure 1). Recent studies at the Wave Hub site suggest that wave induced currents are important in controlling sediment movement (SWRDA, 2006). Better understanding of tidal effects on waves and sand transport is crucial to wave resource characterization and environmental impact assessment of the wave farm at the Wave Hub site.

A modelling study done by SWRDA (2006) suggests that the wave energy converters (WECs) installed at Wave Hub would cause a reduction between 3% - 5% of wave height on the coast off to the Wave Hub site, as well as changes in surface tidal currents and offshore bed elevations. Key areas of study are the estimated wave height attenuation and tidal currents in the lee of the Wave Hub site and the associated impact on sedimentation, beach topography and beach state. From the perspective of the effect on the coast, the tidal control on sand transport is weak and regionally uncertain, and volumes of sand involved are limited in comparison with other sectors of the English coast. Wave induced currents are more important in controlling sediment movement. The prevailing winds are from the south and west, but easterly winds can produce significant movement of sediment. Storm events cause movement of sand on the inner shelf but the effects are greater in the narrow, shallower near-shore zone. Also cross-shore sediment transport takes place. (Buscombe & Scott, 2008).

Millar et al (2006) carried out a study at the Wave Hub site with to estimate the impacts of WECs on the near-shore wave climate by analysing the wave energy transmitted to the devices and to the shoreline. They applied the SWAN model and used field observations from wave buoys. They concluded that at 90% transmission the average reduction in significant wave height was of the order of 1cm, and that the stretch of the coast most likely to be affected was between Godrevy and Towan Heads. The admiralty pilot reports tidal streams on the north coast of Cornwall at a spring rate of 1 to 2 knots (0.5 to 1.0 m/s). In the modelling study published by SWRDA (2006), the deployed buoy recorded wave parameters and tidal currents, maximum velocities of 1.2 m/s were measured, the hydrodynamic model applied (Flow3D) was forced by four tidal constituents during a storm to assess the impact of the deployed devices on tidal currents, sediment regime and wave buoy data from 03/02 to 14/02 2005 was used in the calibration of the model. The devices used for worst case scenarios in the simulation were the wave dragons. The sediment transport was modelled with and without the presence of wave and current regime, results of the sediment transport for the worst case scenario shows significant changes at the Wave Hub site.

The aim of this study is to investigate wave-tide interactions, in particular their effects on sediment transport at the wave-farm coast, looking at the vertical column stratification through the relationships of wave-currents and bottom stresses. This project includes the use of a very complex numerical modelling

system. The main question to answer is how waves, tidal currents and winds affect the bottom friction at the Wave Hub site and the near-shore zone, as well as their impact on the sediment transport.

THE WAVE-CURRENT MODELLING SYSTEM

The SWAN model

The Simulating WAves in the Near-shore (SWAN) wave model is a phase averaged wind wave model developed by Booij et al. (1999) that is widely used to simulate wave conditions in coastal areas, where propagation, wave generation and dissipation processes are represented as: refraction and shoaling, reflection, diffraction, bottom friction, and depth induced breaking. The model solves the action balance equation, where action density is $N(\sigma, \theta)$, which is the energy density $E(\sigma, \theta)/\sigma$. The relative wave frequency σ is related to the fixed wave frequency ω by the wave number vector $\boldsymbol{k}$ and mean current vector $\boldsymbol{u}$.

$$\sigma = \omega - \boldsymbol{k} \cdot \boldsymbol{u} \tag{1}$$

The evolution of the wave field in SWAN is described by the action balance equation

$$\frac{\partial}{\partial t}N + \frac{\partial}{\partial x}(c_x + u)N + \frac{\partial}{\partial y}(c_y + v)N + \frac{\partial}{\partial \sigma}c_\sigma N + \frac{\partial}{\partial \theta}c_\theta N = \frac{S_{tot}}{\sigma} \tag{2}$$

which describes the local rate of change of action density with time, t, and the propagation of action density in each dimension. Velocities c_x and c_y are spatial x and y components of the group velocity c_g, the speed at which wave action is transported. c_σ and c_θ are the rate of change in spectral space, which describe the directional (θ) rate of turning and frequency shifting due to changes in currents (u, v) and water depth. Wave propagation on the left-hand side of equation (2) is balanced by local changes to the wave spectrum from energy density source terms S_{tot} on the right hand side, which describes the sources, sinks and distribution of energy in the wave spectrum (Booij et al., 1999). Radiation stresses are determined from spatial gradients in the directional energy spectrum $E(\sigma, \theta)$, the strongest gradients in radiation stress may occur where depth-induced breaking happens (Mulligan et al, 2008).

The ROMS model

The Regional Ocean Modeling System (ROMS) is a fully 3D baroclinic circulation model which solves the Reynolds-averaged Navier-Stokes equations using the hydrostatic and Boussinesq assumptions (Warner et al, 2008). The vertical coordinate is implemented as being a sensible way to handle variations in the water depth. The ROMS equations have been modified to include wave induced momentum flux (horizontal and vertical wave radiation stresses) that are important in near-shore regions by adding depth-dependent radiation stress terms in the three-dimensional momentum equations and depth-independent terms to the two-dimensional momentum equations, neglecting Coriolis, density variations, and scalar transport (Haas and Warner, 2009). The governing equations in Cartesian coordinates are:

$$\frac{\partial(H_z u)}{\partial t} + \frac{\partial(u H_z u)}{\partial x} + \frac{\partial(v H_z u)}{\partial y} + \frac{\partial(\Omega H_z u)}{\partial s} = -H_z g \frac{\partial \eta}{\partial x} - \frac{\partial(\overline{u'w'})}{\partial s} - \frac{\partial(H_z S_{xx})}{\partial x} - \frac{\partial(H_z S_{xy})}{\partial y} + \frac{\partial S_{px}}{\partial s} \tag{3}$$

$$\frac{\partial(H_z v)}{\partial t} + \frac{\partial(u H_z v)}{\partial x} + \frac{\partial(v H_z v)}{\partial y} + \frac{\partial(\Omega H_z v)}{\partial s} = -H_z g \frac{\partial \eta}{\partial y} - \frac{\partial(\overline{v'w'})}{\partial s} - \frac{\partial(H_z S_{xy})}{\partial x} - \frac{\partial(H_z S_{yy})}{\partial y} + \frac{\partial S_{py}}{\partial s} \tag{4}$$

$$0 = -\frac{1}{\rho_0}\frac{\partial p}{\partial s} - \frac{g}{\rho_0}H_z \rho \tag{5}$$
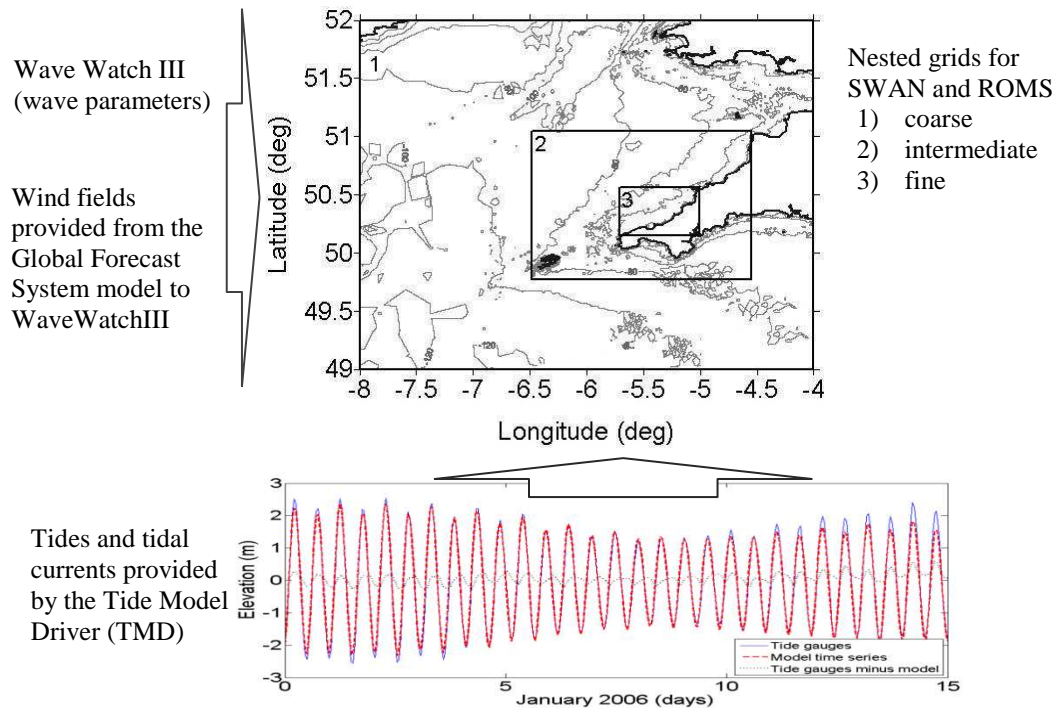
with continuity as

$$\frac{\partial \eta}{\partial t} + \frac{\partial(H_z u)}{\partial x} + \frac{\partial(H_z v)}{\partial y} + \frac{\partial(\Omega H_z)}{\partial s} = 0 \tag{6}$$

where **u, v** and Ω are the mean components in the horizontal (x and y) and vertical (s) directions respectively; the vertical sigma coordinate $s = (z - \eta)/D$ ranges from s= -1 at the bottom to s= 0 at the free surface; z is the vertical coordinate positive upwards with z=0 at mean sea level; η is the wave-averaged free surface elevation; D is the total water depth $D=h+\eta$; h is the depth below mean sea level of

the sea floor; H_z is the grid cell thickness. An overbar represents a time average, and a prime(') represents turbulent fluctuations. Pressure is p; ρ and ρ_o are total and reference densities; g is acceleration due to gravity; and a fuction $\rho=f(C)$ where C represents a tracer quantity (e.g. salt, temperature, suspended sediement) is required to close the density relation. These equations are closed by parameterizing the Reynolds stress using one of the five options for turbulent-closure models in ROMS (Hass and Warner, 2009).

In equations (3) and (4) the terms on the left side are: the change rate, horizontal advection and vertical advection; on the right side: surface pressure gradient, vertical viscosity, horizontal radiation and vertical radiation (where the surface roller term is included). Equation (5) represents the hydrostatic buoyancy force and the equation (6) represents the continuity equation. The above equations neglect Coriolis force, density variations and scalar transport, as well as the momentum transfer term that correlates wind-induced surface pressure fluctuations and wave slope. The horizontal radiation stress terms can be seen in full detail in Warner et al (2008) and Hass and Warner (2009).

The coupled system

Wave Watch III (wave parameters)

Wind fields provided from the Global Forecast System model to WaveWatchIII

Nested grids for SWAN and ROMS
1) coarse
2) intermediate
3) fine

Tides and tidal currents provided by the Tide Model Driver (TMD)

**Figure 1. Model boundary conditions and nested grid domains.**

The complex numerical modelling system consists of two main open source models; the spectral wave model SWAN and the circulation ROMS model, which are a fully two way coupled, with a sediment transport module embedded system. The modelling system was set in the Wave Hub site. In operation the wave model is fed by the output of the global wave spectral model Wave Watch III (NOAA http://polar.ncep.noaa.gov), wind fields are provided from the Global Forecast System (GFS) model to WaveWatch III model, then, a tidal model provides tidal currents and water elevations to both SWAN and ROMS wave and circulation models. As shown in Figure 1, the coupled modelling system was run with three nested domains with a progressively finer grid resolution. In addition, a sediment transport model was incorporated in the modelling system for computing beach morphological changes, the results of which, however, are not discussed in this paper.

The wave model needs water elevations and tidal currents on the whole domain (not as boundary conditions), the circulation models requires tidal currents and water elevations to be forced as boundary conditions. The Tide Model Driver (TMD), a tidal prediction software through the Artic Ocean Tidal Inverse model (Padman and Erofeeva, 2004) based on the TOPEX/POSEIDON altimeter data, was used to obtain predictions of tidal currents and water elevations from eleven harmonic constituents (M_2, S_2, N_2, K_2, K_1, O_1, P_1, Q_1, M_4, MS_4, MN_4) for the studied area. At the bottom of the Figure 1 the predicted elevations and tidal currents are shown and they are in a good agreement with tide gauges. The test period for the study was from 1st to 31st January of 2006 with the available wave buoy data.

RESULTS

Model tests were first carried out with the SWAN model setting conditions of variation of tidal levels, tidal currents and constant wind. It was observed that normal conditions have a quicker numerical stabilisation rather than the extreme conditions, also it was observed a non-steady state produced by currents and water elevations.

Figure 3 shows the effect of tidal currents on spatial wave heights for the fine grid domainfor spring tides at high tidal level (top) and low tidal level (bottom). With tidal currents, the computed significant wave heights at the Wave Hub are higher by approximately 0.4 m in comparison with those computed without tidal currents at high water level. However, at the low tidal level, the magnitude of the increase is smaller, in a range of about 0.2 m.
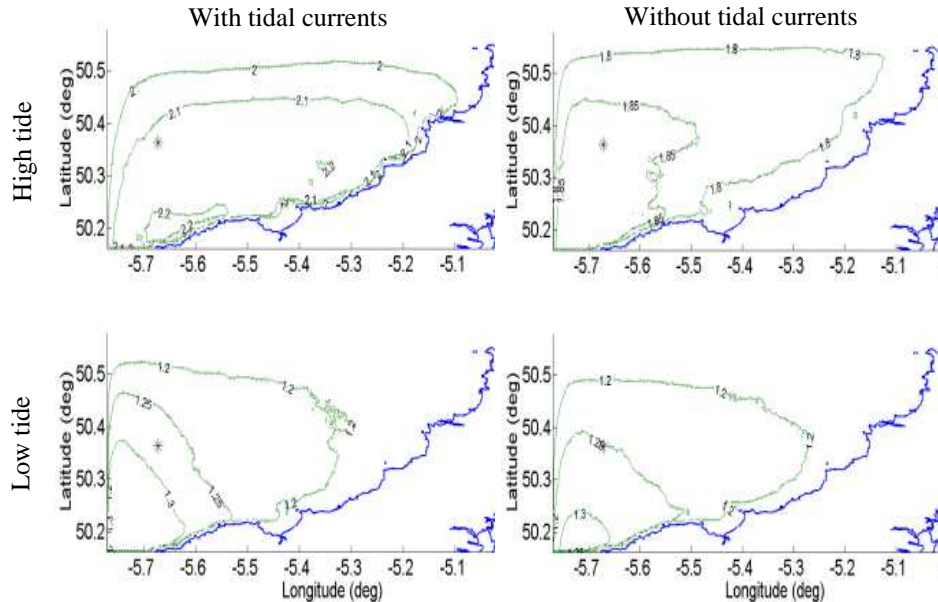
Figure 2. Snapshots of contours of the fine nested grid at the Wave Hub region at spring tide. (Left) Significant wave height (m) with tidal currents. (Right) Significant wave height (m) without tidal currents. (Top) High tide. (Bottom) Low tide. (*) Wave Hub site.

Bed shear stress

To understand the sediment transport due to waves and currents, it is necessary to calculate the bed shear stress (Wolf and Prandle, 1999). These results generate a wave-induced current and additional drift (long-shore current) (Figure 6), typically along the coast (Pleskachevsky et al, 2009).The water depth influences the wave: low tide affects the waves more due to bottom influence than in high water.

The next test-cases take into account analytical waves which were provided to the circulation model to interact with the tidal currents, analytical stands for wave parameters imposed as constant boundary conditions. Three main cases of wave and current interactions have been tested: firstly, with the influence

of tidal currents only; secondly, tidal currents and the influence of analytical waves and; thirdly, currents, waves and analytical wind stress.

For further model tests, both tidal elevation and currents are included together with the wave-induced current. Figure 3 shows that the depth-averaged long-shore and cross-shore components of current velocities at the Wave Hub site. For the sake of clarity, the computed current velocities have been decomposed into long shore and cross-shore directions based on the main direction of the shoreline at the site, neglecting the vertical structure of the horizontal velocities.

As shown in Figure 3, the velocities computed for tide only and combined tide and wave without wave-current interaction are found to be almost identical. However, when the wave-current interaction is included, the computed velocities are clearly enhanced, particularly for the long shore component. By removing the underlying tidal velocity, the impact of wave-current interaction on the computed current velocities is clearly illustrated during the spring tides, as shown in Figure 4.

The anomalies of the currents were calculated using a least square method (harmonic analysis), so that the general tidal variation can be removed. Figure 5 shows the kinematic bottom stresses. Similar as velocities, the long-shore component at a spring tide has major impacts on the bed shear rather than the cross-shore component.
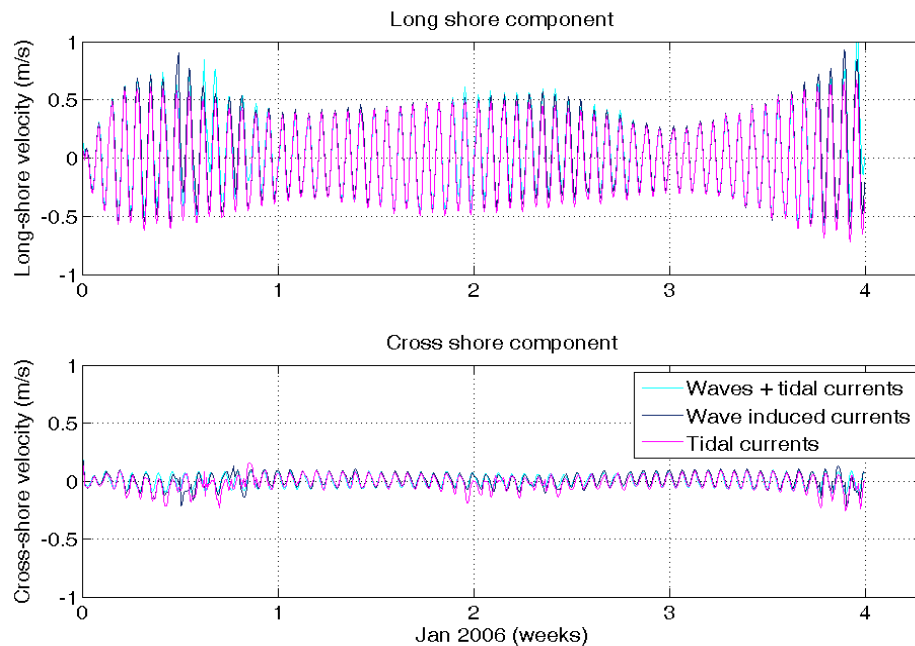
Figure 3. The long-shore and cross-shore components of the current velocities at the Wave Hub site. The legend at the bottom applies for the two figures.
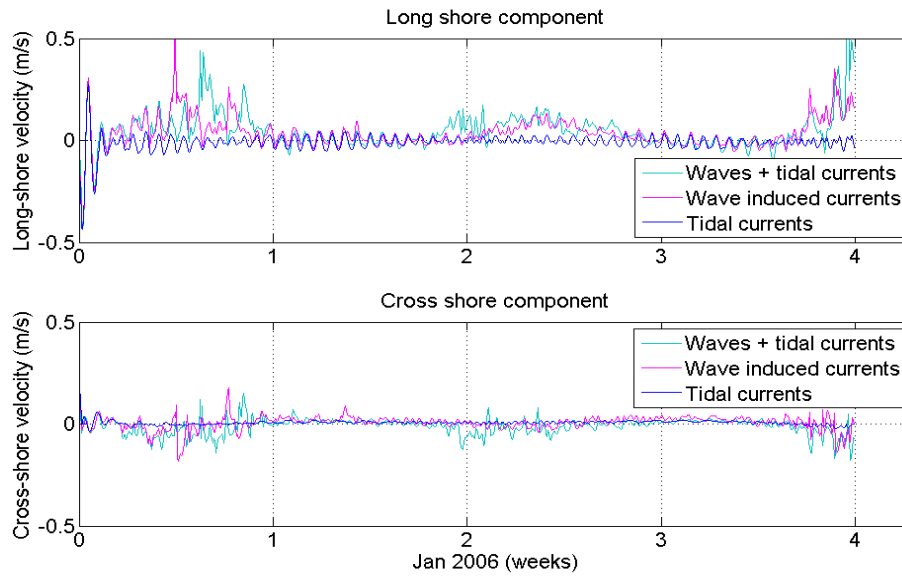
Long shore component

Cross shore component

Jan 2006 (weeks)

Figure 4. Anomalies of the current velocities for long-shore and cross-shore components, at the Wave Hub site.

Long shore component

Jan 2006 (weeks)

Cross shore component
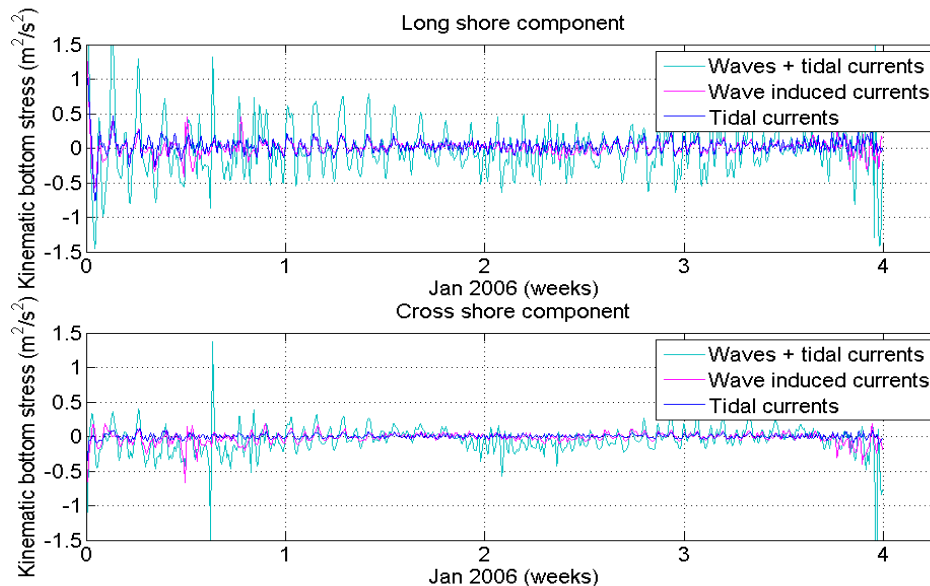
Jan 2006 (weeks)

Figure 5. Anomalies of the kinematic bottom stress for long-shore and cross-shore components, at the Wave Hub site.

Wave effects on tidal currents (radiation stress influence)

In order to study the wave-tide interactions the concept of radiation stress must be included, which is the flux of momentum carried by the ocean waves, when these waves break, that momentum is transferred to the water column, forcing near-shore currents. Radiation stress theory has been successfully used to explain the presence of long-shore currents (Bowen, 1969). Significant momentum can be transferred from wave to current especially where strong radiation stress gradient occurs due to breaking and bottom friction in the near-shore region.

Figure 6 shows a snap shot of current velocities with (left) and without (right) radiation stress influence, again the long-shore component has more impact on the general circulation of the area of study. It is worth mentioning that for these cases the surface stress has been idealised over the whole domain.
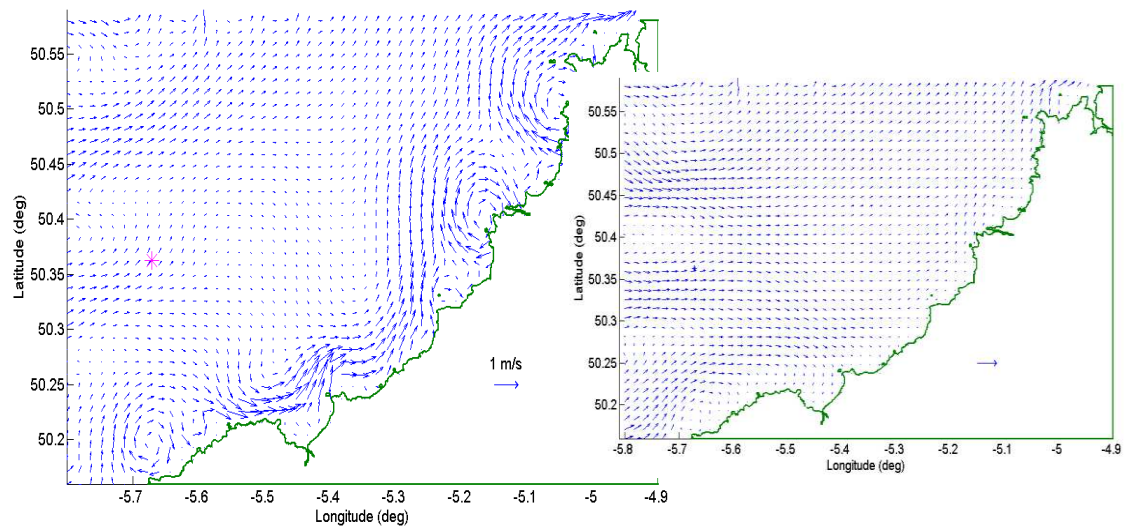
Figure 6. Velocity currents with (left) and without (right) radiation stress influence.

To assess the impact of waves on tidal currents a series of different cases combining spring and neap tides, high and low waters, high and low wave conditions, were tested to obtain current velocities and bottom stresses. In Figure 7 the significant wave height is plotted for the SWAN case only and for the coupled system against the sea surface elevation and buoy observations.
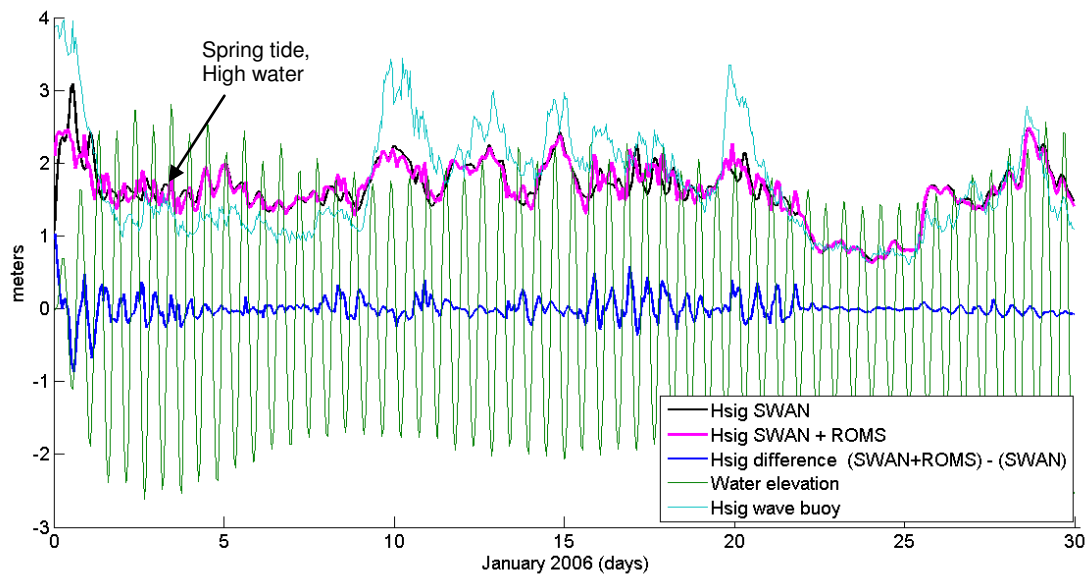

Figure 7. Significant wave heights with and without tidal currents and water elevations effects

In order to see the effects of waves on tidal currents, the change of currents or the magnitude of the velocity differences with and without the wave influence, the following formulation was applied to the velocity field:

$$V_{diff} = \sqrt{\left(U_{wy} - U_{wn}\right)^2 + \left(V_{wy} - V_{wn}\right)^2} \qquad (7)$$

where U_{wy} and U_{wy} are the x-horizontal velocity components with wave interaction and without wave interaction, respectively. V_{wy} and V_{wn} similarly for y-horizontal velocity components.

In Figure 8 the magnitude of velocity differences is shown, notice that in the near-shore region waves have a major impact on current velocities close to 1m/s of difference, in a similar way, the bottom stress difference has been mapped Figure (10), as well as velocity differences, the waves have the greatest impact on the bottom stress for the case indicated in Figure 7.
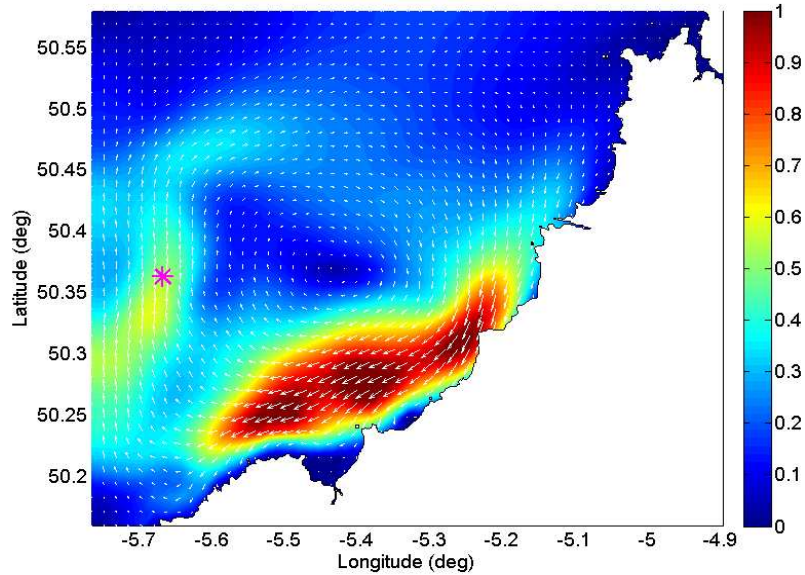

Figure 8. Current differences between ROMS+SWAN and ROMS for the point indicated by the arrow in Figure 7.
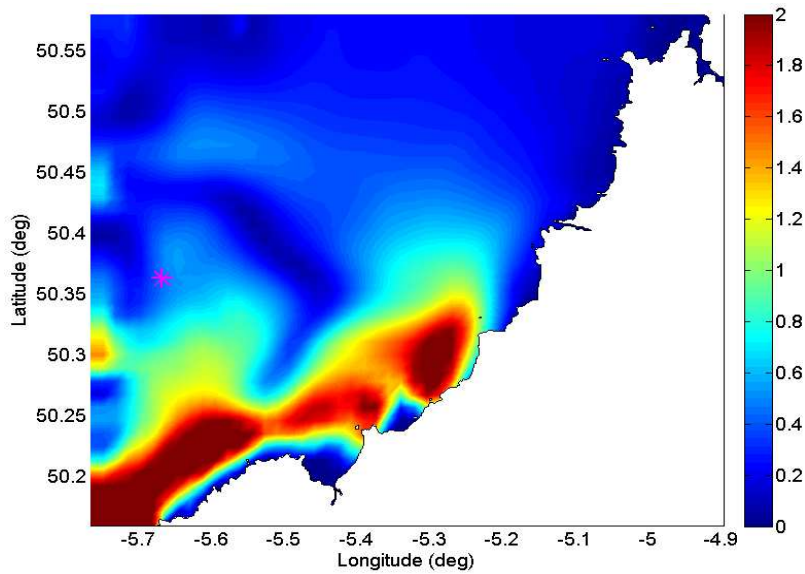

Figure 9. Bottom stress differences between ROMS+SWAN and ROMS for the point indicated by the arrow in Figure 7.

CONCLUSIONS

The wave model has been nested from coarse to fine grids, as shown in Figure 1, it has been forced by wave parameters and wind fields from global models. Model results have been compared against tide gauges and wave buoy observations with reasonable agreement. The circulation model has been forced by the tide model and wave parameters as radiation stress from the wave model. Also wind induced waves has been tested to improve the wave-current effect on the bed shear stress and velocity current fields.

The tidal elevation and tidal currents have a significant effect on the wave height predictions, tidal currents and wind waves have a significant effect on the bed shear-stress, relevant to sediment transport.

Waves via radiation stresses have an important effect on the long-shore and cross-shore velocity components, particularly during spring tides. Waves can impact on the bottom boundary layer and the mixing in the water column.

Significant wave heights are improved when the coupled modelling system is implemented. Also velocity currents and bed shear stresses show the significant influence from waves via radiation stress.

Interaction between waves and tides at the Wave Hub site is important when modelling sediment transport influenced by wave energy devices. The addition of wind fields on the circulation model are compulsory to determine the effect of surface stresses on waves and currents, moreover, the sediment transport study is being implemented in future works.

The results of this study will help the wave energy resource assessment and potential environment impact of the wave farm. Model results will be validated against the wave and current measurements by HF RADAR, ADCP and Directional Waverider buoys during the on-going Wave Hub projects.

ACKNOWLEDGMENTS

REFERENCES

Booij, N., Ris, R.C., Holthuijsen, L.H. (1999). A third generation wave model for coastal regions, part I, model description and validation. Journal of Geophysical Research 104 (C4), 7649-7666.

Buscombe D.D. & Scott T.M. (2008). The Coastal Geomorphology of North Cornwall, Wave Hub Impact on Seabed and Shoreline Processes – Report, http://www.research.plymouth.ac.uk/whissp/index.html

Haas K.A., Warner J.C. (2009), Comparing a quasi-3D to a full 3D nearshore circulation model: SHORECIRC and ROMS, Ocean Modelling 26, 91-103.

Millar D.L., Smith H.C.M., Reeve D.E. (2007). Modelling analysis of the sensitive of shoreline change to a wave farm. Ocean Engineering 34, 884-901.

Mulligan, R. P., A. E. Hay, and A. J. Bowen (2008), Wave-driven circulation in a coastal bay during the landfall of a hurricane, J. Geophys. Res., 113, C05026, doi:10.1029/2007JC004500.

NOAA Wavewatch III. NOAA/NCEP Operational Wave Models [online]. Available from: http://polar.ncep.noaa.gov/waves.

Padman L. and Erofeeva S. (2004), A barotropic inverse tidal model for the Artic Ocean, Geophysical Research Letters, vol. 31.

Pleskachevsky Eppel DP, Kapitza H. (2009), Interaction of waves, currents and tides, and wave-energy impact on the beach area of Sylt Island, Ocean Dynamics 59, 451 – 461.

Bowen, A. J. (1969), The generation of longshore currents on a plane beach, J. Mar. Res., 27, 206–214

SWRDA - South West of England Development Agency (2006). Wave Hub Development and Design Phase, SWRDA Group Limited, Coastal Processes Study Report. http://www.wavehub.co.uk/.

SWAN Cycle III version 40.72ABCDE (2009), Scientific and Technical Documentation, Delft University of Technology, pp. 119.

Warner J.C., Sherwood C.R., Signell R.P., Harris C.K., Arango H.G. (2008). Development of a three dimensional, regional, coupled wave, current, and sediment transport model. Computers & Geosciences 34, 1284-1306.

Wolf J., Prandle D. (1999), Some observations of wave-current interaction, Coastal Engineering 37, 471 – 485.